frontiers | Research Topics

Characterization of major traits and identification of functional genes for potato

Edited by
Botao Song, Juan Du and Vivianne Vleeshouwers

Published in
Frontiers in Plant Science

ISSN 1664-8714
ISBN 978-2-8325-2668-2
DOI 10.3389/978-2-8325-2668-2

About Frontiers

Frontiers is more than just an open access publisher of scholarly articles: it is a pioneering approach to the world of academia, radically improving the way scholarly research is managed. The grand vision of Frontiers is a world where all people have an equal opportunity to seek, share and generate knowledge. Frontiers provides immediate and permanent online open access to all its publications, but this alone is not enough to realize our grand goals.

Frontiers journal series

The Frontiers journal series is a multi-tier and interdisciplinary set of open-access, online journals, promising a paradigm shift from the current review, selection and dissemination processes in academic publishing. All Frontiers journals are driven by researchers for researchers; therefore, they constitute a service to the scholarly community. At the same time, the *Frontiers journal series* operates on a revolutionary invention, the tiered publishing system, initially addressing specific communities of scholars, and gradually climbing up to broader public understanding, thus serving the interests of the lay society, too.

Dedication to quality

Each Frontiers article is a landmark of the highest quality, thanks to genuinely collaborative interactions between authors and review editors, who include some of the world's best academicians. Research must be certified by peers before entering a stream of knowledge that may eventually reach the public - and shape society; therefore, Frontiers only applies the most rigorous and unbiased reviews. Frontiers revolutionizes research publishing by freely delivering the most outstanding research, evaluated with no bias from both the academic and social point of view. By applying the most advanced information technologies, Frontiers is catapulting scholarly publishing into a new generation.

What are Frontiers Research Topics?

Frontiers Research Topics are very popular trademarks of the *Frontiers journals series*: they are collections of at least ten articles, all centered on a particular subject. With their unique mix of varied contributions from Original Research to Review Articles, Frontiers Research Topics unify the most influential researchers, the latest key findings and historical advances in a hot research area.

Find out more on how to host your own Frontiers Research Topic or contribute to one as an author by contacting the Frontiers editorial office: frontiersin.org/about/contact

Characterization of major traits and identification of functional genes for potato

Topic editors

Botao Song — Huazhong Agricultural University, China

Juan Du — Huazhong Agricultural University, China

Vivianne Vleeshouwers — Wageningen University and Research, Netherlands

Citation

Song, B., Du, J., Vleeshouwers, V., eds. (2023). *Characterization of major traits and identification of functional genes for potato*. Lausanne: Frontiers Media SA.

doi: 10.3389/978-2-8325-2668-2

Cover image

VectoryFloor/Shutterstock.com

Table of contents

frontiers | Frontiers in Plant Science

TYPE Editorial
PUBLISHED 26 May 2023
DOI 10.3389/fpls.2023.1204304

OPEN ACCESS

EDITED AND REVIEWED BY
Leo Marcelis,
Wageningen University and Research, Netherlands

*CORRESPONDENCE
Botao Song
songbotao@mail.hzau.edu.cn

RECEIVED 12 April 2023
ACCEPTED 02 May 2023
PUBLISHED 26 May 2023

CITATION
Du J, Vleeshouwers VGAA and Song B (2023) Editorial: Characterization of major traits and identification of functional genes for potato.
Front. Plant Sci. 14:1204304.
doi: 10.3389/fpls.2023.1204304

Editorial: Characterization of major traits and identification of functional genes for potato

Juan Du[1,2,3], Vivianne G. A. A. Vleeshouwers[4] and Botao Song[1,2]*

[1]National Key Laboratory for Germplasm Innovation & Utilization of Horticultural Crops, Huazhong Agricultural University, Wuhan, China, [2]Key Laboratory of Potato Biology and Biotechnology, Ministry of Agriculture and Rural Affairs, Huazhong Agricultural University, Wuhan, China, [3]College of Life Science and Technology, Huazhong Agricultural University, Wuhan, China, [4]Plant Breeding, Wageningen University and Research, Wageningen, Netherlands

KEYWORDS

potato, gene, development, yield, nutrition, abiotic/biotic, plant immunity, disease resistance

Editorial on the Research Topic
Characterization of major traits and identification of functional genes for potato

Potato, *Solanum tuberosum*, is the fourth largest food crop and the most important non-grain crop in the world, as well as the model plant for the development of abnormal organs. It originates from the mountains of the Andes, and a great diversity of related wild tuber-bearing *Solanum* species thrive in South, Central, and North America. The widely cultivated potato has wide adaptability, high yield, and comprehensive nutrition. It can be used as the main food as well as vegetable and feed. Potato cultivars are autotetraploid (2n = 4x = 48), with highly heterozygous chromosomes and complex inheritance. Besides, artificial selection during cultivation has resulted in a relatively narrow genetic base, low heterosis, poor biotic and abiotic resistance, and so on. Unclear mechanisms of major potato traits, including growth and development, tuber nutrition and morphology, tolerance to abiotic and resistance to the many diseases, are key bottlenecks restricting potato genetic improvement. The decoding of several cultivated and wild potato genomes coupled with rapid advances in bioinformatics has provided powerful tools for detailed genetic and functional analysis. This Research Topic showcases exciting findings in potato ranging from tuber development, potato yield, tuber quality, abiotic and biotic stress resistance.

Potato tubers provide starch, which is the largest source of carbohydrates in the human diet. Cell wall invertase (CWI) is an essential coordinator in carbohydrate partitioning and sink strength determination, thereby playing key roles in plant development. Liu et al. identified StInvInh1 as a key inhibitor of CWI and demonstrated that its inhibition leads to improved microtuber development and higher accumulations of dry matter. These findings provide new insights into the regulation of tuber development. In addition to nutrient composition, tuber shape is one of the most important traits for potato breeding. To efficiently identify QTL for tuber shape, Huang et al. performed QTL-Seq analysis and linkage analysis in a diploid potato population-PM7. They identified a major stable QTL *TScha6* in a 1.85 Mb interval on chr 6 for tuber shape, and subsequently verified the QTL in a natural mapping population. Potato tuber sprouting has a great impact on processing and storage, but the molecular mechanism of sprouting is unclear.

Wang et al. found that overexpression of *StTCP15* leads to early sprouting of potato tubers, while down-regulated expression of the *StTCP15* gene leads to the dormancy of potato tubers. Through further research, they suggested that *StTCP15* regulated potato tuber dormancy and sprouting by affecting the dynamic balance between ABA and GA3. Altogether, these studies provide insight in the starch content, size, shape and sprouting of potato tubers.

The major threat to the sustainable production of potatoes remains the pressure of many diseases and pests. The most devastating disease is late blight caused by the oomycete *Phytophthora infestans*. Breeding for resistance to late blight has so far mainly been focused on the introgression of resistance genes, which are typically quickly defeated by this pathogen. Pattern-triggered immunity (PTI) mediated by plant pattern recognition receptors (PRRs) provides a promising alternative as they recognize conserved MAMPs, leading to enhanced broad-spectrum disease resistance. To study the mechanisms of PTI against *P. infestans*, Mu et al. performed a sequential windowed acquisition of all theoretical mass spectra (SWATH-MS) based quantitative proteomics analysis of differentially expressed proteins (DEPs) at different time points after infiltration of *P. infestans* culture filtrate in *N. benthamiana*. They identified a total of 4401 proteins and 1429 DEPs, of which 6 DEPs were proved to be involved in PTI responses. An additional study on PRR-based resistance in potato is targeting Pep-13/25, which are well-characterized MAMPs in *Phytophthora* species. Lin et al. conducted genetic mapping and characterization of a potato locus conferring perception of Pep-13/Pep-25 present in *P. infestans* and other plant pathogenic *Phytophthora* species. They developed a mapping population using wild potato species and use bulked-segregant RNAseq to map the putative receptor to a 0.081 cM region on the top of chr 3.

Plant viruses also represent limiting factors leading to a loss in the quality and quantity of potato. Due to their limited coding capacity, plant viruses depend on various host factors for successful infection. Loss of function of these factors will result in recessively inherited resistance, and therefore, are also described as recessive resistance or susceptibility genes. Chen et al. discovered the role of a plant eukaryotic translation initiation factor StnCBP as a recessive resistance factor for potato virus S (PVS) by recognizing the viral coat protein.

A major bacterial pathogen is *Ralstonia solanacearum* (Rs), the causal agent of potato bacterial wilt. Type III Secretion System Effectors (T3Es) play a vital role in the interaction. Investigating the T3Es that are recognized by host resistance proteins is an effective method to uncover the resistance mechanism of potato against *R. solanacearum*. Huang et al. employed comparative genomics to identify novel effectors of the Rs strain HA4-1, which is specifically recognized by the wild potato ALB28-1. They found that ectopic expression of two effectors, RipA5 and the newly identified RipBS, in the pathogenic strain HZAU091 of ALB28-1 partially reduced virulence, whereas individual mutations in four unique effectors RipS6, RipO1, RipBS, and Hyp6 in HA4-1 promote virulence.

The soil-borne fungus *Synchytrium endobioticum* is causing potato wart disease. Yan et al. investigated the response of potato cultivar 'Qingshu9' against *S. endobioticum* at the transcriptional level, and identified differentially expressed genes (DEGs) in the early and advanced stages of infection. They also identified 17 distinct modules of co-expressed genes using gene co-expression networks.

Altogether, these studies on the diversity of potato pathogens, including oomycetes, virus, bacteria and fungi, promise to contribute to achieving genetic disease resistance in potato.

Abiotic stresses are becoming increasingly important worldwide due to the ongoing global climate change and the increase in agrochemical utilization. Salt stress is a significant threat to potato production in facility cultivation environments, and the mining of salt tolerance genes requires further study. Jing et al. showed that proline homeostasis is critical for potato plantlet growth under salt stress, and identified the TF-hub gene *StGLK014720* as a regulator of two structural genes.

Additionally, environmental factors such as light and temperature influence anthocyanin biosynthesis. The molecular mechanisms regulating anthocyanin biosynthesis were profiled in potato tubers. Zhang et al. studied the gene expression and anthocyanin metabolites of Purple Viking tubers and its red and purple-skin mutants. They discovered that the conversion of certain anthocyanins was blocked in the red tubers and identified a specific gene, *OMT30376*, involved in the transformation of anthocyanins in potato tubers. Zhao et al. analyzed potato RM-210 tubers that turn purple when exposed to light and found that the *StMYBA1* gene was highly correlated with anthocyanin accumulation and could activate the expression of structural genes under light conditions, promoting anthocyanin biosynthesis in potato.

Continuous potato cropping systems cause yield reduction, soil-borne disease aggravation, and soil degradation, but crop rotation can alleviate these negative effects. Qin et al. explored the effects of continuous cropping obstacles on soil biochemical properties and microbial communities in North China. Data from their 4-year field work provided valuable information to improve the management of potato cultivation.

In sum, in this special issue, a diversity of major traits that are essential for a sustainable production of the potato crop are presented. The underlying genes are identified and characterized, and their function in growth and development, tuber nutrition and morphology, abiotic stress, and disease resistance and cropping systems.

Author contributions

JD prepared the first draft of this editorial. VV and BS revised the editorial. All authors approved the editorial for publication.

Funding

The work was partially supported by the National Science Foundation of China (31401436) and the Key-Area Research and Development Program of Guangdong Province (2022B0202060001).

Conflict of interest

The authors declare that the research was conducted in the absence of any commercial or financial relationships that could be construed as a potential conflict of interest.

Publisher's note

frontiers | Frontiers in Plant Science

ORIGINAL RESEARCH
published: 29 June 2022
doi: 10.3389/fpls.2022.865716

Integrative Analysis of Genes Involved in the Global Response to Potato Wart Formation

*Lang Yan[1], Yan Li[2], Yuan Qing[1], Xiang Tao[2], Haiyan Wang[3], Xianjun Lai[1]*and Yizheng Zhang[3]*

[1]Panxi Crops Research and Utilization Key Laboratory of Sichuan Province, College of Agricultural Science, Xichang University, Liangshan, China, [2]College of Life Sciences, Sichuan Normal University, Chengdu, China, [3]Sichuan Key Laboratory of Molecular Biology and Biotechnology, College of Life Sciences, Sichuan University, Chengdu, China

Synchytrium endobioticum, the causal agent of potato wart disease, poses a major threat to commercial potato production. Understanding the roles of transcriptionally regulated genes following pathogen infection is necessary for understanding the system-level host response to pathogen. Although some understanding of defense mechanisms against *S. endobioticum* infection has been gained for incompatible interactions, the genes and signaling pathways involved in the compatible interaction remain unclear. Based on the collection of wart diseased tubers of a susceptible cultivar, we performed phenotypic and dual RNA-Seq analyses of wart lesions in seven stages of disease progression. We totally detected 5,052 differentially expressed genes (DEGs) by comparing the different stages of infection to uninfected controls. The tendency toward differential gene expression was active rather than suppressed under attack by the pathogen. The number of DEGs step-up along with the development of the disease and the first, third and seventh of the disease stages showed substantially increase of DEGs in comparison of the previous stage. The important functional groups identified *via* Gene ontology (GO) and KEGG enrichment were those responsible for plant-pathogen interaction, fatty acid elongation and phenylpropanoid biosynthesis. Gene coexpression networks, composed of 17 distinct gene modules that contained between 25 and 813 genes, revealed high interconnectivity of the induced response and led to the identification of a number of hub genes enriched at different stages of infection. These results provide a comprehensive perspective on the global response of potato to *S. endobioticum* infection and identify a potential transcriptional regulatory network underlying this susceptible response, which contribute to a better understanding of the potato–*S. endobioticum* pathosystem.

Keywords: potato, *Synchytrium endobioticum*, transcriptional profiling, gene coexpression networks, susceptible response

OPEN ACCESS

Edited by:
Maria Raffaella Ercolano, University of Naples Federico II, Italy

Reviewed by:
Bharat Bhusan Patnaik, Fakir Mohan University, India
M. Gonzalo Claros, University of Malaga, Spain

****Correspondence:***
Xianjun Lai
laixianj@hotmail.com

Specialty section:
This article was submitted to Plant Pathogen Interactions, a section of the journal Frontiers in Plant Science

Received: *30 January 2022*
Accepted: *17 May 2022*
Published: *29 June 2022*

Citation:
Yan L, Li Y, Qing Y, Tao X, Wang H, Lai X and Zhang Y (2022) Integrative Analysis of Genes Involved in the Global Response to Potato Wart Formation. Front. Plant Sci. 13:865716. doi: 10.3389/fpls.2022.865716

INTRODUCTION

Potato wart disease, at present the most severe quarantine disease affecting cultivated potato production worldwide, is caused by the soilborne obligate biotrophic fungus *Synchytrium endobioticum* (Schilb.) Percival (Curtis, 1921; Hampson and Coombes, 1985). The potato host cell greatly enlarges and surrounding cells divide irregularly, resulting in wart-like malformations

and a nutrient sink (Hampson and Coombes, 1985). The tumor-like tissue of the wart progressively increases in size at the expense of the tubers, leading to unmarketable tubers and complete yield losses (Hampson, 1993). *Synchytrium endobioticum* exhibits a life cycle with a haploid sorus. Summer sporangia release several hundred zoospores that infect new tissue and transform under unfavorable conditions into diploid zygotes, resting or winter sporangia that penetrate host tissue and release to the soil when the host tissue decays (Busse et al., 2017). Because resting sporangia can survive and remain viable and infectious in the soil for decades, the major problem in current potato production is the contamination of the soil. There are no effective chemical control agents for eradicating the pathogen from contaminated soil (Obidiegwu et al., 2014). The only strategies to confine the disease are strict quarantine and phytosanitary measures as well as cultivation of resistant cultivars (De Boer, 2001; Flath et al., 2014; Obidiegwu et al., 2014; Przetakiewicz, 2015).

Plant–fungi interactions have evolved over millions of years, resulting in complicated mechanisms on both incompatible and compatible interaction (Asai and Shirasu, 2015; Cook et al., 2015; Wang and Wang, 2018). Although resistance and susceptibility are opposite sides of the same coin, most studies have focused for a long time on the resistance side in search for plant resistance genes (R-genes) and other defense genes (Pavan et al., 2010). Systematic studies on resistance of potato cultivars to *S. endobioticum* started a century ago. Conventional breeding schemes were successful in developing resistant varieties early in the twentieth century while are currently challenged by *S. endobioticum* pathotypes evolving and the increased risk of dissemination by potato tuber trade (Baayen et al., 2006; Obidiegwu et al., 2014). Several quantitative resistance loci for *S. endobioticum* resistance have been identified, in which the first one was a single dominant gene *Sen 1* located on potato chromosome IX, bringing resistance to pathotype 1(D1) through the recognition of the pathogen effector AvrSen1 (Hehl et al., 1999; Brugmans et al., 2006; van de Vossenberg et al., 2019). Based on two mapping populations, the quantitative resistance locus (QRL) *Sen2/6/18* on chromosome I were identified, which expressed resistance to pathotypes 2(G1), 6(O1), and 18(T1) respectively (Ballvora et al., 2011). Recently, newly locus *Sen2* located on chromosome XI which provides resistance to at least seven various virulent pathotypes of *S. endobioticum* were reported (Plich et al., 2018).

Although some understanding of defense mechanisms against *S. endobioticum* infection has been gained for incompatible interactions, including identification of several *Sen* loci conferring qualitative or quantitative potato resistance, the genes and signaling pathways involved in the compatible interaction remain unclear, especially the molecular basis of the induction of neo-plastic growth by this fungus. Insight into the molecular basis of plant disease susceptibility can be in further applied in breeding for resistance against a wide spectrum of pathogens. Besides the employment of multiple resistance genes in resistance breeding, knocking out (down) key susceptible genes could be an alternative method to develop cultivars with durable resistance. For example, the molecular responses of a susceptible wheat to *Fusarium graminearum* infection fit over the grain development processes depicted new clues to the understanding of effector-triggered susceptibility in plant–pathogen interactions (Chetouhi et al., 2016). Several host genes necessary for pathogen growth and infectious cycle were reported in other pathosystems (Pavan et al., 2010; Jia et al., 2011). A loss of functional mutations of such genes has already been successful in providing durable and broad-spectrum plant resistance, making the susceptibility genes (S-genes) a promising source of resistance in breeding strategies.

Although increasing knowledge is available, identifying S-genes still requires a better understanding of the molecular determinism of the plant-pathogen interacting system, including genome-wide approaches. Given the rapid development of high-throughput sequencing technology, RNA-Seq has been widely used to explore genome-wide gene expression patterns in compatible interaction (Tremblay et al., 2010; Tan et al., 2015). Although differential gene expression analyses have been carried out comparing transcription profiles, most of them provide a limited picture of the whole infection dynamics, prioritizing either on different stages of disease establishment or on organ-specific responses. In this study, we combined transcriptome and gene coexpression network (GCN) analyses to characterize regulated genes and signaling pathways in potato tuber tissue underlying global responses to *S. endobioticum* infection at the transcriptional level. GCNs constructed from gene expression data through the calculation of pairwise correlation coefficients could enrich genes' causal susceptibility and correlate with certain immune responses in modules, representing well-defined biological interactions deduced by differentially expressed genes (DEGs). Also, GCNs helps in noise reduction by eliminating non-responding genes during pathogen attacks, providing better insights into molecular mechanisms of the host response during wart formation and pathogenesis. Comparing patterns of gene expression among samples with varying stages of infection highlights some of the potential genes in biological pathways leading to susceptibility, which could help explain the compatible interactions in the potato–*S. endobioticum* pathosystem. Identifying key functional genes and pathways in susceptible responses will ultimately be powerful for developing diagnostic markers, which may aid in the identification of novel pathotype-specific effector genes and the development of new interventions against this pathogenic fungus.

MATERIALS AND METHODS

Plant Collection and Disease Assessment

The potato cultivar Qingshu 9, which is susceptible to potato wart disease, was grown in a field affected by potato wart disease the previous year. The field was located in Puge county, Liangshan, in southwestern China (E102°41′, N26°64′, elevation: 2,521 m a.s.l.). During the harvest, potato wart disease appeared in parts of the field. Diseased tubers were collected, and the lengths of the lesions were measured. The percentage of wart infection was calculated as the PLL: the maximum tumor diameters divided by the diameters of transverse sections of

tubers multiplied by 100. A total of 24 tubers were classified into eight groups (disease stages DS0–DS7) according to the PLL. The PLL was further used to quantify the area under the disease progress curve, which was calculated with the trapezoidal integration method (Silva et al., 2019). Data were analyzed by ANOVA, with each data point representing the average of three replicates.

RNA Isolation and Transcriptome Sequencing

Tissue protruding from the surface of the tuber was trimmed off, and the tuber flesh in the lesion was dug out, immediately frozen in liquid nitrogen, and stored at −80°C. Total RNA was isolated from infected and control samples with TRIzol reagent (Thermo Fisher Scientific, Waltham, MA, United States) according to the manufacturer's recommendations. Briefly, tissue from each sample was ground in TRIzol reagent with four ceramic beads with a tissue homogenizer (MP Biomedicals, Solon, OH, United States) after separation with chloroform, RNA precipitation with isopropanol, and washing of the RNA pellet with 75% ethanol. The air-dried RNA samples were dissolved in water treated with DEPC. The quantity of extracted RNA was detected with a spectrophotometer (NanoDrop™, Thermo Scientific), and the quality was measured by gel electrophoresis.

To construct the library of RNA sequences, we used a NEBNext Ultra RNA Library Prep Kit for an Illumina platform (New England Biolabs, Ipswich, MA, United States) according to the manufacturer's instructions. We generated the RNA-seq libraries using the NEBNext UltraTM RNA Library Prep Kit for Illumina (NEB) according to the manufacturer's instructions. Each library was indexed using NEBNext Multiplex Oligos for Illumina (Index Primers Set 1). The 24 libraries were paired-end sequenced by Illumina's HiSeq 2500 system (Illumina, United States). All raw sequence data as fastq files from the 24 libraries were deposited in the National Center for Biotechnology Information (NCBI)'s sequence read archive (SRA) database with respective accession numbers under BioProject accession number PRJNA803348.

RNA-Seq Data Processing and Differential Gene Expression

We assessed the quality of the raw reads with Cutadapt v1.10 (Martin, 2011). Reads were aligned with the potato reference genome (group Phureja DM v4.04; Diambra, 2011) with Gmap/Gsnap (Wu et al., 2016) and Samtools (Li et al., 2009). Normalized gene expression levels were calculated with Cufflinks v2.2.1 (Trapnell et al., 2012) and reported as FPKM. The extremely low expressed genes with an average FPKM value below four were excluded from analysis. To understand variability among biological replicates, pearson correlation coefficients were calculated for the log2 transformed FPKM values of the genes expressed in both replicates at a particular disease stage.

Based on the alignments, the read counts were used to perform differential gene expression analysis with DESeq2 (Love et al., 2014). Briefly, we compared infected samples (DS1–DS7) to controls with no symptoms of *S. endobioticum* infection (DS0) using a generalized linear model to obtain log2 fold change differences and corresponding value of p for individual transcripts. Also, we compared the samples in the latter disease stage with the previous disease stage (DSn vs. DSn-1). To define DEGs, we subjected the DESeq2 output to the Benjamini–Hochberg method (Ferreira, 2007) for multiple hypothesis testing and filtered it to retain genes with $|\log2FC| \geq 1$, false discovery rate < 0.05.

To determine the functional annotation of DEGs, the Database for Annotation, Visualization, and Integrated Discovery (DAVID, 2021 Update) was used for Gene ontology (GO) terms annotation and KEGG pathways analysis, with enrichment score >1, and value of $p < 0.05$ defined as significant.

GCN Analysis

The normalized read counts obtained from DESeq2 were used to construct GCNs with the weighted gene coexpression network analysis (WGCNA) package in R (Langfelder and Horvath, 2008). A one-step network building and module detection approach was used to build a GCN. WGCNA defines a network by connecting all variables in the data set, then detects modules with highly similar expression patterns. First an unsigned topological overlap matrix (TOM) is created to identify a threshold value for module detection. The network construction parameters included a threshold power of nine, a minimum module size equal to 30, and a branch merge cut height of 0.25. The resulting coexpression modules were visualized in Cytoscape v3.6.1 (Shannon et al., 2003). For each module, the top 10 percent of the nodes ranked by connectivity were recognized as hub nodes (genes). To identify the functions of each coexpression module, we performed GO and KEGG enrichment analysis using DAVID. Each gene set was compared against the fully expressed genes as background. Raw value of p were corrected for multiple tests and false discovery rate < 0.05 were identified as significantly enriched.

Confirmation and Quantification of the DEGs

For the confirmation and quantification of the DEGs obtained by the NGS analysis, we conducted RT-qPCR, respectively, for seven DEGs belonging to hub genes in GCN analysis with specific primers (**Supplementary Table S1**). Total RNA was treated with DNase I (Takara Bio, Shiga, Japan) and reverse-transcribed using the PrimeScript Reverse Transcription reagent Kit (Takara Bio, Shiga, Japan) following the manufacturer's instructions. RT-qPCR reactions were performed in a CFX Connect Real-Time PCR system (Bio-Rad Laboratories, Hercules, CA, United States), using TB Green Premix Ex Taq II Kit (Takara Bio Inc., Shiga, Japan). TB green RT-qPCR amplification was carried out in 20 µl reaction volumes that contained 2 µl of cDNA template, 10 µl of TB Green Premix Ex Taq II and 0.4 µM each of the forward and reverse primers, respectively, with the following conditions: initial denaturation at 95°C for 2 min, followed by 40 cycles at 95°C for 15 s and 60°C for 30 s. The relative quantification of four DEGs in different DS was carried out using the protocol described above and

normalized with internal controls GADPH according to the $2^{-\Delta\Delta CT}$ method (Livak and Schmittgen, 2001). Three biological replicates were run for each RT-qPCR reaction. Gene expression data were subjected to one-way ANOVA, followed by the Tukey's HSD *post hoc* test ($p \leq 0.05$).

RESULTS

Assessment of Disease in Potato Tubers Exposed to *Synchytrium endobioticum* Infection

To correlate observable symptoms of disease caused by the pathogen with gene expression in host responses, we monitored *S. endobioticum* infections of varying severity in tuber warts of the susceptible potato cv. Qingshu 9. Samples were classified into disease stages DS0–DS7 based on maximum tumor diameters divided by the diameters of transverse sections of tubers, also called the percent lesion length (PLL). ANOVA revealed mutually exclusive stages (**Figure 1**). DS0 represented the controls, with no symptoms; increasing stages revealed the development of the wart lesions until the tumor size exceeded 60%. Spots of *S. endobioticum* infection were first visible by DS1, on which no tumors yet appeared, corresponding to zoospore encystment and initial penetration through the stomata into the host. The first visible wart was apparent by DS2; warts increased in intensity and became slightly necrotic at the center by DS6. The mean severity of the entire sample was 47.05%, which fell just below the middle stage (DS4) on the scale. The area under the disease progress curve (AUDPC), assessed by one-way ANOVA, was lowest for DS1 at 17.84 and highest for DS7 at 190.83 and also demonstrated that the progression of the disease was in line with the scale.

Global Transcriptome Patterns Related to *Synchytrium endobioticum* Infection

We performed dual mRNA-Seq profiling of wart sites in infected tubers. Three biological replicates were sequenced for each severity level, yielding approximately 1.72 billion raw reads of 24 samples, with 32.11–42.63 million reads per sample. The libraries were constructed from infected potato tubers, and therefore the reads represented transcripts from the host (potato) and the pathogen (*S. endobioticum*). Raw reads were quality-filtered and aligned against the latest potato reference genome (with mapping rates ranging from 32.90% to 89.58%) as well as the *S. endobioticum* reference genome (with mapping rates ranging from 1.42% to 30.26%; **Supplementary Table S2**). In the early stages of infection, nearly all reads were of host origin. Susceptible interaction in advanced stages of infection led to an increase in pathogen biomass as well as pathogen transcripts in the transcriptome pools. To study the consistency in sampling and biological replicates, we used principal component analysis (PCA) to cluster samples. The results showed the co-localization of biological replicates at each stage

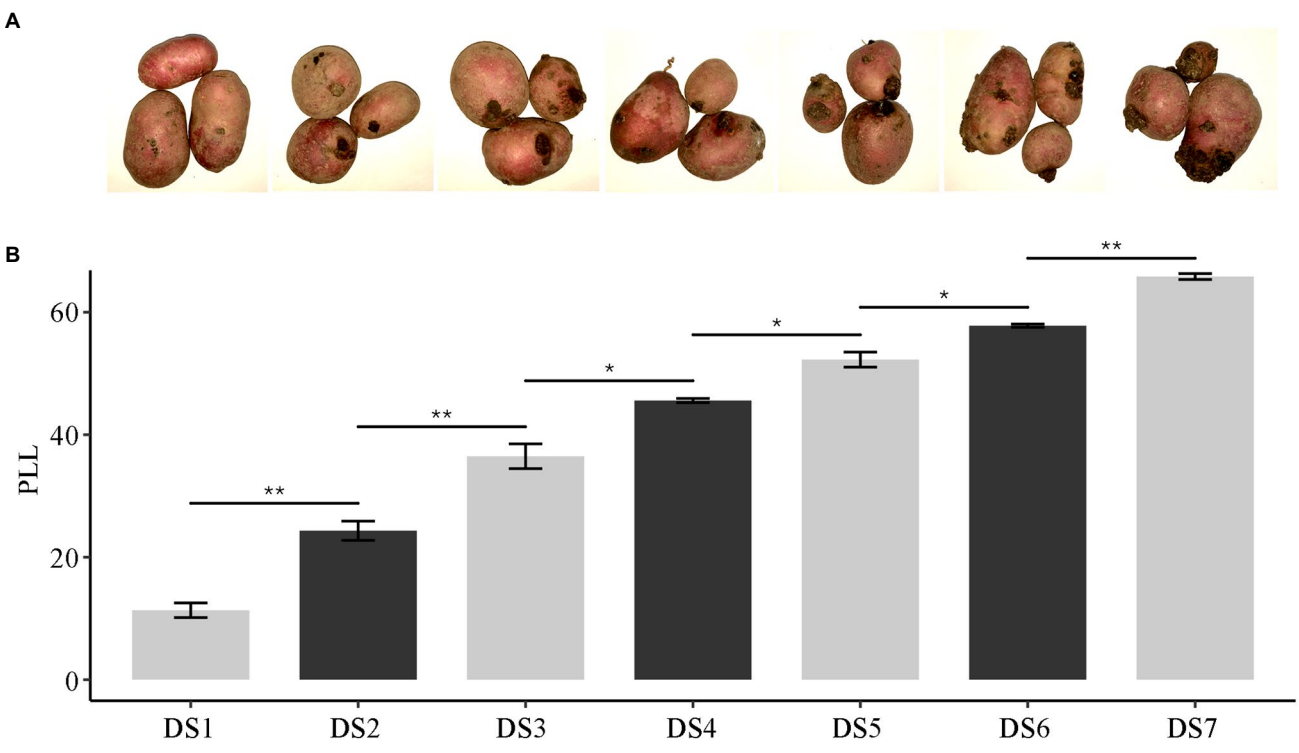

FIGURE 1 | The severity of potato wart disease in tubers infected by *Synchytrium endobioticum*. **(A)** Photographs showing the progression of disease over seven stages. **(B)** The severity of disease expressed as the percent lesion length (PLL). * means $p < 0.05$ and ** means $p < 0.01$, assessed by one-way ANOVA.

(**Figure 2A**), indicating severity-specific clustering in the wart infection transcriptomes explained by differences in gene expression patterns.

Over all infected samples, a total of 5,052 potato genes were differentially expressed compared to the control samples. A heat map of genes differentially expressed between the control and infected samples is shown in **Figure 2B**. The dendogram on the x axis showed that genes in DS0 clustered together, all infected sample clusters tended to group together by severity of disease. We compared the gene expression patterns and identified up- and down-regulated DEGs between the infected and control samples (**Figure 2C**). In general, 15.06%–80.17% out of DEGs were identified in different disease stages and the number of DEGs tended to increase along with the development of the disease. The proportion of DEGs in the early disease stages as DS1 and DS2 were below 20% while increased substantially after DS3 which exceeding 50% as the severity of disease increased (50.68%–60.87% from DS3 to DS6) and jumped to 80% in the last stage DS7. It was suggested a correlation between gene expression and the severity of infection. To elaborate on this step-up trend, we compared the DEG numbers in the latter disease stage with the previous disease stage (DSn vs. DSn-1). As shown in **Figure 2D**, the DS1, DS3 and DS7 showed substantially increase of DEGs in comparison of the previous stage, representing the early, intermediate and advanced stages of disease development.

A Venn diagram of DEGs showed that only 384 DEGs were common to all seven stages of infection. More important, DS7 had the most unique DEGs (1,027), and the number of unique DEGs decreased as the severity of disease decreased, to only 43 unique DEGs in DS1 (**Figure 3A**). Although DS3 and DS4 had more unique DEGs than DS5 and DS6, the difference was not significant. The differential number of unique DEGs demonstrated that different sets of response genes were

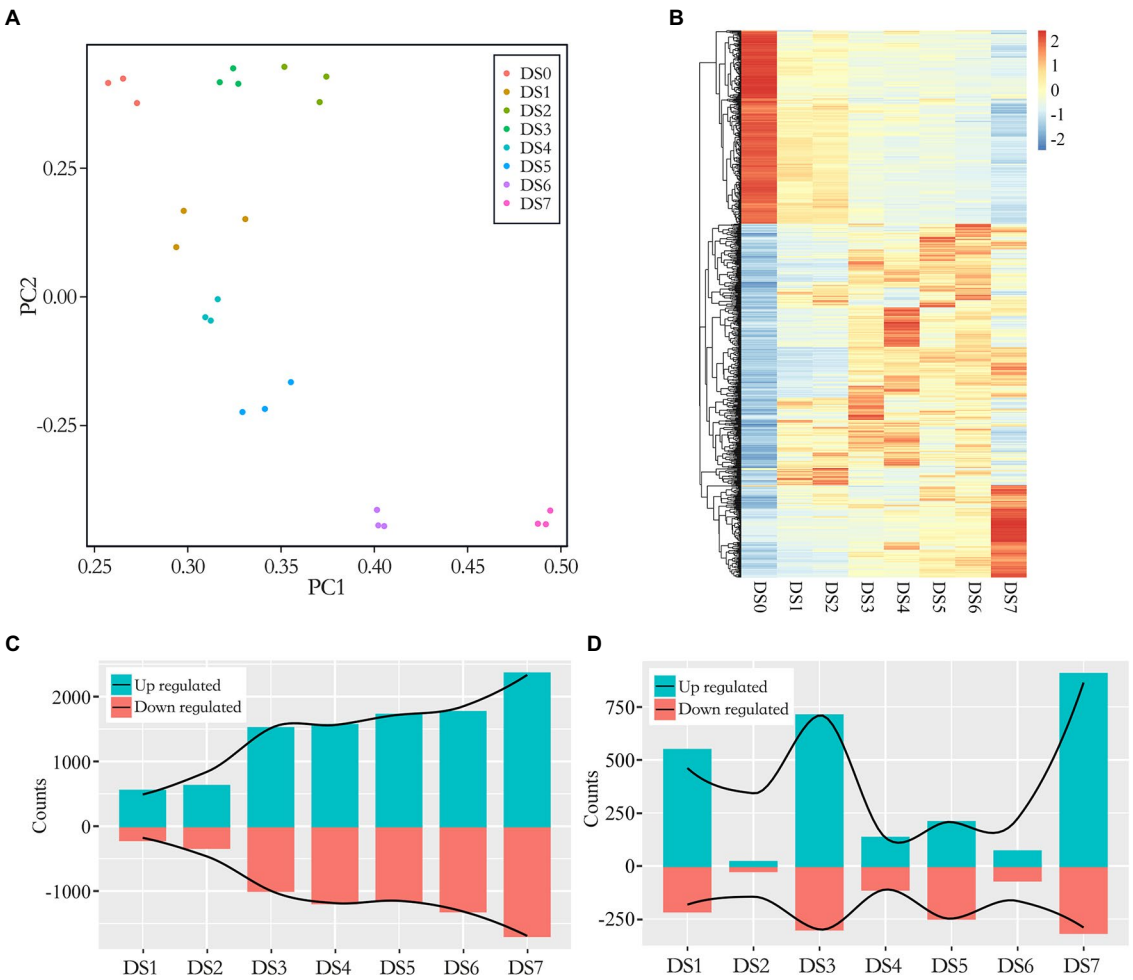

FIGURE 2 | Multiple plots of differentially expressed genes (DEGs) in seven disease stages. **(A)** Principal component analysis (PCA) of log2-transformed normalized gene expression in control and infected samples. **(B)** Clustered heat map of DEGs. Expression was calculated as the log2 fold change (LFC) of the FPKM value. The *x*-axis shows the disease stage, and the *y*-axis shows a dendrogram of samples at each individual stage, indicated by color; genes are represented by individual lines on the *y*-axis. **(C,D)** Bar graphs of the number of up- and down-regulated genes between the control and infected samples (**C**, DSn vs. DS0) as well as between the latter disease stage with the previous disease stage (**D**, DSn vs. DSn-1).

likely activated in severely infected samples. As shown in **Figure 3B**, in the comparison of DSn and DSn-1, the stage with substantial increase of DEG numbers also had a large number of unique DEGs, in which DS1, DS3 and DS7 had 299, 399 and 577 unique DEGs, respectively. Comparisons of the DEGs between early (DS1) and advanced (DS7) stages showed an absolutely higher number of unique DEGs in DS7. However, when compared with the intermediate stage DS3, the DS7-unique DEGs decreased and an increase number of DEGs were common in both stages. Comparison of two adjacent stages (DS6 vs. DS7) showed that most of the DEGs were common, which suggests that several different genes were involved in the host response to pathogen along with the development of the disease (**Figure 3C**).

Also, the results of pathogen mapping demonstrated the gene expression pattern in *S. endobioticum* during infection. Compared with DS0, the mapping rate of which was 1.46% in average, the vast majority of pathogen genes (6,398 out of 8,031) expressed differentially in the infected samples. Different from potato DEG patterns, the number of pathogen-DEGs increase in DS1 sharply to 4,573 and stabilize within the range between 4,890 and 5,485 in the subsequent disease stages (**Supplementary Figure S1**). The most interesting is that the number of upregulated DEGs was 5.2–5.6 times the number of downregulated DEGs, demonstrated that the pathogen gene expression was active rather than suppressed in the process of attacking the host. In addition, few unique DEGs in each stage were identified as 3,223 DEGs were common to all infected stages (**Supplementary Figure S2**).

System-Level Functional Analysis in Response to *Synchytrium endobioticum* Infection

Analyses of GO term and KEGG pathway enrichment were used to identify differential responses to potato wart at system-level functional pathways. To gain further insights about the pathway functions, we separated the up- and down-regulated DEGs between each infected samples and the control, as well as stage-specific DEGs between the latter and the previous disease stages. The top 10 enriched GO terms, including

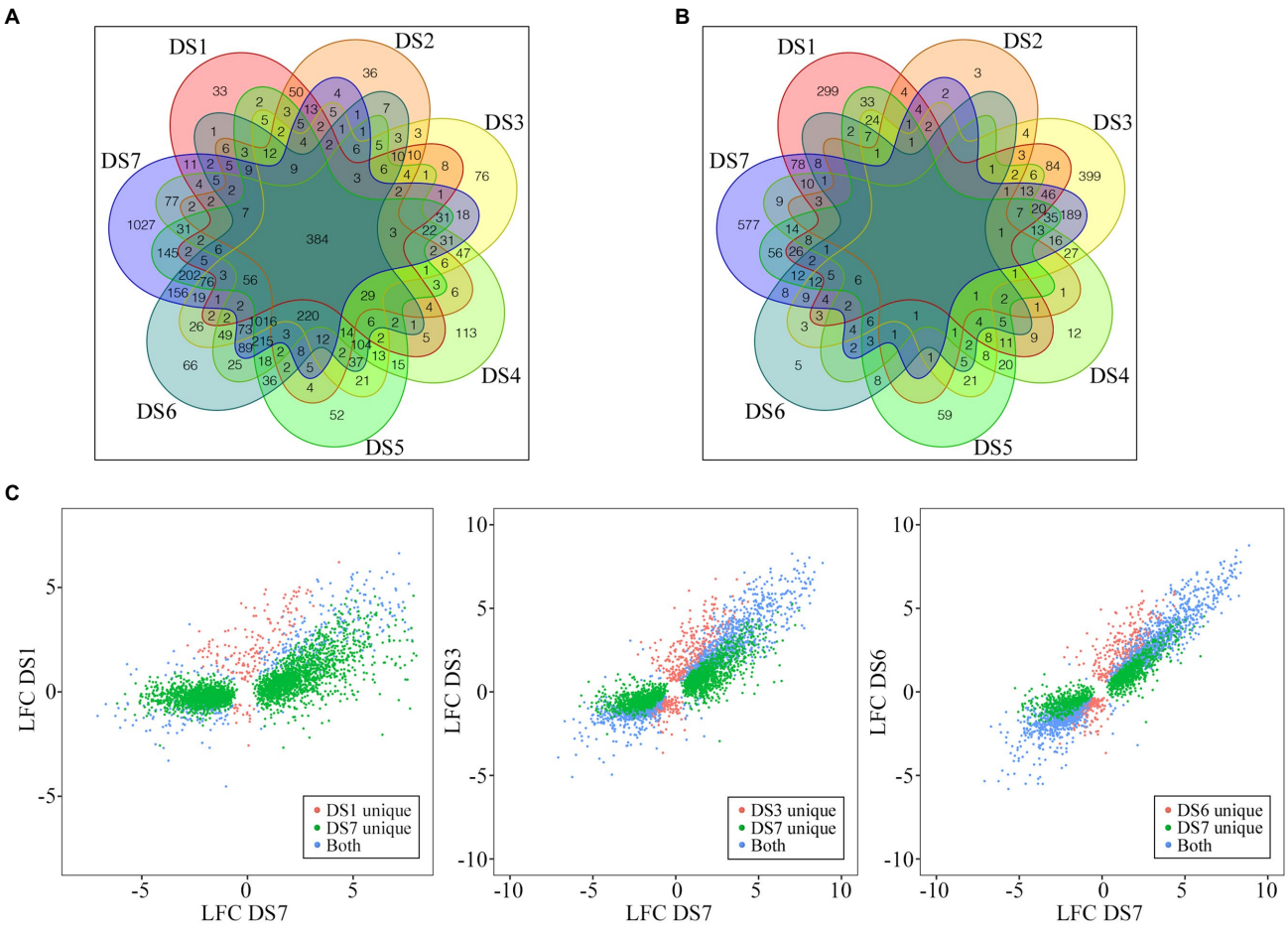

FIGURE 3 | Distribution of the common and unique DEGs among different disease stages. **(A,B)** Evaluation of similarities of DEGs between the control and infected samples (**A**, DSn vs. DS0) as well as between the latter disease stage with the previous disease stage (**B**, DSn vs. DSn-1) using Venn diagrams. **(C)** Pairwise comparisons of unique and conserved genes pair-wisely. Comparisons of DEGs for DS1 vs. DS7, DS3 vs. DS7, and DS6 vs. DS7 are shown.

biological process, molecular function and cellular components were shown in **Figure 4**; **Supplementary Tables S3** and **S4**. Biological process specific to defense response (GO:0006952) were upregulated and organonitrogen compound biosynthetic process (GO:1901566) were downregulated in all infected stages. Photosynthesis (GO:0015979) and cell wall organization (GO:0071555) were only upregulated during the early stage and peptide metabolic process (GO:0006518) were upregulated during the intermediate and advanced stages. In the last stage DS7, nitrogen compound transport (GO:0071705) and ion transport (GO:0006811) were specifically enriched. As to the molecular function, DNA binding (GO:0003677), transferase activity (GO:0016765), lipid binding (GO:0008289) and protein heterodimerization activity (GO:0046982) were shown upregulation whereas RNA binding (GO:0003723) and nucleic acid binding (GO:1901363) were shown downregulation in all infected stages. As the disease progresses, functions related to active transmembrane transporter activity (GO:0022804) and ubiquitin-protein transferase activity (GO:0019787) were induced at DS5-7.

A greater number of significantly ($p < 0.05$) enriched KEGG pathways were identified at each disease stages (**Supplementary Tables S5** and **S6**). Up-regulated DEGs displayed a total of 84 enriched pathways and down-regulated DEGs enriched in 61 pathways. Plant-pathogen interaction (sot04626), fatty acid elongation (sot00062), phenylpropanoid biosynthesis (sot00940), phenylalanine metabolism (sot00360) and glutathione metabolism (sot00480) were associated with the up-regulated genes in all seven infected stages. However, some pathways enriched with up-regulated genes were specifically enriched at different disease

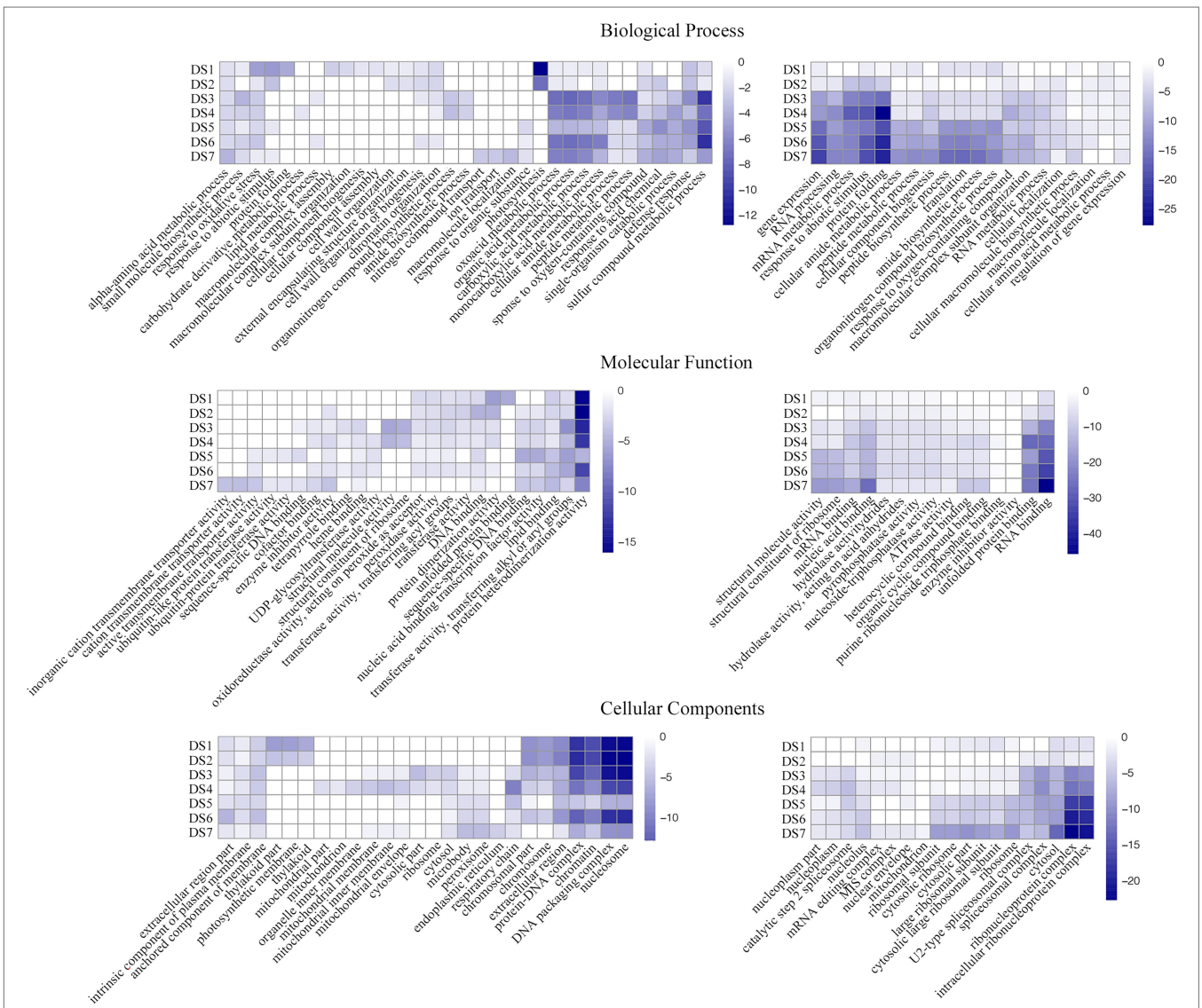

FIGURE 4 | Gene ontology (GO)-term correlation plots comparing probabilities of GO-term enrichments among different disease stages. Heatmaps in left and right represented the GO terms with the up- and down-regulated DEGs between each infected samples and the control, respectively. Color key scale indicates the minus log10 value of *p* GO term significance.

stages. Early stages DS1 and DS2 showed significant enrichment of pathways related to photosynthesis (sot00195) and porphyrin metabolism (sot00860) while pathways related to MAPK signaling pathway (sot04016) was induced since DS3. Interestingly, the last and most advance stage (DS7) had specific gene enrichments for pathways related to phagosome (sot04145) and metabolism of unsaturated fatty acids including biosynthesis of unsaturated fatty acids (sot01040) and α-linolenic acid metabolism (sot00592). In contrast, mRNA surveillance pathway (sot03015) and spliceosome (sot03040) showed downregulation in all seven infected stages. Pathways specific to pantothenate and CoA biosynthesis (sot00770) and ubiquitin mediated proteolysis (sot04120) were downregulated during the intermediate and advanced stages of disease development.

Gene Coexpression Patterns Associated With *Synchytrium endobioticum* Infection

We categorized genes differentially expressed between control samples and samples with varying levels of disease severity into distinct gene networks and used WGCNA to explore gene expression patterns and regulatory network responses to potato wart disease. A total of 4,621 highly correlated genes formed modules in which all members were more highly correlated with each other than they were with genes outside the module. WGCNA identified 17 distinct gene modules that contained between 25 and 813 genes. These highly interconnected GCN modules (subnetworks) were more likely to share common biological function or regulatory mechanisms. To visualize the module traits with respect to the progression of infection, we correlated eigengenes of each module with the different infection stages. As shown in **Figure 5A**, although a few modules included genes that shared broader coexpression patterns across multiple stages of infection, most modules differed significantly at certain stages of the stress response. For example, modules 1 and 6 were representative of genes with correlated coexpression at control, which enriched the largest number of genes highly expressed in uninfected samples and coordinately downregulated their expression after infection. Modules 12 and 10 were representative of genes highly coexpressed in the early stage (DS1 and 2) that might be responsible for inducing defense signaling in the host. The gene expression in modules 4, 11, and 15 showed peak upregulation in DS3, DS4, and DS5, respectively, corresponding to the middle stages of infection. Moreover, modules 16 and 8 had peak expression in DS6 and DS7 alone, which implicated them in serious susceptible responses in the late stages of infection. Gene expression patterns in 17 coexpression modules were shown in **Figures 5B–E**; **Supplementary Figure S3**.

We further performed GO and KEGG enrichment analysis to characterize functional classes and pathways associated with individual coexpression modules (**Supplementary Table S7**). The results of GO enrichment showed system-level functional activity initiated by pathogen infection. Five coexpression modules showed particular overrepresentation for the stress response. Module 1 and 8 had prominent enrichment of response to abiotic stimulus (GO:0009628). In addision, Module 8 showed enrichment for defense response (GO:0006952) and a series of GO terms related to gene positive regulations; Module 9 overrepresented GO terms related to cell wall organization or biogenesis (GO:0071554), response to oxidative stress (GO:0006979) as well as several negative regulations of biosynthetic process. Module 10 had a number of enriched GO terms mainly involved in regulation process and Module 17 showed significant enrichment of defense response to biotic stimulus (GO:0009607). In the results of KEGG enrichment, five modules (M3, M5, M6, M7, and M14) did not show significant enrichment for any KEGG pathway. Some pathways were specifically identified in a single module. Among them, Module 1 had prominent enrichment of spliceosome (sot03040), mRNA surveillance pathway (sot03015) and nucleocytoplasmic transport (sot03013). Module 8 showed enrichment for plant hormone signal transduction (sot04075) and MAPK signaling pathway (sot04016). Biosynthesis of various alkaloids (sot00996) was specifically enriched in Module 10. In contrast, several functional pathways were observed in more than one cluster. For example, both module 4 and 17 showed enrichment for terpenoid backbone biosynthesis (sot00900) and pyruvate metabolism (sot00620); module 2 and 11 revealed the enrichment of ubiquitin mediated proteolysis (sot04120).

Based on the WGCNA results for these notable modules, we identified hub genes that played crucial roles during infection and visualized the functional networks shown in **Supplementary Figure S4**. To validate the expression pattern of identified hub genes in the control and samples of seven infected stages, quantitative RT-qPCR were performed on the hub genes with highest connectivity in Module 1, 8, 9, and 10, respectively. The results of RT-qPCR showed the similar expression pattern of these four genes with RNA-Seq results and pearson correlation coefficients estimated from RNA-Seq and RT-qPCR ranged from 0.778 to 0.956 (**Supplementary Figure S5**). As shown in **Figure 5B**, genes in module 8 were significantly upregulated compared to the uninfected controls. This set of 48 hub genes included a large suite of genes implicated in the pathogen response, including class II chitinase (PGSC0003DMG400001528), Kunitz-type protease inhibitor (PGSC0003DMG400015267), β-ketoacyl-CoA synthase family protein (PGSC0003DMG400007373), nodulin (PGSC0003 DMG400015263), CBL-interacting protein kinase (PGSC0003 DMG400011106), late embryogenesis abundant protein 5 (PGSC0003DMG400017936). The common characteristics of these gene expression patterns were low expression in the controls and increased gene expression to thousands across multiple stages of infection and to peak expression in the last stage (DS7), which suggests an active attempt by the pathogen to alter host defense responses. Similarly, genes in module 10 were significantly upregulated compared to the controls, having the highest expression in the early stage (DS2) but becoming increasingly downregulated as the infection got worse (**Figure 5C**). The 15 hub genes in this module, which were responsible for inducing defense signaling in the early stages of infection, were ethylene response factor 5 (PGSC0003DMG400040046), Avr9/*Cf*-9 rapidly elicited protein (PGSC0003DMG400012296) and kinase interacting protein (PGSC0003DMG400027049). In module 9, we identified 35 hub genes related to plant defense (**Figure 5D**), in which ring finger

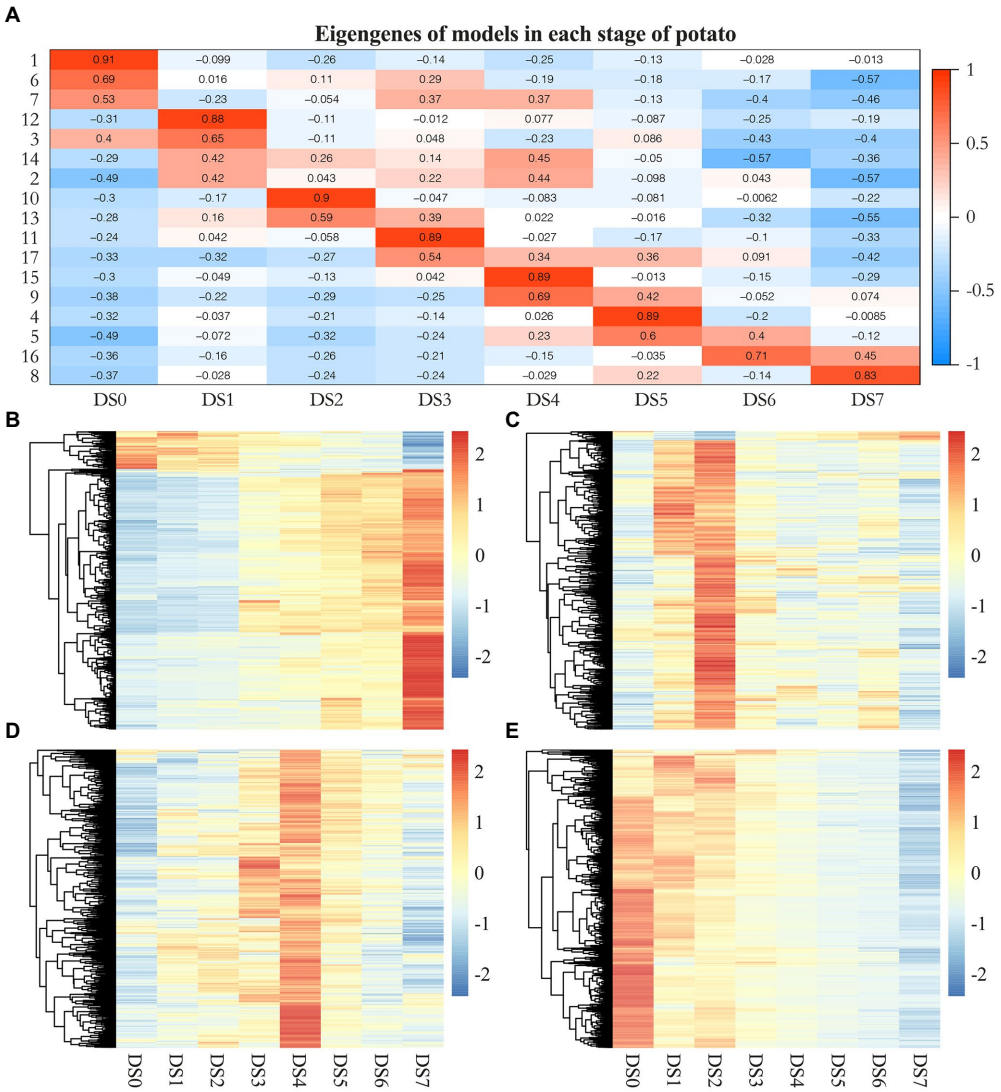

FIGURE 5 | Weighted gene coexpression network analysis (WGCNA) of genes differentially expressed following *S. endobioticum* infection in potato. **(A)** Heat map of eigengenes of each module correlated with the different infection stages. **(B–E)** Gene expression patterns in four coexpression modules that specifically showed enrichment for response to biotic stimuli.

protein (PGSC0003DMG400030821) had the highest connectivity of 155, followed by UDP-glucosyltransferase (PGSC0003DMG 400024618), Class III peroxidase (PGSC0003DMG400000511), NADH dehydrogenase (PGSC0003DMG400005271), extensin (PGSC0003DMG400000776), lipid binding protein (PGSC0003 DMG401023630). They were significantly upregulated in the early stages of infection, reaching peak expression in the middle stage (DS4) of the defense response. Given the fact that the majority of DEGs were upregulated during defense responses, module 1 included genes highly expressed in the controls but increasingly downregulated in infected samples (**Figure 5E**). Among 81 hub genes in this module, gene encoding histone acetyltransferase (PGSC0003DMG401015202) had the highest connectivity of 701. Several other transferase encoding genes such as methyltransferase (PGSC0003DMG400024216), glycosyltransferase (PGSC0003DMG400020103), acetylgluco saminyltransferase (PGSC0003DMG400008939) as well as RNA binding protein such as SGRP-1 protein (PGSC0003DMG 400033903), ran binding protein (PGSC0003DMG400020543), RNA-binding region RNP-1 (PGSC0003DMG400029841) showed either high connectivity in this module.

DISCUSSION

A significant difference was elaborated for gene expression under disease progression when infected with pathogen of potato wart, demonstrating unique biological processes and molecular mechanisms leading to susceptible responses. It is of fundamental importance to uncover gene changes in susceptible

potato cultivars following infection, which will help to exploit systemic response, especially susceptible responses to pathogen. In the biological process enrichment, DEGs up-regulated throughout all disease stages were related to defense response, plant-pathogen interaction as well as fatty acid elongation and phenylpropanoid biosynthesis. The process of fatty acid elongation had been reported in responses of plants to abiotic and biotic stresses, which are of primary importance for many interactions of the plant with its surrounding environment caused by pathogen or insect attacked and serves as a protection against pathogen infection to sustain post-injury survival (Batsale et al., 2021). On the other side, long-chain fatty acids such as sphingolipid was characterized as a positive regulator in biotic response and plant defense against fungi and bacteria pathogens by activating programmed cell death leading to spontaneous necrosis and lesions, also called accelerated cell death phenotype (Michaelson, 2011; Berkey et al., 2012). In plant–pathogen interactions, the phenylpropanoid pathway plays a critical role in plant defense response to fugal pathogen, in which previous studies in lettuce and tomato had been reported gene related to phenylpropanoid biosynthesis induced during the compatible interaction with *Botrytis cinerea* (De Cremer et al., 2013) and *Verticillium dahlia* (Tan et al., 2015).

The GCNs in our study presented distinct modules of genes enriched in the biotic stress response, suggesting a potential transcriptional regulatory network underlying the global response in different stages of infection. In general, pathogen infection should induce the downregulation of metabolic processes to conserve energy for resistance. However, the upregulation of metabolic processes during pathogen infection may trigger signal cascades that lead to host resistance. Module 8, with genes increased expression along with the disease progression, showed enrichment for plant hormone signal transduction and MAPK signaling pathway and involved pathogenesis-related hub genes encoding kunitz-type protease inhibitor and nodulin protein. As far as we know, kunitz-type protease inhibitors, showed high homology with miraculin-like proteins, is involved in the endogenous defense system as it helps regulate and balance protease activity, which plays a pivotal role in maize defense signaling and the regulation of plant cell death associated with the pathogen response involving the interplay of activating triggers and inhibitors (van der Linde et al., 2012). The induction of nodulin proteins in potato–*S. endobioticum* interactions has been associated with improvements in pathogen fitness through control over plant transporters. As reported before, the accumulation of transporters for nutrient uptake represents a shift from the biotrophic phase to the necrotrophic phase in hemibiotrophic pathogens due to the rapid growth of secondary hyphae in the late stages of infection (Zamora-Ballesteros et al., 2021).

Exploration of gene functions in pathways activated in the early stages of infection can provide knowledge about pathogen invasion as well as quick and effective responses among host plants. Module 10 was composed of genes with peak expression in the early stages of infection, and represented groups associated with biological regulation process in functional enrichment. The upregulation of ethylene-responsive transcription factor illustrates the early stress response. In most cases, the induction of ethylene-responsive transcription factor gene expression precedes mRNA accumulation of potential downstream target chitinase genes (Samac et al., 1990; Oñate-Sánchez and Singh, 2002). Although the ethylene-responsive transcription factor gene was upregulated in the early stages of infection and then was quickly tamped down during infection, transcriptional activation cascades may be important for host defense against pathogen attack while inhibited by pathogen with the progression of the infection (Oñate-Sánchez and Singh, 2002). CCR4-associated factor and Avr9/*Cf*-9 rapidly elicited genes had the same expression patterns, which rapidly altered expression in the early stages. CCR4-associated factor is necessary for plant development and defense, and its upregulation might contribute to a thickening of the cell wall through the formation of cellulose, the enlargement of cells, and the fortification of the cell wall through the regulation of downstream peroxidases (Sarowar et al., 2007). Many Avr9/*Cf*-9 rapidly elicited genes encode putative signaling components and regulatory proteins, including protein kinases and transcription factors, and thus may play pivotal roles in the initial development of the defense response (Liang et al., 2009). Specifically, *Cf* genes confer resistance to fungal pathogens by recognizing secreted Avr peptides, and host defense responses are immediately activated when the pathogen is perceived (De Vega et al., 2021). These signaling components could activate downstream R genes such as Rcr-1 and Rcr-2, as could ubiquitylation, which is important for *Cf*-9/Avr9-mediated defense responses (Rowland et al., 2005). Module 1 clearly represented a certain gene expression pattern highly expressed in the controls but increasingly downregulated in infected samples. From the results of functional enrichment in GO and KEGG pathways, we found Module 1 had prominent enrichment of response to abiotic stimulus as well as spliceosome, mRNA surveillance pathway and nucleocytoplasmic transport. And the hub genes in Module 1 contained some known disease resistance genes like transferase encoding genes and RNA binding protein encoding genes. The core hub gene with the highest connectivity was gene encoding histone acetyltransferase. A growing body of evidence suggests epigenetic mechanisms including histone acetylation is pertinent to interactions between hosts and pathogens (Gómez-Díaz et al., 2012). Histone acetyltransferases (HATs) had played a role in the regulation of plant defense responses (Ramirez-Prado et al., 2018). Also, the genes enriched in spliceosome and mRNA surveillance pathway were involved in the main regulatory processes to achieve early effective immunity, through either nonsense-mediated mRNA decay or alternative precursor mRNA splicing variation (Jung et al., 2020). Their downregulation explains their inefficiency in containing infection in earlier stages, which suggests an active virulence mechanism to abrogate host responses associated with stress-induced signaling.

From the results of the functional enrichment, our study showed an activation of basal defense response related genes. It has no doubt that resistant host initiate defense responses in incompatible interactions, while susceptible host can also

launch a series of basal defense responses in compatible interactions. Our results demonstrated that there may be an overlap among the susceptible responses of potato to fungal pathogens. As reported before, compatible response of potato inoculated with *Phytophthora infestans* uncovered significant differential expression of many defense- and disease-responsive genes (Restrepo et al., 2005). In fact, several genes and QTLs for potato wart disease resistance have been in potato populations, in which some *Sen* genes were found to be dominant genes giving a qualitative type of resistance (Prodhomme et al., 2020). Referenced to the flanking intervals of these QTLs, a total of 372 different DEGs in our study were located across the major effect QTL regions (**Supplementary Table S8**). The number of DEGs ranged from 56 for DS1 to 372 for DS7. Analysis of functional annotations of DEGs in potato wart QTLs found candidate gene with previous association with disease resistance. For example, receptor-like protein kinases such as CBL-interacting protein kinase and brassionsteroid insensitive-associated receptor kinase, as well as repeat domain-encoding genes including leucine rich repeat family and F-box/kelch-repeat protein, binding protein encoding genes like MAR-binding protein and ring finger protein were present in QTL regions from all the disease stages. Transcription factors such as WRKY domain, BZIP domain, SCL domain and C3H4 Zinc finger proteins were also among the DEGs in potato wart QTL regions.

Our study of using stages of infection captures the divergent properties observed in the gene expressions of the host and the pathogen by dual RNA-Seq, which was expected to become the gold standard in the studies of host-pathogen interactions (Camilios-Neto et al., 2014). When analyzing the genes expressed by *S. endobioticum*, it was possible to see that the amount of *S. endobioticum* genes detected in the study was highly variable depending on the states of tuber samples, and it ranged from 2,623 to 6,670 genes. The progressive increase of *S. endobioticum* RNA reflected the progression of disease (**Supplementary Figure S1A**) and the sharply increase of the relative amount of *S. endobioticum* RNA in the DS1 indicated the fungal invasion in large numbers (**Supplementary Figure S1B**). The pathogenicity-related transcripts included apoplastic effectors and secreted proteins, which were differentially expressed by *S. endobioticum*. As previously reported, many of them were proteins involved in protein degradation and modification (Brilli et al., 2018). Genes involved periplasmic serine protease and cysteine protease up-regulated by *S. endobioticum* might be important for the pathogenicity of pathogen, which is one of the best-characterized virulence factors and is of fundamental importance for invasion and dissemination of the fungus through the stratum corneum of the host (Leng et al., 2009; Bitencourt et al., 2016). Another important category attributed to the pathogen were associated with necrosis or breakdown of host cells, in which genes encoding lectins, 1,3(4)-β-D-glucanases and cellulose-binding proteins were up-regulated by *S. endobioticum* (Hayden et al., 2014). These effectors above were putatively involved in the hydrolysis of antifungal proteins produced by the host as well as the cell wall degradation during colonization.

In summary, infection by the fungal pathogen *S. endobioticum* activates a system-level response in potato tubers. Although further research is needed to determine whether the expression patterns of hub genes in modules are causative biomarkers or simply an effect of root nodulation or pathogen defense pathways, their identification suggests hypotheses to test.

DATA AVAILABILITY STATEMENT

The datasets presented in this study can be found in online repositories. The names of the repository/repositories and accession number(s) can be found at: https://www.ncbi.nlm.nih.gov/, PRJNA803348.

AUTHOR CONTRIBUTIONS

LY, YZ, and XL designed the research. YQ prepared the plant sample. XL and HW performed the transcriptome sequencing, assembly, and annotation. XL, YL, and XT performed the data analysis. LY and YL performed the RT-qPCR experiment. YZ and HW supervised the experiments and analysis. LY and XL wrote the initial draft. YZ, HW, and XT revised the manuscript. All authors contributed to the article and approved the submitted version.

FUNDING

This work was supported by the Application Fundamental Project of Science and Technology of Sichuan (no. 2019YJ0546) and the National Natural Science Foundation of China (no. 32060720) to LY.

ACKNOWLEDGMENTS

We acknowledge Xuecai Chen from Liangshan Potato Industry Development Center and Peihua Li from Xichang University for their assistance in the process of sampling.

SUPPLEMENTARY MATERIAL

The Supplementary Material for this article can be found online at: https://www.frontiersin.org/articles/10.3389/fpls.2022.865716/full#supplementary-material

Supplementary Figure S1 | Bar graphs of the number of up- and down-regulated pathogen genes between the control and infected samples (**A**, DSn vs. DS0) as well as between the latter disease stage with the previous disease stage (**B**, DSn vs. DSn-1).

Supplementary Figure S2 | A Venn diagrams of common and unique differentially expressed genes (DEGs) in different disease stages compared with control sample.

Supplementary Figure S3 | Heat maps showing the co-expressed genes in 13 modules.

Supplementary Figure S4 | Visualized coexpression network and related modules enriched with infection response genes.

Supplementary Figure S5 | RT-qPCR validation of RNA sequencing results. Four hub genes with the highest connectivity in four modules were selected for the confirmation of differentially expressed genes using the same RNA samples that were used for RNA sequencing. Pearson correlation between the gene expression levels measured using RT-qPCR and RNA-Seq was used for validation. The colors in the heat plot represents values for log2 fold change for each sample.

Supplementary Table S1 | A set of specific primer pairs for four hub genes with the highest connectivity in four modules in RT-qPCR validation.

Supplementary Table S2 | Summary of raw sequence data for dual RNA-Seq and SRA accession number.

Supplementary Table S3 | Functional enrichment of the GO terms with the up- and down-regulated DEGs between each infected samples and the control.

Supplementary Table S4 | Functional enrichment of the GO terms with the stage-specific DEGs between the latter and previous disease stages.

Supplementary Table S5 | Functional enrichment of the KEGG pathways with the up- and down-regulated DEGs between each infected samples and the control.

Supplementary Table S6 | Functional enrichment of the KEGG pathways with the stage-specific DEGs between the latter and previous disease stages.

Supplementary Table S7 | Functional enrichment of the GO terms and KEGG pathways with the coexpression genes in 17 network modules.

Supplementary Table S8 | List of DEGs in the major QTL regions that confer resistance against S. endobioticum infection.

REFERENCES

Asai, S., and Shirasu, K. (2015). Plant cells under siege: plant immune system versus pathogen effectors. *Curr. Opin. Plant Biol.* 28, 1–8. doi: 10.1016/j.pbi.2015.08.008

Baayen, R., Cochius, G., Hendriks, H., Meffert, J., Bakker, J., Bekker, M., et al. (2006). History of potato wart disease in Europe–a proposal for harmonisation in defining pathotypes. *Eur. J. Plant Pathol.* 116, 21–31. doi: 10.1007/s10658-006-9039-y

Ballvora, A., Flath, K., Lübeck, J., Strahwald, J., Tacke, E., Hofferbert, H.-R., et al. (2011). Multiple alleles for resistance and susceptibility modulate the defense response in the interaction of tetraploid potato (*Solanum tuberosum*) with *Synchytrium endobioticum* pathotypes 1, 2, 6 and 18. *Theor. Appl. Genet.* 123, 1281–1292. doi: 10.1007/s00122-011-1666-9

Batsale, M., Bahammou, D., Fouillen, L., Mongrand, S., Joubès, J., and Domergue, F. (2021). Biosynthesis and functions of very-long-chain fatty acids in the responses of plants to abiotic and biotic stresses. *Cell* 10:1284. doi: 10.3390/cells10061284

Berkey, R., Bendigeri, D., and Xiao, S. (2012). Sphingolipids and plant defense/disease: the "death" connection and beyond. *Front. Plant Sci.* 3:68. doi: 10.3389/fpls.2012.00068

Bitencourt, T. A., Macedo, C., Franco, M. E., Assis, A. F., Komoto, T. T., Stehling, E. G., et al. (2016). Transcription profile of Trichophyton rubrum conidia grown on keratin reveals the induction of an adhesin-like protein gene with a tandem repeat pattern. *BMC Genomics* 17, 1–14. doi: 10.1186/s12864-016-2567-8

Brilli, M., Asquini, E., Moser, M., Bianchedi, P. L., Perazzolli, M., and Si-Ammour, A. (2018). A multi-omics study of the grapevine-downy mildew (*Plasmopara viticola*) pathosystem unveils a complex protein coding-and noncoding-based arms race during infection. *Sci. Rep.* 8, 1–12. doi: 10.1038/s41598-018-19158-8

Brugmans, B., Hutten, R. G., Rookmaker, A. N. O., Visser, R. G., and van Eck, H. J. (2006). Exploitation of a marker dense linkage map of potato for positional cloning of a wart disease resistance gene. *Theor. Appl. Genet.* 112, 269–277. doi: 10.1007/s00122-005-0125-x

Busse, F., Bartkiewicz, A., Terefe-Ayana, D., Niepold, F., Schleusner, Y., Flath, K., et al. (2017). Genomic and transcriptomic resources for marker development in *Synchytrium endobioticum*, an elusive but severe potato pathogen. *Phytopathology* 107, 322–328. doi: 10.1094/PHYTO-05-16-0197-R

Camilios-Neto, D., Bonato, P., Wassem, R., Tadra-Sfeir, M. Z., Brusamarello-Santos, L. C., Valdameri, G., et al. (2014). Dual RNA-seq transcriptional analysis of wheat roots colonized by *Azospirillum brasilense* reveals up-regulation of nutrient acquisition and cell cycle genes. *BMC Genomics* 15, 1–13. doi: 10.1186/1471-2164-15-378

Chetouhi, C., Bonhomme, L., Lasserre-Zuber, P., Cambon, F., Pelletier, S., Renou, J.-P., et al. (2016). Transcriptome dynamics of a susceptible wheat upon *Fusarium* head blight reveals that molecular responses to *Fusarium graminearum* infection fit over the grain development processes. *Funct. Integr. Genomics* 16, 183–201. doi: 10.1007/s10142-016-0476-1

Cook, D. E., Mesarich, C. H., and Thomma, B. P. (2015). Understanding plant immunity as a surveillance system to detect invasion. *Annu. Rev. Phytopathol.* 53, 541–563. doi: 10.1146/annurev-phyto-080614-120114

Curtis, K. M. (1921). IX—The life-history and cytology of *Synchytrium endobioticum* (Schilb.), Perc., the cause of wart disease in potato. *Philos. Trans. R. Soc. B* 210, 409–478.

De Boer, S. (2001). Occurrence of potato wart caused by *Synchytrium endobioticum* on Prince Edward Island, Canada. *Plant Dis.* 85:1292. doi: 10.1094/PDIS.2001.85.12.1292A

De Cremer, K., Mathys, J., Vos, C., Froenicke, L., Michelmore, R. W., Cammue, B. P. A., et al. (2013). RNA seq-based transcriptome analysis of *Lactuca sativa* infected by the fungal necrotroph *Botrytis cinerea*. *Plant Cell Environ.* 36, 1992–2007. doi: 10.1111/pce.12106

De Vega, D., Holden, N., Hedley, P. E., Morris, J., Luna, E., and Newton, A. (2021). Chitosan primes plant defence mechanisms against *Botrytis cinerea*, including expression of Avr9/Cf-9 rapidly elicited genes. *Plant Cell Environ.* 44, 290–303. doi: 10.1111/pce.13921

Diambra, L. A. (2011). Genome sequence and analysis of the tuber crop potato. *Nature* 475, 189–195. doi: 10.1038/nature10158

Ferreira, J. A. (2007). The Benjamini-Hochberg method in the case of discrete test statistics. *Int. J. Biol.* 3:11. doi: 10.2202/1557-4679.1065

Flath, K., Przetakiewicz, J., van Rijswick, P., Ristau, V., and van Leeuwen, G. (2014). Interlaboratory tests for resistance to S ynchytrium endobioticum in potato by the G lynne-L emmerzahl method. *EPPO Bull.* 44, 510–517. doi: 10.1111/epp.12167

Gómez-Díaz, E., Jordà, M., Peinado, M. A., and Rivero, A. (2012). Epigenetics of host–pathogen interactions: the road ahead and the road behind. *PLoS Pathog.* 8:e1003007. doi: 10.1371/journal.ppat.1003007

Hampson, M. C. (1993). History, biology and control of potato wart disease in Canada. *Can. J. Plant Pathol.* 15, 223–244. doi: 10.1080/07060669309501918

Hampson, M., and Coombes, J. W. (1985). Stress and stimulus modifications of disease severity in the wart disease of potato. *Phytopathology* 75, 817–820. doi: 10.1094/Phyto-75-817

Hayden, K. J., Garbelotto, M., Knaus, B. J., Cronn, R. C., Rai, H., and Wright, J. W. (2014). Dual RNA-seq of the plant pathogen *Phytophthora ramorum* and its tanoak host. *Tree Genet. Genomes* 10, 489–502. doi: 10.1007/s11295-014-0698-0

Hehl, R., Faurie, E., Hesselbach, J., Salamini, F., Whitham, S., Baker, B., et al. (1999). TMV resistance gene N homologues are linked to *Synchytrium endobioticum* resistance in potato. *Theor. Appl. Genet.* 98, 379–386. doi: 10.1007/s001220051083

Jia, H., Millett, B. P., Cho, S., Bilgic, H., Xu, W. W., Smith, K. P., et al. (2011). Quantitative trait loci conferring resistance to *Fusarium* head blight in barley respond differentially to *Fusarium graminearum* infection. *Funct. Integr. Genomics* 11, 95–102. doi: 10.1007/s10142-010-0192-1

Jung, H. W., Panigrahi, G. K., Jung, G. Y., Lee, Y. J., Shin, K. H., Sahoo, A., et al. (2020). Pathogen-associated molecular pattern-triggered immunity involves proteolytic degradation of core nonsense-mediated mRNA decay

factors during the early defense response. *Plant Cell* 32, 1081–1101. doi: 10.1105/tpc.19.00631

Langfelder, P., and Horvath, S. (2008). WGCNA: an R package for weighted correlation network analysis. *BMC Bioinform.* 9, 1–13. doi: 10.1186/1471-2105-9-559

Leng, W., Liu, T., Wang, J., Li, R., and Jin, Q. (2009). Expression dynamics of secreted protease genes in *Trichophyton rubrum* induced by key host's proteinaceous components. *Sabouraudia* 47, 759–765. doi: 10.3109/13693780802524522

Li, H., Handsaker, B., Wysoker, A., Fennell, T., Ruan, J., Homer, N., et al. (2009). The sequence alignment/map format and SAMtools. *Bioinformatics* 25, 2078–2079. doi: 10.1093/bioinformatics/btp352

Liang, W., Li, C., Liu, F., Jiang, H., Li, S., Sun, J., et al. (2009). The *Arabidopsis* homologs of CCR4-associated factor 1 show mRNA deadenylation activity and play a role in plant defence responses. *Cell Res.* 19, 307–316. doi: 10.1038/cr.2008.317

Livak, K. J., and Schmittgen, T. D. (2001). Analysis of relative gene expression data using real-time quantitative PCR and the $2^{-\Delta\Delta CT}$ method. *Methods* 25, 402–408. doi: 10.1006/meth.2001.1262

Love, M. I., Huber, W., and Anders, S. (2014). Moderated estimation of fold change and dispersion for RNA-seq data with DESeq2. *Genome Biol.* 15, 1–21. doi: 10.1186/s13059-014-0550-8

Martin, M. (2011). Cutadapt removes adapter sequences from high-throughput sequencing reads. *EMBnet j.* 17, 10–12. doi: 10.14806/ej.17.1.200

Michaelson, L. V. (2011). New insights into cell death induced by long chain bases in *Arabidopsis*. *New Phytol.* 191, 909–911. doi: 10.1111/j.1469-8137.2011.03843.x

Obidiegwu, J. E., Flath, K., and Gebhardt, C. (2014). Managing potato wart: a review of present research status and future perspective. *Theor. Appl. Genet.* 127, 763–780. doi: 10.1007/s00122-014-2268-0

Oñate-Sánchez, L., and Singh, K. B. (2002). Identification of *Arabidopsis* ethylene-responsive element binding factors with distinct induction kinetics after pathogen infection. *Plant Physiol.* 128, 1313–1322. doi: 10.1104/pp.010862

Pavan, S., Jacobsen, E., Visser, R. G., and Bai, Y. (2010). Loss of susceptibility as a novel breeding strategy for durable and broad-spectrum resistance. *Mol. Breed.* 25, 1–12. doi: 10.1007/s11032-009-9323-6

Plich, J., Przetakiewicz, J., Śliwka, J., Flis, B., Wasilewicz-Flis, I., and Zimnoch-Guzowska, E. (2018). Novel gene Sen2 conferring broad-spectrum resistance to *Synchytrium endobioticum* mapped to potato chromosome XI. *Theor. Appl. Genet.* 131, 2321–2331. doi: 10.1007/s00122-018-3154-y

Prodhomme, C., van Arkel, G., Plich, J., Tammes, J. E., Rijk, J., van Eck, H. J., et al. (2020). A Hitchhiker's guide to the potato wart disease resistance galaxy. *Theor. Appl. Genet.* 133, 3419–3439. doi: 10.1007/s00122-020-03678-x

Przetakiewicz, J. (2015). First report of new pathotype 39 (P1) of *Synchytrium endobioticum* causing potato wart disease in Poland. *Plant Dis.* 99:285. doi: 10.1094/PDIS-06-14-0636-PDN

Ramirez-Prado, J. S., Piquerez, S. J., Bendahmane, A., Hirt, H., Raynaud, C., and Benhamed, M. (2018). Modify the histone to win the battle: chromatin dynamics in plant–pathogen interactions. *Front. Plant Sci.* 9:355. doi: 10.3389/fpls.2018.00355

Restrepo, S., Myers, K., Del Pozo, O., Martin, G., Hart, A., Buell, C., et al. (2005). Gene profiling of a compatible interaction between *Phytophthora infestans* and *Solanum tuberosum* suggests a role for carbonic anhydrase. *Mol. Plant-Microbe Interact.* 18, 913–922. doi: 10.1094/MPMI-18-0913

Rowland, O., Ludwig, A. A., Merrick, C. J., Baillieul, F., Tracy, F. E., Durrant, W. E., et al. (2005). Functional analysis of Avr9/Cf-9 rapidly elicited genes identifies a protein kinase, ACIK1, that is essential for full Cf-9–dependent disease resistance in tomato. *Plant Cell* 17, 295–310. doi: 10.1105/tpc.104.026013

Samac, D. A., Hironaka, C. M., Yallaly, P. E., and Shah, D. M. (1990). Isolation and characterization of the genes encoding basic and acidic chitinase in *Arabidopsis thaliana*. *Plant Physiol.* 93, 907–914. doi: 10.1104/pp.93.3.907

Sarowar, S., Oh, H. W., Cho, H. S., Baek, K. H., Seong, E. S., Joung, Y. H., et al. (2007). *Capsicum annuum* CCR4-associated factor CaCAF1 is necessary for plant development and defence response. *Plant J.* 51, 792–802. doi: 10.1111/j.1365-313X.2007.03174.x

Shannon, P., Markiel, A., Ozier, O., Baliga, N. S., Wang, J. T., Ramage, D., et al. (2003). Cytoscape: a software environment for integrated models of biomolecular interaction networks. *Genome Res.* 13, 2498–2504. doi: 10.1101/gr.1239303

Silva, K. J. P., Singh, J., Bednarek, R., Fei, Z., and Khan, A. (2019). Differential gene regulatory pathways and co-expression networks associated with fire blight infection in apple (Malus × domestica). *Hortic. Res.* 6, 1–13. doi: 10.1038/s41438-019-0120-z

Tan, G., Liu, K., Kang, J., Xu, K., Zhang, Y., Hu, L., et al. (2015). Transcriptome analysis of the compatible interaction of tomato with *Verticillium dahliae* using RNA-sequencing. *Front. Plant Sci.* 6:428. doi: 10.3389/fpls.2015.00428

Trapnell, C., Roberts, A., Goff, L., Pertea, G., Kim, D., Kelley, D. R., et al. (2012). Differential gene and transcript expression analysis of RNA-seq experiments with TopHat and Cufflinks. *Nat. Protoc.* 7, 562–578. doi: 10.1038/nprot.2012.016

Tremblay, A., Hosseini, P., Alkharouf, N. W., Li, S., and Matthews, B. F. (2010). Transcriptome analysis of a compatible response by *Glycine max* to *Phakopsora pachyrhizi* infection. *Plant Sci.* 179, 183–193. doi: 10.1016/j.plantsci.2010.04.011

van de Vossenberg, B. T., Prodhomme, C., van Arkel, G., van Gent-Pelzer, M. P., Bergervoet, M., Brankovics, B., et al. (2019). The *Synchytrium endobioticum* AvrSen1 triggers a hypersensitive response in Sen1 potatoes while natural variants evade detection. *Mol. Plant-Microbe Interact.* 32, 1536–1546. doi: 10.1094/MPMI-05-19-0138-R

van der Linde, K., Hemetsberger, C., Kastner, C., Kaschani, F., van der Hoorn, R. A., Kumlehn, J., et al. (2012). A maize cystatin suppresses host immunity by inhibiting apoplastic cysteine proteases. *Plant Cell* 24, 1285–1300. doi: 10.1105/tpc.111.093732

Wang, Y., and Wang, Y. (2018). Trick or treat: microbial pathogens evolved apoplastic effectors modulating plant susceptibility to infection. *Mol. Plant-Microbe Interact.* 31, 6–12. doi: 10.1094/MPMI-07-17-0177-FI

Wu, T. D., Reeder, J., Lawrence, M., Becker, G., and Brauer, M. J. (2016). "GMAP and GSNAP for genomic sequence alignment: enhancements to speed, accuracy, and functionality," in *Statistical Genomics*. eds. E. Mathé and S. Davis (New York, NY: Humana Press), 283–334.

Zamora-Ballesteros, C., Pinto, G., Amaral, J., Valledor, L., Alves, A., Diez, J. J., et al. (2021). Dual RNA-sequencing analysis of resistant (*Pinus pinea*) and susceptible (*Pinus radiata*) hosts during *Fusarium circinatum* challenge. *Int. J. Mol. Sci.* 22:5231. doi: 10.3390/ijms22105231

Conflict of Interest: The authors declare that the research was conducted in the absence of any commercial or financial relationships that could be construed as a potential conflict of interest.

Publisher's Note: All claims expressed in this article are solely those of the authors and do not necessarily represent those of their affiliated organizations, or those of the publisher, the editors and the reviewers. Any product that may be evaluated in this article, or claim that may be made by its manufacturer, is not guaranteed or endorsed by the publisher.

frontiers | Frontiers in Plant Science

TYPE Original Research
PUBLISHED 08 August 2022
DOI 10.3389/fpls.2022.946873

OPEN ACCESS

EDITED BY
Vivianne Vleeshouwers,
Wageningen University and Research,
Netherlands

REVIEWED BY
Alfonso Muñoz,
University of Córdoba, Spain
Huimin Xu,
Canadian Food Inspection Agency,
Canada
Bai Yanju,
Heilongjiang Academy of Sciences,
China

*CORRESPONDENCE
Bihua Nie
nbihua@mail.hzau.edu.cn
Changzheng He
hecz@hotmail.com

SPECIALTY SECTION
This article was submitted to
Crop and Product Physiology,
a section of the journal
Frontiers in Plant Science

RECEIVED 18 May 2022
ACCEPTED 11 July 2022
PUBLISHED 08 August 2022

CITATION
Chen R, Yang M, Tu Z, Xie F, Chen J, Luo T, Hu X, Nie B and He C (2022) Eukaryotic translation initiation factor 4E family member nCBP facilitates the accumulation of TGB-encoding viruses by recognizing the viral coat protein in potato and tobacco. *Front. Plant Sci.* 13:946873. doi: 10.3389/fpls.2022.946873

Eukaryotic translation initiation factor 4E family member nCBP facilitates the accumulation of TGB-encoding viruses by recognizing the viral coat protein in potato and tobacco

Ruhao Chen[1,2], Manhua Yang[2], Zhen Tu[2], Fangru Xie[2], Jiaru Chen[2], Tao Luo[2], Xinxi Hu[1], Bihua Nie[2]* and Changzheng He[1]*

[1]ERC for Germplasm Innovation and New Variety Breeding of Horticultural Crops, Key Laboratory for Vegetable Biology of Hunan Province, Hunan Agricultural University, Changsha, China, [2]Key Laboratory of Potato Biology and Biotechnology (HZAU), Ministry of Agriculture and Rural Affairs, Key Laboratory of Horticultural Plant Biology (HZAU), Ministry of Education, Huazhong Agricultural University, Wuhan, China

Due to their limited coding capacity, plant viruses have to depend on various host factors for successful infection of the host. Loss of function of these host factors will result in recessively inherited resistance, and therefore, these host factors are also described as susceptibility genes or recessive resistance genes. Most of the identified recessive resistance genes are members of the *eukaryotic translation initiation factors 4E* family (*eIF4E*) and its isoforms. Recently, an eIF4E-type gene, *novel cap-binding protein* (*nCBP*), was reported to be associated with the infection of several viruses encoding triple gene block proteins (TGBps) in Arabidopsis. Here, we, for the first time, report that the knockdown of *nCBP* in potato (*StnCBP*) compromises the accumulation of potato virus S (PVS) but not that of potato virus M (PVM) and potato virus X (PVX), which are three potato viruses encoding TGBps. Further assays demonstrated that StnCBP interacts with the coat proteins (CPs) of PVS and PVM but not with that of PVX, and substitution of PVS CP in the PVS infectious clone by PVM CP recovered the virus infection in *StnCBP*-silenced transgenic plants, suggesting that the recognition of PVS CP is crucial for *StnCBP*-mediated recessive resistance to PVS. Moreover, the knockdown of nCBP in *Nicotiana benthamiana* (*NbnCBP*) by virus-induced gene silencing suppressed PVX accumulation but not PVM, while NbnCBP interacted with the CPs of both PVX and PVM. Our results indicate that the *nCBP* orthologues in potato

and tobacco have conserved function as in Arabidopsis in terms of recessive resistance against TGB-encoding viruses, and the interaction between nCBP and the CP of TGB-encoding virus is necessary but not sufficient to determine the function of *nCBP* as a susceptibility gene.

KEYWORDS

susceptibility genes, recessive resistance, eukaryotic translation initiation factors 4E, nCBP, TGB-encoding virus, coat protein

Introduction

Potato (*Solanum tuberosum* L.) is currently the third most important food crop worldwide next to rice and wheat for direct human consumption and food security (Hardigan et al., 2017; van der Waals and Krüger, 2020). However, plant viruses are one of the main limiting factors leading to a loss in quality and quantity of potato (Wang et al., 2011; Rashid et al., 2021). Due to their limited coding capacity, plant viruses recruit various host factors to help their infection (Truniger and Aranda, 2009). These host factors, whose mutation confers loss of susceptibility to related viruses, are called susceptibility genes or recessive resistance genes (Truniger and Aranda, 2009; Hashimoto et al., 2016; Garcia-Ruiz, 2018; Mäkinen, 2020).

The eukaryotic translation initiation factor 4E (eIF4E) and its isoforms [eIF(iso)4E] are mRNA 5' cap-binding proteins which control cap-dependent translation initiation (Gingras et al., 1999). They are also the most extensively studied susceptibility genes (Lellis et al., 2002), and particular research attention has been paid to the relationship between *eIF4E/eIF(iso)4E* and potyvirus infection. For instance, mutation in *eIF4E/eIF(iso)4E* resulted in loss of susceptibility to potyviruses in multiple hosts, such as Arabidopsis, tomato, pepper, lettuce, pea, peanut, and sugarcane (Ruffel et al., 2002, 2005; Nicaise et al., 2003; Gao et al., 2004; Xu et al., 2017; Yang et al., 2021). In most cases, the interaction between eIF4E/eIF(iso)4E and the viral genome-linked proteins (VPgs) of potyviruses is required for virus infection (Léonard et al., 2000; Charron et al., 2008; Tavert-Roudet et al., 2017; Yang et al., 2021). Moreover, *eIF4E/eIF(iso)4E* was also found to mediate recessive resistance to other viruses. The recessive mutant *cum1* in Arabidopsis showed reduced accumulation of a cucumovirus, and *cum1* was found to encode an eIF4E protein (Yoshii et al., 2004). The recessive bymovirus resistance locus *rym4* in barley was proved to correspond to the *eIF4E* gene (Kanyuka et al., 2005). In melon, an *eIF4E* allele confers resistance to a carmovirus, depending on the inefficient interaction between the viral 3' cap-independent translational enhancer and eIF4E (Nieto et al., 2006; Truniger et al., 2008). In addition, the mutation of tobacco *eIF(iso)4E* genes was found to reduce the susceptibility to an umbravirus (Udagawa et al., 2020).

Another less studied *eIF4E* family member, *novel cap-binding protein* (*nCBP*), has been identified in Arabidopsis showing 41.44 and 40.50% nucleotide sequence identity with *eIF4E* and *eIF(iso)4E*, respectively, (Ruud et al., 1998). The nCBP protein also supports the translation initiation of capped mRNA *in vitro* and *in vivo* (Bush et al., 2009). In addition, nCBP has been reported to be involved in the infection of different viruses in various crops. *ncbp-1/ncbp-2* mutants in cassava exhibited high resistance to cassava brown streak disease (Gomez et al., 2019), and the *ncbp* mutant in Arabidopsis displayed resistance to several viruses in *Alphaflexiviridae* and *Betaflexiviridae*, which encode triple gene block proteins (TGBps; Keima et al., 2017). These results indicate that *nCBP*, similar to *eIF4E/eIF(iso)4E*, has the potential to act as a recessive resistance gene, which is worthy of further investigation in other crops.

Potato virus S (PVS, *Carlavirus*), potato virus M (PVM, *Carlavirus*), and potato virus X (PVX, *Potexvirus*), which all encode TGBps, are important viruses posing great threats to potato production (Wang et al., 2011, 2016; Keima et al., 2017). In this study, we found that *StnCBP* knockdown compromised PVS accumulation but not PVM and PVX. Further analysis demonstrated that the interaction between StnCBP and PVS coat protein (CP) is crucial for the *StnCBP*-mediated recessive resistance to PVS, while StnCBP interacts with the CPs of both PVS and PVM. Moreover, *NbnCBP* knockdown significantly reduced PVX accumulation but not PVM, and NbnCBP also interacted with both their CPs in *N. benthamiana*. These results indicate that the interaction between nCBP and CP is necessary but not sufficient for facilitating the accumulation of TGB-encoding viruses, which improves the understanding of the underlying mechanism for *nCBP* to act as a susceptibility gene.

Materials and methods

Plant materials and virus isolates

Potato variety (Eshu 3) and three transgenic lines with *StnCBP* silencing were used in the study. The plants were maintained on MS medium (Murashige and Skoog, 1962) supplemented with 4% sucrose *in vitro* under a 16 h of

light/8 h of dark photoperiod with 400–1,000 μmol photons m^{-2} s^{-1} light intensity at 20°C and were transplanted into pots (12 cm) containing premixed soil in the greenhouse located in Huazhong Agricultural University (HZAU) under a 12 h of light/dark photoperiod with 90 μmol photons m^{-2} s^{-1} light intensity at 18–22°C.

Three virus isolates used in this study, PVS-HB7, PVX-HB3, and PVM-HB36, were collected from a local potato virus survey and maintained in tobacco or potato host plants under greenhouse conditions at HZAU. The virus identity and purity were determined as described previously (Nie et al., 2012; Wang et al., 2016).

BLAST search and cloning

A BLASTn search was performed using the *AtnCBP* (Accession number: AF028809) nucleotide sequence as a query against the *S. tuberosum* genome (Spud DB) and the *Solanaceae* Genomics Network (SGN) to retrieve *nCBP* homolog sequences in potato and *N. benthamiana*, respectively. *StnCBP* and *NbnCBP* were amplified with specific primers (**Supplementary Table 1**) from the potato cultivar Eshu 3 and *N. benthamiana*, respectively, using Phanta Super-Fidelity DNA polymerase (Vazyme, China). Then, the PCR amplicons were cloned into the pCE-Zero vector (Vazyme, China). Five colonies were randomly selected and sent for sequencing (Sangon Biotech, China). To analyze the phylogenetic relationships of eIF4E orthologues in *S. tuberosum, Arabidopsis thaliana, Solanum lycopersicum,* and *Nicotiana benthamiana*, we performed a BLASTp search against the NCBI and SGN databases using the amino acid sequences of potato *eIF4E* family members as queries. The phylogenetic tree was generated using MEGA5.2 with neighbor-joining tree and 1000 bootstraps. The nCBP orthologues in *Oryza sativa* and *Zea mays* were also obtained by a BLASTp against the NCBI database. Then, an amino acid sequence alignment of nCBP orthologues from the above species was performed by DNAMAN to analyze whether the nCBP orthologues are conserved across species.

Generation of transgenic potato lines

Based on the design principles of RNAi fragments (Wesley et al., 2001; Reynolds et al., 2004), a fragment with 249 bp near the 5' end of *StnCBP* gene was selected as the target fragment for RNA interference. The nucleotide sequence of the target fragment returned no other homologous genes except for *StnCBP* in a BLASTn search against the *S. tuberosum* genome. The fragment was recombined into the *Xho*I and *Xba*I sites of the pHellsGate8 vector. *Agrobacterium tumefaciens* (*A. tumefaciens*) strain GV3101 containing the recombined pHellsGate8 constructs was employed to transform the microtuber slices of Eshu 3 for transgenic lines as previously described (Zhou et al., 2019). Primers for constructing the RNAi vector are shown in **Supplementary Table 1**.

Virus-induced gene silencing assay

A 270-bp region in the 5'-terminus of *NbnCBP* was selected as the virus-induced gene silencing (VIGS) target using SGN VIGS Tool[1] (Fernandez-Pozo et al., 2015). Then, it was amplified and inserted into the *Eco*RI and *Bam*HI sites of pTRV2 vector (named pTRV2: NbnCBP), and the correct construction of the vector was confirmed by sequencing. The plasmids pTRV1, pTRV2, and pTRV2: NbnCBP were transformed into *A. tumefaciens* strain GV3101 by electroporation. The leaves of 4-week-old *N. benthamiana* plants were inoculated with a mixture of *Agrobacterium* cultures containing pTRV1 and pTRV2: NbnCBP (final OD600 = 0.5) to induce NbnCBP silencing; a mixture of *Agrobacterium* cultures containing pTRV1 and empty pTRV2 was used as a negative control (Control). Two weeks later, the upper leaves were collected to identify the silencing efficiency. Primers for constructing the VIGS vector are shown in **Supplementary Table 1**.

Virus inoculation

Potato plants at the 4–6 leaf stage were mechanically inoculated with wild-type virus inocula (leaf extract: about 1 *g*/10 ml leaf tissue homogenized in 10 mM phosphate buffer with 32 mM sodium sulfite, pH 7.5) as described previously (Singh et al., 2003) or agro-infiltrated with virus infectious clones as described previously (Sun et al., 2017). Foliage symptoms were monitored daily post-inoculation until harvest. For resistance assays, the upper non-inoculated leaves were sampled at 10 and 15 days post-inoculation (dpi).

Identification of virus accumulation

Total RNA of partially collected samples was extracted by Total RNApure Kit (ZOMANBIO, Beijing, China). The first-strand cDNA synthesis was performed by All-In-One 5X RT MasterMix (Applied Biological Materials, Vancouver, Canada). Then, the accumulation level of the viruses was detected through quantitative reverse-transcription polymerase chain reaction (qRT-PCR). The qRT-PCR analyses were carried out in the LightCycler480 Real-Time PCR system[2] using 2X qPCR Real-Time Kit (Applied Biological Materials, Vancouver, Canada). The accumulation level analysis was calculated by the

1 https://vigs.solgenomics.net/

2 https://diagnostics.roche.com

$2^{-\Delta\Delta\ Cq}$ method based on the internal reference gene ef1α (Accession number: AB061263) or *actin* (Accession number: XM_016658880; Nicot et al., 2005). All histograms were made with GraphPad Prism. Primers for qRT-PCR are shown in **Supplementary Table 1**.

Another part of the collected samples was analyzed by double-antibody sandwich enzyme-linked immunosorbent assay to detect the accumulation of viruses at the protein level using virus-specific polyclonal antibodies (Agdia, Elkhart, IN, United States) according to the manufacturer's protocol as previously described (Wang et al., 2016). Five drops (∼100 μl) of leaf sap obtained by a tuber slicer (Elektrowerk, Hannover, Germany) were used as samples for the ELISA assay. The sap from virus-containing plants and virus-free plants was used as the positive controls and negative controls, respectively. After the samples were incubated with specific primary and secondary antibodies in 96-well ELISA plates, the chromogenic substrate pNPP was added and the absorbance value at 405 nm (A_{405}) was measured using an ELx800 Universal Microplate Reader (Bio-Tek Instruments, Winooski, United States).

Yeast-two-hybrid assay

StnCBP, NbnCBP, and AtnCBP were recombined between the *Bam*HI and *Eco*RI sites of the pGBKT7 vector, while the proteins of PVX and PVS were recombined between the *Bam*HI and *Eco*RI sites of the pGADT7 vector using SE cloning kit (Applied Biological Materials, Vancouver, Canada). Pairwise combinations for interaction analyses were co-transformed into yeast strain AH109 following BD Matchmaker Screening Kit. The interactions were identified through a medium that lacks tryptophan, leucine, adenine, and histidine and contains X-α-GAL (20 mg/L) as the interaction leads to blue plaques. Primers for constructing yeast-two-hybrid (Y2H) vectors are shown in **Supplementary Table 2**.

Bimolecular fluorescent complimentary

Paired combinations for interaction analysis were inserted into nYFP and cYFP plasmids, respectively, through restriction endonuclease sites *Bam*HI and *Sal*I, and were introduced into *Agrobacterium* strain GV3101. Then, a mixture of *Agrobacterium* cultures containing the two recombinant plasmids (final OD600 = 0.2) was infiltrated into *N. benthamiana* leaves at the 4–6 leaf stage, and the fluorescence signal of YFP was observed at 48 h post-infiltration using a confocal laser scanning microscope (SP8, Leica, Wetzlar, Germany). Primers for constructing bimolecular fluorescent complimentary (BiFC) vectors are shown in **Supplementary Table 3**.

Subcellular localization

The sequences coding for amino acids in protein (CDS) of *StnCBP* and PVS *CP* were amplified with specific primers and recombined into the *Bsp*1407I site of pK7WGF2 where fused behind eGFP for subcellular localization, and CDS of St*nCBP* was also inserted into the *Bsp*1407I site of pK7WGR2 where fused behind RFP for co-localization analysis. The vectors were electroporated into *Agrobacterium tumefaciens* strain GV3101 and agro-infiltrated the leaves of 4-week-old *N. benthamiana* as protocols previously described (Zhan et al., 2019). The fluorescence signal was observed at 48 h post-infiltration using a confocal laser scanning microscope (SP8, Leica, Wetzlar, Germany). Primers for constructing subcellular localization vectors are shown in **Supplementary Table 3**.

Western blotting

Total proteins were extracted from leaves of *N. benthamiana* which expressed the GFP fused StnCBP and CP proteins using a protein extraction buffer [100 mM Tris–HCl (pH 8), 150 mM NaCl, 2 mM dithiothreitol, 5 mM EDTA, 10% glycerol, 2 mM phenylmethylsulfonyl fluoride, and 1% protease inhibitor tablets (A32955; Thermo Fisher Scientific)]. About 20 μl of 5× SDS-PAGE loading buffer with 5 μM β-mercaptoethanol was added to 80 μl of the extracted protein supernatant. The supernatant was heated to 95°C for 5 min to denature the protein, and then, these samples were loaded for Western blotting analysis. Probes with specific anti-GFP antibodies at 1:5,000 dilution (MBL, Japan) were used for Western blotting as protocols previously described (Cheng et al., 2021; Wang et al., 2021).

Results

StnCBP was an *eIF4E* gene belonging to the nCBP subgroup in potato

A BLASTn search against *the S. tuberosum* genome in the Spud DB database[3] was performed using the nucleotide sequence of *nCBP* in *A. thaliana* (*AtnCBP*, Accession number: AT5G18110) as a query to identify *nCBP* orthologues in potato. As a result, a unique *nCBP* gene (named as *StnCBP*; Accession number: Soltu.DM.10G026730) was identified, which exhibited 59.6 and 70.0% homology to *AtnCBP* in nucleic acid and amino acid sequence, respectively. Potato has four members of the *eIF4E* family, including *SteIF4E* (Accession number: Soltu.DM.03G000970), *SteIF4E-2* (Accession number: Soltu.DM.02G002530), *SteIF(iso)4E* (Accession number:

3 http://spuddb.uga.edu/

10.3389/fpls.2022.946873

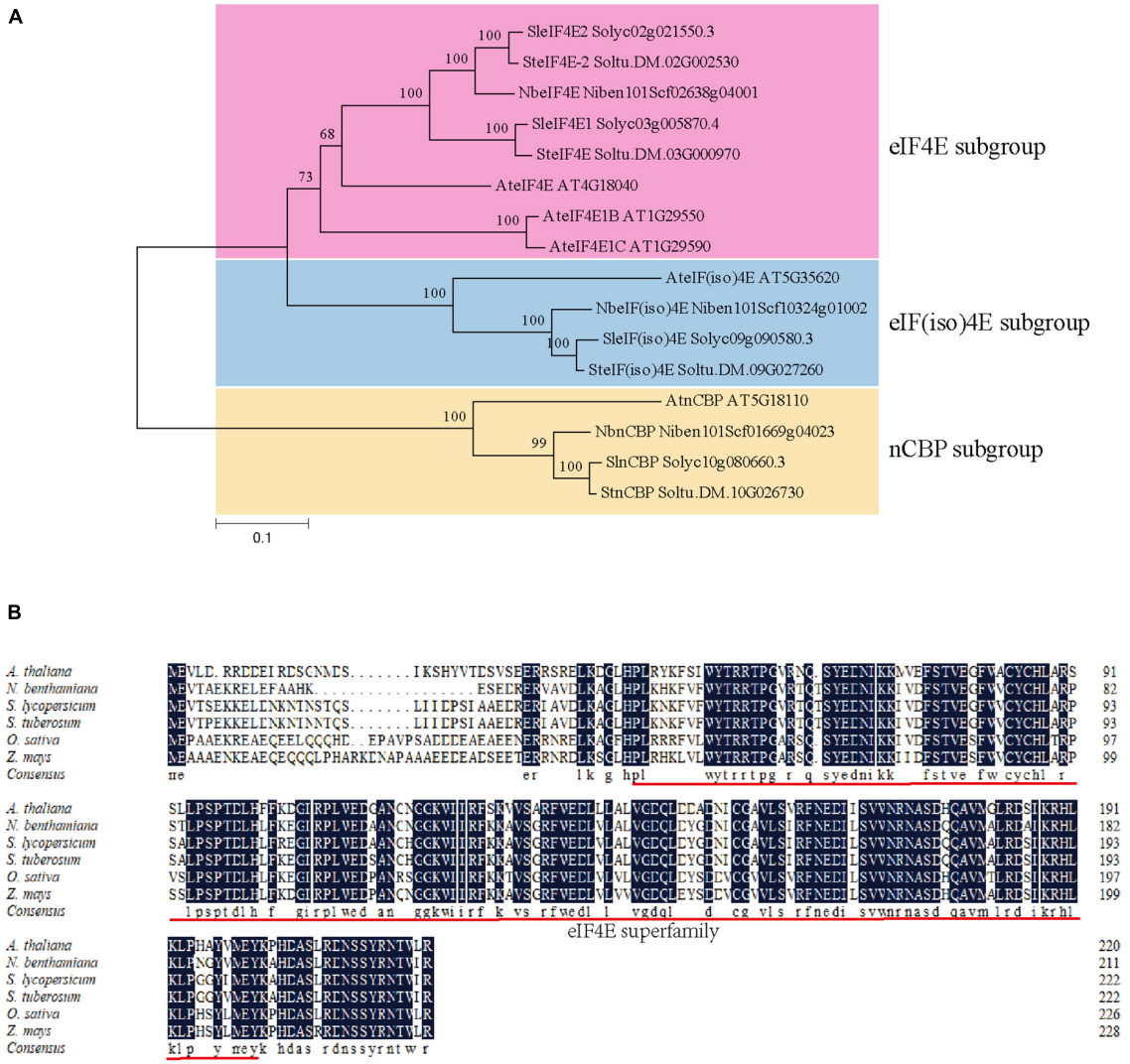

FIGURE 1
Phylogenetic analysis of *eIF4E* genes in potato, Arabidopsis, tobacco, and tomato **(A)**, and an amino acid sequence alignment of ncbp proteins from various species **(B)**. The prefix of accession numbers with "Soltu.DM" represents proteins from *S. tuberosum*; the prefix of accession numbers with "AT" represents proteins from *A. thaliana*; the prefix of accession numbers with "Solyc" represents proteins from *S. lycopersicum*; the prefix of accession numbers with "Niben101Scf" represents proteins from *N. benthamiana*. The eIF4E subgroup, eIF(iso)4E subgroup, and nCBP subgroup are distinguished by pink, blue, and yellow regions, respectively. The phylogenetic tree was generated with neighbor-joining tree and 1000 bootstraps. The red underline represents the eIF4E superfamily domain.

Soltu.DM.09G027260), and *StnCBP*. Then, we performed a BLASTp search against the NCBI and SGN databases using the amino acid sequences of potato *eIF4E* family members as queries. As a result, 12 eIF4E proteins were obtained from *A. thaliana* and two other *Solanaceae* crops (*N. benthamiana* and *S. lycopersicum*). The phylogenetic tree analysis of eIF4E proteins from the above species indicated that StnCBP belongs to the nCBP subgroup (Figure 1A). In addition, an amino acid sequence alignment of nCBP proteins from various species (including the above species, and *O. sativa*, and *Z. mays*) revealed that they contain an eIF4E superfamily domain and share a high homology of 82.32%, indicating that *nCBP* is highly conserved among different species and may have similar functions (Figure 1B).

StnCBP knockdown compromised potato virus S accumulation

To determine whether StnCBP is also involved in the infection of important potato viruses encoding TGBps, RNA interference was performed to silence *StnCBP* expression. Several RNAi transgenic lines were obtained (the interference efficiency is shown in Supplementary Figure 1). The three

transgenic lines with the highest interference efficiency (RiStnCBP-1, RiStnCBP-2, and RiStnCBP-3) were selected for further experiments. As shown in **Figure 2A**, *StnCBP* knockdown resulted in deformed compound leaves, indicating that *StnCBP* plays an important role in leaf development, but does not affect plant growth, which may be due to functional redundancy among eIF4Es. The expression of other members of the *SteIF4E* family was also examined in the RiStnCBP lines, and the results showed that the expression of *SteIF4E*, *SteIF4E-2,* and *SteIF(iso)4E* was not affected by the transgenic events (**Supplementary Figure 2**). Then, the RiStnCBP lines were mechanically inoculated with three TGB-encoding viruses, PVS, PVM, and PVX. No apparent symptom was observed after inoculation. The upper non-inoculated leaves were collected from control plants (WT) and transgenic lines at 10 and 15 dpi. Subsequently, the accumulation of these viruses was determined by qRT-PCR and ELISA assays. PVS accumulation was drastically reduced in the transgenic lines compared with that in WT plants (**Figure 2B**). In contrast, the accumulation of PVM and PVX in the RiStnCBP lines was at a similar level to that in WT plants (**Figures 2C,D**). These results indicated that *StnCBP* knockdown suppresses PVS accumulation but not PVM and PVX, which is the first report that a member of the *eIF4E* family is involved in PVS infection.

StnCBP interacted with potato virus S coat protein

Many susceptibility factors have been proved to function by directly interacting with viral proteins (Roudet-Tavert et al., 2007; Hwang et al., 2015; Zhang et al., 2015). To determine whether StnCBP directly interacts with any protein of PVS, we tested the interaction between StnCBP and six proteins of PVS (including RdRp, TGB1, TGB2, TGB3, CP, and NaBp proteins) in Y2H assays (**Figure 3A**). The results revealed that StnCBP interacted with the CP of PVS, which was further demonstrated *via* BiFC assays in *N. benthamiana* (**Figure 3B**). Moreover, the results of BiFC demonstrated that StnCBP and PVS CP interacted in the nucleus and cytoplasm. Therefore, we further observed their subcellular localization and co-localization. StnCBP and PVS CP tagged with a GFP at the C-terminus were co-expressed with an RFP-empty vector (RFP-EV) in the leaves of *N. benthamiana* to observe their subcellular localization. As a result, the GFP fluorescence of StnCBP and PVS CP was both localized in the nucleus and cytoplasm (**Figure 3C**). To validate the successful expression of full-length StnCBP and PVS CP with GFP, Western blotting was performed to identify the protein size expressed by the vectors GFP-EV, StnCBP-GFP, and CP-GFP. They were predicted to encode proteins with sizes of 25.6, 52.5, and 59.4 kD, respectively, and the Western blotting results were consistent with expectation (**Figure 3D**), indicating the correct expression of proteins and accurate subcellular localization. Moreover, StnCBP-RFP and CP-GFP were found to be co-localized in the nucleus and cytoplasm (**Figure 3C**). These results indicated that StnCBP and PVS CP interact with each other and may function in the nucleus and cytoplasm.

We also tested the interaction between StnCBP and the proteins of PVX or PVM (**Supplementary Figure 3**). No interaction was observed between StnCBP and any PVX protein. Surprisingly, StnCBP also interacted with PVM CP, but *StnCBP* knockdown did not affect PVM infection. Therefore, we further determined whether PVS CP is critical for *StnCBP*-mediated recessive resistance to PVS.

Potato virus S coat protein played a vital role in *StnCBP*-mediated recessive resistance to potato virus S

Construction of plant RNA virus infectious clones has become a powerful tool to study virus molecular biology (Bao et al., 2020). Therefore, we constructed a PVS infectious clone to test whether PVS CP plays an important role in *StnCBP*-mediated recessive resistance to PVS. According to the previously described method (Sun et al., 2017), the PVS genome was divided into three partially overlapping cDNA fragments (PVS-A, PVS-B, and PVS-C), followed by amplification using specific primers (**Supplementary Table 4**) and homologous recombination assembly in the yeast with an expression vector pCB301-2μ-HDV to construct the full-length clone of PVS (named as pCB301-2μ: PVS; **Figure 4A**). Then, the CP in PVS infectious clone was replaced by the CP of PVM or PVX, and the infectious clones were designated as $PVS^{CP/S}$, $PVS^{CP/M}$, and $PVS^{CP/X}$, respectively, (**Supplementary Figure 4**).

To confirm the infectivity, we inoculated the WT plants with the three infectious clones by *Agrobacterium* infiltration and detected the presence of the virus in the upper non-inoculated leaves by PCR assays at 14 dpi, with two pairs of primers. The first pair of primers (named as detection primers) were designed on the *TGB1* region of PVS for general detection. The other pair of primers (named as CP-flanking primers) were designed based on the sequences flanking the *CP* region, to confirm the substitution of viral CP according to the different sizes of CPs from PVS, PVM, and PVX (**Supplementary Figure 5**). As a result, $PVS^{CP/S}$ and $PVS^{CP/M}$ infectious clones successfully infected the plants as indicated by the amplification of PCR products with expected sizes (**Figure 4B**). In addition, the nucleotide lengths of *CP* genes of PVS and PVM were 885 bp and 915 bp, respectively. As expected, the PCR product amplified by CP-flanking primers from the $PVS^{CP/M}$ inoculated plants was slightly larger than that from $PVS^{CP/S}$ inoculated plants (**Figure 4B**), indicating correct substitution of the CP. Surprisingly, $PVS^{CP/X}$ showed no infection ability since no PCR product was amplified

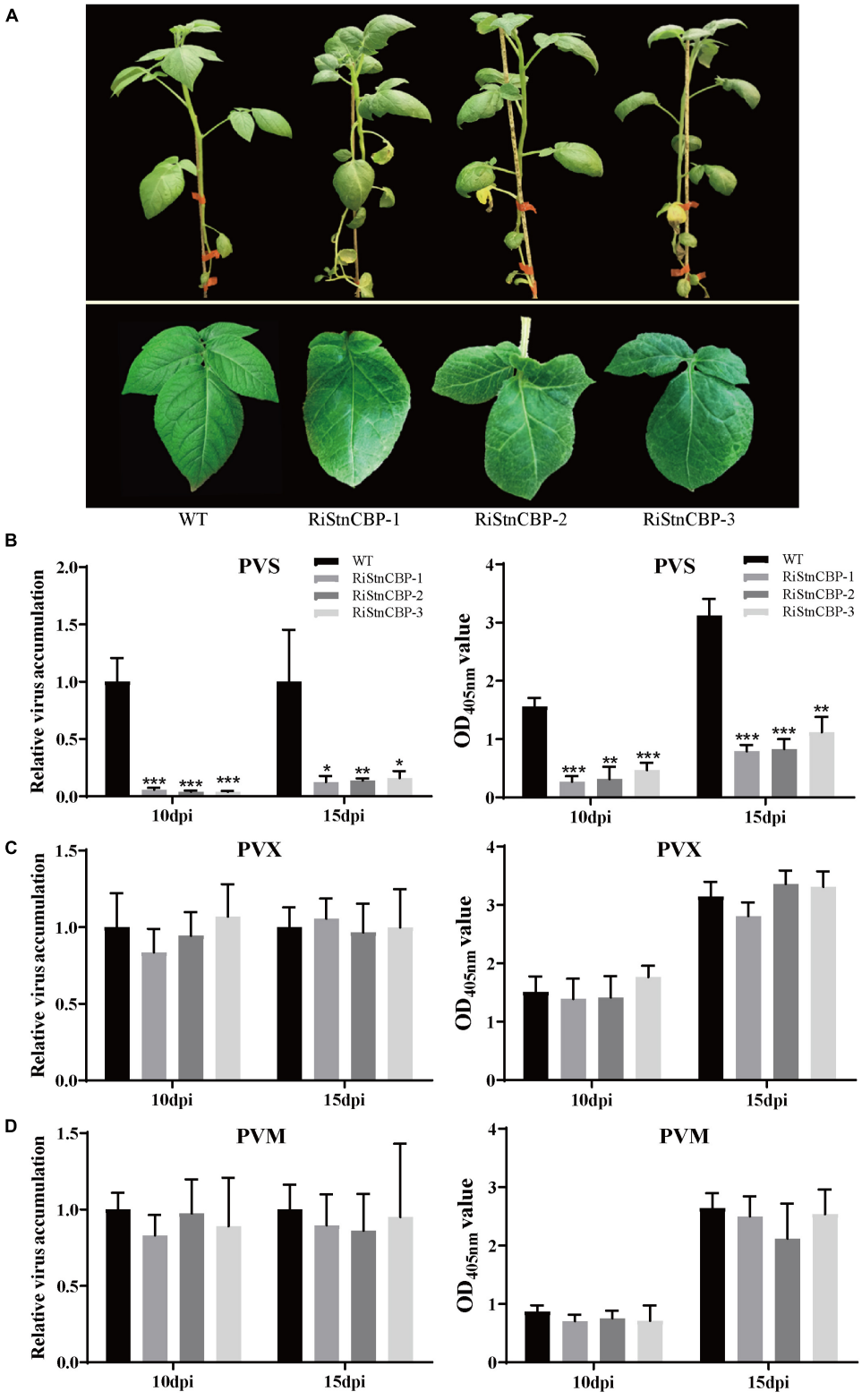

FIGURE 2
Morphology and virus resistance identification of the RiStnCBP transgenic lines. **(A)** Morphology of RiStnCBP transgenic lines under field conditions. **(B–D)** Virus resistance identification in RiStnCBP transgenic lines against PVS **(B)**, PVM **(C)**, and PVX **(D)**, respectively. The virus accumulation was determined using qRT-PCR (left) and ELISA (right). Error bars indicate ± SD of three replicates (n = 3). Three independent experiments were performed with similar results. $p < 0.05$*, $p < 0.01$**, and $p < 0.001$*** (Student's t-test).

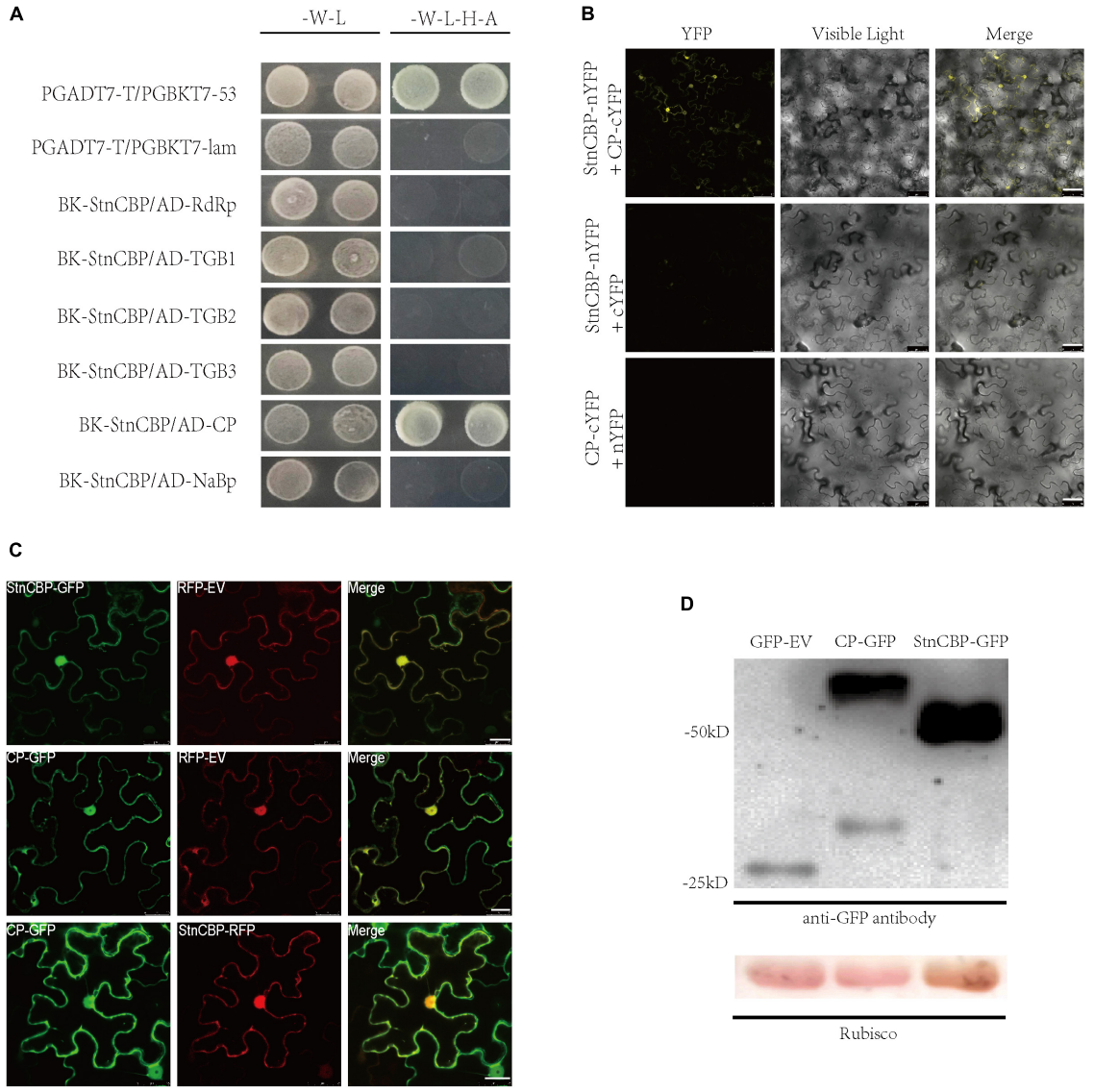

FIGURE 3
StnCBP interacted with PVS CP in the nucleus and cytoplasm. **(A)** Interaction between StnCBP and proteins of PVS in Y2H assays. -W-L represents a medium lacking tryptophan and leucine, while -W-L-H-A represents a medium lacking tryptophan, leucine, histidine, and adenine. Paired combinations PGADT7-T/PGBKT7-53 and PGADT7-T/PGBKT7-lam represent positive and negative controls, respectively. **(B)** Interaction between StnCBP and PVS CP in BiFC assays. Merge means the overlay of YFP and visible light on single confocal planes. Scale bar: 50 μm. **(C)** Subcellular localization and co-localization of StnCBP and PVS CP. Merge means the overlay of GFP and RFP on single confocal planes. Scale bar: 20 μm. **(D)** Identification of full-length proteins of StnCBP and PVS CP successfully expressed with GFP in the Western blotting. Total proteins were immunoprecipitated with anti-GFP antibody, and Rubisco was stained with Ponceau S as a loading control.

(Figure 4B). A plausible explanation is that both PVS and PVM belong to the *Carlavirus* genus with mutually compatible CPs, while PVX belongs to the *Potexvirus* genus with an incompatible CP.

Furthermore, the RiStnCBP lines were inoculated with the $PVS^{CP/S}$ and $PVS^{CP/M}$ infectious clones by *Agrobacterium* infiltration. The upper non-inoculated leaves were collected at 10 and 15 dpi to determine the virus accumulation using qRT-PCR and ELISA assays. The RiStnCBP lines also had significantly lower accumulation of $PVS^{CP/S}$ infectious clone than the control plants (Figure 4C). In contrast, the accumulation of $PVS^{CP/M}$ infectious clone showed no significant difference between the RiStnCBP and control plants (Figure 4D). These results indicated that PVS CP is vital for *StnCBP*-mediated recessive resistance to PVS. However, the interaction between StnCBP and CP may be necessary but not sufficient for the *StnCBP*-mediated recessive resistance to TGB-encoding viruses.

10.3389/fpls.2022.946873

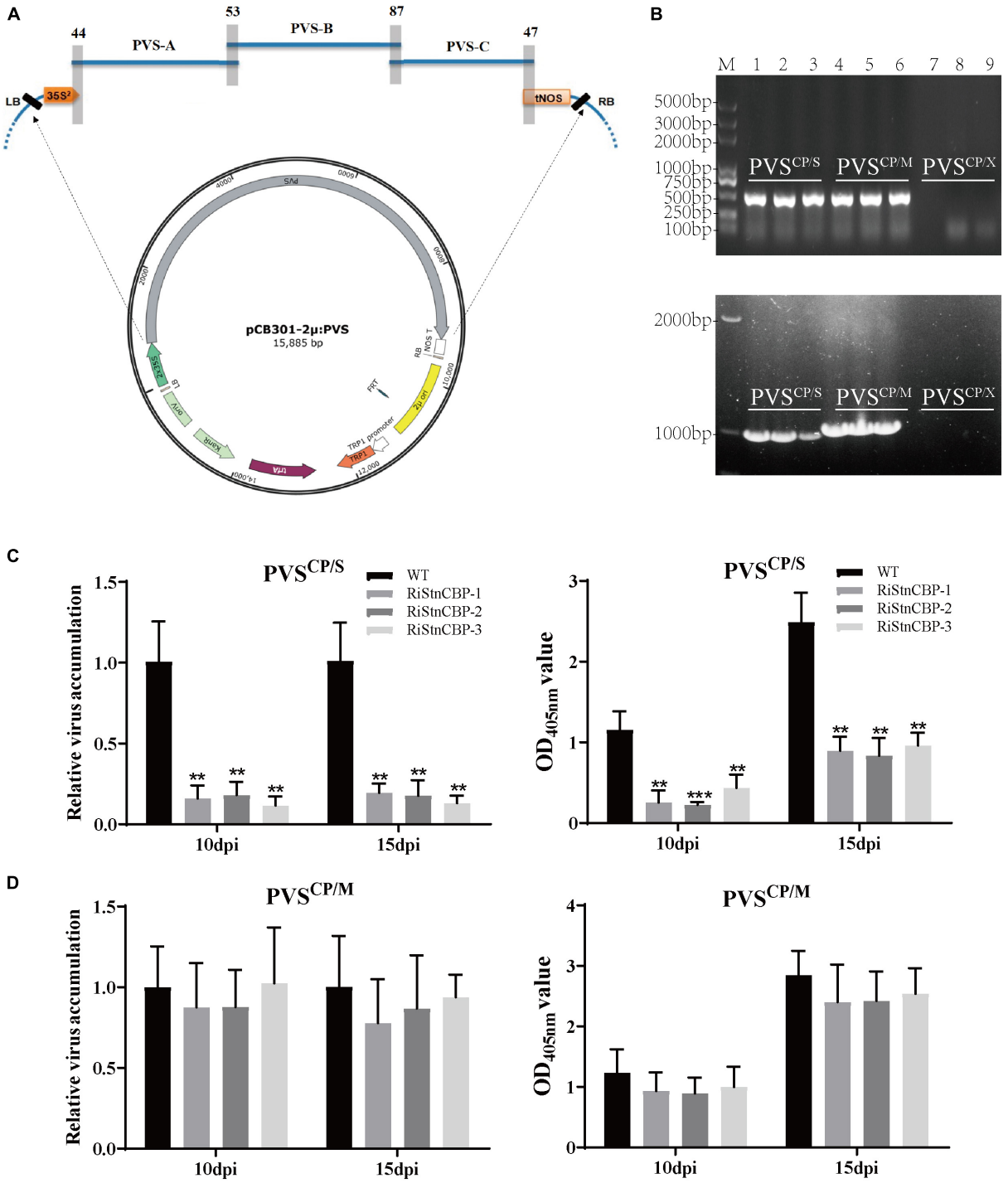

FIGURE 4
PVS CP played a vital role in the *StnCBP*-mediated recessive resistance to PVS. **(A)** Schematic illustration of the construction of PVS infectious clone. PVS-A, PVS-B, and PVS-C represent the fragments from PVS for the assembly. The gray shadow bars indicate the overlapping regions of adjacent fragments, with the number of overlapping nucleotides. **(B)** Electrophoretic separation of PCR products amplified with detection primers (above) and CP-flanking primers (below) from plants agroinoculated with $PVS^{CP/S}$ (1–3), $PVS^{CP/M}$ (4–6), and $PVS^{CP/X}$ (7–9). M: Trans2K® Plus DNA Marker. The upper non-inoculated leaves were collected 14 days after inoculation. **(C,D)** The accumulation of $PVS^{CP/S}$ **(C)** and $PVS^{CP/M}$ **(D)** infectious clones in the RiStnCBP and control plants (WT). The virus accumulation was determined using qRT-PCR (left) and ELISA (right). Error bars indicate ± SD of three replicates (n = 3). Three independent experiments were performed with similar results. $p < 0.01$** and $p < 0.001$*** (Student's t-test).

10.3389/fpls.2022.946873

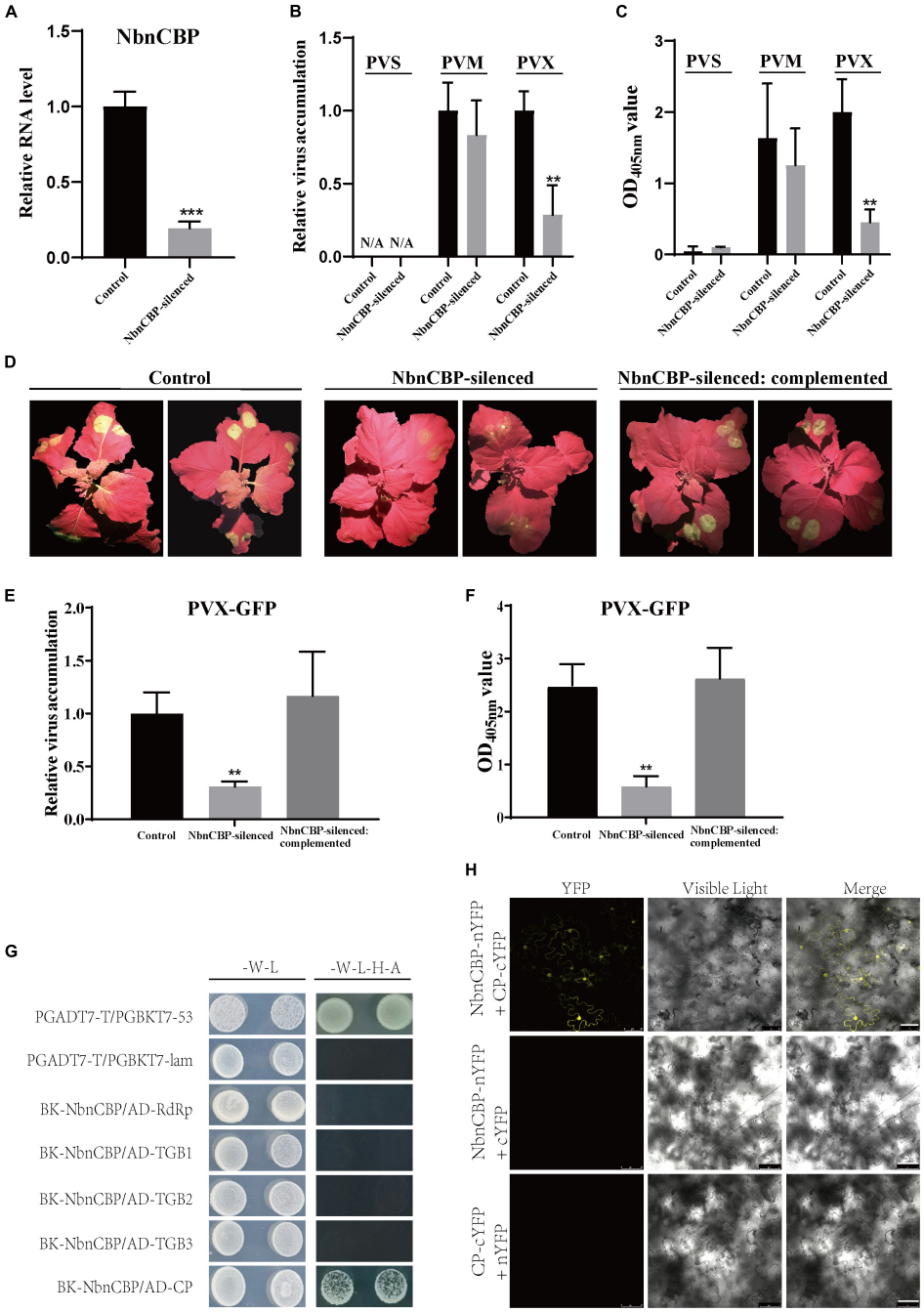

FIGURE 5

Antiviral identification of *NbnCBP* against PVX, and interaction analyses between NbnCBP and proteins of PVX. **(A)** The silencing efficiency of *NbnCBP* in *N. benthamiana* by VIGS. The gene expression was determined using qRT-PCR. Error bars indicate ± SD of five replicates (n = 5). $p < 0.001$*** (Student's t-test). **(B,C)** The determination of PVM and PVX accumulation in the control and *NbnCBP*-silenced plants by RT-qPCR **(B)** and ELISA **(C)**. Error bars indicate ± SD of three replicates (n = 3). Three independent experiments were performed with similar results. $p < 0.01$** (Student's t-test). **(D)** Green fluorescence emission in PVX-GFP inoculated leaves of the control, *NbnCBP*-silenced, and *NbnCBP*-silenced: complemented plants. The photographs were taken at 8 dpi. **(E,F)**. The determination of PVX-GFP accumulation in inoculated leaves of the control, *NbnCBP*-silenced and *NbnCBP*-silenced: complemented plants by RT-qPCR **(E)** and ELISA **(F)**. Error bars indicate ± SD of three replicates (n = 3). Three independent experiments were performed with similar results. $p < 0.01$** (Student's t-test). **(G)** Interaction analysis between NbnCBP and the proteins of PVX in Y2H. -W-L represents a medium lacking tryptophan and leucine, while -W-L-H-A represents a medium lacking tryptophan, leucine, histidine, and adenine. Paired combinations PGADT7-T/PGBKT7-53 and PGADT7-T/PGBKT7-lam represent positive and negative controls, respectively. **(H)** Interaction analysis between NbnCBP and PVX CP in BiFC assay. nYFP and cYFP represent their empty vectors. Merge means the overlay of YFP and visible light on single confocal planes. Scale bar: 50 μm.

The *nCBP* orthologue in *N. benthamiana* was involved in potato virus X infection

The function of *nCBP* gene in the infection of TGB-encoding viruses was first reported in Arabidopsis and then in potato in this study. However, it remains unknown whether the function of *nCBP* homolog is also conserved in *N. benthamiana*, which also belongs to the *Solanaceae* as potato. Therefore, the TRV-mediated VIGS assay was employed to silence the *nCBP* homolog in *N. benthamiana* (*NbnCBP*; accession number: Niben101Scf01669g04023.1). The silencing efficiency of *NbnCBP* by VIGS reached 80% (**Figure 5A**). The *NbnCBP*-silenced plants were then mechanically inoculated with PVS, PVM, and PVX. At 6 dpi, the upper non-inoculated leaves were collected to determine the virus accumulation by qRT-PCR and ELISA assays. Surprisingly, the accumulation of PVX was significantly reduced, while that of PVM was not affected in the *NbnCBP*-silenced plants, which was inconsistent with the results obtained for potato (**Figures 5B,C**). In addition, *N. benthamiana* exhibited resistance to PVS as no virus was detected in both *NbnCBP*-silenced and control plants (**Figures 5B,C**). It was reported that many tobacco varieties could not be infected by PVS in mechanical inoculation (De Bokx, 1970; Brattey et al., 2002; Nie and Singh, 2013), indicating that *N. benthamiana* may have some unknown resistance against PVS like these tobaccos. Therefore, it remains unclear whether NbnCBP is involved in the infection of PVS.

To provide more intuitive results, the *NbnCBP*-silenced plants were inoculated with a PVX infectious clone tagged with a green fluorescent protein (hereafter referred to as PVX-GFP) by agroinfiltration. The GFP fluorescence at 8 dpi revealed that PVX-GFP accumulation drastically decreased in the inoculated leaves, and the systemic infection was significantly delayed (**Figure 5D**). Further qRT-PCR and ELISA assays demonstrated that both the PVX RNA and protein levels decreased in *NbnCBP*-silenced plants compared with those in the control (**Figures 5E,F**). Obviously, these results were consistent with those of GFP fluorescence emission, indicating that *NbnCBP* knockdown compromises PVX-GFP accumulation.

A transient complementation assay was performed to confirm that the decrease in the accumulation of PVX in *NbnCBP*-silenced plants was directly caused by loss of *NbnCBP*. The leaves of *NbnCBP*-silenced plants were agro-infiltrated with a mixture of *Agrobacterium* cultures carrying the PVX-GFP infectious clone and a full-length cDNA of *NbnCBP*. As a result, the GFP fluorescence of PVX-GFP was recovered in the inoculated leaves of *NbnCBP*-silenced: complemented plants. However, the systemic infection of PVX-GFP was still delayed (**Figure 5D**). In addition, the qRT-PCR and ELISA results also revealed the PVX-GFP accumulation in the inoculated leaves of *NbnCBP*-silenced: complemented plants was comparable to the control plants (**Figures 5E,F**). Thus, it could be speculated that *NbnCBP* is required for PVX infection in *N. benthamiana*.

Then, a Y2H assay showed that the CP was the only protein interacting with NbnCBP in the five proteins coded by PVX, which was similar to the relationship between StnCBP and PVS CP (**Figure 5G**), and the interaction between NbnCBP and CP of PVX was further confirmed by the BiFC assay (**Figure 5H**). Thus, PVX CP may also have a critical function in *NbnCBP*-mediated recessive resistance against PVX. In addition, we analyzed the interaction between NbnCBP and the proteins of PVM and PVS. Interestingly, like the case in potato, NbnCBP interacted with PVM CP, though *NbnCBP* knockdown did not affect PVM infection (**Supplementary Figures 6A,B**). NbnCBP also interacted with PVS CP (**Supplementary Figures 6C,D**), even if PVS did not infect *N. benthamiana*. This result implies that NbnCBP may also have the function to facilitate PVS accumulation, but this phenotype was masked by other possible anti-PVS mechanisms prevalent in tobacco.

In summary, our results indicated that the *nCBP* orthologues have conserved functions in potato and tobacco as in Arabidopsis in terms of recessive resistance against TGB-encoding viruses, and the interaction between nCBP and CP is necessary but not sufficient to determine the recessive resistance of *nCBP*.

Discussion

Recessive resistance genes have become a very important resource in plant breeding for virus resistance (Truniger and Aranda, 2009). *eIF4Es* are the most extensively studied recessive resistance genes involved in the infection of various viruses (Hashimoto et al., 2016; Xu et al., 2017; Yang et al., 2021). This study for the first time reports that *StnCBP*, a member of the *eIF4E* family in potato, is involved in PVS infection as a recessive resistance gene. PVS has become an important virus in all potato-growing areas worldwide (Song et al., 2017). However, compared with potato virus Y resistance, potato resistance to PVS has been much less studied, except for the chromosomal localization of a dominant gene (*Ns*) against PVS (Marczewski et al., 2002). This study identified a recessive resistance gene (*StnCBP*) to PVS, which may provide a new strategy for developing potato varieties resistant to PVS.

Numerous studies of *eIF4Es* have suggested that their interactions with VPg proteins are responsible for the susceptibility to potyviruses. For instance, the mutation of *eIF4Es* that abolishes their interaction with VPg proteins confers resistance to potyviruses, and, in turn, some isolates of potyviruses can restore the interaction to lead to a resistance-breaking phenotype (Yeam et al., 2007; Charron et al., 2008; Truniger and Aranda, 2009). In this study, *StnCBP* knockdown compromised PVS accumulation but not PVX and PVM (**Figure 2**), and further assays demonstrated that StnCBP

directly interacts with PVS CP both *in vitro* and *in vivo* (**Figure 3**). These results indicated that PVS CP may also be crucial for the function of *StnCBP* just like VPgs for *eIF4Es*. We further confirmed the speculation since the substitution of PVS CP by PVM CP recovered the virus accumulation in the RiStnCBP lines (**Figure 4**). Furthermore, our results also suggested that *NbnCBP* is required for PVX infection when it interacts with PVX CP (**Figure 5**), indicating that nCBP-CP interaction may be a common mode in *nCBP*-mediated recessive resistance against TGB-encoding viruses.

However, how nCBP facilitates TGB-encoding virus accumulation is still elusive. nCBP was found to be a component of the 5 'cap complex in Arabidopsis and supports the translation initiation of capped mRNA, like eIF4E/eIF(iso)4E (Ruud et al., 1998; Bush et al., 2009). The genomes of PVS, PVM, and PVX consist of five or six open reading frames, a 5' cap and a 3' poly(A) tail (Poke, 2008; Petrova et al., 2013). Studies on the PVX suggested that the 5' cap structure of RNA and PVX CP plays crucial role for viral ribonucleoprotein (vRNP) assembly (Petrova et al., 2013, 2015). Therefore, the interaction between nCBP and viral CP may promote vRNP assembly, thereby regulating viral translation and facilitating the accumulation of TGB-encoding viruses.

Notably, the knockdown of *StnCBP* and *NbnCBP* did not affect PVM infection in *S. tuberosum* and *N. benthamiana*, respectively, whereas both StnCBP and NbnCBP interacted with PVM CP. One reasonable explanation is that knockdown instead of knockout was used to identify the function of *nCBP* homolog genes, which still produced a certain amount of transcripts. Thus, it is possible that the effect on PVM would only be observed in a knockout situation. In fact, the *ncbp* mutation in Arabidopsis significantly reduced the accumulation of PVM (Keima et al., 2017), and AtnCBP was found to interact with PVM CP in both the Y2H and BiFC assays (**Supplementary Figures 7A,B**), which supports this explanation. Further knockout analysis is needed to confirm the recessive resistance of the *nCBP* orthologues in potato and tobacco to these TGB-encoding viruses.

Another possible explanation is that the nCBP-CP interaction may be a necessary but not sufficient condition for *nCBP* to act as a susceptibility gene, and some other viral proteins may also be critical in the process. The TGBps are considered as conserved gene modules involved in the viral movement, which is similar to movement proteins (MPs) of some viruses (Morozov and Solovyev, 2003; Keima et al., 2017). TGB-encoding viruses are classified into two classes: the hordei-like class in which the CP is dispensable for cell-to-cell movement of viruses, and the potex-like class in which the CP is required for cell-to-cell movement (Forster et al., 1992; Solovyev et al., 1996; Wong et al., 1998; Lin et al., 2006). The potex-like class viruses have a TGB1 ranging from 24 to 26 kDa and a TGB3 of about 7 kDa, while hordei-like class viruses contain a TGB1 ranging from 39 to 63 kDa and a TGB3 of about 15 kDa (Morozov and Solovyev, 2003; Lauber et al., 2005). In addition, the hordei-like class viruses are multicomponent viruses with rigid rod-shaped virions, while the potex-like class viruses are monopartite viruses with filamentous virions (Lauber et al., 2005). Thus, the TGBps of PVS, PVM, and PVX can be classified into the potex-like class (Morozov and Solovyev, 2003), implying that their CPs may be required for TGBps to establish the cell-to-cell movement and systemic infection of viruses. In addition, a previous study has shown that *ncbp* mutation in Arabidopsis conferred resistance to serval potex-like viruses (Keima et al., 2017). Among these viruses, the cell-to-cell movement of plantago asiatica mosaic virus (*Potexvirus*) was significantly delayed, and the accumulation of TGB2 and TGB3 was reduced, which established the association between the function of AtnCBP and TGBps. In addition, we analyzed the interaction between AtnCBP and the proteins of PVX by Y2H assays. As a result, AtnCBP interacted with the TGB2, TGB3, and CP of PVX (**Supplementary Figure 7C**), indicating the association among nCBP, TGBps, and CP.

In summary, this study identified *StnCBP* as a susceptibility gene required for the accumulation of a TGB-encoding virus PVS by recognizing its CP in potato. Our findings revealed that the nCBP-CP interaction may also contribute to the function of *nCBP* orthologues for other TGB-encoding viruses. Moreover, the cassava nCBP was found to interact with the VPgs of two ipomoviruses, which do not encode TGBps (Gomez et al., 2019). It will be meaningful to further study whether *nCBP* is required for the infection of other types of viruses and the underlying mechanism for *nCBP* to facilitate the infection of TGB-encoding and non-TGB-encoding viruses.

Data availability statement

The original contributions presented in this study are included in the article/**Supplementary material**, further inquiries can be directed to the corresponding authors.

Author contributions

CH, BN, RC, and XH conceived and designed the experiments. RC, MY, FX, and TL performed the experiments. RC, ZT, and JC analyzed the data. RC, CH, and BN prepared the manuscript. CH, BN, and XH revised the manuscript. All authors contributed to the article and approved the submitted version.

Funding

This research was supported by the National Natural Science Foundation of China (31971989), China Agricultural Research

System of MOF and MARA (CARS-09-ES16 and CARS-09-P07), and the Modern Agricultural Industrial Technology System of Hubei Province (HBHZD-ZB-2020-005).

Acknowledgments

The authors gratefully acknowledge Zhenghe Li of Zhejiang University for providing the pCB301-2μ-HDV plasmid.

Conflict of interest

The authors declare that the research was conducted in the absence of any commercial or financial relationships that could be construed as a potential conflict of interest.

Publisher's note

Supplementary material

The Supplementary Material for this article can be found online at: https://www.frontiersin.org/articles/10.3389/fpls.2022.946873/full#supplementary-material

References

Bao, W., Yan, T., Deng, X., and Wuriyanghan, H. (2020). Synthesis of full-length cDNA infectious clones of Soybean mosaic virus and functional identification of a key amino acid in the silencing suppressor Hc-Pro. *Viruses* 12:886. doi: 10.3390/v12080886

Brattey, C., Badge, J., Burns, R., Foster, G., George, E., Goodfellow, H., et al. (2002). Potato latent virus: a proposed new species in the genus Carlavirus. *Plant Pathol.* 51, 495–505. doi: 10.1046/j.1365-3059.2002.00729.x

Bush, M. S., Hutchins, A. P., Jones, A. M., Naldrett, M. J., Jarmolowski, A., Lloyd, C. W., et al. (2009). Selective recruitment of proteins to 5' cap complexes during the growth cycle in Arabidopsis. *Plant J.* 59, 400–412. doi: 10.1111/j.1365-313X.2009.03882.x

Charron, C., Nicolaï, M., Gallois, J. L., Robaglia, C., Moury, B., Palloix, A., et al. (2008). Natural variation and functional analyses provide evidence for co-evolution between plant eIF4E and potyviral VPg. *Plant J.* 54, 56–68. doi: 10.1111/j.1365-313X.2008.03407.x

Cheng, D., Zhou, D., Wang, Y., Wang, B., He, Q., Song, B., et al. (2021). Ralstonia solanacearum type III effector RipV2 encoding a novel E3 ubiquitin ligase (NEL) is required for full virulence by suppressing plant PAMP-triggered immunity. *Biochem. Biophys. Res. Commun.* 550, 120–126. doi: 10.1016/j.bbrc.2021.02.082

De Bokx, J. (1970). Reactions of various plant species to inoculation with potato virus S. *Neth. J. Plant Pathol.* 76, 70–78. doi: 10.1007/BF01974435

Fernandez-Pozo, N., Rosli, H. G., Martin, G. B., and Mueller, L. A. (2015). The SGN VIGS tool: user-friendly software to design virus-induced gene silencing (VIGS) constructs for functional genomics. *Mol. Plant* 8, 486–488. doi: 10.1016/j.molp.2014.11.024

Forster, R. L., Beck, D. L., Guilford, P. J., Voot, D. M., Van Dolleweerd, C. J., and Andersen, M. T. (1992). The coat protein of white clover mosaic potexvirus has a role in facilitating cell-to-cell transport in plants. *Virology* 191, 480–484. doi: 10.1016/0042-6822(92)90215-B

Gao, Z., Johansen, E., Eyers, S., Thomas, C. L., Noel Ellis, T., and Maule, A. J. (2004). The potyvirus recessive resistance gene, sbm1, identifies a novel role for translation initiation factor eIF4E in cell-to-cell trafficking. *Plant J.* 40, 376–385. doi: 10.1111/j.1365-313X.2004.02215.x

Garcia-Ruiz, H. (2018). Susceptibility genes to plant viruses. *Viruses* 10:484. doi: 10.3390/v10090484

Gingras, A. C., Raught, B., and Sonenberg, N. (1999). eIF4 initiation factors: effectors of mRNA recruitment to ribosomes and regulators of translation. *Annu. Rev. Biochem.* 68, 913–963. doi: 10.1146/annurev.biochem.68.1.913

Gomez, M. A., Lin, Z. D., Moll, T., Chauhan, R. D., Hayden, L., Renninger, K., et al. (2019). Simultaneous CRISPR/Cas9-mediated editing of cassava eIF4E isoforms nCBP-1 and nCBP-2 reduces cassava brown streak disease symptom severity and incidence. *Plant Biotechnol. J.* 17, 421–434. doi: 10.1111/pbi.12987

Hardigan, M. A., Laimbeer, F. P. E., Newton, L., Crisovan, E., Hamilton, J. P., Vaillancourt, B., et al. (2017). Genome diversity of tuber-bearing Solanum uncovers complex evolutionary history and targets of domestication in the cultivated potato. *Proc. Natl. Acad. Sci. U.S.A.* 114, E9999–E10008. doi: 10.1073/pnas.1714380114

Hashimoto, M., Neriya, Y., Yamaji, Y., and Namba, S. (2016). Recessive resistance to plant viruses: potential resistance genes beyond translation initiation factors. *Front. Microbiol.* 7:1695. doi: 10.3389/fmicb.2016.01695

Hwang, J., Lee, S., Lee, J. H., Kang, W. H., Kang, J. H., Kang, M. Y., et al. (2015). Plant translation elongation factor 1Bβ facilitates potato virus X (PVX) infection and interacts with PVX triple gene block protein 1. *PLoS One* 10:e0128014. doi: 10.1371/journal.pone.0128014

Kanyuka, K., Druka, A., Caldwell, D. G., Tymon, A., McCallum, N., Waugh, R., et al. (2005). Evidence that the recessive bymovirus resistance locus rym4 in barley corresponds to the eukaryotic translation initiation factor 4E gene. *Mol. Plant Pathol.* 6, 449–458. doi: 10.1111/j.1364-3703.2005.00294.x

Keima, T., Hagiwara-Komoda, Y., Hashimoto, M., Neriya, Y., Koinuma, H., Iwabuchi, N., et al. (2017). Deficiency of the eIF4E isoform nCBP limits the cell-to-cell movement of a plant virus encoding triple-gene-block proteins in Arabidopsis thaliana. *Sci. Rep.* 7:39678. doi: 10.1038/srep39678

Lauber, E., Jonard, G., Richards, K., and Guilley, H. (2005). Nonregulated expression of TGBp3 of hordei-like viruses but not of potex-like viruses inhibits beet necrotic yellow vein virus cell-to-cell movement. *Arch. Virol.* 150, 1459–1467. doi: 10.1007/s00705-005-0516-y

Lellis, A. D., Kasschau, K. D., Whitham, S. A., and Carrington, J. C. (2002). Loss-of-susceptibility mutants of Arabidopsis thaliana reveal an essential role for eIF (iso) 4E during potyvirus infection. *Curr. Biol.* 12, 1046–1051. doi: 10.1016/S0960-9822(02)00898-9

Leònard, S., Plante, D., Wittmann, S., Daigneault, N., Fortin, M. G., and Laliberteì, J. F. ((2000). Complex formation between potyvirus VPg and translation eukaryotic initiation factor 4E correlates with virus infectivity. *J. Virol.* 74, 7730–7737. doi: 10.1128/jvi.74.17.7730-7737.2000

Lin, M. K., Hu, C. C., Lin, N. S., Chang, B. Y., and Hsu, Y. H. (2006). Movement of potexviruses requires species-specific interactions among the cognate triple gene block proteins, as revealed by a trans-complementation assay based on the bamboo mosaic virus satellite RNA-mediated expression system. *J. Gen. Virol.* 87, 1357–1367. doi: 10.1099/vir.0.81625-0

Mäkinen, K. (2020). Plant susceptibility genes as a source for potyvirus resistance. *Ann. Appl. Biol.* 176, 122–129. doi: 10.1111/aab.12562

Marczewski, W., Hennig, J., and Gebhardt, C. (2002). The Potato virus S resistance gene Ns maps to potato chromosome VIII. *Theor. Appl. Genet.* 105, 564–567. doi: 10.1007/s00122-002-0976-3

Morozov, S. Y., and Solovyev, A. G. (2003). Triple gene block: modular design of a multifunctional machine for plant virus movement. *J. Gen. Virol.* 84, 1351–1366. doi: 10.1099/vir.0.18922-0

Murashige, T., and Skoog, F. (1962). A revised medium for rapid growth and bio assays with tobacco tissue cultures. *Physiol. Plantar.* 15, 473–497. doi: 10.1111/j.1399-3054.1962.tb08052.x

Nicaise, V., German-Retana, S., Sanjuán, R., Dubrana, M. P., Mazier, M., Maisonneuve, B., et al. (2003). The eukaryotic translation initiation factor 4E controls lettuce susceptibility to the potyvirus Lettuce mosaic virus. *Plant Physiol.* 132, 1272–1282. doi: 10.1104/pp.102.017855

Nicot, N., Hausman, J. F., Hoffmann, L., and Evers, D. (2005). Housekeeping gene selection for real-time RT-PCR normalization in potato during biotic and abiotic stress. *J. Exp. Bot.* 56, 2907–2914. doi: 10.1093/jxb/eri285

Nie, B., Singh, M., Murphy, A., Sullivan, A., Xie, C., and Nie, X. (2012). Response of potato cultivars to five isolates belonging to four strains of Potato virus Y. *Plant Dis.* 96, 1422–1429. doi: 10.1094/PDIS-01-12-0018-RE

Nie, X., and Singh, M. (2013). Response of potato, tobacco and Physalis floridana plants to mixed infection with PVX, PVYNTN and PVY strains. *Can. J. Plant Pathol.* 35, 390–401. doi: 10.1080/07060661.2013.812581

Nieto, C., Morales, M., Orjeda, G., Clepet, C., Monfort, A., Sturbois, B., et al. (2006). An eIF4E allele confers resistance to an uncapped and non-polyadenylated RNA virus in melon. *Plant J.* 48, 452–462. doi: 10.1111/j.1365-313X.2006.02885.x

Petrova, E. K., Nikitin, N. A., Protopopova, A. D., Arkhipenko, M. V., Yaminsky, I. V., Karpova, O. V., et al. (2013). The role of the 5'-cap structure in viral ribonucleoproteins assembly from potato virus X coat protein and RNAs. *Biochimie* 95, 2415–2422. doi: 10.1016/j.biochi.2013.09.004

Petrova, E. K., Nikitin, N. A., Trifonova, E. A., Protopopova, A. D., Karpova, O. V., and Atabekov, J. G. (2015). The 5 '-proximal region of Potato virus X RNA involves the potential cap-dependent "conformational element" for encapsidation. *Biochimie* 115, 116–119. doi: 10.1016/j.biochi.2015.05.012

Poke, F. S. (2008). Hop mosaic virus: complete nucleotide sequence and relationship to other carlaviruses. *Arch. Virol.* 153, 1615–1619. doi: 10.1007/s00705-008-0157-z

Rashid, M. O., Li, J. H., Liu, Q., Wang, Y., and Han, C. G. (2021). Molecular detection and identification of eight potato viruses in Gansu province of China. *Curr. Plant Biol.* 25:100184. doi: 10.1016/j.cpb.2020.100184

Reynolds, A., Leake, D., Boese, Q., Scaringe, S., Marshall, W. S., and Khvorova, A. (2004). Rational siRNA design for RNA interference. *Nature Biotechnol.* 22, 326–330. doi: 10.1038/nbt936

Roudet-Tavert, G., Michon, T., Walter, J., Delaunay, T., Redondo, E., and Le Gall, O. (2007). Central domain of a potyvirus VPg is involved in the interaction with the host translation initiation factor eIF4E and the viral protein HcPro. *J. Gen. Virol.* 88, 1029–1033. doi: 10.1099/vir.0.82501-0

Ruffel, S., Dussault, M. H., Palloix, A., Moury, B., Bendahmane, A., Robaglia, C., et al. (2002). A natural recessive resistance gene against potato virus Y in pepper corresponds to the eukaryotic initiation factor 4E (eIF4E). *Plant J.* 32, 1067–1075. doi: 10.1046/j.1365-313X.2002.01499.x

Ruffel, S., Gallois, J. L., Lesage, M., and Caranta, C. (2005). The recessive potyvirus resistance gene pot-1 is the tomato orthologue of the pepper pvr2-eIF4E gene. *Mol. Genet. Genomics* 274, 346–353. doi: 10.1007/s00438-005-0003-x

Ruud, K. A., Kuhlow, C., Goss, D. J., and Browning, K. S. (1998). Identification and characterization of a novel cap-binding protein from *Arabidopsis thaliana*. *J. Biol. Chem.* 273, 10325–10330. doi: 10.1074/jbc.273.17.10325

Singh, R. P., McLaren, D. L., Nie, X., and Singh, M. (2003). Possible escape of a recombinant isolate of Potato virus Y by serological indexing and methods of its detection. *Plant Dis.* 87, 679–685. doi: 10.1094/pdis.2003.87.6.679

Solovyev, A., Savenkov, E., Agranovsky, A., and Morozov, S. Y. (1996). Comparisons of the genomiccis-elements and coding regions in RNAβ components of the hordeiviruses Barley stripe mosaic virus, Lychnis ringspot virus, and Poa semilatent virus. *Virology* 219, 9–18. doi: 10.1006/viro.1996.0217

Song, G., Wu, J. Y., Xie, Y., Liu, Y., Qian, Y. J., Zhou, X. P., et al. (2017). Monoclonal antibody-based serological assays for detection of Potato virus S in potato plants. *J. Zhejiang Univ. Sci. B* 18, 1075–1082. doi: 10.1631/jzus.B1600561

Sun, K., Zhao, D., Liu, Y., Huang, C., Zhang, W., and Li, Z. (2017). Rapid construction of complex plant RNA virus infectious cDNA clones for agroinfection using a yeast-*E. coli*-Agrobacterium shuttle vector. *Viruses* 9:332. doi: 10.3390/v9110332

Tavert-Roudet, G., Anne, A., Barra, A., Chovin, A., Demaille, C., and Michon, T. (2017). The potyvirus particle recruits the plant translation initiation factor eIF4E by means of the VPg covalently linked to the viral RNA. *Mol. Plant Microbe Interact.* 30, 754–762. doi: 10.1094/MPMI-04-17-0091-R

Truniger, V., and Aranda, M. A. (2009). Recessive resistance to plant viruses. *Adv. Virus Res.* 75, 119–231. doi: 10.1016/s0065-3527(09)07504-6

Truniger, V., Nieto, C., González-Ibeas, D., and Aranda, M. (2008). Mechanism of plant eIF4E-mediated resistance against a Carmovirus (*Tombusviridae*): cap-independent translation of a viral RNA controlled in cis by an (a) virulence determinant. *Plant J.* 56, 716–727. doi: 10.1111/j.1365-313X.2008.03630.x

Udagawa, H., Koga, K., Shinjo, A., Kitashiba, H., and Takakura, Y. (2020). Reduced susceptibility to a tobacco bushy top virus Malawi isolate by loss of function in host eIF(iso)4E genes. *Breed. Sci.* 19135. doi: 10.1270/jsbbs.19135

van der Waals, J. E., and Krüger, K. (2020). Emerging potato pathogens affecting food security in southern Africa: Recent research. *S. Afr. J. Sci.* 116, 30–36. doi: 10.17159/sajs.2020/8055

Wang, B., He, T., Zheng, X., Song, B., and Chen, H. (2021). Proteomic analysis of potato responding to the invasion of Ralstonia solanacearum UW551 and its type III secretion system mutant. *Mol. Plant Microbe Interact.* 34, 337–350. doi: 10.1094/mpmi-06-20-0144-r

Wang, B., Ma, Y., Zhang, Z., Wu, Z., Wu, Y., Wang, Q., et al. (2011). Potato viruses in China. *Crop Prot.* 30, 1117–1123. doi: 10.1016/j.cropro.2011.04.001

Wang, J., Meng, F., Chen, R., Liu, J., Nie, X., and Nie, B. (2016). RT-PCR differentiation, molecular and pathological characterization of Andean and ordinary strains of Potato virus S in potatoes in China. *Plant Dis.* 100, 1580–1585. doi: 10.1094/pdis-11-15-1257-re

Wesley, S. V., Helliwell, C. A., Smith, N. A., Wang, M. B., Rouse, D. T., Liu, Q., et al. (2001). Construct design for efficient, effective and high-throughput gene silencing in plants. *Plant J.* 27, 581–590. doi: 10.1046/j.1365-313X.2001.01105.x

Wong, S. M., Lee, K. C., Yu, H. H., and Leong, W. F. (1998). Phylogenetic analysis of triple gene block viruses based on the TGB1 homolog gene indicates a convergent evolution. *Virus Genes* 16, 295–302. doi: 10.1023/a:1008034807216

Xu, M., Xie, H., Wu, J., Xie, L., Yang, J., and Chi, Y. (2017). Translation initiation factor eIF4E and eIFiso4E are both required for peanut stripe virus infection in peanut (*Arachis hypogaea* L.). *Front. Microbiol.* 8:338. doi: 10.3389/fmicb.2017.00338

Yang, Z., Dong, M., Cheng, G., Liu, S., Zhang, H., Shang, H., et al. (2021). Selective interaction of sugarcane eIF4E with VPgs from sugarcane mosaic pathogens. *Viruses Basel* 13:518. doi: 10.3390/v13030518

Yeam, I., Cavatorta, J. R., Ripoll, D. R., Kang, B. C., and Jahn, M. M. (2007). Functional dissection of naturally occurring amino acid substitutions in eIF4E that confers recessive potyvirus resistance in plants. *Plant Cell* 19, 2913–2928. doi: 10.1105/tpc.107.050997

Yoshii, M., Nishikiori, M., Tomita, K., Yoshioka, N., Kozuka, R., Naito, S., et al. (2004). The Arabidopsis Cucumovirus multiplication 1 and 2 loci encode tip translation initiation factors 4E and 4G. *J. Virol.* 78, 6102–6111. doi: 10.1128/jvi.78.12.6102-6111.2004

Zhan, X., Zhang, F., Zhong, Z., Chen, R., Wang, Y., Chang, L., et al. (2019). Generation of virus-resistant potato plants by RNA genome targeting. *Plant Biotechnol. J.* 17, 1814–1822. doi: 10.1111/pbi.13102

Zhang, L., Chen, H., Brandizzi, F., Verchot, J., and Wang, A. (2015). The UPR branch IRE1-bZIP60 in plants plays an essential role in viral infection and is complementary to the only UPR pathway in Yeast. *PloS Genetics* 11:1005164. doi: 10.1371/journal.pgen.1005164

Zhou, T., Song, B., Liu, T., Shen, Y., Dong, L., Jing, S., et al. (2019). Phytochrome F plays critical roles in potato photoperiodic tuberization. *Plant J.* 98, 42–54. doi: 10.1111/tpj.14198

frontiers | Frontiers in Plant Science

TYPE Original Research
PUBLISHED 16 September 2022
DOI 10.3389/fpls.2022.1009552

OPEN ACCESS

EDITED BY
Juan Du,
Huazhong Agricultural University, China

REVIEWED BY
Liqin Li,
Sichuan Agricultural University, China
Yingchun Wang,
Inner Mongolia University, China

*CORRESPONDENCE
Ning Zhang
ningzh@gsau.edu.cn

SPECIALTY SECTION
This article was submitted to Crop and Product Physiology, a section of the journal Frontiers in Plant Science

RECEIVED 02 August 2022
ACCEPTED 29 August 2022
PUBLISHED 16 September 2022

CITATION
Wang K, Zhang N, Fu X, Zhang H, Liu S, Pu X, Wang X and Si H (2022) *StTCP15* regulates potato tuber sprouting by modulating the dynamic balance between abscisic acid and gibberellic acid.
Front. Plant Sci. 13:1009552.
doi: 10.3389/fpls.2022.1009552

StTCP15 regulates potato tuber sprouting by modulating the dynamic balance between abscisic acid and gibberellic acid

Kaitong Wang[1,2], Ning Zhang[1,3]*, Xue Fu[1,2], Huanhuan Zhang[1,2], Shengyan Liu[1,2], Xue Pu[3], Xiao Wang[3] and Huaijun Si[1,3]

[1]State Key Laboratory of Aridland Crop Science, Gansu Agricultural University, Lanzhou, China, [2]College of Agronomy, Gansu Agricultural University, Lanzhou, China, [3]College of Life Science and Technology, Gansu Agricultural University, Lanzhou, China

The major stages of the potato life cycle are tuber dormancy and sprouting, however, there is still known very little of the mechanisms that control these processes. TCP (Theosinte branch I, Cycloidea, proliferationcell factors 1 and 2) transcription factors play a key role in plant growth and dormancy related developmental processes. Previous researches demonstrated that TCP transcription factor *StTCP15* had a function in the promotion of dormancy. To elucidate the function of *StTCP15* gene, it was cloned from potato cultivar "Desiree," which encodes a polypeptide consisting of 414 amino acids and is mainly found in the nucleus. The potato tubers of *StTCP15* overexpression lines sprouted in advance, while the potato tubers of *StTCP15* down-regulated expression lines showed delayed sprouting. In addition, it was also found that overexpression lines of *StTCP15* extremely significantly reduced the ratio of abscisic acid (ABA)/gibberellic acid (GA_3), while the superoxide dismutase activity decreased, and the activity of peroxidase and catalase increased compared with the wild type. The opposite result was found in the down-regulated expression lines of *StTCP15* gene. Three interacting proteins, StSnRK1, StF-Box and StGID1, were screened by Yeast two-hybrid, and verified by Bimolecular Fluorescence Complementation and Split-luciferase, indicating that *StTCP15* could affect ABA and GA_3 signaling pathways to regulate potato tuber dormancy and sprouting. Together, these results demonstrated that *StTCP15* regulated potato tuber dormancy and sprouting by affecting the dynamic balance between ABA and GA_3. The result could provide some information on the molecular mechanism of *StTCP15* regulating potato tuber dormancy and sprouting.

KEYWORDS

potato, *StTCP15*, dormancy, sprouting, ABA, GA_3

Introduction

Potato (*Solanum tuberosum* L.) is a vital meal crop grown in many countries and regions around the world. Potato tuber dormancy has a great impact on its cultivation, processing and storage. People have different demands on potatoes and different requirements on the length of the dormancy period, which makes the length of the resting period of potatoes of great biological significance (Deligios et al., 2020; Gong et al., 2021). Numerous studies have shown that seed dormancy and germination are controlled by multiple hormones and environmental signals, among which plant hormones abscisic acid (ABA) and gibberellic acid (GA_3) are the major endogenous hormones antagonizing seed dormancy and germination (Gubler et al., 2005; Finkelstein et al., 2008). It has been shown that seed germination is determined by the homeostasis of endogenous ABA and GA_3 levels in seeds, germination is usually accompanied by decreased ABA levels and increased GA_3 levels. Therefore, lower ABA levels and improve the level of GA_3 is necessary for seed dormancy release and then sprouting (Yang et al., 2020), but the balance of how to regulate it is unclear.

TCP (Teosinte branched I, Cycloidea, Proliferating Cell Factors 1 and 2) is a group of plant-specific transcription factors that contain a basic helix-loop-helix (bHLH) motif consisting of 59 amino acids, which is responsible for DNA binding and protein-protein interactions (Cubas et al., 1999; Heim et al., 2003). From the similarity of amino acid sequences in the TCP domain, TCP proteins can be divided into two categories: class I (PCF or TCP-P) and class II (TCP-c, CYC/TB1/CIN-like). Class I proteins participate in the regulation of growth patterns by controlling cell proliferation and hormone signaling pathways (Camoirano et al., 2020), but class II protein members inhibit these processes (Herve et al., 2009; Li et al., 2019). In *Arabidopsis thaliana*, class I family members *AtTCP14* and *AtTCP15* participate in the gibberellin signaling pathway to promote embryonic development, thereby regulating seed dormancy in advance (Tatematsu et al., 2008). AtTCP14 indirectly inhibits ABA biosynthesis gene *ABA1* and stress-related genes regulated by ABA through interaction with DOF6, resulting in delayed germination (Rueda-Romero et al., 2012). Resentini et al. (2021) found that AtTCP15 interacted with DELLA protein GAI and RGL2 to mediate GA to promote *A. thaliana* seed germination. *AtTCP20* has also been reported to play a role in different developmental stages, jasmonic acid synthesis and leaf senescence in *A. thaliana* (Guan et al., 2014). *GhTCP19* transcription factor affects the regulation of dormancy release in gladiolus corms by repressing *GhNCED* (ABA biosynthesis gene) expression (Wu et al., 2019). Guo et al. (2018) showed that peach *PpTCP.A2* could regulate fruit ripening process by affecting the expression of ET biosynthesis 1-aminocyclopropane-1-carboxyla synthase (*PpACS1*) gene. Overexpression of *OsTCP19* in *Arabidopsis* leads to up-regulation of *IAA3*, *ABI3* and *ABI4* and down-regulation of *LOX2*, resulting in developmental abnormalities (Mukhopadhyay and Tyagi, 2015). In class II family members, AtTCP3 indirectly activates transcription of DELLA protein-coding gene *GAI*, thereby regulating gibberellin activity (Nicolas and Cubas, 2016). *SlTCP26* negatively regulates auxin signal to reduce apical dominance and inhibits abscisic acid signal to release lateral bud dormancy and promote lateral branch development (Wei et al., 2021). The TCP family gene *CsBRC1* directly inhibited the expression of *CsPIN3*, promoted the accumulation of IAA in axillary buds, and inhibited the germination of axillary buds (Shen et al., 2019). *VcTCP18* negatively regulated the dormancy release of flower buds, and the seed germination rate of transgenic *A. thaliana* was lower than that of the wild-type. In transgenic plants, *VcTCP18* showed later flowering and less rose inflorescence and main stem (Li Y. et al., 2021).

In our previous studies, we found that the expression level of potato *StTCP15* (GenBank No. Xm_006364123.2) was continuously up-regulated during tuber dormancy release Wang et al. (2019), suggesting that this gene may regulate the function of tuber dormancy release and sprouting. In this study, tissue specific expression of *StTCP15* was verified by quantitative real-time polymerase chain reaction (qRT-PCR). The expression site of StTCP15 in cells was determined by subcellular localization. The overexpression and down-regulated expression plants of *StTCP15* of potato cultivar "Desiree" were used as materials, for analysis of transgenic tuber dormancy release and sprouting response. The protein interacting with StTCP15 was screened by Y2H (Yeast two-hybrid), and the reliability of interaction was verified by BiFC (Bimolecular Fluorescence Complementation) and Split-LUC Complementation. This study provided a theoretical and applicable framework for further study of dormancy release and sprouting in potato tubers.

Materials and methods

Plant growth conditions and treatments

Potato (*Solanum tuberosum* L. cv. "Desiree") containing two pieces of leaves *in vitro* plantlet successive transfer culture to Murashige-Skoog (MS) solid media containing 3 and 6% sucrose under (23 ± 1)°C, 16-h light/8-h dark cycle. After 4 weeks of culture, MS solid media containing 6% sucrose was cultured in darkness for 1 month to obtain microtubers (Zhang et al., 2005). For tissue specificity and tuber dormancy analysis, "Desiree" grown in 3% MS media for 4 weeks was transplanted into a flower pot with a diameter of 30 cm and a height of 25 cm, and placed at the optimum temperature of (23 ± 2)°C in the

greenhouse of Gansu Agricultural University. After 2 weeks of culture, roots, stems and leaves were collected and quickly frozen in liquid nitrogen at a temperature below −80°C. The tubers were harvested after 12 weeks and stored at (23 ± 2)°C and under dark conditions. Samples were collected from the beginning of storage (0 day), dormancy release (30 day) and sprouting (bud length > 0.2 cm; 45 day) with a sampler with a diameter of 0.8cm (Van Ittersum et al., 1992). The samples were frozen with liquid nitrogen and stored in a −80°C refrigerator for subsequent experiments.

Tobacco (*Nicotiana Benthamian* L.) was grown and cultured in a pot of 10 cm × 10 cm filled with nutrient soil (nutrient soil: vermiculite = 1:1) under the conditions of light intensity of 2000 Lx, photoperiod of 16-h light/8-h dark and temperature of (23 ± 2)°C. The relevant experiment could be carried out after about 30 days of culture.

Bioinformatics analysis

The *StTCP15* sequence (ID: Soltu.DM.03G03040.1) was retrieved from the potato database Spud DB[1] and the location of chromosome exon-intron structure was searched. The divergence of exon-intron structures was analyzed using NCBI Splign. NCBI conservative Domains were used to analyze the conservative domain of StTCP15 protein. The homologous species evolutionary tree was constructed by MEGA 7.0 software. The ExPASy ProtParam[2] tools ExPASy and ProtScale[3] were used online they predict physicochemical properties of the protein. The NetPhos 3.1[4] online analysis software was used to predict StTCP15 protein phosphorylation site distribution. The SPSS 13.0 software was processed to analyze the data.

StTCP15 expression analysis by qRT-PCR

FastKing RT Kit with gDNase (Tiangen Biotechnology, Beijing) was used for first-strand cDNA synthesis. Super Real PreMix Plus (SYBR Green; Tiangen Biotech, Beijing) was used to analyze the expression level of *StTCP15* with gene-specific primers (**Supplementary Table 1**). Polymerase chain reaction (PCR) solution (20 μl) contained 10 μl 2 × SuperReal PreMix Plus, 0.6 μl forward and reverse primers, 1 μL cDNA (100 ng) template, and 7.4 μl nuclease-free water. qRT-PCR was performed in the Light Cycler 96 system (Roche, Diagnostics GmbH) with the following parameters: 95°C for 15 min, followed by 40 cycles of 95°C for 10 s, 60°C for 20 s, and 72°C for 30 s. The *StEF1α* (GenBank ID: AB061263.1) gene was used as a standardized reference gene (Tang et al., 2017). The primer sequences are shown in **Supplementary Table 1**. All experiments were performed with three biological replicates and three technical replicates. The relative expression levels of the *StTCP15* gene in different tissues and dormancy times were calculated by $2^{-\Delta\Delta Ct}$ method (Rao et al., 2013).

Cloning and subcellular localization of StTCP15

The *StTCP15* gene sequence (ID: Soltu.DM.03G03040.1) was retrieved from potato database Spud DB (see text footnote 1). The subcellular localization vector was constructed by homologous recombination. According to the vector pCAMBIA1300-35S-EGFP sequence and *StTCP15* sequence, Using TaKaRa primer design software[5] online design specific primers (**Supplementary Table 1**). The CDS sequences of *StTCP15* gene without terminator were amplified from the cDNA of potato cv. "Desiree." The PCR product was inserted into the vector pCAMBIA1300-35S-EGFP containing *Kpn*I and *Xba*I restriction sites to obtain the recombinant plasmid pCAMBIA1300-EGFP-StTCP15. Plasmid pCAMBIA1300-EGFP-StTCP15 and empty vector pCAMBIA1300-35S-EGFP were transformed into *Agrobacterium tumefaciens* GV3101. The second to fourth leaves of tobacco were selected from the new leaves at the age of 5–6 weeks old. A small hole was punctured on the back of the tobacco with a sterile syringe needle as the injection entrance for *Agrobacterium* infection. The infection solution was injected slowly into the tobacco leaves with a syringe and the infection area was marked. *Agrobacterium* infected plants were cultured in darkness for 1 day in a 25°C incubator and then transferred to light for 1–2 days. GFP signals were detected with a confocal scanning electron microscope (CARI ZEISS, LSCM 800, Germany) at a 488 nm laser wavelength (Qi et al., 2020).

Construction of plant expression vector

For the *StTCP15* gene sequence and the expression vector pBI121 sequence, specific primers were used to amplify the CDS sequence of *StTCP15* gene, and the gene was cloned by PCR, Primer sequences are shown in **Supplementary Table 1**. The PCR product was inserted into the linearized vector pBI121 containing *Bam*HI and *Sac*I restriction sites according to the homologous recombinase specification. After PCR detection, double enzyme digestion verification and sequencing, the ligated

1 http://spuddb.uga.edu

2 http://web.expasy.org/protparam/

3 https://web.expasy.org/cgi-bin/protscale/protscale.pl/

4 http://www.cbs.dtu.dk/services/NetPhos/

5 https://www.takarabio.com/learning-centers/cloning/primer-design-and-other-tools

product was successfully named pBI121-StTCP15. To down-regulate *StTCP15* gene in potatoes, this experiment designed the sequence of aimRNA using the WMD3 website (**Supplementary Table 1** and **Supplementary Figure 1**; Li et al., 2020). Standard PCR was used for cloning. PCR products to the pMD18-T vector (TaKaRa Bio, Beijing) verified PCR detection, the double enzyme digestion and sequencing, connecting the effective sequence with *Kpn*I and *Sac*I double enzyme pCPB121 vector, sequencing the right named pCPB121-amiR-StTCP15. The successfully identified recombinant plasmid vector was transformed into *Agrobacterium tumefaciens* GV3101 by repeated freezing and thawing (Hayta et al., 2018; Li S. et al., 2021).

Potato transformation and identification

The genetic transformation of potato cultivar "Desiree" microtuber was based on the transformation method of Si et al. (2003). The microtubers were cut by a sterile blade into pieces that were 0.2–0.3 cm thick. Potato chips were transferred to *Agrobacterium* solution containing recombinant plasmids pBI121-StTCP15 and pCPB121-amiR-StTCP15 for 7–10 min. The remaining bacterial solution on potato slices was dried with sterile dry filter paper and placed in a petri dish containing solid MS for 2 days at 28°C under light protection. The co-cultured potato slices were transferred to the differentiation media and cultured at 2500 Lx at 25°C. The media was changed once a week. When the differentiated shoots grew to about 1.5 cm, they were cut and transferred to the rooting medium containing 50 mg/L kanamycin and 200 mg/L carbenicillin for rooting screening (Qi et al., 2020; Zhu et al., 2021). After about 7 days, the plants rooting on the media were preliminarily identified as transformed plants.

To identify transgenic plants, the neomycin phosphotransferase (*NPT* II) gene on the expression vector was used for PCR detection. Genomic DNA of transgenic plants was extracted by CTAB method (Li S. et al., 2021). The wild type potato cultivar "Desiree" were used as a negative control, and the constructed plant expression vector plasmid was used as a positive control. Electrophoresis detected the fragment size of 676 bp, which was transformed into pBI121-StTCP15 and pCPB121-amiR-StTCP15 transgenic potato plants, named OE-n and RNAi-n, respectively, and used for. Further identification by qRT-PCR was performed to identify successful transgenic potato plants for later experiments.

Analysis of transgenic potato tuber

Wild-type (WT) potato plants, transgenic lines OE-n and RNAi-n were propagated and transplanted to pots to obtain potato tubers. After harvesting potato tubers, they were allowed to air dry and stored in darkness at (23 ± 2)°C. A total of 100 transgenic and WT potato tubers of the same size were selected, and the dormancy and germination of tubers were observed every 5 days since the date of harvest. The sign of dormancy removal of tubers is that at least one bud larger than 2 mm grows on tubers (Van Ittersum et al., 1992). All comparative sprouting tests were conducted using batches of tubers harvested at the same time from plants growing under the same environmental conditions.

Measurement of superoxide dismutase, peroxidase, catalase, ABA and GA_3 in transgenic potato tuber

The transgenic and WT potato tubers were used as materials. During the dormancy release period of tubers, tissue samples were collected from the bud eye area using a 0.5 cm diameter sampler, and the fresh plant materials were quickly placed in liquid nitrogen and stored in a low-temperature refrigerator at −80°C. Superoxide dismutase (SOD) activity was measured by NBT method (Johnson-Flanagan and Owens, 1985). The activity of peroxidase (POD) activity was determined by guaiacol method (Maehly and Chance, 1954). Catalase (CAT) activity was quantified using the method of Rajinder et al. (1982). ABA and GA_3 contents were determined by ELISA kit (Shanghai Jianglai Biotechnology Co., Ltd., Shanghai, China) according to the instructions of the kit, as described by Zhang et al. (2009). Each experiment was set up with three biological replicates.

Yeast two-hybrid assay

According to the vector pGBKT7 sequence and *StTCP15* gene sequence, specific primers are used to amplify the *StTCP15* sequence, and the specific primers were shown in **Supplementary Table 1**. The PCR product was inserted into bait vector pGBKT7 containing *Nde*I and *Not*I restriction sites, and the recombinant plasmid pGBKT7-StTCP15 was obtained. The bait vector pGBKT7-StTCP15 was co-transformed into yeast strain AH109 (Clontech) with cDNA library of potato cultivar "Zihuabai," which was constructed by fusing cDNA with GAL4 activation domain in pGADT7-Rec vector. The inverters were screened on selective media SD/-Leu/-Trp/-His/-Ade/X-α-gal, and then the interaction of each of the two protein combinations was determined by the blue color of the colony. Further identification of blue positive clones by sequence. All assays were performed according to the protocol described in the YEASTMAKER Yeast Transformation System User Manual (Clontech).

Bimolecular fluorescence complementarity assay

In order to verify the reliability of the Y2H, this research will PCR amplification without termination codon *StTCP15* coding sequence containing *Bam*HI and *Sam* I restriction sites in the pSPYCE-35S vector; The full-length coding sequences of *StSnRK1*, *StF-box* and *StGID1* without termination codon were inserted into pSPYNE-35S containing *Bam*HI and *Sam* I restriction sites. pSPYCE-StTCP15 and pSPYNE-35S empty vectors were used as negative controls for BiFC analysis. The constructed BiFC vector was transformed into *Agrobacterium tumefaciens* GV3101, and the bacterial solution was mixed 1:1 with a sterile syringe. The injection and infection methods were the same as the subcellular localization method. After 48–72 h, the yellow fluorescent protein (YFP) signal was observed by confocal scanning electron microscope (CARI ZEISS, LSCM 800, Germany; Ma et al., 2021).

Split-LUC complementation assay

The CDS of *StTCP15* was cloned into the *Kpn*I and *Xba*I sites of the pCAMBIA1300-cLUC vector, and the *StSnRK1*, *StF-box*, and *StGID1* without terminator CDS were ligated to the *Sac*I and *Sal*I sites of the pCAMBIA1300-nLUC vector. Specific primers were shown in **Supplementary Table 1**. The recombinant plasmid was transformed into *Agrobacterium tumefaciens* strain GV3101. As described by Chen et al., pCAMBIA1300-cLUC-StTCP15 and pCAMBIA1300-nLUC-StSnRK1/StF-box/StGID1 were mixed in equal volumes, and the injection and infection methods were the same as the subcellular localization methods. pCAMBIA1300-cLUC and pCAMBIA1330-nLUC served as blank controls. *Nicotiana benthamiana* leaves were sprayed with D-luciferin potassium salt (Solarbio, Beijing, China), and the fluorescence was detected by a plant live imaging system (BLT PlantView100, Guangzhou Biolight Biotechnology Co., Ltd., Guangzhou, China; Chen et al., 2022).

Results

Bioinformatics and expression analysis of *StTCP15* gene

The potato *StTCP15* gene bioinformatics analysis results showed that *StTCP15* gene is 1981 bp in length, which contains 1245 bp CDS sequence, encoding a polypeptide of 414 amino acids. By analyzing NCBI Splign, *StTCP15* genes were found to contain one intron and two exons, which was a discontinuous gene (**Supplementary Figure 2A**). The gene was located on chromosome 3 (PGSC gene ID: Soltu.DM.03G03040.1; Chromosome location: chr03:54904362-54906342). According to NCBI conservative domain analysis, it was found that StTCP15 contains TCP domain (95-166AA; **Supplementary Figure 2B**). The total molecular weight of the protein was 44.26 KD and PI 7.06, indicating that the protein was neutral. The grand average of hydropathy is –0.713, which is a hydrophilic protein. There were 63 phosphorylation sites with a total score of 0.5–1, accounting for 15.22% (**Supplementary Figure 2C**), which provided conditions for the function of transcription factors (Yang et al., 2021).

The phylogenetic relationship between PCF class and StTCP15 protein in *A. thaliana* was analyzed, and it was found that StTCP15 and AtTCP15/14 had the closest homology (**Figure 1A**). Studies have shown that AtTCP15/14 has a regulatory role in the process of seed dormancy release and germination (Tatematsu et al., 2008), and StTCP15 may regulate the dormancy release and sprouting of potato tubers.

Based on the qRT-PCR results, the *StTCP15* gene was expressed in all potato tissues with significant difference ($P < 0.01$). The relative expression level in leaves was 9.91 times that in roots with the lowest relative expression level, and the expression level in stems, tubers and buds was 5.26, 1.40, and 3.14 times that in roots, respectively (**Figure 1B**). The expression of *StTCP15* gene increased during dormancy release, and the difference between dormancy and dormancy release was extremely significant ($P < 0.01$), dormancy release and sprouting were about 4.35 and 9.00 times that in dormancy, respectively (**Figure 1C**).

Subcellular localization of StTCP15-EGFP fusion protein

StTCP15-EGFP fusion protein was injected into tobacco by *Agrobacterium*-mediated transformation and expressed in leaf cells of tobacco. The expression of the fusion protein was observed under a laser confocal scanning microscope (pCAMBIA1300-35S-EGFP empty vector as negative control). The results showed that StTCP15-EGFP fusion protein had strong GFP fluorescent signal mainly in the nucleus and a weak GFP fluorescent signal in the cell membrane. However, the control GFP fluorescent signal was located in the whole tobacco cell, including the cell membrane, cytoplasm, and nucleus, without specific compartmentalization (**Figure 2**).

Genetic transformation of *StTCP15* and identification of transgenic potato plants

The potato cultivar "Desiree" plantlets *in vitro* were infected with *Agrobacterium tumefaciens* containing pBI121-StTCP15 overexpression vector and pCPB121-amiR-StTCP15 down-regulated expression vector, respectively, and were cultured in

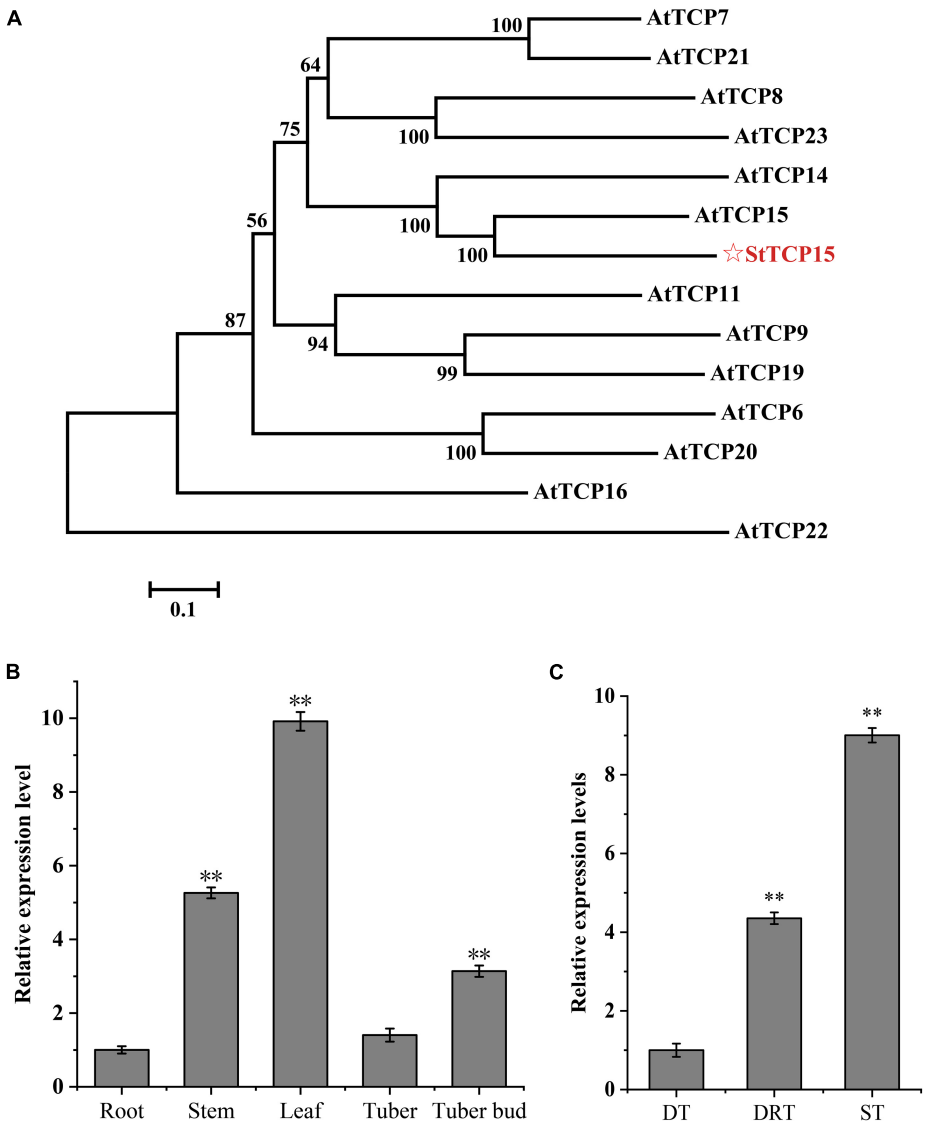

FIGURE 1
Analysis of potato StTCP15. **(A)** The phylogenetic tree of PCF class and StTCP15 in *Arabidopsis thaliana*. **(B)** The relative expression level of *StTCP15* in different organs of potato. **(C)** The relative expression levels of *StTCP15* genes during release of tuber dormancy. DT: Dormant tuber (0 day); DRT: Dormant release tuber (30 day); ST: Sprouting tuber (45 day). Relative expression levels, determined by qRT-PCR, relative to the expression of the *StEF1α* gene, expressed as $2^{-\Delta\Delta Ct}$. Each column represents the mean values ± SE (n = 3; $^{**}P < 0.01$).

differentiation media to form calli and plants (Figure 3A). Transgenic plants were screened by rooting media containing kanamycin (Figures 3B,C).

The putative transformed buds were verified by amplification of reporter *NPT* II on the expression vector. Genomic DNA of transformed plants was extracted by CTAB method and analyzed by PCR and agarose gel electrophoresis. *NPT* II gene of 676 bp could be amplified from transgenic plants, but *NPT* II gene could not be amplified from WT plants, which was consistent with the expected experimental purpose. Therefore, this indicated that transgenic lines of overexpression pBI121-StTCP15 and down-regulated overexpression pCPB121-amiR-StTCP15 have been successfully obtained (Figure 3D).

StTCP15 promotes sprouting of potato tubers

The total RNA of WT and transgenic plants were extracted and reverse transcribed into cDNA. The relative expression levels of *StTCP15* gene in dormancy released tubers were analyzed by qRT-PCR. The results showed that the relative expression level of *StTCP15* gene in pBI121-StTCP15 transgenic

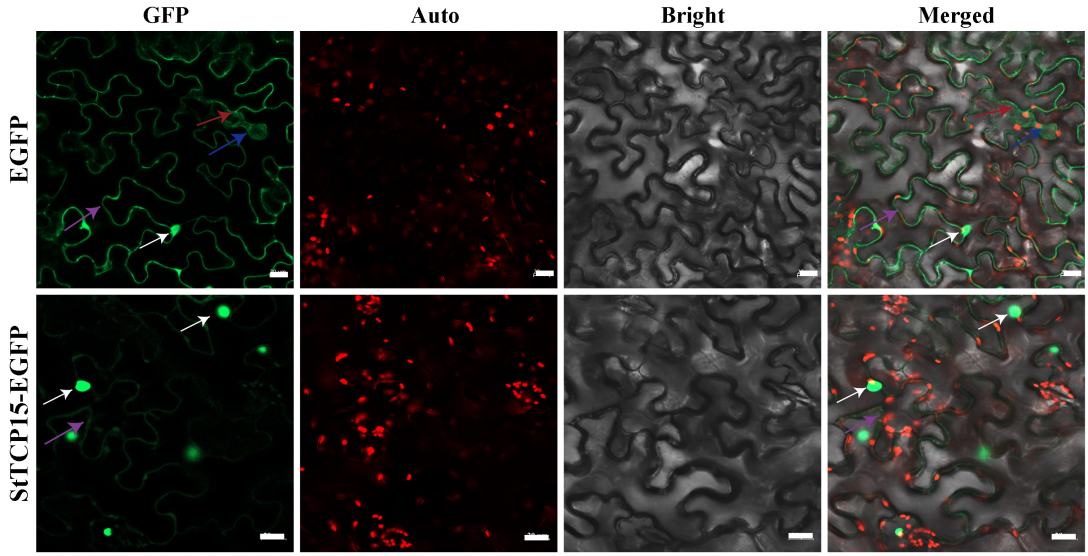

FIGURE 2
Subcellular localization of StTCP15 protein in *Nicotiana benthamiana* leaf cells. The EGFP and StTCP15-EGFP fusion protein transiently expressed in tobacco. The white arrows indicate the nucleus, blue arrows indicate cytoplasm, purple arrows indicate cytoplasmic membrane, and red arrows indicate chloroplasts. GFP: EGFP fluorescence signal in the dark field; Auto: Autofluorescence of chlorophyll; Bright: Cell morphology under bright field; Merged: Combination field. The scale bale represents 20 μm.

dormancy released tubers was significantly higher than that of WT, and the relative expression levels of OE-1, OE-2, and OE-3 were 2.87, 1.88, and 2.39 times of WT, respectively (**Figure 3E**). The relative expression of *StTCP15* gene in pCPB121-amiR-StTCP15 dormancy release tuber was significantly lower than WT, and the relative expression levels of RNAi-1, RNAi-2, and RNAi-3 were 0.27, 0.42, and 0.44 times of WT, respectively (**Figure 3F**).

To further clarify the role of *StTCP15* in potato dormancy release and sprouting, the dormancy release and sprouting of transgenic tubers were measured. According to Ittersum et al. (1992), when the sprouting percentage reached 80% and the length of at least one bud on the tuber was more than 0.2 cm as tubers sprouting time, the time of overexpression transgenic tubers (OE-1, OE-2, and OE-3) was 4.30, 3.67, and 3.54 d earlier than that of the wild type, respectively. However, the time for down-regulated expression transgenic tubers (RNAi-1, RNAi-2, and RNAi-3) was delayed by 6.16, 5.57, and 5.10 d, respectively, compared with WT (**Figures 4A,B**). These results showed that *StTCP15* could promote potato tuber dormancy release and sprouting.

Analysis of superoxide dismutase, peroxidase, catalase, ABA, and GA_3 in transgenic potato tuber

SOD, POD, and CAT, as protective enzymes of plant system defense system, can remove excessive free radicals and peroxides from potato tuber, increase the sugar content of potato tubers, and could help germination of plants (Gong et al., 2021). SOD activity of dormancy released tubers of overexpression (OE-1, OE-2, and OE-3) transgenic lines decreased by 22.8, 39.8, and 35.7%, respectively, compared to wild type, whereas SOD activity of down-regulated expression (RNAi-1, RNAi-2, and RNAi-3) transgenic lines increased by 58.7, 55.2, and 47.4%, respectively, compared to wild type (**Figure 5A**). POD activity increased by 23.0, 16.6, and 20.8% in overexpression transgenic lines, and decreased by 18.2, 24.4, and 20.6% in RNAi-n transgenic lines (**Figure 5B**). CAT activity increased significantly in overexpression transgenic lines compared with wild type, but decreased significantly in down-regulated expression transgenic lines (**Figure 5C**).

Abscisic acid and GA_3 are the main endogenous hormones that antagonize seed dormancy and germination (Gubler et al., 2005; Finkelstein et al., 2008). The content of endogenous hormones ABA and GA_3 was determined. The results showed that the ABA content of dormancy released tubers of OE-2 transgenic lines was significantly higher than that of wild type ($P < 0.05$), and the content of OE-1 and OE-3 transgenic lines was extremely significant ($P < 0.01$). Only OE-3 transgenic lines showed no difference in GA_3 content, while OE-1 and OE-2 transgenic lines showed extremely significant differences ($P < 0.01$) and significant differences ($P < 0.05$), respectively. There was no difference in ABA content of dormancy released tubers of RNAi-1 transgenic lines, but there was an extremely significant difference ($P < 0.01$) and significant difference ($P < 0.05$) in RNAi-2 and RNAi-3 transgenic lines. The

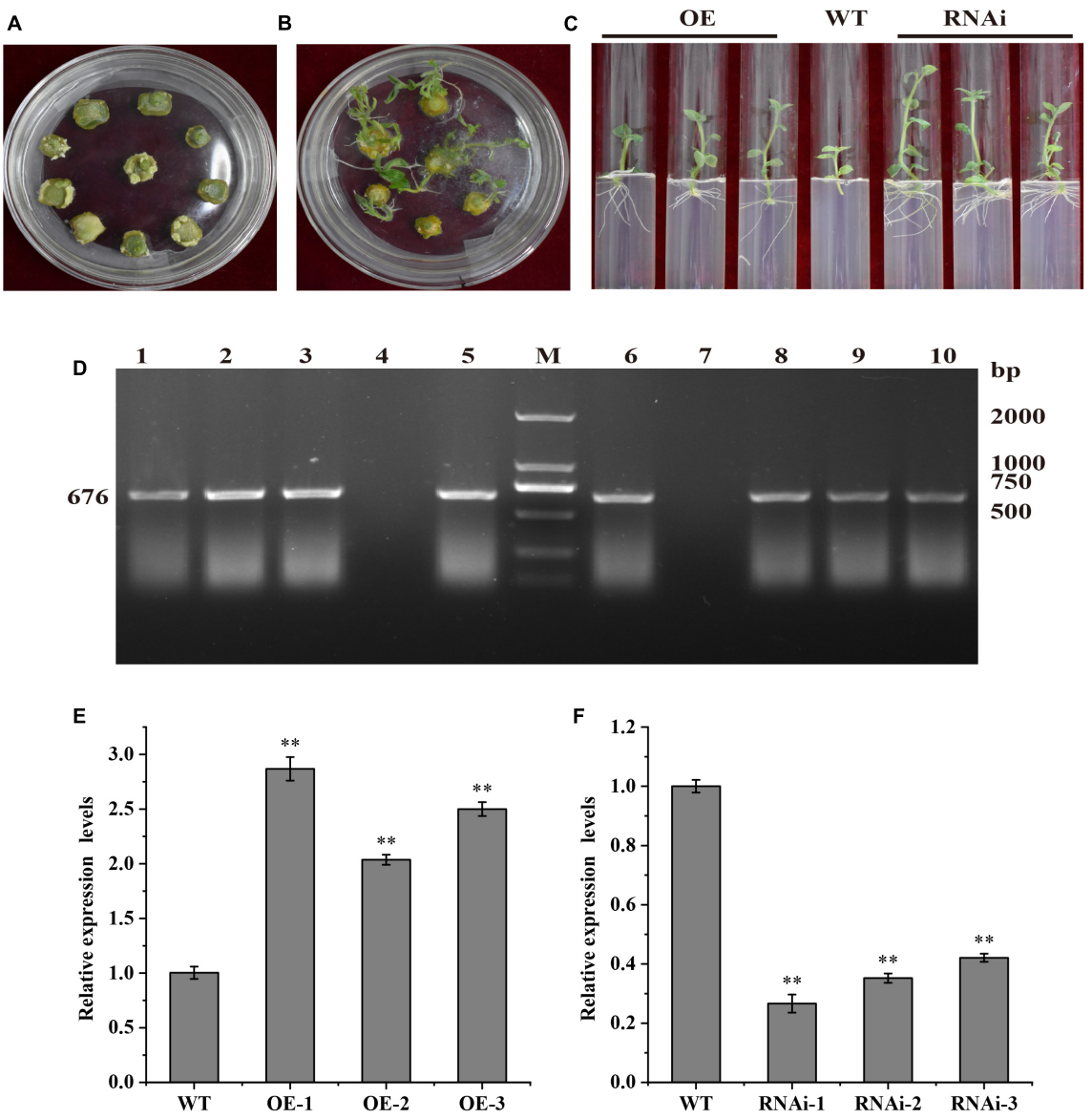

FIGURE 3
Acquisition and identification of transgenic potato. **(A)** Calli; **(B)** Differentiation and rooting transgenic plants; **(C)** Rooting and screening transgenic plants. OE, Transgenic plant "Desiree" carrying recombinant plasmids pBI121-StTCP15; WT, Wild-type plant "Desiree"; RNAi: Transgenic plant "Desiree" carrying recombinant plasmids pCPB121-amiR-StTCP15. **(D)** PCR detection of transgenic plants. M: DL 2000 marker; 1–3: pBI121-StTCP15 transformed plants; 4: Negative control; 5: Positive control pBI121-StTCP15 plasmid; 6: Positive control pCPB121-amiR-StTCP15 plasmid; 7: Negative control; 8–10: pCPB121-amiR-StTCP15 transformed plants. **(E,F)** The relative expression level *StTCP15* in the transgenic plants and WT plants. WT: Wild-type tubers of "Desiree"; OE-1~OE-3: Transgenic tubers of "Desiree" carrying recombinant plasmids pBI121-StTCP15; RNAi-1~RNAi-3: Transgenic tubers of "Desiree" carrying recombinant plasmids pCPB121-amiR-StTCP15. Each column represents the mean values ± SE (n = 3; $^{*}P < 0.05$; $^{**}P < 0.01$).

content of GA_3 in dormancy released tubers of down-regulated expression (RNAi-1, RNAi-2, and RNAi-3) transgenic lines were extremely significantly higher than that of the wild type ($P < 0.01$; Figures 5D,E). It has been shown that seed germination is not determined by ABA or GA_3 alone, but by the dynamic balance of endogenous ABA and GA_3 levels in seeds (Seo et al., 2009; Liu and Hou, 2018; Chen et al., 2020). Therefore, the ratios of ABA and GA_3 in dormancy released tubers was compared in this study. The results showed that the ABA/GA_3 ratio in OE-1, OE-2, and OE-3 transgenic lines were 0.62, 0.67, and 0.64, respectively, which was extremely significantly lower than that in the wild type (0.74). The ABA/GA_3 ratio of RNAi-1, RNAi-2, and RNAi-3 transgenic lines were 0.88, 0.89, and 0.87, respectively, which were extremely significantly higher than those of the wild type (Figure 5F). According to the dynamic equilibrium theory, a

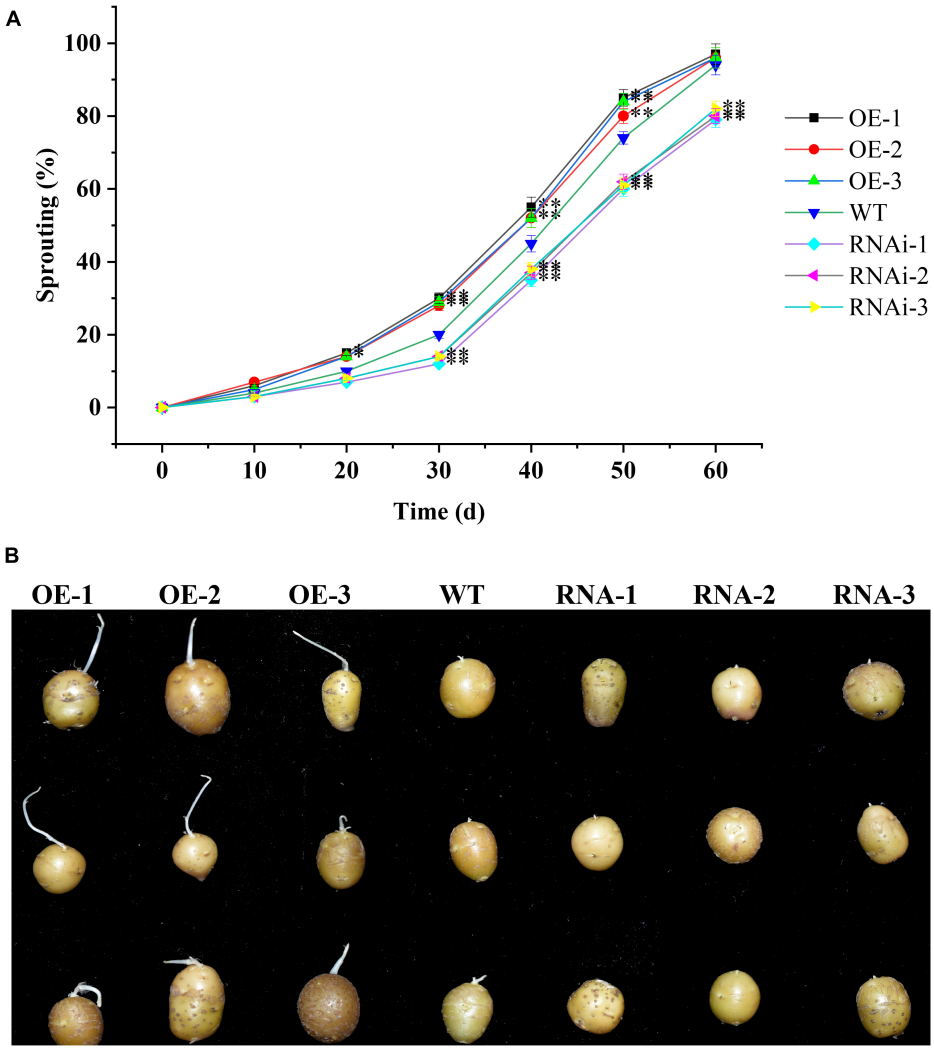

FIGURE 4
StTCP15 promotes sprouting of potato tubers. **(A)** Sprouting percentages of *StTCP15* transgenic and WT tubers. **(B)** Sprouting of transgenic tubers (partial) in 40 days. WT, Wild-type tubers of "Desiree"; OE-1∼OE-3, Transgenic tubers of "Desiree" carrying recombinant plasmids pBI121-StTCP15; RNAi-1∼RNAi-3, Transgenic tubers of "Desiree" carrying recombinant plasmids pCPB121-amiR-StTCP15.

high ABA/GA_3 ratio is beneficial to dormancy, while a low ABA/GA_3 ratio is beneficial to germination, suggesting that *StTCP15* has the function of positively regulating dormancy release of potato tubers.

StTCP15 interacts with StSnRK1, StF-box and StGID1

To further explore the molecular mechanism of StTCP15 in regulating potato tuber sprouting, yeast two-hybrid screening was performed to identify the proteins interacting with StTCP15. Among the various proteins identified, we focused on StSnRK1 (XM_006345112.2), StF-box (CP046683.1) and StGID1 (XM_006358383.1) for further analysis, because they were previously reported to affect seed germination (McGinnis et al., 2003; Qu et al., 2020; Song et al., 2021). Yeast cells co-transformed by pGADT7-StSnRK1, pGADT7-StF-box and pGADT7-StGID1 with pGBKT7-StTCP15 and cells transformed by positive control plasmid were grown on SD/-Ade/-His/-Leu/-Trp/X-α-gal media, respectively. Moreover, it turned blue on SD/-Ade/-His/-Leu/-Trp/X-α-gal media, respectively, while the negative control did not (**Figure 6A**). This demonstrated that StTCP15 interacted with StSnRK1, StF-box and StGID1, respectively. To further characterize this interaction, BiFC experiments were performed. It is connected StTCP15 to pSPYCE-35S, the interacting protein to pSPYNE-35S, and mixed injection into the *N. benthamiana* leaves. YFP fluorescence signal was found to be expressed in both the nucleus and the cell membrane (**Figure 6B**). This is

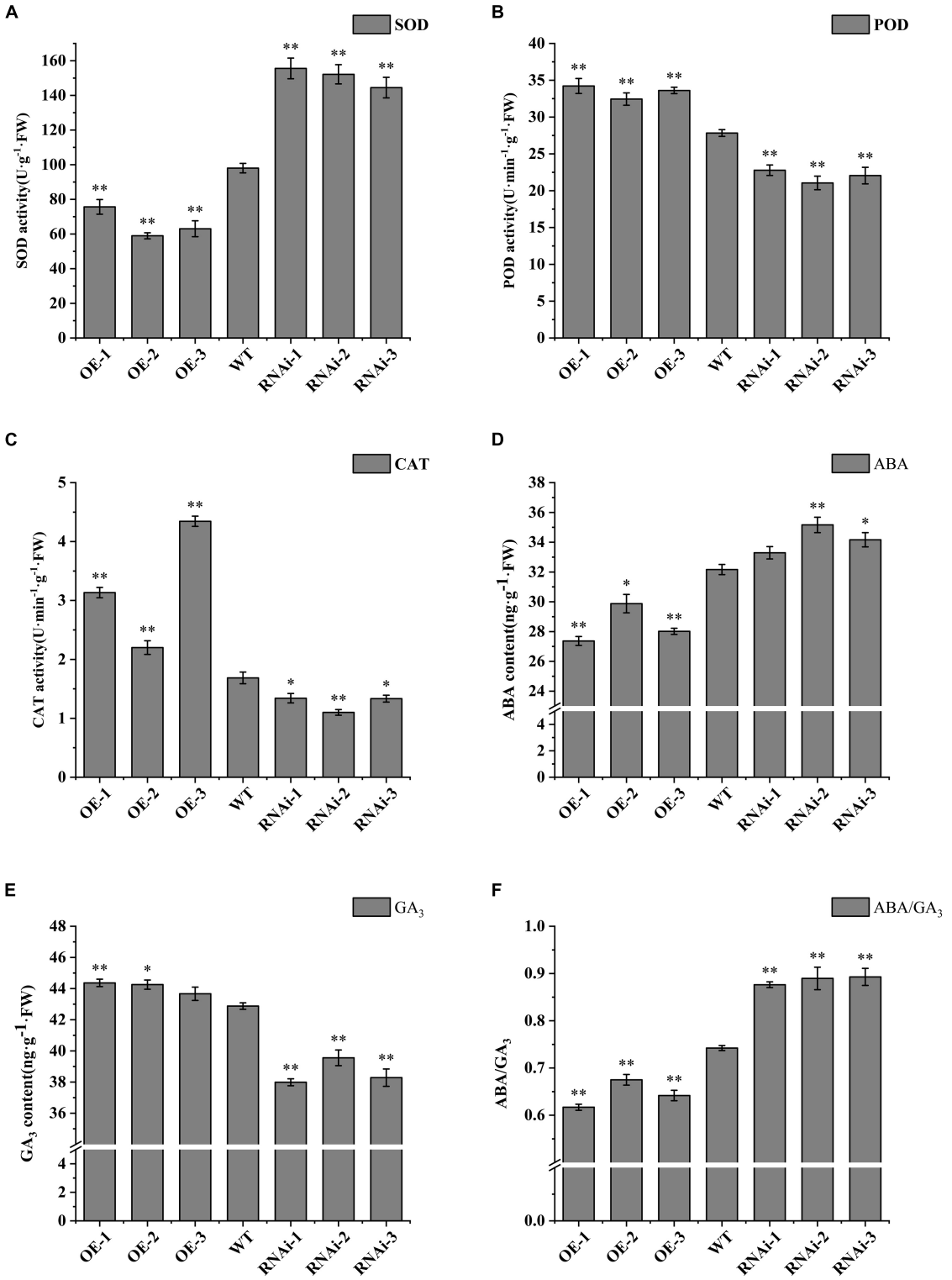

FIGURE 5
Antioxidant-related enzyme activity and endogenous hormone ABA/GA3 in tubers released from dormancy. **(A)** SOD activity; **(B)** POD activity; **(C)** CAT activity; **(D)** ABA content; **(E)** GA3 content; **(F)** ABA/GA3 ratio. WT: Wild-type tubers of "Desiree"; OE-1 ~OE-4, Transgenic tubers of "Desiree" carrying recombinant plasmids pBI121-StTCP15; RNAi-1 RNAi-4, Transgenic tubers of "Desiree" carrying recombinant plasmids pCPB121-amiR-StTCP15. Each column represents the mean values SE (n=3; *P < 0.05; **P < 0.01).

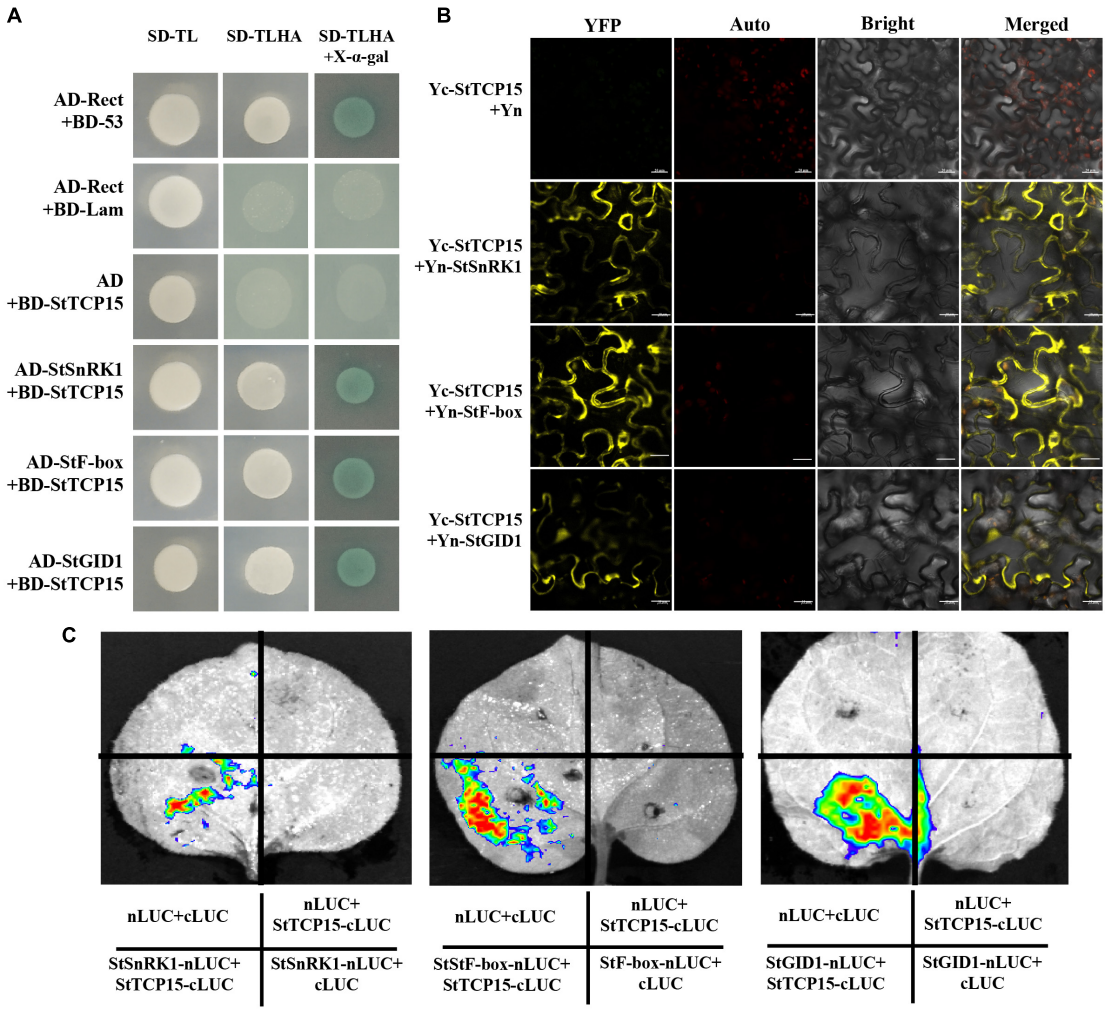

FIGURE 6
(A) The Y2H reciprocal interactions between the interacting protein and the StTCP15 protein. AD, pGADT7. SD-TL stands for -Trp-Leu auxotrophic media; SD-TLHA stands for -Trp-Leu-His-Ade auxotrophic media, where x-α-gal was added to promote blue. **(B)** BiFC analysis was used to detect the interaction of StTCP15 in tobacco. Yc-StCTP15 + Yn-StSnRK1/StF-bos/StGID1 was used as the experimental group; Yc-StCTP15 + Yn were used as negative controls; Yellow indicates YFP fluorescence. The scale bale represents 20 μm. **(C)** Split-LUC complementation assay showing that StTCP15 could interact with StSnRK1, StF-box and StGID1 in cells of *Nicotiana benthamiana* leaves, respectively. The LUC signals were not detected in the corresponding negative controls.

consistent with the subcellular localization of StTCP15 in the nucleus and cell membrane (Figure 2). In addition, Split-LUC Complementation analysis of *N. benthamiana* leaves showed that only LUC signals were detected in the combined region of StSnRK1, StF-box and StGID1 by StTCP15, and no LUC signals were detected in other regions (Figure 6C). Based on these results, this research concluded that StTCP15 interacts with StSnRK1, StF-box and StGID1, respectively.

Discussion

In the whole life cycle of the potato tuber, tuber dormancy and sprouting are the key components of tuber physiological characteristics, which determine the growth and yield of the potato (Sonnewald and Sonnewald, 2014). The dormancy release process of potato tubers was the result of a variety of molecular regulations working together. However, the participation of specific molecular mechanisms in potato dormancy release remains to be seen (Gong et al., 2021).

T are plant-specific transcription factors involved in multiple processes of biological function (Broholm et al., 2008; Tatematsu et al., 2008; Koyama et al., 2010; Danisman et al., 2012; Davière et al., 2014; Nicolas et al., 2015; Wu et al., 2019). In the previous study, Wang et al. (2019) found that the expression level of PCF gene *StTCP15* was continuously up-regulated during the dormancy release of potato tubers. In this research, the relative expression level of *StTCP15* was analyzed

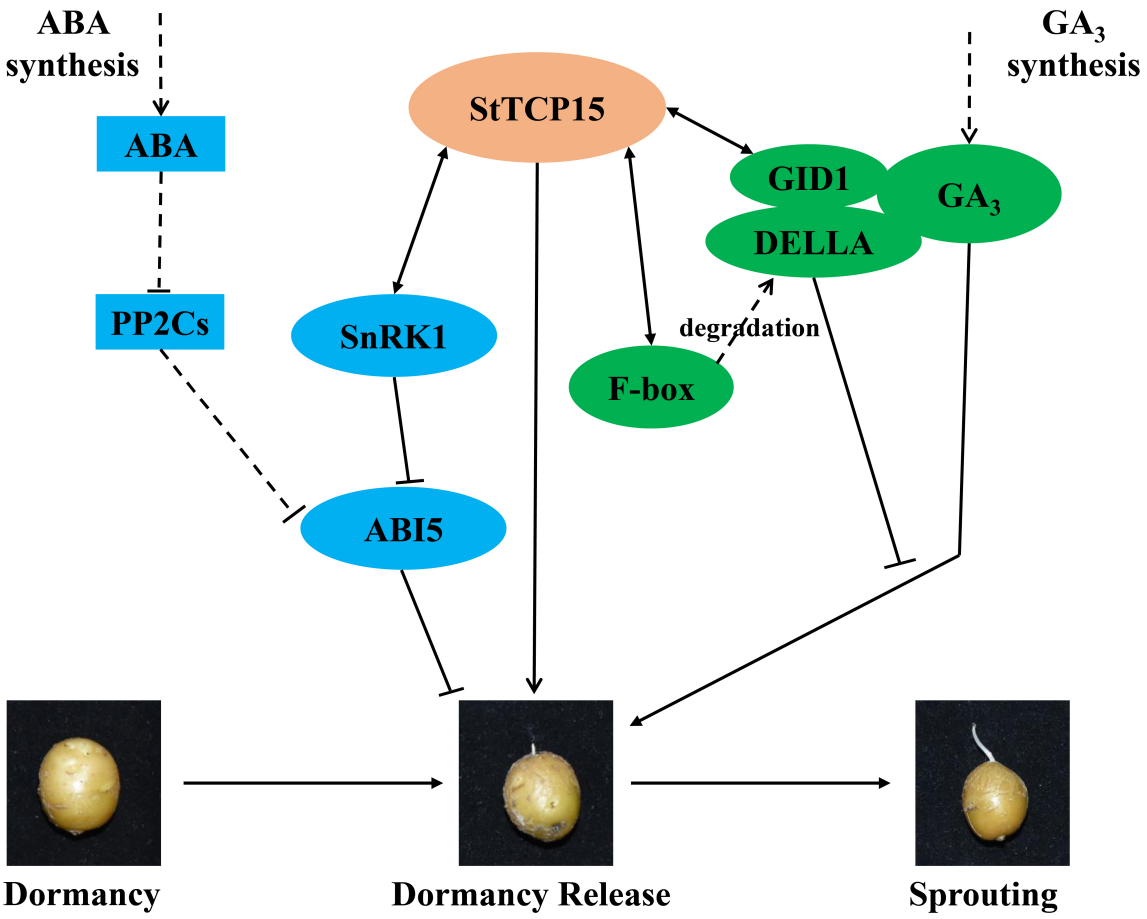

FIGURE 7
The putative pathway model of StTCP15 in potato tuber dormancy release. StTCP15 regulates the dormancy and sprouting of potato tubers by regulating the dynamic balance between ABA and GA_3. GID1 senses GA signals promotes the formation of GID1/GA/DELLA complex, and SLY1 F-Box protein recognizes, binds and degrades DELLA, thus promoting the dormancy release and sprouting of tubers. SnRK1 binds to ABI5, down-regulates the expression of ABI5, participates in ABA signal transduction, and regulates tuber dormancy. Solid lines represent pathways that have been experimentally confirmed to have direct or inhibitory effects, and dashed lines represent pathways that have indirect stimulatory and inhibitory effects.

during the tuber dormancy release of potato cultivar "Desiree" by qRT-PCR (**Figure 1C**) and it was steady with the results of Wang et al. (2019). By constructing PCF class and StTCP15 homologous evolutionary tree of *A. thaliana*, it was found that StTCP15 sequence was related to AtTCP14/15 (**Figure 1A**). Steiner et al. (2012) showed that AtTCP14 and AtTCP15 regulate cell proliferation in developing leaves and specific flower tissues. Tatematsu et al. (2008) showed a functional relationship between *AtTCP14* and GA, and the activation of *AtTCP14* used to be vital for seed germination. Lacking this activity, seeds are hypersensitive to the negative effects on germination of GA biosynthesis inhibitor paclobutrazol. Resentini et al. (2021) research showed that *AtTCP14* and *AtTCP15* mediate the promotion of seed germination by gibberellins in *A. thaliana*. In this study, the *StTCP15* gene was transformed into potato cultivar "Desiree" by *Agrobacterium*-mediated method. Phenotypic analysis confirmed that *StTCP15* gene had no effect on potato plants (**Supplementary Figure 3**). Overexpression potato tubers dormancy released and sprouted earlier than wild-type tubers, while down-regulated expression tubers delayed dormancy released and sprouted (**Figures 4A,B**). The results showed that *StTCP15* gene promotes the dormancy release and sprouting of potato tubers.

The activity of antioxidant enzymes and the content of endogenous hormones ABA and GA_3 in transgenic tubers had been determined. It was found that SOD activity decreased, and POD activities and CAT activities increased in dormancy released tubers of overexpression transgenic lines (**Figures 5A–C**), which was the same as results of Wang et al. (2020). Gong et al. (2021) showed that POD and CAT can remove excessive free radicals and peroxides in plants, increase the sugar content in potato tubers and promote sprouting. In overexpression transgenic lines, ABA content was always significantly lower than that of wild type and inhibited transgenic lines, and

GA_3 was always significantly higher than that of wild type and inhibited transgenic lines (**Figures 5D,E**). However, studies have shown that seed germination is not affected by ABA or GA_3 hormones, and is determined by the dynamic balance of endogenous ABA and GA_3 levels in seeds. A low ABA/GA_3 ratio is conducive to seed dormancy release and germination (Finkelstein et al., 2008; Seo et al., 2009; Yang et al., 2020). In the research, ABA/GA_3 ratio in overexpression transgenic lines was extremely significantly lower than that in the wild type, while ABA/GA_3 ratio in down-regulated expression transgenic lines was extremely significantly higher than that in the wild type (**Figure 5F**). Teh et al. (2014) showed that during the ripening process of oil palm fruits, the increase in ABA/GA_3 ratio was consistent with ripening. Ge (2019) found that GA_3/ABA ratio of oat seeds with different maturity increased with storage time, and ABA/GA_3 ratio was positively correlated with germination rate of oat seeds. Ling and Zhang (2022) recently reported that ABA levels were significantly reduced during seed development in *Paris polyphylla* var. *yunnanensis,* while GA_3 levels were significantly increased in nine endogenous gibberellins (GAs), resulting in a significantly increased GA_3/ABA ratio in germinated seeds. These results provide evidence that *StTCP15* regulates the dynamic balance of endogenous ABA and GA_3 levels during the dormancy release and sprouting of potato tubers.

In order to further clarify the molecular mechanism of StTCP15 in the dormancy release and sprouting of potato tubers, the proteins interacting with StTCP15 were screened using Y2H system (**Figure 6A**), which were as follows: StSnRK1, StF-box and StGID1 have been proved by BiFC and Split-LUC techniques (**Figures 6B,C**). Resentini et al. (2021) found that AtTCP14 and AtTCP15 interact with DELLA protein GAI and RGL2 to mediate GA to promote *A. thaliana* seed germination. It has also been reported that AtTCP14, through its interaction with DOF6, indirectly inhibits ABA biosynthesis gene ABA1 and ABA-regulated related stress genes, resulting in delayed germination (Rueda-Romero et al., 2012). Song et al. (2021) found that SnRK1 binds to ABI5 and down-regulates the expression of ABI5, thereby affecting ABA signal transduction and promoting seed germination. F-box protein is the most important SCF (SKP1, Cullin/CDC53, F-box protein) complex subunit in Ubiquitin (Ub)-26S proteasome system. It mediates various physiological processes from hormone signaling cascade to environmental stress response (Santner and Estelle, 2010). Song et al. (2012) found that the overexpression of *OsFbx352* reduced the expression of genes involved in ABA synthesis and increased the expression of genes encoding ABA catabolism, and the germination of seeds overexpressing *OsFbx352* was less inhibited by glucose than that of non-transgenic seeds. GID1, as GA receptor, promotes the formation of GID1/GA/DELLA complex, leading to DELLA degradation by 26S proteasome and release of transcription factors (Ariizumi et al., 2011), thus releasing seed dormancy in advance. Combined with the experimental results, it was proposed the pathway model of StTCP15 regulating potato tuber dormancy and sprouting (**Figure 4C**), and StTCP15 may interact with StSnRK1 to regulate the expression of ABI5, and thus regulate the ABA signaling pathway. StTCP15 interacts with StF-Box and StGID1 to reduce DELLA expression and regulate GA_3 signaling (**Figure 7**). However, it is still not clear whether StSnRK1, StF-box and StGID1 proteins are necessary for regulating potato tuber dormancy and sprouting, and further experiments are needed to prove it.

Conclusion

In this study, the potato *StTCP15* gene was cloned. qRT-PCR analysis showed that *StTCP15* gene was expressed in different tissues of potato, the relative expression level in bud was higher than that in tuber, and the relative expression level continued to increase during tuber dormancy release. The expression of *StTCP15* gene reduced SOD activity, increased POD activity and CAT activity in the antioxidant system of potato tubers. It was found that *StTCP15* could promote sprouting of potato tubers by affecting the dynamic balance between ABA and GA. These results could provide insights into the molecular mechanisms of potato tuber dormancy and sprouting and their potential roles in genetic improvement.

Data availability statement

The datasets presented in this study can be found in online repositories. The names of the repository/repositories and accession number(s) can be found in the article/**Supplementary material**.

Author contributions

HS and NZ conceived and designed the experiments. KW, XF, HZ, SL, XP, and XW performed the laboratory experiments. KW, NZ, and HS performed the data analysis and interpretation and wrote the manuscript. All authors contributed to the article and approved the submitted version.

Funding

This research was sponsored by National Natural Science Foundation of China (Nos. 31960444 and 31560413), Science and Technology Partnership Program of Ministry of Science and Technology of China (No. KY201901015), and Gansu Major Science and Technology Project (No. GZGG-2021-6).

Conflict of interest

The authors declare that the research was conducted in the absence of any commercial or financial relationships that could be construed as a potential conflict of interest.

Publisher's note

All claims expressed in this article are solely those of the authors and do not necessarily represent those of their affiliated organizations, or those of the publisher, the editors and the reviewers. Any product that may be evaluated in this article, or claim that may be made by its manufacturer, is not guaranteed or endorsed by the publisher.

Supplementary material

The Supplementary Material for this article can be found online at: https://www.frontiersin.org/articles/10.3389/fpls.2022.1009552/full#supplementary-material

References

Ariizumi, T., Lawrence, P. K., and Steber, C. M. (2011). The role of two f-box proteins, SLEEPY1 and SNEEZY, in Arabidopsis gibberellin signaling. *Plant Physiol.* 155, 765–775. doi: 10.1104/pp.110.166272

Broholm, S. K., Tahtiharju, S., Laitinen, R. A., Albert, V. A., Teeri, T. H., and Elomaa, P. (2008). A TCP domain transcription factor controls flower type specification along the radial axis of the Gerbera (Asteraceae) inflorescence. *Proc. Natl. Acad. Sci. U.S.A.* 105, 9117–9122. doi: 10.1073/pnas.0801359105

Camoirano, A., Arce, A. L., Ariel, F. D., Alem, A. L., Gonzalez, D. H., and Viola, I. L. (2020). Class I TCP transcription factors regulate trichome branching and cuticle development in Arabidopsis. *J. Exp. Bot.* 71, 5438–5453. doi: 10.1093/jxb/eraa257

Chen, H., Ruan, J., Chu, P., Fu, W., Liang, Z., Li, Y., et al. (2020). AtPER1 enhances primary seed dormancy and reduces seed germination by suppressing the ABA catabolism and GA biosynthesis in Arabidopsis seeds. *Plant J.* 101, 310–323. doi: 10.1111/tpj.14542

Chen, Z., Teng, S., Liu, D., Chang, Y., Zhang, L., Cui, X., et al. (2022). RLM1, encoding an R2R3 MYB transcription factor, regulates the development of secondary cell wall in rice. *Front. Plant Sci.* 13:905111. doi: 10.3389/fpls.2022.905111

Cubas, P., Lauter, N., Doebley, J., and Coen, E. (1999). The TCP domain: A motif found in proteins regulating plant growth and development. *Plant J.* 18, 215–222. doi: 10.1046/j.1365-313x.1999.00444.x

Danisman, S., van der Wal, F., Dhondt, S., Waites, R., de Folter, S., Bimbo, A., et al. (2012). Arabidopsis class I and class II TCP transcription factors regulate jasmonic acid metabolism and leaf development antagonistically. *Plant Physiol.* 159, 1511–1523. doi: 10.1104/pp.112.200303

Davière, J. M., Wild, M., Regnault, T., Baumberger, N., Eisler, H., Genschik, P., et al. (2014). Class I TCP-DELLA interactions in inflorescence shoot apex determine plant height. *Curr. Biol.* 24, 1923–1928. doi: 10.1016/j.cub.2014.07.012

Deligios, P. A., Rapposelli, E., Mameli, M. G., Baghino, L., Mallica, G. M., and Ledda, L. (2020). Effects of physical, mechanical and hormonal treatments of seed-tubers on bud dormancy and plant productivity. *Agronomy* 10:33. doi: 10.3390/agronomy10010033

Finkelstein, R., Reeves, W., Ariizumi, T., and Steber, C. (2008). Molecular aspects of seed dormancy. *Annu. Rev. Plant Biol.* 59, 387–415. doi: 10.1146/annurev.arplant.59.032607.092740

Ge, J. (2019). Effects of GA3 and aba on the germination of dormant oat (Avena Sativa L.) seeds. *Appl. Ecol. and Env. Res.* 17, 11175–11189. doi: 10.15666/aeer/1705_1117511189

Gong, H., Dusengemungu, L., Igiraneza, C., and Rukundo, P. (2021). Molecular regulation of potato tuber dormancy and sprouting: A mini-review. *Plant Biotechn. Rep.* 15, 417–434. doi: 10.1007/s11816-021-00689-y

Guan, P., Wang, R., Nacry, P., Breton, G., Kay, S. A., Pruneda-Paz, J. L., et al. (2014). Nitrate foraging by Arabidopsis roots is mediated by the transcription factor TCP20 through the systemic signaling pathway. *Proc. Natl. Acad. Sci. U.S.A.* 111, 15267–15272. doi: 10.1073/pnas.1411375111

Gubler, F., Millar, A. A., and Jacobsen, J. V. (2005). Dormancy release, ABA and pre-harvest sprouting. *Curr. Opin. Plant Biol.* 8, 183–187. doi: 10.1016/j.pbi.2005.01.011

Guo, Z., Shu, W., Cheng, H., Wang, G., Qi, K., Zhang, S., et al. (2018). Expression analysis of TCP genes in peach reveals an involvement of PpTCP.A2 in ethylene biosynthesis during fruit ripening. *Plant Mol. Bio. Rep.* 36, 588–595. doi: 10.1007/s11105-018-1105-z

Hayta, S., Smedley, M. A., Li, J., Harwood, W. A., and Gilmartin, P. M. (2018). Agrobacterium-mediated transformation systems of Primula vulgaris. *Plant Methods* 14:93. doi: 10.1186/s13007-018-0360-1

Heim, M. A., Jakoby, M., Werber, M., Martin, C., Weisshaar, B., and Bailey, P. C. (2003). The basic helix-loop-helix transcription factor family in plants: A genome-wide study of protein structure and functional diversity. *Mol. Biol. Evol.* 20, 735–747. doi: 10.1093/molbev/msg088

Herve, C., Dabos, P., Bardet, C., Jauneau, A., Auriac, M. C., Ramboer, A., et al. (2009). In vivo interference with AtTCP20 function induces severe plant growth alterations and deregulates the expression of many genes important for development. *Plant Physiol.* 149, 1462–1477. doi: 10.1104/pp.108.126136

Ittersum, M. K., Aben, F. C. B., and Keijzer, C. J. (1992). Morphological changes in tuber buds during dormancy and initial sprout growth of seed potatoes. *Potato Res.* 35, 249–260. doi: 10.1007/BF02357705

Johnson-Flanagan, A. M., and Owens, J. N. (1985). Peroxidase activity in relation to suberization and respiration in white spruce (picea glauca) seedling roots. *Plant Physiol.* 79, 103–107. doi: 10.1104/pp.79.1.103

Koyama, T., Mitsuda, N., Seki, M., Shinozaki, K., and Ohme-Takagi, M. (2010). TCP transcription factors regulate the activities of ASYMMETRIC LEAVES1 and miR164, as well as the auxin response, during differentiation of leaves in Arabidopsis. *Plant Cell* 22, 3574–3588. doi: 10.1105/tpc.110.075598

Li, D., Zhang, H., Mou, M., Chen, Y., Xiang, S., Chen, L., et al. (2019). Arabidopsis class II TCP transcription factors integrate with the FT-FD module to control flowering. *Plant Physiol.* 181, 97–111. doi: 10.1104/pp.19.00252

Li, S., Zhang, N., Zhu, X., Ma, R., Liu, S., Wang, X., et al. (2021). Genome-wide analysis of NF-Y genes in potato and functional identification of StNF-YC9 in drought tolerance. *Front. Plant Sci.* 12:749688. doi: 10.3389/fpls.2021.749688

Li, Y., An, S., Cheng, Q., Zong, Y., Chen, W., Guo, W., et al. (2021). Analysis of evolution, expression and genetic transformation of TCP transcription factors in blueberry reveal that VcTCP18 negatively regulates the release of flower bud dormancy. *Front. Plant Sci.* 12:697609. doi: 10.3389/fpls.2021.697609

Li, S., Zhang, N., Zhu, X., Ma, R., Yang, J., Tang, X., et al. (2020). Enhanced drought tolerance with artificial microRNA-mediated StProDH1 gene silencing in potato. *Crop Sci.* 60, 1462–1471. doi: 10.1002/csc2.20064

Ling, L., and Zhang, S. (2022). Comparative proteomic analysis between mature and germinating seeds in Paris polyphylla var. yunnanensis. *PeerJ.* 10:e13304. doi: 10.7717/peerj.13304

Liu, X., and Hou, X. (2018). Antagonistic regulation of ABA and GA in metabolism and signaling pathways. *Front .Plant Sci.* 9:251. doi: 10.3389/fpls.2018.00251

Ma, R., Liu, W., Li, S., Zhu, X., Yang, J., Zhang, N., et al. (2021). Genome-wide identification, characterization and expression analysis of the CIPK gene family in potato (Solanum tuberosum L.) and the role of StCIPK10 in response to drought and osmotic stress. *Int. J .Mol. Sci.* 22:13535. doi: 10.3390/ijms222413535

Maehly, A. C., and Chance, B. (1954). The assay of catalases and peroxidases. *Methods Biochem. Anal.* 1, 357–424. doi: 10.1002/9780470110171.ch14

McGinnis, K. M., Thomas, S. G., Soule, J. D., Strader, L. C., Zale, J. M., Sun, T. P., et al. (2003). The Arabidopsis SLEEPY1 gene encodes a putative F-box subunit of an SCF E3 ubiquitin ligase. *Plant Cell* 15, 1120–1130. doi: 10.1105/tpc.010827

Mukhopadhyay, P., and Tyagi, A. K. (2015). OsTCP19 influences developmental and abiotic stress signaling by modulating ABI4-mediated pathways. *Sci. Rep.* 5:9998. doi: 10.1038/srep09998

Nicolas, M., and Cubas, P. (2016). TCP factors: New kids on the signaling block. *Curr. Opin. Plant Biol.* 33, 33–41. doi: 10.1016/j.pbi.2016.05.006

Nicolas, M., Rodríguez-Buey, M. L., Franco-Zorrilla, J. M., and Cubas, P. (2015). A recently evolved alternative splice site in the BRANCHED1a gene controls potato plant architecture. *Curr. Biol.* 25, 1799–1809. doi: 10.1016/j.cub.2015.05.053

Qi, X., Tang, X., Liu, W., Fu, X., Luo, H., Ghimire, S., et al. (2020). A potato RING-finger protein gene StRFP2 is involved in drought tolerance. *Plant Physiol. Biochem.* 146, 438–446. doi: 10.1016/j.plaphy.2019.11.042

Qu, L., Sun, M., Li, X., He, R., Zhong, M., Luo, D., et al. (2020). The Arabidopsis F-box protein FOF2 regulates ABA-mediated seed germination and drought tolerance. *Plant Sci.* 301:110643. doi: 10.1016/j.plantsci.2020.110643

Rajinder, S. D., Plumb-Dhindsa, P. L., and Reid, D. M. (1982). Leaf senescence and lipid peroxidation: Effects of some phytohormones, and scavengers of free radicals and singlet oxygen. *Physiol. Plantarum* 56, 453–457. doi: 10.1111/j.1399-3054.1982.tb04539.x

Rao, X., Huang, X., Zhou, Z., and Lin, X. (2013). An improvement of the $2^{-\Delta\Delta}$CT method for quantitative real-time polymerase chain reaction data analysis. *Biostat. Bioinforma. Biomath.* 3, 71–85.

Resentini, F., Felipo-Benavent, A., Colombo, L., Blázquez, M. A., Alabadi, D., and Masiero, S. (2021). TCP14 and TCP15 mediate the promotion of seed germination by gibberellins in Arabidopsis thaliana. *Mol. Plant* 14:1771. doi: 10.1016/j.molp.2021.09.012

Rueda-Romero, P., Barrero-Sicilia, C., Gómez-Cadenas, A., Carbonero, P., and Oñate-Sánchez, L. (2012). Arabidopsis thaliana DOF6 negatively affects germination in non-after-ripened seeds and interacts with TCP14. *J. Exp. Bot.* 63, 1937–1949. doi: 10.1093/jxb/err388

Santner, A., and Estelle, M. (2010). The ubiquitin-proteasome system regulates plant hormone signaling. *Plant J.* 61, 1029–1040. doi: 10.1111/j.1365-313X.2010

Seo, M., Nambara, E., Choi, G., and Yamaguchi, S. (2009). Interaction of light and hormone signals in germinating seeds. *Plant Mol. Biol.* 69, 463–472. doi: 10.1007/s11103-008-9429-y

Shen, J., Zhang, Y., Ge, D., Wang, Z., Song, W., Gu, R., et al. (2019). CsBRC1 inhibits axillary bud outgrowth by directly repressing the auxin efflux carrier CsPIN3 in cucumber. *Proc. Natl. Acad. Sci. U.S.A.* 116, 17105–17114. doi: 10.1073/pnas.1907968116

Si, H., Xie, C., and Liu, J. (2003). An efficient protocol for Agrobacterium-mediated transformation with microtuber and the introduction of an antisense class i patatin gene into potato. *Acta. Agron. Sin.* 29, 801–805.

Song, J., Shang, L., Wang, X., Xing, Y., Xu, W., Zhang, Y., et al. (2021). MAPK11 regulates seed germination and ABA signaling in tomato by phosphorylating SnRKs. *J. Exp. Bot.* 72, 1677–1690. doi: 10.1093/jxb/eraa564

Song, S., Dai, X., and Zhang, W. (2012). A rice F-box gene, OsFbx352, is involved in glucose-delayed seed germination in rice. *J. Exp. Bot* 63, 5559–5568. doi: 10.1093/jxb/ers206

Sonnewald, S., and Sonnewald, U. (2014). Regulation of potato tuber sprouting. *Planta* 239, 27–38. doi: 10.1007/s00425-013-1968-z

Steiner, E., Yanai, O., Efroni, I., Ori, N., Eshed, Y., and Weiss, D. (2012). Class I TCPs modulate cytokinin-induced branching and meristematic activity in tomato. *Plant Signal. Behav.* 7, 807–810. doi: 10.4161/psb.20606

Tang, X., Zhang, N., Si, H., and Calderón-Urrea, A. (2017). Selection and validation of reference genes for RT-qPCR analysis in potato under abiotic stress. *Plant Methods* 13:85. doi: 10.1186/s13007-017-0238-7

Tatematsu, K., Nakabayashi, K., Kamiya, Y., and Nambara, E. (2008). Transcription factor AtTCP14 regulates embryonic growth potential during seed germination in Arabidopsis thaliana. *Plant J.* 53, 42–52. doi: 10.1111/j.1365-313X.2007.03308.x

Teh, H. F., Neoh, B. K., Wong, Y. C., Kwong, Q. B., Ooi, T. E., Ng, T. L., et al. (2014). Hormones, polyamines, and cell wall metabolism during oil palm fruit mesocarp development and ripening. *J. Agric. Food Chem.* 62, 8143–8152. doi: 10.1021/jf500975h

Van Ittersum, M. K., Aben, F. C. B., and Keijzer, C. J. (1992). Morphological changes in tuber buds during dormancy and initial sprout growth of seed potatoes. *Potato Res.* 35, 249–260. doi: 10.1007/BF02357705

Wang, Y., Zhang, N., Li, T., Yang, J., Zhu, X., Fang, C., et al. (2019). Genome-wide identification and expression analysis of StTCP transcription factors of potato (*Solanum tuberosum* L.). *Comput. Biol. Chem.* 78, 53–63. doi: 10.1016/j.compbiolchem.2018.11.009

Wang, Z., Ma, R., Zhao, M., Wang, F., Zhang, N., and Si, H. (2020). NO and ABA interaction regulates tuber dormancy and sprouting in potato. *Front. Plant. Sci.* 11:311. doi: 10.3389/fpls.2020.00311

Wei, X., Yang, J., Lei, D., Feng, H., Yang, Z., Wen, G., et al. (2021). The SlTCP26 promoting lateral branches development in tomato. *Plant Cell Rep.* 40, 1115–1126. doi: 10.1007/s00299-021-02680-x

Wu, J., Wu, W., Liang, J., Jin, Y., Gazzarrini, S., He, J., et al. (2019). GhTCP19 transcription factor regulates corm dormancy release by repressing GhNCED expression in Gladiolus. *Plant Cell Physiol.* 60, 52–62. doi: 10.1093/pcp/pcy186

Yang, L., Liu, S., and Lin, R. (2020). The role of light in regulating seed dormancy and germination. *J. Integr. Plant Biol.* 62, 1310–1326. doi: 10.1111/jipb.13001

Yang, S., Zhou, J., Watkins, C. B., Wu, C., Feng, Y., Zhao, X., et al. (2021). NAC transcription factors SNAC4 and SNAC9 synergistically regulate tomato fruit ripening by affecting expression of genes involved in ethylene and abscisic acid metabolism and signal transduction. *Postharvest Biol. Techno.* 178:111555. doi: 10.1016/j.postharvbio.2021.111555

Zhang, N., Si, H., and Wang, D. (2005). Cloning of rd29A gene promoter from Arabidopsis thaliana and Its application in stress-resistance transgenic potato. *Acta. Agron. Sin.* 31, 159–164.

Zhang, Y., Tan, J., Guo, Z., Lu, S., Shu, W., and Zhou, B. (2009). Increased ABA levels in transgenic tobacco over-expressing 9-*cis*-epoxycarotenoid dioxygenase influences H_2O_2 and NO production and antioxidant defenses. *Plant Cell Environ.* 32, 509–519. doi: 10.1111/j.1365-3040.2009.01945.x

Zhu, X., Zhang, N., Liu, X., Li, S., Yang, J., Hong, X., et al. (2021). Mitogen-activated protein kinase 11 (MAPK11) maintains growth and photosynthesis of potato plant under drought condition. *Plant Cell Rep.* 40, 491–506. doi: 10.1007/s00299-020-02645-6

frontiers | Frontiers in Plant Science

TYPE Original Research
PUBLISHED 29 September 2022
DOI 10.3389/fpls.2022.999730

OPEN ACCESS

EDITED BY
Botao Song,
Huazhong Agricultural University, China

REVIEWED BY
Xu Cheng,
Agricultural Genomics Institute at Shenzhen (CAAS), China
Jiasui Zhan,
Swedish University of Agricultural Sciences, Sweden

*CORRESPONDENCE
Liping Jin
jinliping@caas.cn
Guangcun Li
liguangcun@caas.cn

SPECIALTY SECTION
This article was submitted to Crop and Product Physiology, a section of the journal Frontiers in Plant Science

RECEIVED 11 August 2022
ACCEPTED 13 September 2022
PUBLISHED 29 September 2022

CITATION
Qin J, Bian C, Duan S, Wang W, Li G and Jin L (2022) Effects of different rotation cropping systems on potato yield, rhizosphere microbial community and soil biochemical properties. *Front. Plant Sci.* 13:999730. doi: 10.3389/fpls.2022.999730

Effects of different rotation cropping systems on potato yield, rhizosphere microbial community and soil biochemical properties

Junhong Qin, Chunsong Bian, Shaoguang Duan, Wanxing Wang, Guangcun Li* and Liping Jin*

Institute of Vegetables and Flowers, Chinese Academy of Agricultural Sciences/Key Laboratory of Biology and Genetic Improvement of Tuber and Root Crop, Ministry of Agriculture and Rural Affairs, Beijing, China

Continuous potato cropping systems cause yield reduction, soil-borne disease aggravation, and soil degradation, but crop rotation can alleviate these negative effects. However, there are limited studies on the relationships between microbial community and other soil biochemical properties of continuous potato cropping at both pre-planting and harvest in North China. A 4-year study was conducted to explore the effects of different rotation system on soil biochemical properties, microbial community at pre-planting and harvest, and potato yield, tuber number and black scurf incidence at harvest in 2020 and 2021, which included 4 treatments vis. potato-potato-potato-potato (PC), potato-oat-faba bean-potato (PR), oat-faba bean-potato-oat (O), and faba bean-potato-oat-faba bean (B). The results showed that soil biochemical properties and microbial community among all treatments showed no significant difference at pre-planting after a long cold winter generally. At harvest, PC reduced tuber yield and number and significantly increased black scurf incidence relative to potato rotation systems. PC also reduced soil enzyme activities, the content of soil nutrients, and fungal community diversity, and increased bacterial community diversity compared with the other treatments, insignificantly when compared with PR. Relative abundance of microorganisms related to the degradation of organic residues, soil nitrogen cycling, and disease suppression, such as the genera *Devosia*, *Aeromicrobium*, *Paraphoma*, and *Papiliotrema*, were significantly higher in O or B than in PC and PR, while microorganisms related to disease infection such as the genera *Pseudomonas*, *Colletotrichum*, *Plectosphaerella*, *Fusarium*, and *Verticillium* exhibited increased in PC and PR. Principal Coordinates Analysis (PCoA) showed that there were significant differences in the microbial community structure of PC and PR at harvest compared with that of O and B. Redundancy analysis (RDA) revealed that soil available potassium (AK), acid phosphatase (ACP), available phosphorus (AP), sucrase (SUC) and pH were the dominant factors that significantly affected bacterial and fungal community structure. Partial least squares structural equation model

indicated rotation system had significant negative effect on fungal community. It was concluded that growing oat or faba bean after potato can increase soil beneficial microorganisms and maintain the ecosystem healthy, thus reducing the incidence of tuber black scurf and increasing potato yield.

KEYWORDS

potato, continuous cropping, yield, soil biochemical properties, soil microbial communities

Introduction

Potato (*Solanum tuberosum* L.) is ranked as the fourth food crop globally after rice, wheat, and corn. In recent years, potato growers in China have had to cultivate potato consecutively due to limited arable land and the adjustment of planting structures in this country. Consequently, potato yield decreased by 27–85% (Qin et al., 2017), soil-borne disease incidence such as black scurf and common scab increased by 25.9–235.7% and 27.1–60.2%, respectively (Larkin et al., 2011), and soil fertility such as available K and P decreased by 38.1–285.6% and 51.2–59.8%, respectively (Wang et al., 2022). In order to alleviate the problems above, the growers used large amounts of fungicides to control soil-borne disease and applied more and more chemical fertilizer to improve potato yield, which may cause potential environment pollution. Crop rotation is an environment friendly practice that could potentially solve the problems mentioned above (Larkin et al., 2021). For example, green manure-potato rotation (Wang et al., 2022), legume-potato rotation (Qin et al., 2017), and potato-canola-wheat rotation (Mohr et al., 2011) can maintain soil fertility and keep the ecosystem healthy, and thus significantly improving potato yield relative to continuous potato cropping.

Soil microorganisms are instrumental in nutrient cycling and transformation (Kuypers et al., 2018) and soil structure development (Helliwell et al., 2014). Under a cucumber continuous cropping system, the balance of the structure of the soil microbial community was broken, with soil microorganisms shifting significantly from bacteria to fungi (Ma et al., 2004). Tan et al. (2022) recently reported that the diversity of soil bacterial and fungal communities increased and decreased in continuous potato cropping, respectively, but Liu et al. (2014) showed that the diversity of soil bacteria decreased with an increase in continuous cropping years, while the diversity of fungal community was mostly unaffected. This was partially congruent with results from She et al. (2017) that bacterial diversity decreases with continuous cropping years in tobacco. However, Potter et al. (2022) found that the diversity of soil bacterial and fungal community did not differ among maize cropping systems. Beneficial microflora such as *Sphingomonas* and *Haliangium* decreased and pathogenic fungi such as *Fusarium* and *Stagonosporopsis* increased with the continuous years of potato cropping (Wang et al., 2022). *Fusarium* can cause potato stem, root, and tuber rot (Yang et al., 2019). Soil chemical properties are closely related with soil microorganisms. For example, in the continuous cropping of strawberry (Huang et al., 2018) and tobacco (She et al., 2017), soil pH tended to decrease over time and was correlated with low bacterial diversity. With potato, however, soil pH increased with time and had positive and negative correlation with bacterial and fungal content, respectively (Wang et al., 2022). By contrast, Xu et al. (Xu et al., 2015) reported a significant decrease in soil pH with the continuous cropping years. Soil enzymes have a strong positive relationship with bacterial abundance (Taylor et al., 2002). In continuous potato cropping, soil urease and alkaline phosphatase activities gradually decreased, and the numbers of soil bacteria and fungi had significant relationships with alkaline phosphatase activity (Qin et al., 2017). Overall, the relationship between soil biochemical properties and microbial community under continuous cropping systems varied with climate conditions, soil texture, field management and crop species.

In Hebei Province, More than 80% of the potato cultivated in the north, which is the main potato production region in North China. In recent years, continuous cropping obstacles caused problems such as yield reduction and soil-borne disease aggravation became more and more serious in North China (Xu et al., 2019). So, it is urgent to explore the key factors caused these problems and select optimum rotation system to alleviate these problems. However, studies on the continuous cropping system are mainly focus on few single factors such as microbial communities or crop yield at harvest. It is still unclear that how the soil microbial communities change at pre-planting after a long cold winter. In this study, a 4-year oat/faba bean/potato rotation trial with different rotation sequences was conducted in North China from 2018 to 2021 to investigate: 1) the potato yield and soil-borne disease incidence in PC (4-year potato continuous cropping) and PR (potato rotation system, viz. potato oat-faba bean-potato); 2) the soil biochemical properties and microbial community composition in different rotation systems at pre-planting and harvest; and 3) to

determine the key soil biochemical properties that influenced on soil microbial community composition in potato rotation systems.

Materials and methods

Description of the experimental site

The experiment was conducted from 2018 to 2021 at the experimental station (41°25′00″ N, 114°55′57″ E, 1450 m a.s.l.) of the Institute of Vegetables and Flowers of Chinese Academy of Agricultural Sciences in Chabei Administration District, Zhangjiakou City, Hebei Province, China. The region has an average temperature of 2.9°C and an annual precipitation of 381.4 mm. Only one crop per year is cultivated due to the climate features. The soil type was clay loam and its bulk density and field capacity were 1.44 g·cm^{-3} and 24.33%, respectively. D668 (potato genotype), Jican 1(faba bean), and Bayou 18 (fodder oat genotype) were used as crop materials. The potato seeds were produced by our research group, while the seeds of the other two crops were provided by Zhangjiakou Academy of Agricultural Sciences.

Experimental design and soil samplings

The experiment commenced in 2018 and included four crop sequences: 1) potato-oat-faba bean-potato (PR), 2) oat-faba bean-potato-oat (O), 3) faba bean-potato-oat-faba bean (B), and 4) potato-potato-potato-potato (PC). A randomized block design with three replications was used, and each plot size was 500 m^2 (50 m ×10 m) to facilitate mechanized management. The row distance and plant spacing of potato were 0.9 m and 0.18 m, respectively. The oat planting density was 4.5×10^6 plants·ha^{-1} with a row distance of 0.20 m, and the faba bean planting density was 0.33 m (row distance) × 0.12 m (plant spacing). Every year, compound fertilizer (N:P:K=12-19-16) was applied at a rate of 700 kg·ha^{-1} at pre-planting, while nitrogen and potassium were applied during the plant development stage at a rate of 150 kg·ha^{-1} (urea) and 150 kg·ha^{-1} (potassium sulfate), respectively. All plots were fallow before the experiment commenced. Potato and the other two crops were planted in mid- and late-May, respectively, and all crops were harvested in mid-September each year. The investigation began at harvest in 2020 and 2021 for potato yield. At pre-planting and harvest in 2021, soil samples from all crops were collected at five points ("X" sampling method) from each plot and then mixed as one soil sample. Before planting, surface soil (0-20 cm) was collected. At harvest, the whole root of the crop (three plants per point) was completely dug out with a shovel, shaken gently, and then the soil adhering to the root was collected. Samples were passed through a 2-mm sieve and divided into two parts—one was stored at −80°C for microorganism analysis and the other was used for biochemical analysis (Wang et al., 2022).

Analysis of soil biochemical properties

Soil pH was measured with a glass electrode (HQ440D, HACH, USA) (water:soil = 2.5:1). Soil available phosphorus (AP), available potassium (AK), and available nitrogen (AN) were determined by molybdenum blue colorimetric method, flame photometry method, and the alkaline hydrolysable diffusion method, respectively. Soil organic matter (OM) was determined by potassium dichromate titration method (Bao, 2000). Soil acid phosphatase (ACP), alkaline phosphatase (ALP), sucrase (SUC), and urease (URE) were measured using a soil enzyme activity assay kit (Beijing Solarbio Co., Ltd. Beijing, China)

Yield evaluation

The potato yield was determined from each plot at harvest in 2020 (O treatment) and 2021(PR treatment). The black scurf incidence of tubers in 2021 was calculated by the number of tubers with symptoms divided by the total number of tubers per plants and then multiplied by 100.

Soil DNA extraction and illumina sequencing

A PowerSoil DNA Isolation Kit (MoBio Laboratories, Carlsbad, CA, USA) was used to extract soil DNA following the manufacturer's instructions. Purity and quality of the extracted genomic DNA were checked on 1% agarose gels and with a NanoDrop spectrophotometer (Thermo Scientific). The V3-V4 hypervariable regions of bacterial 16S rRNA gene were amplified with primers 338F (5′-ACTCCTACGGG AGGCAGCAG-3′) and 806R (5′-GGACTACNNGGGTATCTAAT-3′). Fungal ITS genes were amplified with the primers ITS5F (5′-GGAAGTAAAAGTCGTAACAAGG-3′) and ITS1R (5′-GCTGCGTTCTTCATCGATGC-3′). PCR amplification was conducted on a Mastercycler Gradient (Eppendorf, Germany) and the cycling parameters were 94°C for 4 min, followed by 28 cycles (16S rRNA gene) or 34 cycles (ITS gene) at 94°C for 30 s, 55°C for 30 s, and 72°C for 60 s, with a final elongation step at 72°C for 7 min. The amplified products were purified using an Agencourt AMPure XP Kit (Beckman Coulter, Brea, CA, USA). High-throughput sequencing was performed using Illumina MiSeq platforms (Beijing Allwegene Co., Ltd.).

High–throughput sequencing data analysis

When adaptors and primer sequences were removed, QIIME (v1.8.0) was used to assemble the raw sequences of each sample according to the unique barcode. The Uparse algorithm of Vsearch (v2.7.1) software was used to cluster

high-quality reads by operational taxonomic units (OTUs) at a similarity threshold of 97%. The Ribosomal Database Project (RDP) Classifier tool was used to divide the sequences into different taxonomic groups against the SILVA128 database. Alpha-diversity indices were then calculated with QIIME1 (v1.8.0). Principal coordinates analysis (PCoA) and heatmap figures were analyzed by R (v3.6.0) based on the Weighted Unifrac distance to analyze the structure and composition of the microbial community. Redundancy analysis (RDA) was used to analyze the multiply relationships between soil biochemical properties and microbial community composition at the genus level by R (v3.6.0). LEfSe (linear discriminant analysis (LDA) Effect Size) was employed to identify the biomarkers of each treatment with an LDA score ≥ 3.0 by Python (v2.7).

Statistical analysis

Multiple comparisons were conducted by one-way analysis of variance (ANOVA) for yield, disease incidence, soil biochemical properties, and microbial relative abundance according to Duncan's test ($p < 0.05$). Pearson correlation analysis was conducted to analyze the relationship between the soil biochemical properties. Spearman correlation analysis was conducted to analyze the relationship between the top twenty microbial communities in genus level and soil biochemical properties. SPSS v22.0 (SPSS Inc., Chicago, IL, United States) was used in all these analyses. SmartPLS v3.3.9 (Ringle et al., 2015) was used to construct partial least squares structural equation model (PLS-SEM) and explore the relationship between rotation system, yield, soil biochemical properties and microbial community.

Results

Potato yield and tuber black scurf incidence

The two-year average potato yield from potato rotation system (PRS) and potato continuous cropping (PC, potato-potato-potato-potato) was showed in Figure 1A. PRS consisted of the potato yield of O treatment (oat-faba bean-potato-oat) in 2020 and PR treatment (potato-oat-faba bean-potato) in 2021. The crop rotation systems significantly affected tuber disease infection and tuber number of potato (Figure 1B). PRS increased potato yield by 23.5%, significantly decreased black scurf incidence by 80% ($p < 0.05$), and increased tuber number by 30.2% compared with PC.

Soil chemical and biological properties

In terms of soil chemical properties, the crop rotation systems only had significant effects on soil AK ($p < 0.05$), as the content of soil AK in PR was significantly higher compared with B and O at pre-planting and B at harvest ($p < 0.05$) (Table 1). The value of other soil chemicals was similar between all treatments at both time points. Among all crops, both soil AP and AK content were significantly higher at harvest than at pre-planting. Compared with PR, PC reduced all soil nutrient content at both time points.

Among soil biological activities, only soil SUC activity was significantly affected ($p < 0.05$) by cropping systems, with that in O significantly higher compared with the other three cropping systems at harvest (Table 2). Compared with pre-planting, soil SUC of O increased by 57.5% at harvest ($p < 0.05$). Soil ACP in

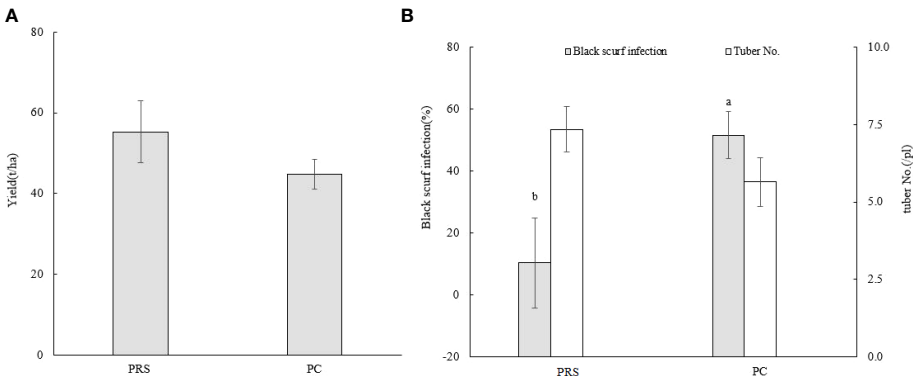

FIGURE 1
Potato yield **(A)** and black scurf infection of tubers **(B)**. PRS indicate the mean yield of potato from O treatment in 2020 and PR treatment in 2021. The grey bar indicates tuber black scurf infection and the white bar indicates tuber No. in **(B)**. Different lowercase letters at the top of the bar indicate significant differences at *P < 0.05*.

10.3389/fpls.2022.999730

TABLE 1 Soil chemical properties at pre-planting and harvest in different cropping systems in 2021.

Treatment	AP(mg/kg)		AK(mg/kg)		AN(mg/kg)		OM(g/kg)		pH	
	Pre-planting	Harvest	Pre-planting	Harvest	Pre-planting	Harvest	Pre-planting	Harvest	Pre-planting	Harvest
PC	17.7 ± 2.1	111.7 ± 12.0 *	28.9 ± 3.9 a	219.3 ± 8.4 a*	64.8 ± 2.8	64.2 ± 4.1	14.4 ± 0.6	15.0 ± 1.5	8.1 ± 0.0	8.2 ± 0.1
PR	15.6 ± 4.7	105.3 ± 25.7 *	30.8 ± 2.3 a	228.0 ± 47.9 a*	72.4 ± 10.3	72.8 ± 9.9	16.4 ± 2.6	15.9 ± 1.8	8.1 ± 0.0	8.2 ± 0.0
B	13.9 ± 2.2	99.7 ± 26.1 *	17.7 ± 0.8 b	103.3 ± 20.1 b*	68.5 ± 7.6	66.6 ± 9.1	16.2 ± 1.9	16.6 ± 2.2	8.1 ± 0.0	8.1 ± 0.1
O	13.6 ± 1.8	98.3 ± 25.6*	20.2 ± 3.2 b	198.0 ± 35.3 a*	70.4 ± 6.4	67.3 ± 2.7	16.0 ± 0.3	15.4 ± 1.6	8.1 ± 0.0	8.1 ± 0.0

Lowercase letters within a column mean significant differences among treatments ($p < 0.05$), and * $p < 0.05$ means significant differences of the same treatment between the two time points. AP, available phosphorus; AK, available potassium; AN, available nitrogen. Data represent mean values ± SE (n = 3).

TABLE 2 Soil enzyme activities at pre-planting and harvest in different cropping systems in 2021.

Treatment	ALP (U/g)		ACP (U/g)		SUC (U/g)		URE (U/g)	
	Pre-planting	Harvest	Pre-planting	Harvest	Pre-planting	Harvest	Pre-planting	Harvest
PC	13270.3 ± 2400.3	15112.5 ± 1067.7	10180.7 ± 950.4	13966.7 ± 612.0 *	18.6 ± 4.0	23.5 ± 3.8 b	28.1 ± 3.7	26.2 ± 3.2
PR	13688.1 ± 4373.0	14979.5 ± 2468.0	12621.4 ± 2915.8	16541.9 ± 1798.1 *	26.7 ± 9.9	24.7 ± 5.4 b	30.4 ± 7.6	30.2 ± 5.7
B	12539.1 ± 3363.3	19243.1 ± 2358.2	11939.2 ± 1709.1	17358.7 ± 1741.8 *	24.3 ± 5.9	26.6 ± 3.6 b	28.1 ± 2.6	30.9 ± 5.8
O	12368.2 ± 1264.7	15055.5 ± 1558.9	13274.9 ± 192.7	17377.9 ± 1093.0 *	21.0 ± 2.5	33.1 ± 1.1 a*	29.2 ± 0.8	32.6 ± 4.9

Lowercase letters within a column mean significant differences among treatments ($p < 0.05$), and *$p < 0.05$ means significant differences of the same treatment between the two time points. ALP, alkaline phosphatase; ACP, acid phosphatase; SUC, sucrase; URE, urease. Data represent mean values ± SE (n = 3).

all treatments at harvest increased by a significant 30.9-45.4% from that at pre-planting ($p < 0.05$). Soil URE and ALP activities were similar among all treatments. However, all the enzyme activities in PC at harvest were lower than those in the other cropping systems. Soil chemical properties had significant correlation with enzyme activities ($p < 0.05$) (Table 3). AK was positively correlated with AP and ACP. OM was positively correlated with all enzymes and AN, but negatively correlated with pH, which in turn was significantly correlated with AN. AN was positively correlated with ALP, ACP and SUC. All these four enzymes were significantly correlated with each other ($p < 0.05$).

α-diversity of microbial community

The cropping system had significant effects on Shannon index of bacterial community and Observed_species and PD_whole_tree indices of fungal community at pre-planting and on all four α-diversity indices of bacterial community and Observed_species and Shannon indices of fungal community at harvest. ($p < 0.05$) (Table 4). Although all the α-diversity indices between PC and PR were not much different at harvest, they were significantly different from those of O and B. At pre-planting, all bacterial community diversity indices except the Shannon index were similar among different cropping systems, while the fungal community diversity indices of PC were lower compared with those of the other cropping systems. Even the indices of Observed_species and PD_wholw_tree were significantly lower ($p < 0.05$). At harvest, the bacterial community diversity indices of PC were the highest, and even significantly higher than those of B and O systems ($p < 0.05$). By contrast, the fungal community diversity indices of PC were the lowest, even significantly lower than those of B and O systems for Observed_species and Shannon indices ($p < 0.05$). In general, the α-diversity indices of bacterial and fungal communities of PC were higher and lower, respectively, compared with those of PR.

Microbial community structure and composition

The different cropping systems significantly affected bacterial and fungal community structure as evident from the PCoA analysis ($p < 0.05$) (Figure 2). The four systems were clustered together at pre-planting and significantly different from harvest along the PCo1 axis. In terms of bacterial community, the relative abundance of 11 phyla, including Proteobacteria, Acidobacteriota, Actinobacteriota, Bacteroidetes, Gemmatimonadota, Chloroflexi, Myxococcota, Verrucomicrobiota, Planctomycetota, Firmicutes, and Patescibacteria, was more than 1% (Figure 3A). However, the dominant phyla with the highest relative abundance in each cropping system was not the same at pre-planting. For example,

10.3389/fpls.2022.999730

TABLE 3 Pearson correlations between soil chemical and biological properties.

	AP	AK	pH	OM	AN	ALP	ACP	SUC
AK	0.514*							
pH	0.386	0.343						
OM	-0.007	-0.017	-0.453*					
AN	0.165	0.175	-0.425*	0.811**				
ALP	0.13	0.289	-0.105	0.534**	0.498*			
ACP	0.306	0.484*	0.024	0.551**	0.531**	0.750**		
SUC	0.181	0.164	-0.07	0.582**	0.546**	0.445*	0.667**	
URE	-0.089	0.148	-0.085	0.416*	0.394	0.449*	0.470*	0.562**

*$p < 0.05$ and **$p < 0.01$ means significant correlations between two properties. ALP, alkaline phosphatase; ACP, acid phosphatase; SUC, sucrase; URE, urease; AP, available phosphorus; AK, available potassium; AN, available nitrogen.

TABLE 4 α-diversity indices of soil samples in all cropping systems.

Period	Treatment	Chao1		Observed_species		PD_whole_tree		Shannon	
		Bacteria	Fungi	Bacteria	Fungi	Bacteria	Fungi	Bacteria	Fungi
Pre-planting	PC	4541.2 ± 144.7	979.9 ± 98.4	3297.5 ± 64.3	764.6 ± 32 b	286.5 ± 7.7	172.1 ± 6.7 b	10.1 ± 0 a	6.4 ± 0.2
	PR	4418.3 ± 114.1	1131.9 ± 60.1	3257.1 ± 39.6	876 ± 5.1 a	284.4 ± 4.4	199 ± 10.8 a	10.1 ± 0 a	6.4 ± 0.3
	B	4454.1 ± 109.6	1142.9 ± 18.0	3204.3 ± 56.6	899.3 ± 29.4 a	276.6 ± 4.2	197.2 ± 3.3 a	10 ± 0 b	6.5 ± 0.2
	O	4442.8 ± 47.1	1139.9 ± 42.0	3226.5 ± 23.2	858 ± 27.9 a	279.6 ± 1.0	192.3 ± 12.1 a	10.1 ± 0 a	6.5 ± 0.1
Harvest	PC	4917.6 ± 104.3 a	1024.3 ± 34.5	3550.1 ± 31.3 a	721.3 ± 46.4 c	306.5 ± 1.8 a	156.8 ± 8.6	10.3 ± 0 a	5 ± 0.4 b
	PR	4864.6 ± 83.5 a	1044 ± 9.2	3499 ± 15.4 a	739.3 ± 29 bc	301.8 ± 1.6 a	159.9 ± 8.2	10.3 ± 0 ab	5.4 ± 0.4 b
	B	4560.3 ± 131.4 b	1102.4 ± 81.7	3222.8 ± 67.5 b	831 ± 45.8 ab	281.5 ± 6.8 b	172.5 ± 6.5	10 ± 0.1 c	6.3 ± 0.2 a
	O	4390.6 ± 155.4 b	1091.2 ± 57.9	3237.1 ± 70.9 b	855.9 ± 34.7 a	280.4 ± 4.6 b	175.7 ± 11.2	10.2 ± 0 b	6.4 ± 0.1 a

Lowercase letters within a column mean significant differences among treatments ($p < 0.05$). Data represent mean values ± SE (n = 3).

Acidobacteriota showed the highest relative abundance in B and PR, while Proteobacteria showed the highest relative abundance in O and PC. Only the relative abundance of Chloroflexi in O was significantly higher than in other cropping systems ($p < 0.05$) (Supplementary Figure 1A). At harvest, the relative abundance of three phyla exhibited significant differences among cropping systems ($p < 0.05$). Myxococcota in O and Patescibacteria in B had significantly higher relative abundance than in the other treatments. The relative abundance of Planctomycetota in PC was significantly higher than in B and O but similar to that in PR. Analysis of the top 20 most abundant bacterial genera revealed that 2 and 10 genera were significantly different among cropping systems at pre-planting and harvest, respectively (Supplementary Figure 1B). At pre-planting, the relative abundance of metagenome genus was significantly higher in PR than in the other cropping systems, and uncultured genera was significantly higher in B than in the other cropping systems. At harvest, the relative abundance of uncultured_bacterium in PC was significantly higher than in the other three systems. The relative abundance of unidentified genera was higher in B than in the other cropping systems and significantly higher than in O. The relative abundance of *Metagenome* and *Devosia* was significantly higher in O. *Allorhizobium-Neorhizobium-Pararhizobium-Rhizobium*, *Aeromicrobium*, and *Lysobacter* had higher relative abundance in B, while *Pseudomonas* and *Methylotenera* showed higher relative abundance in PR.

Among the fungal community, the relative abundance of 9 phyla, including Ascomycota, unidentified, Mortierellomycota, Basidiomycota, Chytridiomycota, Glomeromycota, Rozellomycota, Olpidiomycota, and Zoopagomycota, was more than 1% (Figure 3B). Five of them showed significant differences among all cropping systems at harvest ($p < 0.05$) (Supplementary Figure 2A). For example, the relative abundance of Ascomycota was significantly higher in PC than in the other cropping systems, and significantly higher in PR than in O and B. The relative abundance of Chytridiomycota in PC was significantly lower than in the other treatments. The relative abundance of Basidiomycota in PC and PR were similar but significantly higher than in O and B. At pre-planting, the four cropping systems were similar in all of the phyla. Eighteen of the 20 most abundant fungal genera at harvest belonged to the phyla Ascomycota and Basidiomycota, including nine genera that exhibited significant differences among all cropping systems ($p < 0.05$) (Supplementary Figure 2B). For example, the relative abundance of *Papiliotrema*, *Paraphoma*,

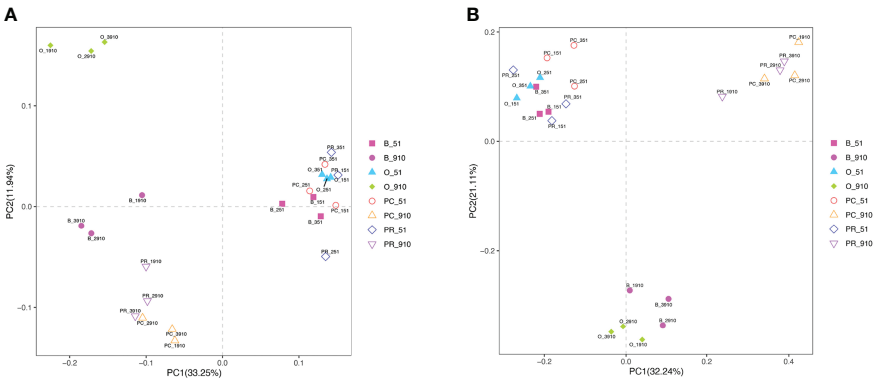

FIGURE 2
Principal coordinate analysis (PCoA) of soil bacterial **(A)** and fungal **(B)** communities. B_51, O_51, PC_51 and PR_51 indicate the samples from B, O, PC and PR treatments at pre-planting, respectively; B_910, O_910, PC_910 and PR_910 indicate the samples from B, O, PC and PR treatments at harvest.

Cladophialophora, *Stachybotrys* and *Humicola* showed the highest value in B, and even were significantly higher than in the other cropping systems except *Humicola*. The relative abundance of *Plectosphaerella* and *Colletotrichum* in PC and PR were similar, but both were significantly higher than in B and O, while *Vishniacozyma* in PC and PR showed the opposite trend. The relative abundance of *Fusarium* and *Verticillium* were higher in PC at harvest compared with other cropping systems but insignificantly (data were not shown).

Biomarkers of all cropping systems were identified by LEfSe, and there were 77 and 121 bacterial communities and 67 and 112 fungal communities (LDA > 3) at all taxonomic levels at pre-planting and harvest, respectively (Figures 4, 5). At harvest, there were more biomarkers for each cropping system than at pre-planting. The PC treatment showed the same number of fungal biomarkers (14) and five less bacterial biomarkers (22) compared to PR treatment. At harvest, the most abundant bacterial biomarkers in PC included Cytophagales (order), Sphingobacteriales (order), Microscillaceae (family), and Bdellovibrionia (phylum), while the most abundant fungal biomarkers in PC were Ascomycota (phylum), Plectosphaerellaceae (family), Glomerellales (order), Sordariomycetes (class), *Plectosphaerella* (genus), *Plectosphaerella niemeijerarum* (species), and *Verticillium* (genus).

Relationship Between Environmental Factors, Microbial Community and Rotation System

Redundancy analysis (RDA) consisted of the soil chemicals and dominant microbial communities at the genus level (Figure 6). The bacterial community structure was significantly affected by soil AK, ACP, pH, SUC and AP, and the fungal community structure was significantly affected by soil AK, ACP, pH, SUC, AP and AN ($p < 0.05$). Spearman correlation analysis between environmental factors and the top 20 microbes at the genus level showed similar results to RDA analysis but differed slightly in that, soil AN had no effect on the fungal genera. In addition, most microbial communities had strong relationship with each other (Supplementary Figure 3). Partial least squares structural equation model (PLS-SEM) was used to assess the relationship between rotation system, environmental factors and microbial community (Figure 7 and Supplementary Table 1). The results showed that rotation system had direct significant negative effects on yield, disease, soil pH and soil NPK with the path coefficients of -0.447, -0.516, -0.334 and -0.306, respectively ($p < 0.05$) and significant negative effect on fungal community with the total path coefficient of -0.756. Both soil enzyme and crop yield had direct significant negative effect on bacterial community with the path coefficients of -0.653 and -1.087, respectively ($p < 0.05$).

Discussion

Many studies have shown that the continuous cropping system not only decreases crop yield but also increases the incidence of disease (Wright et al., 2016). Liu et al. (2014) and Qin et al. (2017) reported that potato yield decreased significantly after two years of continuous potato cropping, and by 85% after 4 years of continuous cropping (Qin et al., 2017). In the current study, potato yield decreased by an insignificant 23.5% after 4 years continuous cropping (PC) relative to potato rotation system, possibly as a result of soil texture and fertility or irrigation management. However, the incidence of potato tuber black scurf was significantly higher in PC, which was congruent with results from Bernard et al. (2014) and Larkin et al. (2011) that different rotation systems could

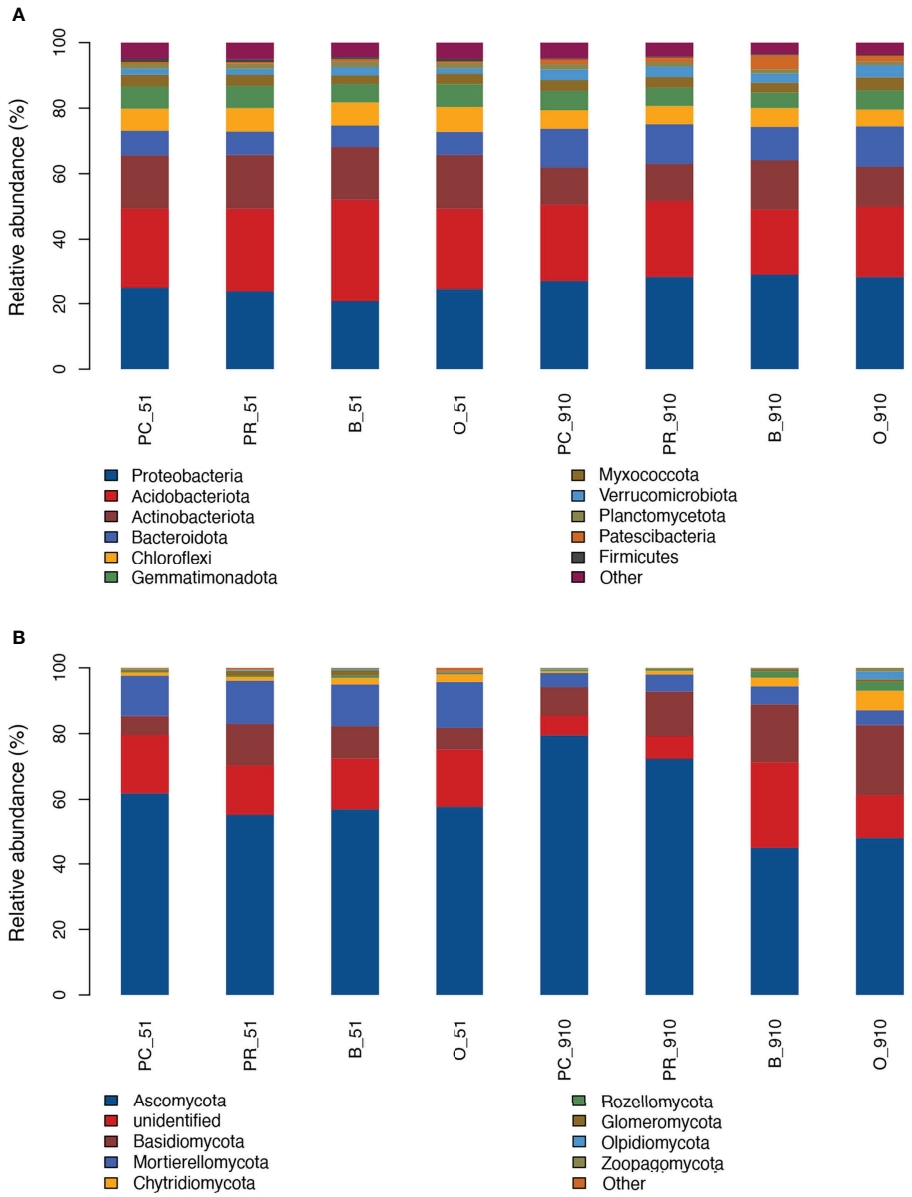

FIGURE 3
Bacterial **(A)** and fungal **(B)** community structure at the phylum level. B_51, O_51, PC_51 and PR_51 indicate the samples from B, O, PC and PR treatments at pre-planting, respectively; B_910, O_910, PC_910 and PR_910 indicate the samples from B, O, PC and PR treatments at harvest.

reduce the incidence of black scurf by18 to 58% relative to PC. Interestingly, PC significantly decreased the tuber number relative to potato rotation system, which was inconsistent with the findings of Mohr et al. (2011) that crop rotations affected the number of large or small tubers but not the total number of tubers.

Different cropping systems had significant effects on soil microbial communities (Larkin et al., 2021). In this study, the rotation system had significant negative effect on fungal community. PR and PC, especially PC, increased the diversity of soil bacterial community and reduced the diversity of soil fungal community, which was consistent with the results of cotton (Xi et al., 2021) and lily (Shi et al., 2021) cropping systems and a 2-11 years continuous potato cropping systems (Zhao et al., 2020). However, this finding was opposite to a study on a 7-year continuous potato cropping system, which showed that the Shannon and Chao1 indices of the fungal community remained consistent over the years but the bacterial community significantly decreased (Liu et al., 2014; Qin et al., 2015); this might be caused by soil type, and was supported by

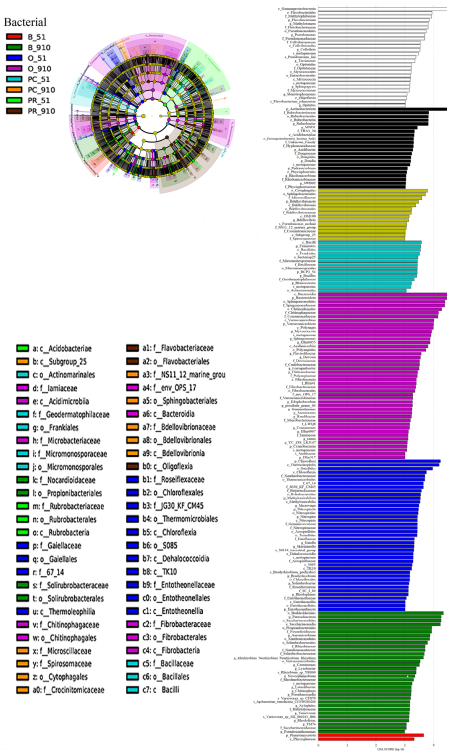

FIGURE 4
LEfSe analysis of soil bacterial community structure at different taxonomic levels among different rotation systems (LDA ≥ 3.0). The left figure is the cladogram of microbial communities. The right graph is the significant different taxa among treatments with LDA ≥3. B_51, O_51, PC_51 and PR_51 indicate the samples from B, O, PC and PR treatments at pre-planting, respectively; B_910, O_910, PC_910 and PR_910 indicate the samples from B, O, PC and PR treatments at harvest.

the study of İnceoğlu et al. (2012) that bacterial communities from the rhizosphere of the same potato cultivar were quite diverse in different soil.

The cropping rotation system significantly affected microbial community structure and composition ($p < 0.05$). In terms of bacterial community, the predominant phyla at pre-planting were similar to harvest. Chloroflexi, which can degrade organic residues (Zeng et al., 2021), was the only phylum that exhibited significant differences in relative abundance among treatments and was significantly higher in O followed by B, PR, and PC at pre-planting. The possible reason was that in all the treatments except for PC, oats were planted in one of the four years and oat straw returned to the field, the degradation of which may lead to higher abundance of Chloroflexi. At harvest, Myxococcota, Patescibacteria, and Planctomycetota showed significant differences in relative abundance among treatments. The abundance of Myxococcota was improved by application of organic materials (Zhang et al., 2022), which was higher in a yam rotation cropping system compared with in continuous cropping systems (Zhou et al., 2021). Patescibacteria is involved in nitrogen, sulfur, and iron cycling (Herrmann et al., 2019). In the present study, the relative abundance of Myxococcota in O and that of Patescibacteria in B were both significantly higher compared with those in other cropping systems. In pepper rotation and intercropping systems, the abundance of Planctomycetota and Acidobacteria increased significantly relative to a continuous cropping system, which accounted for the reduction in soil-borne disease (Dong et al., 2019). However, in the current study, the relative abundance of Planctomycetota was higher in PR and PC relative to B and O. In the present study, Proteobacteria was the dominant phylum in all treatments, which was consistent with the studies that Proteobacteria was, reported as the predominant phylum in potato cultivated soil (Liu et al., 2014; Zhao et al., 2020). At harvest, six known genera of the top 20 bacterial genera presented significant differences among different cropping systems, five of which belonged to the phylum Proteobacteria, including *Pseudomonas*, *Devosia*, *Allorhizobium-Neorhizobium-Pararhizobium-Rhizobium*, *Lysobacter*, and *Methylotenera*. Members of the genus *Devosia* are involved in nitrogen-fixing (Rivas et al., 2002) and straw degradation together with *Allorhizobium-Neorhizobium-Pararhizobium-Rhizobium* (Wang et al., 2019). *Aeromicrobium* can produce erythromycin and may inhibit the Gram-negative bacteria in the soil (Reeves

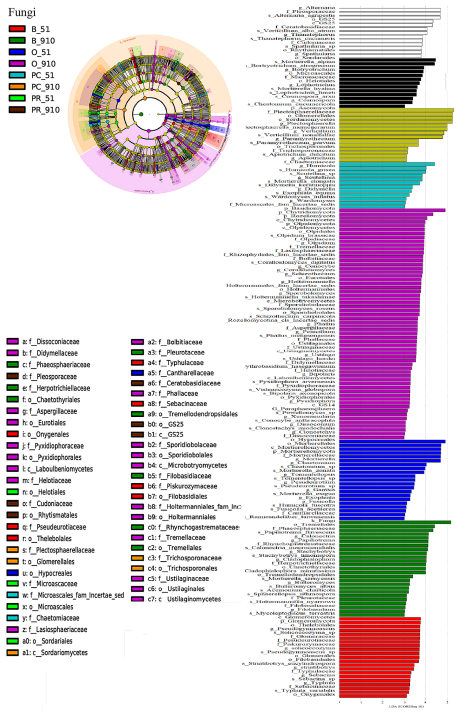

FIGURE 5
LEfSe analysis of soil fungal community structure at different taxonomic levels among different rotation systems (LDA ≥ 3.0). The left figure is the cladogram of microbial communities. The right graph is the significant different taxa among treatments with LDA ≥3. B_51, O_51, PC_51 and PR_51 indicate the samples from B, O, PC and PR treatments at pre-planting, respectively; B_910, O_910, PC_910 and PR_910 indicate the samples from B, O, PC and PR treatments at harvest.

et al., 2004). The abundance of *Devosia* in O and *Allorhizobium-Neorhizobium-Pararhizobium-Rhizobium* and *Aeromicrobium* in B was significantly higher than in other cropping systems. Fluorescent *Pseudomonas* suppressed soil-borne disease (Farah et al., 2008) and *Pseudomonas* sp. RU47 improved P uptake and plant growth (Nassal et al., 2018). However, *Pseudomonas palleroniana* caused potato tuber soft rot (Peng et al., 2022). In the current study, *Pseudomonas* showed significantly higher relative abundance in PC and PR than in B and O, and the functions of members of this genus in these crop systems need to be studied further.

For the fungal community, the main phyla at pre-planting were also similar to harvest. All these fungal phyla showed similar changes among cropping systems at pre-planting, but the first four showed significant differences at harvest. Three of them including Ascomycota, Basidiomycota and Chytridiomycota predominantly belong to the saprotrophic soil fungi and are involved in aerobic cellulose degradation (de Boer et al., 2005), which may improve soil fertility as well as increasing disease incidence during the decomposition and decay process. The relative abundance of the phylum Ascomycota was significantly higher in PC compared with that in PR followed by B and O, but the relative abundance of the phylum Basidiomycota was significantly lower in PC than in O and B. At harvest, eight known genera of the top 20 fungal genera presented significant differences among cropping systems. Members of the genus *Colletotrichum* (Hyde et al., 2009), *Plectosphaerella* (Carlucci et al., 2012; Li et al., 2017) and *Paraphoma* (Cao et al., 2020) are harmful pathogens, and *Paraphoma* can degrade plant residues and biodegradable plastic (Sameshima-Yamashita et al., 2016). The genera *Colletotrichum* and *Plectosphaerella* belonging to phylum Ascomycota presented significantly higher relative abundance in PC and PR than in O and B, which could increase the disease incidence especially in PC. The relative abundance of the genus *Paraphoma* was significantly higher in B than in other treatments, which may be related to plant residue degradation. Genera *Stachybotrys*, *Cladophialophora*, *Humicola* and *Papiliotrema* showed the highest abundance in B relative to in other cropping systems. Members of the genus *Papiliotrema* can control head blight (Khan et al., 2001) and crown rot (Liu et al., 2021) of wheat caused by *Fusarium*, which also causes potato dry rot and wilt. The incidence of the two diseases increased with increasing years of continuous cropping (Mendes et al., 2013). *Stachybotrys elegans* can decrease *Rhizoctonia solani* infection due to degradation of the host hyphae and cell wall of sclerotia

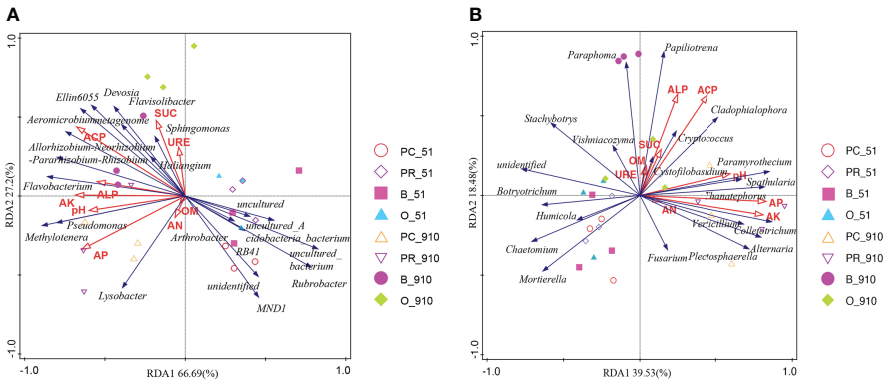

FIGURE 6
Redundancy analysis (RDA) of bacterial **(A)** and fungal **(B)** communities (genera) and soil biochemical properties. B_51, O_51, PC_51 and PR_51 indicate the samples from B, O, PC and PR treatments at pre-planting, respectively; B_910, O_910, PC_910 and PR_910 indicate the samples from B, O, PC and PR treatments at harvest.

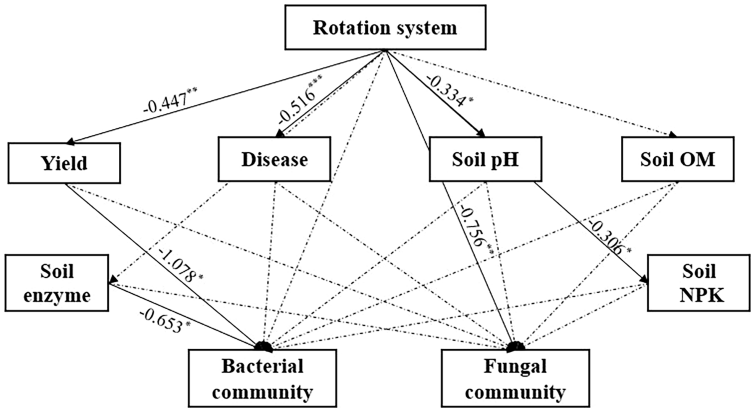

FIGURE 7
Partial least squares structural equation model (PLS-SEM) graph. Solid line and Dash line with arrow indicate significant and insignificant effect between the two measurements, respectively. Bacterial community and fungal community consisted of the top 20 bacterial and fungal genera, respectively. The numbers next to the line indicate the path coefficient. *$P < 0.05$, **$P < 0.01$ and ***$P < 0.001$ indicate significant effect between the two measurements.

(Benyagoub et al., 1994). The abundance of *Rhizoctonia solani*, which causes black scurf, was significantly higher in PC relative to that in PR. The genus *Cladophialophora* includes many plant saprophytes and endophytes, which can degrade cell walls of dead host plants or aromatic-ring based compounds (Davey and Currah, 2007).

Soil nutrient imbalances is one of the main obstacles of continuous cropping (Puniya et al., 2019). In the present study, PC treatment reduced all soil nutrient content and enzyme activities compared to the other three cropping systems, with its value close to that of PR. This was similar to the results from Ma et al. (2015) that soil nutrients did not show significant deficiency and imbalance between PC and PR but the structure of soil microbial community changed significantly. Soil enzymes are predominantly produced by soil microbes and plant roots (Schloter et al., 2003) and play a key role in nutrient cycling and energy flow in the soil ecosystem (Wang et al., 2016). In the current study, soil enzyme had direct significant effect on bacterial community. Li et al. (2018) reported that soil SUC activity was significantly higher in oat rotation and continuous cropping than in potato continuous cropping, which lead to the degradation of plant residues and an increase in soil organic matter. Similar results were obtained in the current study that SUC activity and phyla Chloroflexi related to organic residues

degradation were significantly higher in O. Soil physical and chemical properties and enzymes can affect microbial community abundance and composition (Qin et al., 2017). In this study, soil AK, ACP, SUC, pH and AP affected both bacterial and fungal community significantly, which was in agreement with that soil fungal community was strongly influenced by soil AP (Li et al., 2020) and pH (Zhao et al., 2014). In addition, the rotation system had significant negative effect on fungal community, which was in consistent with the results from Wang et al. (2022) that fungal community was more sensitive to the rotation system.

At pre-planting, the bacterial and fungal community diversity and structure as well as soil chemical properties were similar among all four cropping systems, which could be mainly caused by the low temperature in winter (average temperature -12.5°C) that kept the relative abundance of soil microorganisms in a low level (Zhang et al., 2017) or caused the death of some sensitive organisms. (Shi et al., 2015). Additionally, the microbial community and soil chemical properties changed significantly at harvest than at pre-planting. So, further studies need to determine if the crop exudates recruited some specific microorganisms or they had strong mutual relations to change the diversity and structure of soil microorganisms leading to yield reduction and disease aggravation.

Conclusion

Growing oat or faba bean can increase microorganisms related to plant residues degradation, nitrogen cycling and disease suppression. At pre-planting, the soil biochemical properties and microbial community among four different cropping systems were similar after a long cold winter. However, at harvest, a 4-year potato continuous cropping system (PC) reduced potato yield and tuber number and significantly increased the incidence of black scurf relative to PR. Furthermore, PC also decreased fungal community diversity, soil nutrient contents, and soil enzyme activities, and increased bacterial community diversity compared with the other treatments. Soil AK, ACP, SUC, pH and AP were the key factors to affect bacterial and fungal community structure. In summary, oat and faba bean can increase soil beneficial microorganisms and maintained a healthy ecosystem, thus potato rotated with them can decrease the incidence of tuber black scurf and increase potato yield.

Data availability statement

The datasets presented in this study can be found in onlinerepositories (https://www.ncbi.nlm.nih.gov/bioproject/PRJNA741081/).

Author contributions

JQ, JL and GL designed the research. JL and GL supervised the whole work, JQ carried out the experiments, collected and analyzed the data, and prepared the manuscript. CB, SD and WW provided suggestions for data analysis. All authors approved the manuscript for publication.

Funding

This research was funded by National Key R&D Program of China (2020YFD1000800) and China Agriculture Research System (CARS-09-P11).

Acknowledgments

We thank Xiuhan Liang for language revision and Shuxin Li for figures modification.

Conflict of interest

The authors declare that the research was conducted in the absence of any commercial or financial relationships that could be construed as a potential conflict of interest.

The reviewer XC declared a shared second affiliation with the authors at the time of the review.

Publisher's note

Supplementary material

The Supplementary Material for this article can be found online at: https://www.frontiersin.org/articles/10.3389/fpls.2022.999730/full#supplementary-material

SUPPLEMENTARY FIGURE 1
Relative abundance of dominant bacterial phyla (A) and genera (B) among different treatments. Lowercase letters indicate significant differences at $P < 0.05$ level. B_51, O_51, PC_51 and PR_51 indicate the samples from B, O, PC and PR treatments at pre-planting, respectively; B_910, O_910, PC_910 and PR_910 indicate the samples from B, O, PC and PR treatments at harvest.

SUPPLEMENTARY FIGURE 2
Relative abundance of dominant fungal phyla (A) and genera (B) among different treatments. Lowercase letters indicate significant differences at $P < 0.05$ level. B_910, O_910, PC_910 and PR_910 indicate the samples from B, O, PC and PR treatments at harvest.

SUPPLEMENTARY FIGURE 3
Correlation analysis of soil biochemical properties and the dominant bacterial (A) and fungal (B) genera. * and ** indicate significant differences between two indices at $P < 0.05$ and $P < 0.01$ level, respectively. ALP, alkaline phosphatase; ACP, acid phosphatase; SUC, sucrase; URE, urease; AP, available phosphorus; AK, available potassium; AN, available nitrogen.

References

Bao, S. D. (2000). *Soil agrochemical analysis* (Beijing: Chinese Agricultural Science and Technology Press), 81:106.

Benyagoub, M., Jabaji-Hare, S. H., Banville, G., and Charest, P. M. (1994). Stachybotrys elegans: A destructive mycoparasite of rhizoctonia solani. *Mycol. Res.* 98 (5), 493–505. doi: 10.1016/S0953-7562(09)80467-X

Bernard, E., Larkin, R. P., Tavantzis, S., Erich, M. S., Alyokhin, A., and Gross, S. D. (2014). Rapeseed rotation, compost and biocontrol amendments reduce soilborne diseases and increase tuber yield in organic and conventional potato production systems. *Plant Soil* 374, 611–627. doi: 10.1007/s11104-013-1909-4

Cao, S., Liang, Q. W., Nzabanita, C., and Li, Y. Z. (2020). *Paraphoma* root rot of alfalfa (Medicago sativa) in inner Mongolia, China. *Plant Pathol.* 69 (2), 231–239. doi: 10.1111/ppa.13131

Carlucci, A., Raimondo, M. L., Santos, J., and Phillips, A. J. (2012). Plectosphaerella species associated with root and collar rots of horticultural crops in southern Italy. *Persoonia* 28, 34–48. doi: 10.3767/003158512X638251

Davey, M. L., and Currah, R. S. (2007). A new species of cladophialophora (hyphomycetes) from boreal and montane bryophytes. *Mycol. Res.* 111 (1), 106–116. doi: 10.1016/j.mycres.2006.10.004

de Boer, W., Folman, L. B., Summerbell, R. C., and Boddy, L. (2005). Living in a fungal world: Impact of fungi on soil bacterial niche development. *FEMS Microbiol. Rev.* 29 (4), 795–811. doi: 10.1016/j.femsre.2004.11.005

Dong, Y. F., Lyu, X. Z., Zhang, Z. K., He, H. J., Yu, J. Q., and Zhou, Y. H. (2019). Effects of different cultivation patterns on soil microbial community and enzyme activity in continuous cropped pepper field. *Acta Agric. Zhejiangensis* 31 (9), 1485–1492. doi: 10.13930/j.cnki.cjea.140755

Farah, A., Iqbal, A., and Khan, M. S. (2008). Screening of free-living rhizospheric bacteria for their multiple plant growth promoting activities. *Microbiol. Res.* 163 (2), 173–181. doi: 10.1016/j.micres.2006.04.001

Helliwell, J. R., Miller, A. J., Whalley, W. R., Mooney, S. J., and Sturrock, C. J. (2014). Quantifying the impact of microbes on soil structural development and behaviour in wet soils. *Soil Biol. Biochem.* 74, 138–147. doi: 10.1016/j.soilbio.2014.03.009

Herrmann, M., Wegner, C. E., Taubert, M., Geesink, P., Lehmann, K. , Yan, L., et al. (2019). Predominance of cand. patescibacteria in groundwater is caused by their preferential mobilization from soils and flourishing under oligotrophic conditions. *Front. Microbiol.* 101407. doi: 10.3389/fmicb.2019.01407

Huang, Y., Xiao, X., Huang, H., Jing, J., Zhao, H., Wang, L., et al. (2018). Contrasting beneficial and pathogenic microbial communities across consecutive cropping fields of greenhouse strawberry. *Appl. Microbiol. Biotechnol.* 102, 5717–5729. doi: 10.1007/s00253-018-9013-6

Hyde, K. D., Cai, L., Cannon, P. F., Crouch, J. A., Crous, P. W., Damm, U., et al. (2009). Colletotrichum-names in current use. *Fungal Divers.* 39, 147–182.

İnceoğlu, Ö., Falcão Salles, J., and van Elsas, J. D. (2012). Soil and cultivar type shape the bacterial community in the potato rhizosphere. *Microb. Ecol.* 63, 460–470. doi: 10.1007/s00248-011-9930-8

Khan, N. I., Schisler, D. A., Boehm, M. J., Slininger, P. J., and Bothast, R. J. (2001). Selection and evaluation of micro-organisms for biocontrol of fusarium head blight of wheat incited by gibberella zeae. *Plant Dis.* 85, 1253–1258. doi: 10.1094/PDIS.2001.85.12.1253

Kuypers, M., Marchant, H., and Kartal, B. (2018). The microbial nitrogen-cycling network. *Nat. Rev. Microbiol.* 16, 263–276. doi: 10.1038/nrmicro.2018.9

Larkin, R. P., Honeycutt, C. W., Griffin, T. S., Olanya, O. M., Halloran, J. M., and He, Z. (2011). Effects of different potato cropping system approaches and water management on soilborne diseases and soil microbial communities. *Phytopathology* 101 (1), 58–67. doi: 10.1094/PHYTO-04-10-0100

Larkin, R. P., Honeycutt, C. W., Griffn, T. S., Olanya, O. M., and He, Z. Q. (2021). Potato growth and yield characteristics under different cropping system management strategies in northeastern U.S. *Agron.* 11 (1), 165. doi: 10.3390/agronomy11010165

Li, P. L., Chai, A. L., Shi, Y. X., Xie, X. W., and Li, B. J. (2017). First report of root rot caused by plectosphaerella cucumerina on cabbage in China. *Mycobiology* 45 (2), 110–113. doi: 10.5941/MYCO.2017.45.2.110

Li, N., Gao, D., Zhou, X., Chen, S., Li, C., and Wu, F. (2020). Intercropping with potato-onion enhanced the soil microbial diversity of tomato. *Microorganisms* 8 (6), 834. doi: 10.3390/microorganisms8060834

Li, X. T., Li, L. J., Li, Y., and Liu, X. F. (2018). Effect of different crop rotation methods on soil microbial biomass and enzyme activity. *Chin. Agric. Sci. Bull.* 34 (9), 68–73.

Liu, Z. W., Sun, Z. C., Yang, Y. M., and Wang, Z. M. (2021). Colonization characteristics of seed-soaking and root irrigation with papiliotrema flavescens in wheat seedling and the control of wheat crown rot. *J. China Agric. Univ.* 26 (2), 24–31. doi: 10.11841/j.issn.1007-4333.2021.02.03

Liu, X, Zhang, J, Gu, T, Zhang, W, Shen, Q, and Yin, S (2014). Microbial community diversities and taxa abundances in soils along a seven-year gradient of potato monoculture using high throughput pyrosequencing approach. *PLoS One* 9 (1):e86610. doi: 10.1371/journal.pone.0086610

Ma, L., Ma, K., Yang, G. L., Niu, H. X., and Dai, X. H. (2015). Effects of continuous potato cropping on the diversity of soil microorganisms. *Chin. J. Eco-Agric.* 23 (5), 589–596. doi: 10.13930/j.cnki.cjea.140888

Ma, Y. H., Wei, M., and Wang, X. F. (2004). Variation of microflora and enzyme activity in continuous cropping cucumber soil in solar greenhouse. *Chin. J. Appl. Ecol.* 15 (6), 1005–1008.

Mendes, R., Garbeva, P., and Raaijmakers, J. M. (2013). The rhizosphere microbiome: significance of plant beneficial, plant pathogenic, and human pathogenic microorganisms. *FEMS Microbiol. Rev.* 37 (5), 634–663. doi: 10.1111/1574-6976.12028

Mohr, R. M., Volkmar, K., Derksen, D. A., Irvine, R. B., Khakbazan, M., Mclaren, D. L., et al. (2011). Effect of rotation on crop yield and quality in an irrigated potato system. *Am. J. Potato Res.* 88, 346–359. doi: 10.1007/s12230-011-9200-9

Nassal, D., Spohn, M., Eltlbany, N., Jacquiod, S., Smalla, K., Marhan, S., et al. (2018). Effects of phosphorus-mobilizing bacteria on tomato growth and soil microbial activity. *Plant Soil* 427, 17–37. doi: 10.1007/s11104-017-3528-y

Peng, S. Q., Ren, Y. Y., Yao, T., Chu, H. L., Gao, Y., Tian, X. L., et al. (2022). First report of pseudomonas palleroniana causing potato soft rot in China. *Plant Dis.* doi: 10.1094/PDIS-04-22-0816-PDN

Potter, T. S., Vereecke, L., Lankau, R. A., Sanford, G. R., Silva, E. M., and Ruark, M. D. (2022). Long-term management drives divergence in soil microbial biomass, richness, and composition among upper Midwest, USA cropping systems. *Agric. Ecosyst. Environ.* 325, 107718. doi: 10.1016/j.agee.2021.107718

Puniya, R., Pandey, P. C., Bisht, P. S., Singh, D. K., and Singh, A. P. (2019). Effect of long-term nutrient management practices on soil micronutrient concentrations and uptake under a rice-wheat cropping system. *J. Agric. Sci.*, 157 (3), 226–234. doi: 10.1017/S0021859619000509

Qin, Y., Ma, K., and Liu, P. (2015). Effect of potato continuous cropping on genetic diversity of soil microorganisms. *Chin. J. Eco-Agric.* 23 (2), 225–232. doi: 10.13930/j.cnki.cjea.140755

Qin, S., Yeboah, S., Cao, L., Zhang, J., Shi, S., and Liu, Y. (2017). Breaking continuous potato cropping with legumes improves soil microbial communities, enzyme activities and tuber yield. *PloS One* 12 (5), e0175934. doi: 10.1371/journal.pone.0175934

Qin, S., Yeboah, S., Xu, X., Liu, Y., and Yu, B. (2017). Analysis on fungal diversity in rhizosphere soil of continuous cropping potato subjected to different furrow-ridge mulching managements. *Front. Microbiol.* 8. doi: 10.3389/fmicb.2017.00845

Reeves, A. R., Cernota, W. H., Brikun, I. A., Wesley, R. K., and Weber, J. M. (2004). Engineering precursor flow for increased erythromycin production in aeromicrobium erythreum. *Metab. Eng.* 6 (4), 300–312. doi: 10.1016/j.ymben.2004.03.003

Ringle, C. M., Wende, S., and Becker, J. M. (2015). *SmartPLS 3* (Boenningstedt: SmartPLS GmbH). Available at: http://www.smartpls.com.

Rivas, R., Velázquez, E., Willems, A., Vizcaíno, N., and Martínez-Molina, E. (2002). A new species of devosia that forms a unique nitrogen-fixing root-nodule symbiosis with the aquatic legume neptunia natans (L.f.) druce. *Appl. Environ. Microbiol.* 68 (11), 5217–5222. doi: 10.1128/AEM.68.11.5217-5222.2002

Sameshima-Yamashita, Y., Koike, H., Koitabashi, M., Saika, A., Morita, T., Yarimizu, T., et al. (2016). Draft genome sequence of the fungus paraphoma sp. B47-9, a producer of a biodegradable plastic-degrading enzyme. *Genome Announc.* 4 (5), e01159–e01116. doi: 10.1128/genomeA.01159-16

Schloter, M., Dilly, O., and Munch, J. C. (2003). Indicators for evaluating soil quality. *Agric. Ecosyst. Environ.* 98, 255–262. doi: 10.1016/S0167-8809(03)00085-9

She, S., Niu, J., Zhang, C., Xiao, Y., Chen, W., Dai, L., et al. (2017). Significant relationship between soil bacterial community structure and incidence of bacterial wilt disease under continuous cropping system. *Arch. Microbiol.* 199 (2), 267–275. doi: 10.1007/s00203-016-1301-x

Shi, Y., Lalande, R., Hamel, C., and Ziadi, N. (2015). Winter effect on soil microorganisms under different tillage and phosphorus management practices in eastern Canada. *Can. J. Microbiol.* 61 (5), 315–326. doi: 10.1139/cjm-2014-0821

Shi, G., Sun, H., Calderón-Urrea, A., Li, M., Yang, H., Wang, W., et al. (2021). Bacterial communities as indicators for soil health under continuous cropping system. *Land Degrad. Dev.* 32, 2393–2408. doi: 10.1002/ldr.3919

Tan, X. L., Guo, T. W., Hu, X. Y., Zhang, P. L., Zeng, J., and Liu, X. W. (2022). Characteristics of microbial community in the rhizosphere soil of continuous potato cropping in arid regions of the loess plateau. *Acta Agron. Sin.* 48 (3), 682–694. doi: 10.3724/SP.J.1006.2022.14015

Taylor, J. P., Wilson, B., Mills, M. S., and Burns, R. G. (2002). Comparison of microbial numbers and enzymatic activities in surface soils and subsoils using various techniques. *Soil Biol. Biochem.* 34, 387–401. doi: 10.1016/S0038-0717(01)00199-7

Wang, Z. F., Chen, J., Dai, J. P., Glnur, A., Wang, X. W., Qin, X. Z., et al. (2019). Analysis on the diversity of bacterial flora during the natural decomposing process of corn straws by illumina miseq sequencing. *Xinjiang Agric. Sci.* 56 (1), 111–119.

Wang, X. Y., Duan, Y., Zhang, J., Ciampitti, J. A., Cui, J. W., Qiu, S. J., et al. (2022). Response of potato yield, soil chemical and microbial properties to different rotation sequences of green manure-potato cropping in north China. *Soil Till. Res.* 217, 105273. doi: 10.1016/j.still.2021.105273

Wang, L. D., Wang, F. L., Guo, C. X., Han, F. G., Wei, L. Y., and Li, F. M. (2016). Review: Progress of soil enzymology. *Soil* 48 (1), 12–21. doi: 10.13758/j.cnki.tr.2016.01.002

Wright, P., Falloon, R., and Hedderley, D. (2016). A long-term vegetable crop rotation study to determine effects on soil microbial communities and soilborne diseases of potato and onion. *New Zeal. J. Crop Hortic.* 45, 1–26. doi: 10.1080/01140671.2016.1229345

Xi, H., Zhang, X., Qu, Z., Yang, D., and Zhu, L. (2021). Effects of cotton–maize rotation on soil microbiome structure. *Mol. Plant Pathol.* 22, 673–682. doi: 10.1111/mpp.13053

Xu, X. F., Hui, Z. L., Li, Z. L., Zhang, J. L., and Li, C. Z. (2015). Relationship between potato continuous cropping obstacle and soil environmental factors. *Agric. Res. Arid Areas* 33 (4), 16–23. doi: 10.7606/j.issn.1000-7601.2015.04.03

Xu, J., Zhu, J. H., Yang, Y. L., Tang, H., Ly, H. P., Fan, M. S., et al. (2019). Status of major disease and insect pest of potato and pesticide usage in China. *Sci. Agricultura Sin.* 52 (16), 2800–2808. doi: 10.3864/j.issn.0578-1752.2019.16.006

Yang, B., Guo, C. J., Wang, X. G., and Shen, R. Q. (2019). Investigation and pathogen identification of potato root rot caused by fusarium in xinjiang. *Acta Agric. Boreali-occidentalis Sin.* 28 (12), 2069–2077. doi: 10.7606/j.issn.1004-1389.2019.12.020

Zeng, Y. H., Wu, N. C., Madsen, A. M., Chen, X. H., Gardiner, A. T., and Koblížek, M. (2021). Gemmatimonas groenlandica sp. nov. is an aerobic anoxygenic phototroph in the phylum gemmatimonadetes. *Front. Microbiol.* 11. doi: 10.3389/fmicb.2020.606612

Zhang, H., Tang, J., and Liang, S. (2017). Effects of snow cover plus straw mulching on microorganisms in paddy soil during winter. *Appl. Soil Ecol.* 119, 339–344. doi: 10.1016/j.apsoil.2017.05.023

Zhang, R., Wang, H. H., Zhao, Y. Y., Cheng, Y. Y., Wu, J., and Shi, H. Z. (2022). Effects of organic materials with different carbon sources on soil carbon and nitrogen and bacterial communities in tobacco planting soil. *J. Henan Agric. Sci.*, 51 (3), 84–94. doi: 10.15933/j.cnki.1004-3268.2022.03.010

Zhao, S. C., Qiu, S. J., Cao, C. Y., Zheng, C. L., Zhou, W., and He, P. (2014). Responses of soil properties, microbial community and crop yields to various rates of nitrogen fertilization in a wheat-maize cropping system in north-central China. *Agric. Ecosyst. Environ.* 194, 29–37. doi: 10.1016/j.agee.2014.05.006

Zhao, J., Zhang, D., Yang, Y., Pan, Y., Zhao, D., Zhu, J., et al. (2020). Dissecting the effect of continuous cropping of potato on soil bacterial communities as revealed by high-throughput sequencing. *PloS One* 15 (5), e0233356. doi: 10.1371/journal.pone.0233356

Zhou, L. Z., Lan, C. Y., Shen, Z. Y., Li, Y. Y., Huang, Y. L., Wei, B. H., et al. (2021). Analysis of diversity of rhizosphere soil bacterial community of yam in directional cultivation in continuous cropping. *Southwest China J. Agric. Sci.* 34 (8), 1601–1607. doi: 10.16213/j.cnki.scjas.2021.8.004

frontiers | Frontiers in Plant Science

TYPE Original Research
PUBLISHED 03 October 2022
DOI 10.3389/fpls.2022.1015815

OPEN ACCESS

EDITED BY
Vivianne Vleeshouwers,
Wageningen University and Research, Netherlands

REVIEWED BY
Huaijun Si,
Gansu Agricultural University, China
Rozenn Le Hir,
INRA UMR1318 Institut Jean Pierre Bourgin, France

*CORRESPONDENCE
Xun Liu
liuxun828@swu.edu.cn

SPECIALTY SECTION
This article was submitted to Crop and Product Physiology, a section of the journal Frontiers in Plant Science

RECEIVED 10 August 2022
ACCEPTED 20 September 2022
PUBLISHED 03 October 2022

CITATION
Liu C, Hu S, Liu S, Shi W, Xie D, Chen Q, Sun H, Song L, Li Z, Jiang R, Lv D, Wang J and Liu X (2022) Functional characterization of a cell wall invertase inhibitor StInvInh1 revealed its involvement in potato microtuber size *in vitro*. *Front. Plant Sci.* 13:1015815. doi: 10.3389/fpls.2022.1015815

Functional characterization of a cell wall invertase inhibitor StInvInh1 revealed its involvement in potato microtuber size *in vitro*

Cheng Liu, Shuting Hu, Shuyi Liu, Weiling Shi, Debin Xie, Qi Chen, Hui Sun, Linjing Song, Ziyu Li, Rui Jiang, Dianqiu Lv, Jichun Wang and Xun Liu*

Integrative Science Center of Germplasm Creation in Western China (CHONGQING) Science City, Chongqing Key Laboratory of Biology and Genetic Breeding for Tuber and Root Crops, Engineering Research Center of South Upland Agriculture, Ministry of Education, Southwest University, Chongqing, China

Cell wall invertase (CWI) is as an essential coordinator in carbohydrate partitioning and sink strength determination, thereby playing key roles in plant development. Emerging evidence revealed that the subtle regulation of CWI activity considerably depends on the post-translational mechanism by their inhibitors (INHs). In our previous research, two putative INHs (StInvInh1 and StInvInh3) were expected as targets of CWI in potato (*Solanum tubersum*), a model species of tuberous plants. Here, transcript analysis revealed that *StInvInh1* showed an overall higher expression than *StInhInh3* in all tested organs. Then, *StInvInh1* was further selected to study. In accordance with this, the activity of *StInvInh1* promoter increased with the development of leaves in plantlets but decreased with the development of microtubers *in vitro* and mainly appeared in vascular bundle. The recombinant protein StInvInh1 displayed inhibitory activities on the extracted CWI *in vitro* and StInvInh1 interacted with a CWI StcwINV2 *in vivo* by bimolecular fluorescence complementation. Furthermore, silencing *StInvInh1* in potato dramatically increased the CWI activity without changing activities of vacuolar and cytoplasmic invertase, indicating that StInvInh1 functions as a typical INH of CWI. Releasing CWI activity in *StInvInh1* RNA interference transgenic potato led to improvements in potato microtuber size in coordination with higher accumulations of dry matter *in vitro*. Taken together, these findings demonstrate that *StInvInh1* encodes an INH of CWI and regulates the microtuber development process through fine-tuning apoplastic sucrose metabolism, which may provide new insights into tuber development.

KEYWORDS

potato, cell wall invertase, invertase inhibitor, sucrose metabolism, microtuber

Introduction

Invertases are key metabolic enzymes regulating sink activity through the hydrolytic cleavage of sucrose into glucose and fructose, which are used for diverse metabolic and signaling pathways to regulate plant growth and development (Ruan, 2014). Invertases are classified as cell wall/apoplastic invertase (CWI), vacuolar invertase (VI) and cytosolic neutral/alkaline invertase (CI) on the basis of their cellular targets (Sturm, 1999). The conserved domain of CWI and VI protein belong to glycoside hydrolase family 32 (GH32) enzymes with an optimal pH of 3.5–5.0. Both CWIs and VIs are glycosylated enzymes and intrinsically stable. However, CIs are not glycosylated and clustered to GH100 with an optimal pH of 6.8–9.0 (Coculo and Lionetti, 2022). CIs function in oxidative stress defense (Xiang et al., 2011), and cellulose biosynthesis (Rende et al., 2017; Barnes and Anderson, 2018). VIs often play major roles in hexoses accumulation and osmotic regulation (Klann et al., 1996; Bhaskar et al., 2010; Wang et al., 2010). Molecular genetic studies showed that CWIs are required for seed development and fruit set in some instances, probably by controlling cell division in endosperm and embryo. An endosperm-specific *CWI* mutation in maize resulted in a miniature seed phenotype owing to reduced mitotic activity and cell size in the endosperm (Miller and Chourey, 1992; Cheng et al., 1996; Vilhar et al., 2002). A similar phenotype of *CWI* mutation in seed development was documented in rice (Wang et al., 2008) and tomato (Zanor et al., 2009). Conversely, constitutive expression of *CWI* genes dramatically increases grain yield and total starch content in maize (Li et al., 2013). However, ectopic expression of a CWI gene *GIF1* with the CaMV35S or rice *waxy* promoter resulted in smaller grains in rice, whereas overexpression of *GIF1* driven by its native promoter increased grain production (Wang et al., 2008). These results indicate that CWIs function as determinates of crop yield or production in a gene-dosage-dependent manner or spatial-temporal dependent manner in different plants.

Earlier research on the control of CWI/VI activities mainly focused on transcriptional regulation by modulating their transcripts. However, the proteins of CWI/VIs are intrinsically stable due to glycosylation (Ruan et al., 2010). Thus, their activities are also regulated largely at the protein level. Recent studies have shown that the CWI/VI activities were regulated on the post-translational mechanism through protein–protein interaction between CWIs/VIs and their inhibitors (INHs). The INHs directly target the active site of invertase and compete with sucrose (the substrate of the invertase) for the same binding site (Hothorn et al., 2010). This protein was discovered as early as 1961 when studying the dynamics of potato tuber invertases (Schwimmer et al., 1961). While, the first plant INH of CWI was isolated from tobacco (Greiner et al., 1998). Subsequently, the physiological functions of these INHs in the regulation of seed development have been well documented in maize (Bate et al., 2004; Chen et al., 2019), tomato (Jin et al., 2009), *Arabidopsis* (Su et al., 2016), and soybean (Tang et al., 2017), reflecting that it is a promising strategy to improve seed yield *via* fine-tuning manipulation of CWI activities.

Potato, a model species of tuberous plants, is the most important non-cereal staple crop that widely used throughout the world. The improvement of potato yield potential remains a major challenge for modern agriculture. To understand the effect of the elevating CWI activity on potato tuber development, overexpression of apoplastic yeast invertase in potato was performed. Initially, the constitutive overexpression of apoplastic yeast invertase caused the plants to appear to be under stress and yield penalty (Heineke et al., 1992; Büssis et al., 1997). Subsequently, the tuber-specific overexpression of apoplastic yeast invertase resulted in an increase in tuber size and total yield owing to increased water content (Sonnewald et al., 1997; Hajirezaei et al., 2000; Ferreira and Sonnewald, 2012), further indicated that the CWI activity need to be finely regulated to improve tuber development. Although increasing CWI activities *via* these approaches have been studied for the formation and development of tubers, the CWI activities have been finely regulated at the molecular level, especially during the stolon-tuber formation period, and its influence on the formation and development of tubers still remains unknown.

In our previous study, four putative *INHs* were isolated from potato (Liu et al., 2010). Among them, both StInvInh2A and StInvInh2B function as INHs of VI to diminish cold-induced sweetening in cold-stored tubers (Liu et al., 2010; Liu et al., 2013; Lin et al., 2015). However, the physiological functions of another two putative INHs of CWI are still unknown. In this study, StInvInh1 was identified as an important INH of CWI related to biological processes during potato growth and development. In order to have a better understanding of the importance of the apoplastic sucrose metabolism for potato development, the transgenic plants with released CWI activities were made by silencing *StInvInh1*. Knockdown of *StInvInh1* in potato exclusively increased the CWI activity and led to improvement in potato microtuber size and weight in coordination with higher accumulations of dry matter *in vitro*. The results will help clarify the function of endogenous CWI activity in regulating tuber development and provide a potential avenue for improving tuber production.

Materials and methods

Plant materials and growth conditions

The wild-type (WT) and transgenic plantlets were multiplied in tissue culture on semisolid (7 g L^{-1} agar) Murashige & Skoog (MS) medium with 4% sucrose and incubated at 20 ± 1°C with a photoperiod of 16/8 h day/night

(light intensity 100 μmol m^{-2} s^{-1}). The second or the third single stem nodes from the uppermost of 4-week-old plantlets were transferred to the microtuber induction MS medium with 8% sucrose, 0.7% agar, and 0.2% activated carbon and then incubated at 20 ± 1°C with 8/16 h day/night photoperiods (Liu and Xie, 2001). The characteristics of microtuberization *in vitro* were investigated by using 200 plantlets for each line. Four-week-old microtubers were harvested for microtuber size observation. The samples of various organs in potato were prepared for the expression patterns of *StInvInh1* and *StInvInh3* in our previous study (Liu et al., 2011).

Isolation and analysis of the *StInvInh1* promoter sequence

A pair of specific primers were designed to amplify 5'-flanking sequences of *StInvInh1* based on the *StInvInh1* (Soltu.DM.12G001750.1) genome sequence. The CTAB method was used to isolate the genomic DNA from leaves of three-week-old plantlets of potato cultivar E3. The final PCR products were gel-purified and cloned into the pEASY simple blunt vector (BioGene, Beijing, China), and subjected to sequencing. Putative cis-elements in the *StInvInh1* promoter sequence were searched using the Plant-CARE (http://bioinformatics.psb.ugent.be/webtools/plantcare/html) and PLACE (http://www.dna.affrc.go.jp/PLACE/signalscan.html) databases.

Transient transcription dual-LUC assay

For the promoter activity assay, the *StInvInh1* promoter sequence was subcloned into the pGreenII 0800-LUC double-reporter vector. Dual-LUC assays were performed on *N. benthamiana* plants as described previously (Liu et al., 2021). The Firefly luciferase (LUC) and Renillia (REN) luciferase activity of the plant protein extract was analyzed by a Promega GloMax 20/20 Luminometer (Promega, Madison, USA) using the dual luciferase assay kit (Vazyme, Nanjing, China). The results were calculated by the LUC/REN ratio. At least three measurements were calculated for each assay, and three individual replicates were performed.

Vector construction and plant transformation

For constructing the *StInvInh1* promoter:: *GUS* binary vector, an approximate 2.2-kb fragment from -2157 to the translation start codon was sub-cloned into the pBI121 vector (Invitrogen, Carlsbad, CA, USA). For constructing the *CaMV35S*:: *StInvInh1* RNAi vector, a 348-bp fragment starting from 69 bp downstream of the start codon of the *StInvInh1* cDNA was subcloned into pENTR/D cloning vector (Invitrogen, USA). The fragment was further subcloned into pHellsGate8 vector with the recombination method (Helliwell et al., 2002). Sequences in the recombinant pHellsGate8-*StInvInh1* plasmid were confirmed by restriction digestion (*Xho* I and *Xba* I) and sequencing of inserts to ensure that the *StInvInh1* sequences recombined in sense and antisense orientations. The resulting constructs were transformed into the *Agrobacterium tumefaciens* GV3101 strain and transformed into potato E3 as previously described (Liu et al., 2013). The four-week-old plantlets and microtubers *in vitro* were sampled, used immediately for GUS staining, or frozen in liquid nitrogen and stored -80°C for GUS expression analysis. The characteristics of microtuberization *in vitro* were investigated by using 200 plantlets for each RNAi line. Four-week-old microtubers were harvested for observation of the size of microtubers.

Histochemical determination of GUS activity

Fresh samples (the plantlets or microtubers slices) were subjected to the X-Gluc solution (Sangon, Shanghai, China) for histochemical determination of GUS activity (Liu et al., 2017).

RNA extraction and RT-qPCR

All the samples are quick-frozen in liquid nitrogen and stored in -80°C refrigerator. The tissues were grounded, and total RNA was extracted using the RNA purification kit (Tiangen, Beijing, China). The quantitative RT-PCR (RT-qPCR) was performed as previously described by Liu et al. (2010). The procedure was as follows: 95°C 30 s, 40 cycles, 95°C 15 s, 55°C 30 s, 72°C 5 s. The specificity of the individual PCR amplification was confirmed by a dissociation curve protocol from 60 to 95°C and electrophoresis on agarose gel after the last cycle of real-time qPCR. Potato gene *ef1α* (AB061263) was used as an internal control (Nicot et al., 2005). All primers used in this study are presented in Supplemental Table S1.

Determination of invertase activity *in planta* and *in vitro*

Samples of plantlets and microtuber slices were fixed with the fixation buffer (2% paraformaldehyde, 2% polyvinylpyrrolidone 40, 10 mM dithiothreitol, pH=7.0) for 1 h at 4°C. After fixation, samples were washed overnight in water and refreshed at least five times to get rid of the soluble sugar. The analyses of invertase activity *in planta* and *in vitro* were performed as previously

described (Sergeeva et al., 2006; Liu et al., 2013). Samples of plantlets and microtuber slices were ground in liquid nitrogen.

Quantification of the fresh and dry weight, the contents of dry matter, starch, sucrose, fructose and glucose in microtubers

One hundred four-week-old microtubers were collected and weighed as one biological replicate, and three biological replicates were sampled for each transgenic line. The fresh weight was determined by the average weight of the microtubers. Then, the microtubers were dried at 80°C for 48 h in an oven. The dry weight was determined by calculating the average weight of the dried microtubers. Dried tuber samples were grounded to fine powder. The starch, sucrose, fructose and glucose in each sample were extracted and determined following the instructions provided with the starch, sucrose, fructose and glucose assay kits (Solarbio, Beijing, China), respectively.

Functional assays of recombinant *StInvInh1*

The coding sequence (without signal peptide) of *StInvInh1* was sub-cloned into expression vector E6 (GenScript, USA) with an N-terminal 6× His tag. The *E. coli* strain Rosetta-gami™ (DE3) (Novagen, USA) was used as host for the protein expression. Expression and purification of recombinant StInvInh1 protein was performed following the protocol reported by Liu et al. (2010). Assay for inhibitor function of recombinant StInvInh1 protein *in vitro* were performed as described by Link et al. (2004).

Protein-protein interaction between *StInvInh1* and *StcwINV2*

For the bimolecular fluorescence complementation (BiFC) analysis, the full-length cDNA fragments of *StInvInh1* and *StcwINV2* without their stop codon were amplified and subcloned into the BiFC vectors, respectively (Walter et al., 2004). The subsequent constructs were transformed into the BY-2 cells by particle bombardment as previously described (Liu et al., 2010). Afterwards, the transformants were incubated at 26°C for 24 h in dark. Fluorescence signals for YFP (excitation 514 nm) of the successful transformants were detected and recorded by confocal laser scanning microscope (LSM510 Meta, Zeiss, Germany).

Statistical analyses

One-way ANOVA test was accomplished for data analyses using IBM SPSS Statistics 20. The student's t-test was carried out using the software in Excel 2017 (Microsoft, USA). Data are means ± SD from at least three independent replicates. Differences depicted as "*" and "**" were accepted as significant at $P < 0.05$ or 0.01.

Results

Expression patterns of *StInvInh1* in various organs of potato

In our previous study, two putative cell wall invertase inhibitor genes (*StInvInh1* and *StInvInh3*) were isolated (Liu et al., 2010). To compare the expression levels of *StInvInh1* and *StInvInh3* in various organs, their transcripts were estimated by RNA-seq data from potato genotype RH (http://spuddb.uga.edu/). The results revealed a low or undetectable expression of *StInvInh3* in various organs, whereas *StInvInh1* showed an overall higher expression, with the highest transcript levels in flower and stamen (Figure 1A). The expression patterns of *StInvInh1* and *StInvInh3* were further analyzed in various organs by RT-qPCR (Figure 1B). Consistent with the RNA-seq data, RT-qPCR analysis showed that *StInvInh3* was only detectable in flower and flower bud with a low abundance, whereas *StInvInh1* exhibited constitutive expression with a higher expression level in flower and flower buds, senescence leaves, and stems. Notably, the mRNA level of *StInvInh1* decreased with the development of tubers from stolon to tuber. These results indicated that *StInvInh1* may work as an important *INH* gene involved in biological processes of potato growth and development. Thus, *StInvInh1* was selected for further study.

For more detail on *StInvInh1* expression, its promoter activity was further analyzed. According to the *StInvInh1* gene sequence (Soltu.DM.12G001750.1) in potato reference genome of *S. tuberosum* group *Phureja* clone DM 1-3 (Pham et al, 2020), an approximate 2.2 kb length of 5'-flanking sequences of *StInvInh1* was isolated from E3 genomic DNA (Figure S1). The sequencing results indicated that an abscisic acid (ABA)-responsive element (ABRE), a methyl jasmonate-responsive element (CGTAC-motif), an auxin-responsive element (TGA-element), a gibberellin-responsive element (P-box), a stress-responsive element (TC-rich element), and several light-responsive elements (I-box and Box4) were predicted over the 2.2-kb promoter region, suggesting that the expression of *StInvInh1* may be regulated by different physiological and environmental factors. Subsequently, to estimate the promoter activity of the

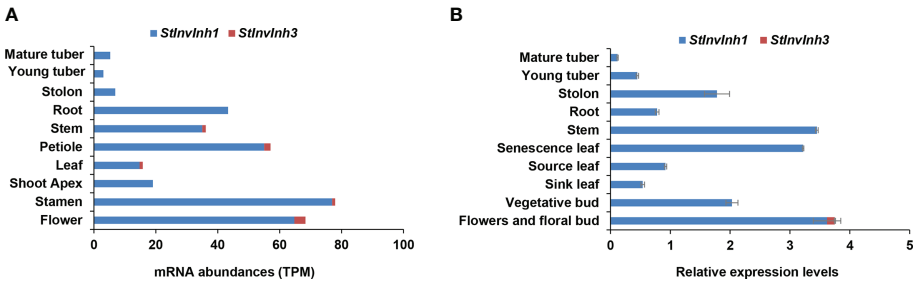

FIGURE 1
Relative expression levels of putative cell wall invertase inhibitor genes in various organs of potato plants. **(A)** The mRNA abundances of *StInvInh1* and *StInvInh3* are estimated from RNA-seq data of potato genotype RH *in silico*. **(B)** The relative expression levels of *StInvInh1* and *StInvInh3* genes are presented in relation to the expression levels of *ef1α* (AB061263) transcripts (100) by RT-qPCR. Data are means ± SD of three independent samples.

isolated promoter sequence, the transient expression assays were performed using the dual-luciferase reporter assays. The dual luciferase reporter plasmids harboring the 2.2-kb *StInvInh1* promoter sequence were fused to *LUC*, and the *REN* driven by the CaMV35S promoter was used as an internal control (Figure 2A). Compared with the empty control, the promoter activity of the 5'-flanking sequence of *StInvInh1* was detectable. In addition, its promoter activity was activated by ABA (Figure 2B). These results suggested that the 2.2-kb promoter region of *StInvInh1* is a functional promoter.

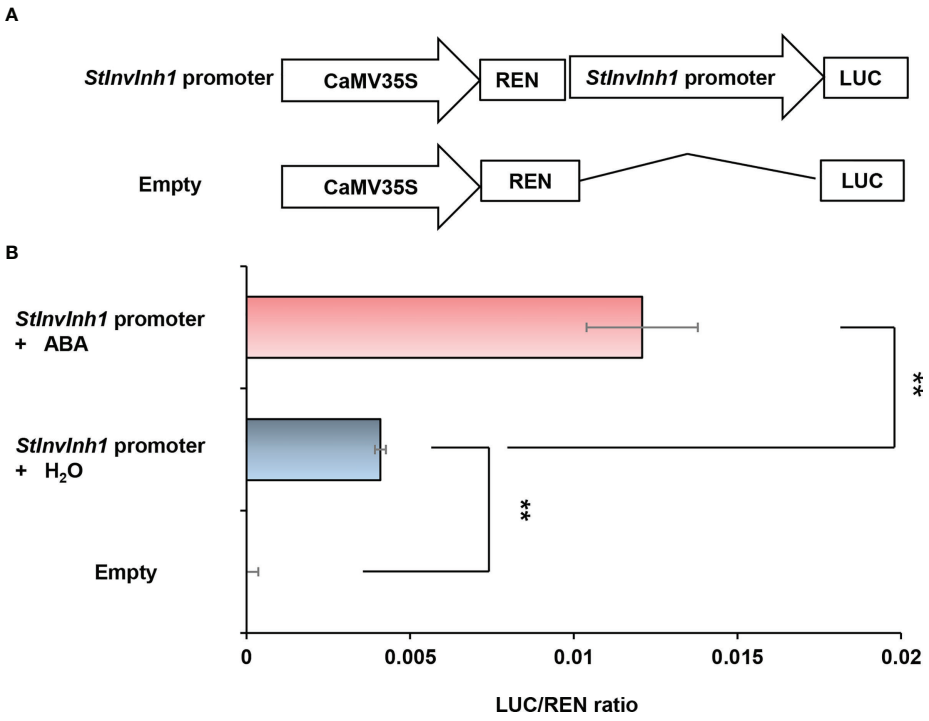

FIGURE 2
Estimation of the promoter activity of the 2.2-kb *StInvInh1* promoter sequence by the dual-luciferase reporter assays. **(A)** Schematic representation of the double-reporter plasmids used in the assay. The double-reporter plasmids contain the *StInvInh1* or empty promoter fused to LUC luciferase and REN luciferase driven by CaMV35S. **(B)** The promoter activity of the 2.2-kb *StInvInh1* promoter sequence. The dual-luciferase reporter vectors were introduced into tobacco leaves by *Agrobacterium tumefaciens* strain GV3101. The infiltrated tobacco leaves were spayed by ABA (50 mM) or H_2O. After 48 h from the infiltration, LUC and REN luciferase activities were assayed. Each value represents the means of three biological replicates, and vertical bars represent the S.D. **Significant differences in values ($P < 0.01$) by Student's t-test.

Then, the promoter sequence was fused to the coding sequence of β-glucuronidase (GUS) to construct a vector denoted as *pInh1::GUS*, and transformed to potato E3. The four-week-old plantlets of the transgenic lines were stained blue by X-Gluc solution (Figure 3), further demonstrating that the 5'-flanking sequence of *StInvInh1* possessed promoter activity. The GUS signal was detected in almost all tested organs and seems to mainly appear in the vascular bundles of stems. The strength of the GUS signal increased with the development of leaves in plantlets but decreased with the development of micro-tubers *in vitro* (Figures 3B, C). The RT-qPCR analysis revealed that the mRNA abundances of *GUS* were in accordance with the histochemical assay. Furthermore, a similar expression pattern was also observed between *GUS* and *StInvInh1* in transgenic lines (Figure 3D), indicating that the promoter function of the isolated sequence is similar with that of the *StInvInh1* native promoter.

Inhibitory functions of StInvInh1

To determine whether StInvInh1 is a functional INH of CWI, the recombinant StInvInh1 protein's inhibitory activity was tested by incubating with CWI fractions from potato leaves. Heterologous expression in the *E. coli* strain Rosetta-gami^{TM} (DE3) yielded N-terminal His fusion proteins of StInvInh1. The purified StInvInh1 was recovered by Ni-TED affinity chromatography (Figure 4A). A decrease in the CWI activity levels was observed upon increasing the recombinant StInvInh1 protein concentration (Figure 4B), suggesting the StInvInh1 function as an INH of CWI *in vitro*.

A further confirmation of the protein–protein interaction between StInvInh1 and CWI was performed in living plant cells using the BiFC. Since *StcwINV2* was potentially co-expressed with *StInvInh1* in tested organs (Liu et al., 2011), it was selected as a representative of CWIs in potato. Sets of pSPYNE-35S and pSPYCE-35S constructs of *StInvInh1* and *StcwINV2* were transformed the tobacco BY-2 cells. A fluorescence signal was observed when *StcwINV2-YFP^{C}* was co-expressed with *StInvInh1-YFP^{N}*, while the control cells transformed with any combination with empty vectors produced no fluorescence (Figure 4C). The results indicated that StInvInh1 interacted with StcwINV2 *in vivo*. Taken together, these results clearly defined the StInvInh1 targeted CWI *in situ*.

Silencing *StInvInh1* expression specifically releases CWI activities in transgenic plantlets

To investigate the physiological roles of *StInvInh1 in vivo*, transgenic potatoes were generated by a RNA interference (RNAi) approach to downregulate the *StInvInh1* mRNA abundances. No obvious phenotypic difference was observed in four-week-old plantlets between RNAi lines and WT (Figure S2). Three independent RNAi transgenic lines (RNAi29, RNAi50 and RNAi60) with transcripts suppressed by over 80% (82.8% – 95.1%) in plantlets were selected for detailed further characterization. Since StInvInh1 possessed its inhibitory function *in vitro*, its cognate invertase activities were investigated in plantlets. Firstly, the acid invertase activities in the 10-day-old plantlets were visualized by a histochemical activity stain *in situ*. The NBT staining of the RNAi plantlets resulted in a darker blue than that of WT control, suggesting elevated acid invertase activities, while no color appearing in either RNAi plants or WT in the absence of substrate (sucrose) (Figure 5A). The invertase activity was then assayed *via* an enzyme assay *in vitro*. The results clearly indicated that only the CWI activities were increased significantly in the RNAi plantlets, while the activities of VI and CI showed little variation in comparison with WT control (Figure 5B). In addition, the expression levels of *CWI* genes (*StcwINV1* and *StcwINV2*) were not affected in the RNAi plantlets (Figure 5C). These results suggest that the CWI activity may be mostly regulated by StInvInh1 at post-translational level *in vivo*. Taken together, the results showed that the silencing of *StInvInh1* expression resulted in significant elevations of CWI activities in the RNAi plantlets, suggesting that StInvInh1 is a physiological target of CWI.

Silencing *StInvInh1* expression enlarges size of micro-tuber *in vitro*

The characteristics of microtuberization were further investigated *in vitro*, and no significant difference was observed in either the percentage of microtuber formation by plantlets, the number of microtuber per plantlet, or the time of microtuber formation between WT and RNAi lines (data not shown). As excepted, significant increases in CWI activities were also observed in microtubers of the RNAi lines (Figures 6A–C). Interestingly, RNAi lines produced larger microtubers than the WT control (Figure 6D). The length and width of microtubers in RNAi lines were 9.37% –19.49% and 6.15% – 14.26% higher than that in WT control, respectively (Figure 6E). The length/width ratio in microtuber is similar between WT and RNAi lines. Compared with WT, the fresh weight of microtubers in RNAi lines increased by 33.35% – 64.15% with an evident increase in microtubers size. In addition, the dry weight of microtubers in RNAi lines also increased by 17.66% – 39.79%. However, the dry matter contents in two RNAi lines decreased significantly (Table 1). These findings demonstrate that the proportion of water content increased is higher than that of dry matter in microtuber production of RNAi lines. Furthermore, a significant increase in contents of sucrose, glucose and starch in the RNAi lines, while a little variation of fructose in comparison with the WT control (Table 1). These findings suggest that the elevated

10.3389/fpls.2022.1015815

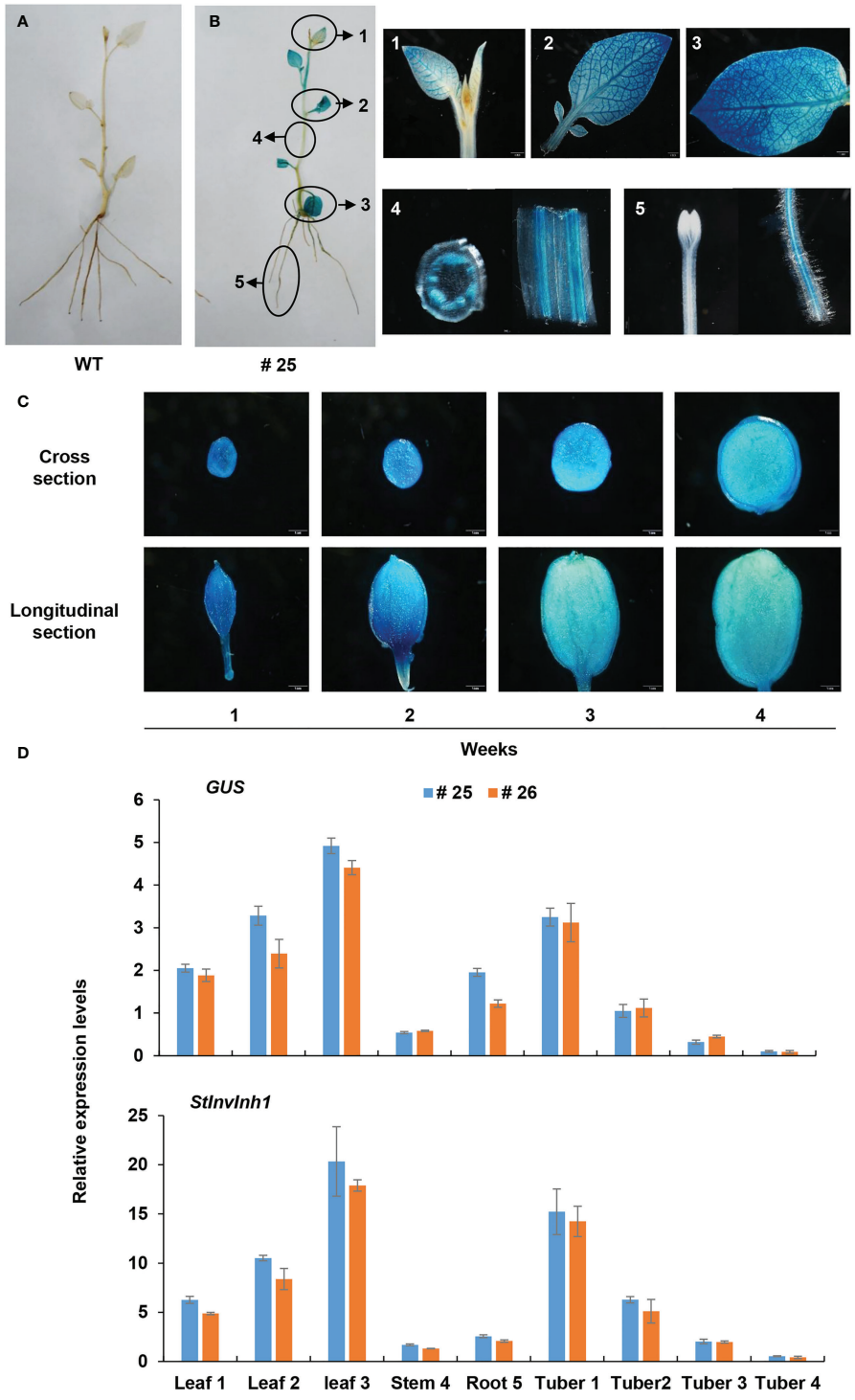

FIGURE 3
Expression pattern of GUS under the control of the *StInvInh1* promoter. **(A)** GUS staining in plantlets of WT; **(B)** GUS staining in plantlets of a representative transgenic line (#25); **(C)** GUS staining in micro-tubers of a representative transgenic line (#25); **(D)** The relative expression levels of *GUS* and *StInvInh1* in two representative transgenic line (#25 and #26). The 4-week-old plantlets and micro-tubers *in vitro* were subjected to the GUS staining and *GUS* expression. Leaves, stems, roots and developing micro-tubers were observed. Each repeat sample contains at least 6 plantlets or micro-tubers. Each sample was distributed into two groups. One was used for histochemical GUS staining; the other was frozen in liquid nitrogen and stored at -80°C for *GUS* expression analysis. The expression level of potato *ef1α* (AB061236) was set as 100 and used for normalization. Each data point is mean value of triplicate readings.

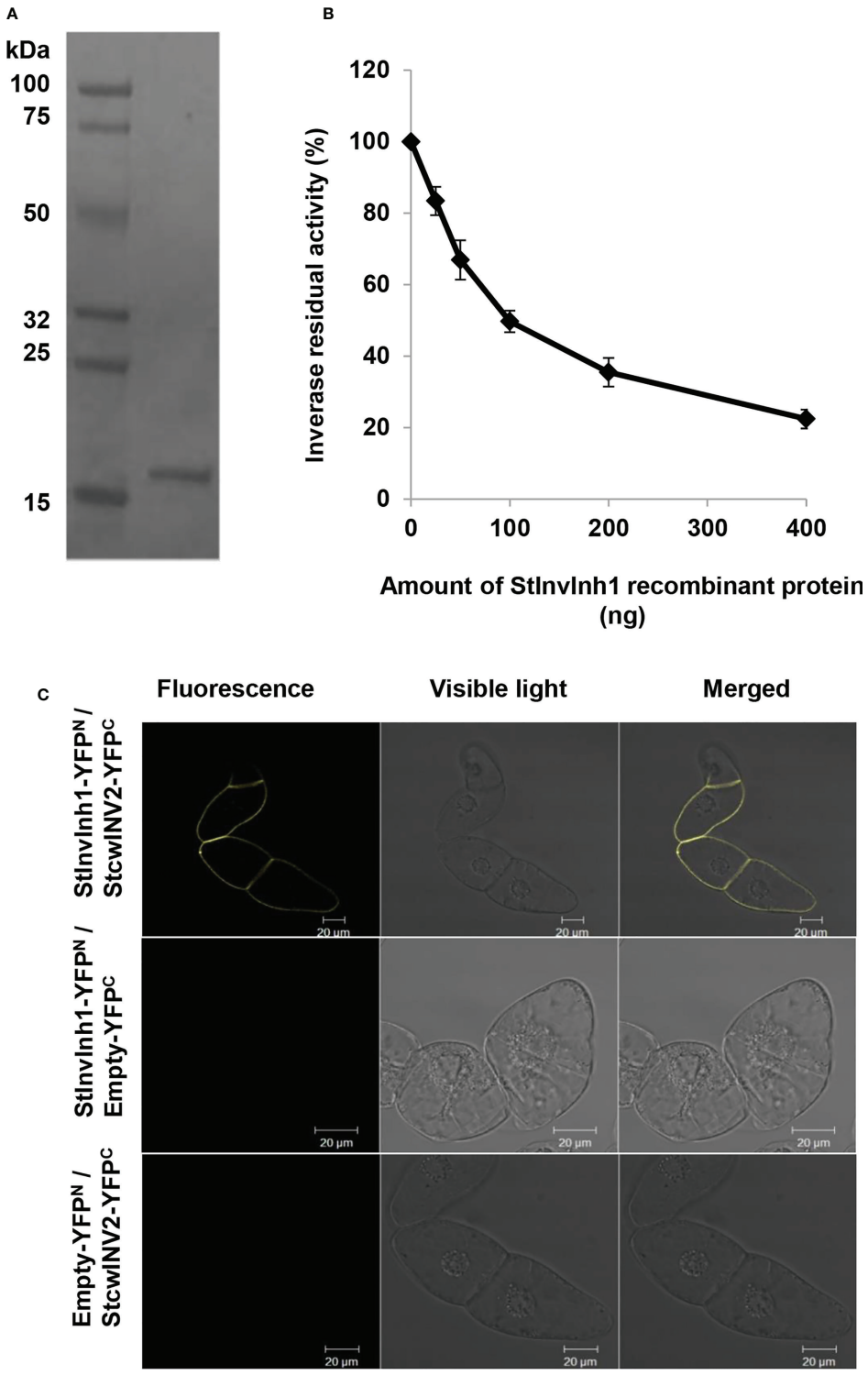

FIGURE 4
Inhibitory functions of StInvInh1. **(A)** The purified recombinant StInvInh1 protein; **(B)** Inhibitory effects of recombinant StInvInh1 protein on CWI activity in potato. Dose-dependent effects of StInvInh1 protein on CWI activity isolated from potato leaves are shown. Residual invertase activity was measured at pH 4.6 and 37°C after 30 min pre-incubation of the recombinant StInvInh1 protein and crude CWI in potato leaves. **(C)** Interaction of StInvInh1 and StcwINV2 proteins in tobacco BY-2 cells by bimolecular fluorescence complementation. Tobacco BY-2 cells were transformed by particle bombardment with a set of constructs for StInvInh1-YFP^N and StcwINV2-YFP^C, StInvInh1-YFP^N and empty-YFP^C, empty -YFP^N and StcwINV2-YFP^C, respectively.

10.3389/fpls.2022.1015815

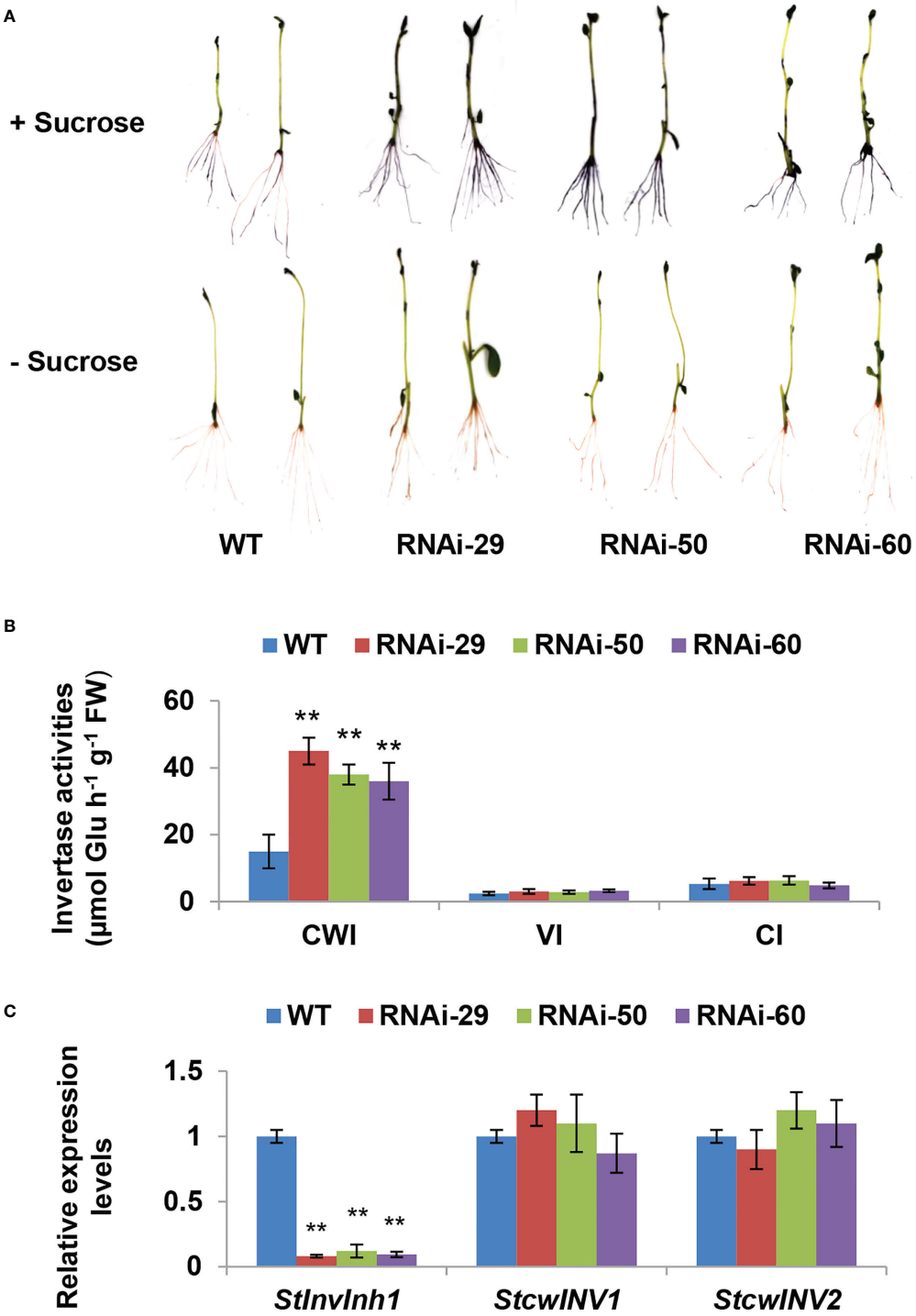

FIGURE 5
Silencing *StInvInh1* expression specifically releases CWI activity in transgenic plantlets. **(A)** Histochemical staining of NBT indicating the increased acid invertase activities in the RNAi plantlets. **(B)** The invertase activity determined by enzyme assay *in vitro* indicating the significantly increased the CWI activity in the RNAi plantlets without impacting the activities of VI and NI. **(C)** RT-qPCR analysis revealed that *StInvInh1* was suppressed in the RNAi plantlets without impact on mRNA levels of the two CWI genes, *StcwINV1* and *StcwINV2*. The relative expression levels of *StInvInh1*, *StcwINV1* and *StcwINV2* are presented in relation to the expression level of *ef1α* (AB061263) transcripts (100). The relative expression level of each gene and each enzyme activity in transgenic lines was compared with that in wild-type control E3. Each value was the mean ± SD of three biological replicates. **Significant differences in values ($P < 0.01$) by Student's t-test.

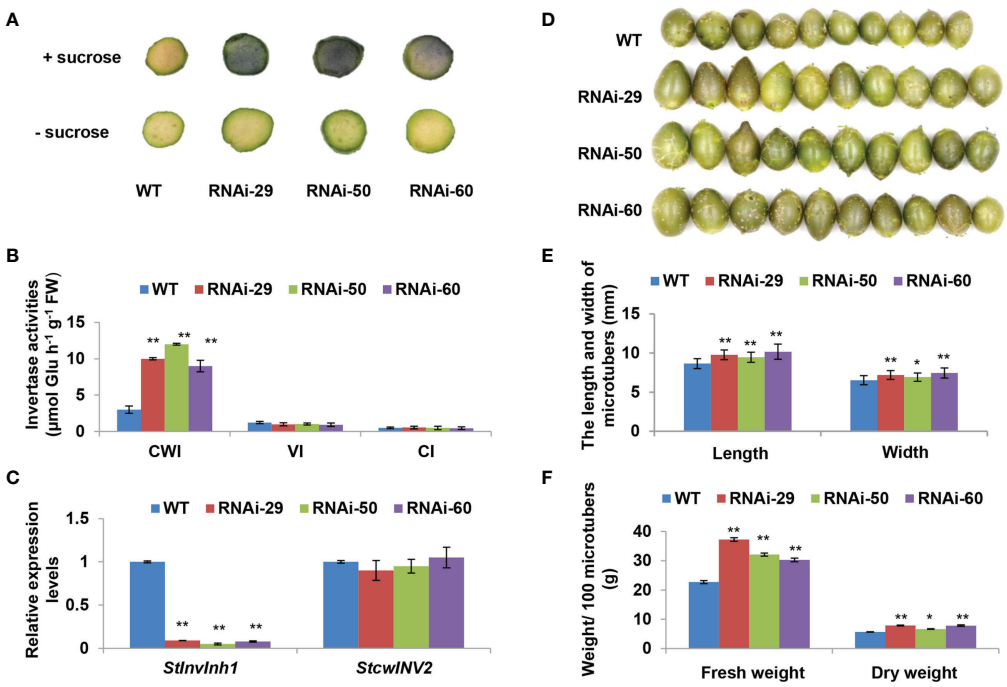

FIGURE 6
Performances of microtuber size and weight in RNAi lines. **(A)** Histochemical staining of NBT indicating the increased acid invertase activities of two-week-old microtubers in the RNAi lines. **(B)** The invertase activity determined by enzyme assay *in vitro* indicating the significantly increased the CWI activity in the RNAi micro-tubers without impacting the activities of VI and NI. **(C)** RT-qPCR analysis revealed that *StInvInh1* was suppressed in the RNAi micro-tubers without impact on mRNA levels of *StcwINV2*. **(D)** Performance of micro-tuber size in RNAi lines (10 four-week-old microtubers are shown in each line). **(E)** The length and width of micro-tubers in RNAi lines. **(F)** The fresh and dry weight of microtubers in RNAi lines. The relative expression levels of *StInvInh1* and *StcwINV2* are presented in relation to the expression levels of *ef1α* (AB061263) transcripts (100). The relative expression level of each gene and each enzyme activity in transgenic lines was compared with that in wild-type control E3. Each value was the mean ± SD of three biological replicates. Significant differences in values (**P < 0.01, *P < 0.05) by Student's t-test.

CWI activities are more closely associated with increases in size and dry matter production of microtubers.

Discussion

CWI-mediated sucrose metabolism and signaling is central to plant development (Ruan, 2014; Ruan, 2022). Apart from the transcriptional regulatory mechanism of invertase activities, emerging evidence also indicates that the subtle control of enzyme activities depends on the post-translational regulatory mechanism through interaction with their inhibitors (INHs) (Rausch and Geiner, 2004). Although the INH was initially discovered in potato as early as in the 1960s (Schwimmer et al., 1961; Pressey and Shaw, 1966), the corresponding cDNAs from *Nicotiana tabacum* was cloned until late 1990s (Greiner et al., 1998; Greiner et al., 1999). Sequence analyses *in silico* suggested that the INH family is moderately conserved within different plant species (Rausch and Greiner, 2004). Both INHs and PMEIs (pectin methylesterase inhibitors) belong to the same superfamily named PMEI-related protein based on their similar protein structure, enabling it's difficult to

TABLE 1 The contents of dry matter, sugar and starch in microtubers of RNAi lines.

Lines	Dry matter content (%)	Sucrose content (mg/g DW)	Glucose content (mg/g DW)	Fructose content (mg/g DW)	Starch content (%)
WT	24.91 ± 0.98	5.37 ± 0.07	2.37 ± 0.14	1.72 ± 0.50	30.28 ± 1.13
RNAi-29	21.21 ± 0.83*	7.43 ± 0.22**	3.74 ± 0.60**	1.78 ± 0.54	36.84 ± 1.18**
RNAi-50	20.71 ± 1.27*	8.77 ± 0.38**	3.16 ± 0.21**	1.75 ± 0.07	33.54 ± 1.05*
RNAi-60	25.85 ± 0.78	8.06 ± 0.13**	3.01 ± 0.72**	1.67 ± 0.15	38.81 ± 1.09**

Data represent mean ± SD of at least three biological replicates. Asterisks indicate significant differences in comparison with the WT as determined by Student's t-test: **P < 0.01, *P < 0.05.

distinguish them from sequence comparisons (Hothorn et al., 2004).

In our previous study, four cDNAs encoding putative INHs were isolated in potato. Among them, both StInvInh2A and StInvInh2B were identified as INHs of VI and play roles in regulating potato CIS by capping VI activity (Liu et al., 2010; Liu et al., 2013; Lin et al., 2015). Based on sequence phylogenetic analyses and subcellular localization, the other two putative INHs, StInvInh1 and StInvInh3, were expected as targets of CWIs (Liu et al., 2010). In combination with RNA-seq data, the RT-qPCR analyses of spatiotemporal expression of *StInvInh1* and *StInvInh3* revealed that *StInvInh1* showed an overall higher expression in all tested organs (Figure 1), indicating that *StInvInh1* may be an important putative *INH* gene related to biological processes in potato growth and development. Interestedly, interaction between StInvInh1 and VI/CWIs was identified in potato using modelling approaches (Datir and Ghosh, 2020). The targets of INHs need to be clarified through both *in vitro* and *in vivo* approaches (Liu et al., 2010; Liu et al., 2013; Coculo and Lionetti, 2022). In this study, enhanced evidences demonstrated that StInvInh1 functions as an INH of CWI in potato. Firstly, the activity of CWI protein from potato was inhibited by the recombinant StInvInh1 protein *in vitro* (Figure 4B). Secondly, the interaction of StInvInh1 and StcwINV2 was confirmed by the BiFC in BY-2 cells (Figure 4C), indicating that StInvInh1 targets CWI *in situ*. Finally, silencing the expression of *StInvInh1* elevated the CWI activity without having impact on expression levels of *CWIs*, suggesting that a high proportion of CWI activity is under post-translational control of StInvInh1 in potato. In addition, altered *StInvInh1* expression did not affect activities of VI and CI (Figure 5), indicating a high specificity of StInvInh1 in capping CWI activity. Collectively, these data strongly indicated that StInvInh1 functions as an INH of CWI in potato.

It is reported that INHs of CWI were shown to be ABA-responsive genes and predominantly expressed in flowers and seeds (Jin et al., 2009; Yang et al., 2020). The seed weight and production were improved by silencing or knock-out of *INHs* in tomato, *Arabidopsis*, and soybean (Jin et al., 2009; Su et al., 2016; Tang et al., 2017). Similarly, *StInvInh1* was also found to have the highest expression in flowers as well as in response to ABA (Figures 1, 2), suggesting its potential conserved role in seed development. In addition, the expression of *StInvInh1* appeared to decrease progressively with tuber development (Figures 1B, 3C, D), providing evidence of its potential role in tuber development. The critical role of CWI in sinks has been demonstrated through mutational and transgenic analyses. An endosperm-specific *CWI* gene mutant in maize resulted in miniature seeds (Cheng et al., 1996). The phenotype is probably caused by the suppression of auxin biosynthesis (LeClere et al., 2010) and reduced mitotic activity and cell size in the endosperm (Vilhar et al., 2002). A similar role for CWI in seed development was found in rice (Wang et al., 2008) and tomato (Zanor et al., 2009). However, it remains a debate whether and how CWI activity plays a role in tuber formation and development, a prerequisite for tuber production. Initially, the constitutive overexpression of the yeast invertase gene in apoplast caused the plants to appear to be under stress and yield penalty (Heineke et al., 1992; Büssis et al., 1997). Subsequently, the tuber-specific overexpression of yeast invertase gene in apoplast resulted in increased tuber size and total yield due to an increase in water content (Sonnewald et al., 1997; Hajirezaei et al., 2000; Ferreira and Sonnewald, 2012). Although these approaches to increasing CWI activities have been studied for the formation and development of tubers, the improvement of dry matter production in potato tubers seemed a failure. CWIs were co-evolved with vascular plants with the gene family expansion in seed plants from gymnosperm to angiosperm (Wan et al., 2018). CWI was reported to be encoded by multiple genes which have distinct but partially overlapping expression patterns in potato (Liu et al., 2011), suggesting a unique function for individual gene. These reports suggest that CWI activity need to be tightly regulated to balance development and stress adaptation for tuber production improvement in potato. Here, transgenic potato plants were generated by RNAi-mediated silencing of *StInvInh1* in order to investigate its effects on tuber formation and development. The microtuberization characteristics of RNAi lines were investigated *in vitro*. Interestingly, the specific suppression of *StInvInh1* expression significantly improved the size, fresh weight, and dry matter production of microtubers with remarkable elevated CWI activities (Figure 6). The results were consistent with the previous reports that the seed weight and production were improved by silencing or knock-out of *INHs* in tomato, *Arabidopsis*, and soybean (Jin et al., 2009; Su et al., 2016; Tang et al., 2017). The improvement of dry matter production of microtubers could result from the elevation of CWI activity during the early stages of tuber formation, because the class I patatin B33 promoter used to design tuber-specific constructs appears to be inactive in stolon and during the early stages of tuber formation (Tauberger et al., 1999). CWI could contribute to sink development by facilitating phloem unloading of sucrose and converting it to glucose and fructose as major nutrients and energy sources. Compared with WT, the sucrose and glucose contents were significantly increased in microtubers of RNAi lines with elevation of CWI activity (Table 1), probably promoting phloem unloading of sucrose. Moreover, CWI-mediated signaling can modulate the expression of sugar transporter and regulatory genes (Ru et al., 2017; Liao et al., 2020). Similarly, functional loss of *SlInvInh1* in tomato by genome editing increased sugar content of fruit (Kawaguchi et al., 2021). In this study, no obvious difference in fructose content was observed between WT and RNAi lines (Table 1). One possible explanation is that the utilization of fructose also was activated in RNAi lines, which resulting in a balance between fructose production and utilization. These findings,

together with evidence of glucose positively regulating cell division (Weber et al., 2005) indicate a role of CWI activity in early tuber development, which could partially explain a bigger microtuber size phenotype under elevation of CWI activity in microtubers. Tuberization in potato involves a switch from CWI-mediated apoplastic to Susy-mediated symplastic phloem unloading (Viola et al., 2001). However, no significant difference was observed in either the percentage of microtuber formation by plantlets, the number of microtuber per plantlet, or the time of microtuber formation between WT and RNAi lines (data not shown). It cannot be ruled out that the possibility of differences from tuberization conditions between *in vitro* and *in vivo*. The potential roles of *StInvInh1* in potato growth and development *in vivo* will be the subject of future investigations.

Conclusion

Emerging evidence has indicated that the CWIs play fundamental roles in plant reproductive development as well as the regulation of sucrose metabolism and homeostasis through fine-tuning the CWI activities. In this study, enhancive evidences demonstrate that StInvInh1 functions as an INH of CWI in potato, which results in an impact on microtuber development *in vitro*. In the future, we will confirm the roles of *StInvInh1* in potato growth and development *in vivo* and decipher the molecular evidence. Our results provide developmental evidence that *StInvInh1* plays a vital role in microtuber development in potato, which may promise great potential to improve tuber performance through manipulation of CWI activity in potato.

Data availability statement

The original contributions presented in the study are included in the article/Supplementary Material. Further inquiries can be directed to the corresponding author.

Author contributions

XL conceived and designed the experiments. CL performed most of the experiments. DX and SH performed the transformation and tuberization of potato. QC and SL helped with the promoter activity analysis. WS, LS, HS, and ZL helped with the vectors construction and biochemical analysis. XL and CL wrote the manuscript. RJ, DL, and JW were involved in data analysis and proofreading. All the authors discussed the results and collectively edited the manuscript. All authors contributed to the article and approved the submitted version.

Funding

This work was supported by the National Key Research and Development Program (NKRDP) (2018YFE0127900), the Natural Science Foundation of China (NSFC) (31571728), the Undergraduate Innovation and Entrepreneurship Training Program in SWU (UIETP) (202210635030), and the Science and Technology Partnership Program (STPP) (KY201904016).

Acknowledgments

The authors would like to thank NKRDP, NSFC, UIETP and STPP for funding this research. We are also grateful to Prof. Zhihua Liao from Southwest University for donating the pGreenII 0800-LUC vector.

Conflict of interest

The authors declare that the research was conducted in the absence of any commercial or financial relationships that could be construed as a potential conflict of interest.

Publisher's note

Supplementary material

The Supplementary Material for this article can be found online at: https://www.frontiersin.org/articles/10.3389/fpls.2022.1015815/full#supplementary-material

References

Barnes, W. J., and Anderson, C. T. (2018). Release, recycle, rebuild: Cell-wall remodeling, autodegradation, and sugar salvage for new wall biosynthesis during plant development. *Mol. Plant* 11, 31–46. doi: 10.1016/j.molp.2017.08.011

Bate, N. J., Niu, X., Wang, Y., Reimann, K. S., and Helentjaris, T. G. (2004). An invertase inhibitor from maize localizes to the embryo surrounding region during early kernel development. *Plant Physiol.* 134, 246–254. doi: 10.1104/pp.103.027466

Bhaskar, P. B., Wu, L., Busse, J. S., Whitty, B. R., Hamernik, A. J., Jansky, S. H., et al. (2010). Suppression of the vacuolar invertase gene prevents cold-induced sweetening in potato. *Plant Physiol.* 154, 939–948. doi: 10.1104/pp.110.162545

Büssis, D., Heineke, D., Sonnewald, U., Willmitzer, L., Raschke, K., and Heldt, H.-W. (1997). Solute accumulation and decreased photosynthesis in leaves of potato plants expressing yeast-derived invertase either in the apoplast, vacuole or cytosol. *Planta.* 202, 126–136. doi: 10.1007/s004250050111

Cheng, W. H., Taliercio, E. W., and Chourey, P. S. (1996). The miniature1 seed locus of maize encodes a cell wall invertase required for normal development of endosperm and maternal cells in the pedicel. *Plant Cell.* 8, 971–983. doi: 10.1105/tpc.8.6.971

Chen, L., Liu, X., Huang, X., Luo, W., Long, Y., Greiner, S., et al. (2019). Functional characterization of a drought-responsive invertase inhibitor from maize (*Zea mays* l.). *Int. J. Mol. Sci.* 20, 17. doi: 10.3390/ijms20174081

Coculo, D., and Lionetii, V. (2022). The plant invertase/pectin methylesterase inhibitor superfamily. *Front. Plant Sci.* 13. doi: 10.3389/fpls.2022.863892

Datir, S., and Ghosh, P. (2020). *In silico* analysis of the structural diversity and interactions between invertases and invertase inhibitors from potato (*Solanum tuberosum* l.). *3. Biotech.* 10 (4), 178. doi: 10.1007/s13205-020-02171-y

Ferreira, S., and Sonnewald, U. (2012). The mode of sucrose degradation in potato tubers determines the fate of assimilate utilization. *Front. Plant Sci.* 3. doi: 10.3389/fpls.2012.00023

Greiner, S., Krausgrill, S., and Rausch, T. (1998). Cloning of a tobacco apoplasmic invertase inhibitor. *Plant Physiol.* 116, 733–742. doi: 10.1104/pp.116.2.733

Greiner, S., Rausch, T., Sonnewald, U., and Herbers, K. (1999). Ectopic expression of a tobacco invertase inhibitor homolog prevents cold-induced sweetening of potato tubers. *Nat. Biotechnol.* 17, 708–711. doi: 10.1038/10924

Hajirezaei, M. R., Takahata, Y., Trethewey, R. N., Willmitzer, L., and Sonnewald, U. (2000). Impact of elevated cytosolic and apoplastic invertase activity on carbon metabolism during potato tuber development. *J. Exp. Bot.* 51, 439–445. doi: 10.1093/jexbot/51.suppl_1.439

Heineke, D., Sonnewald, U., Büssis, D., Günter, G., Leidreiter, K., Wilke, I., et al. (1992). Apoplastic expression of yeast-derived invertase in potato. *Plant Physiol.* 100, 301–308. doi: 10.1104/pp.100.1.301

Helliwell, C. A., Wesley, S. V., Wielopolska, A. J., and Waterhouse, P. M. (2002). High-throughput vectors for efficient gene silencing in plants. *Funct. Plant Biol.* 29, 1217–1225. doi: 10.1071/fp02033

Hothorn, M., Van den Ende, W., Lammens, W., Rybin, V., and Scheffzek, K. (2010). Structural insights into the pH-controlled targeting of plant cell-wall invertase by a specific inhibitor protein. *Proc. Natl. Acad. Sci.* 107, 17427–17432. doi: 10.1073/pnas.1004481107

Hothorn, M., Wolf, S., Aloy, P., Greiner, S., and Scheffzek, K. (2004). Structural insights into the target specificity of plant invertase and pectin methylesterase inhibitory proteins. *Plant Cell.* 16, 3437–3447. doi: 10.1105/tpc.104.025684

Jin, Y., Ni, D.-A., and Ruan, Y.-L. (2009). Posttranslational elevation of cell wall invertase activity by silencing its inhibitor in tomato delays leaf senescence and increases seed weight and fruit hexose level. *Plant Cell.* 21, 2072–2089. doi: 10.1105/tpc.108.063719

Kawaguchi, K., Takei-Hoshi, R., Yoshikawa, I., Nishida, K., Kobayashi, M., Kusano, M., et al. (2021). Functional disruption of cell wall invertase inhibitor by genome editing increases sugar content of tomato fruit without decrease fruit weight. *Sci. Rep.* 11 (1), 21534. doi: 10.1038/s41598-021-00966-4

Klann, E. M., Hall, B., and Bennett, A. B. (1996). Antisense acid invertase (TIV1) gene alters soluble sugar composition and size in transgenic tomato fruit. *Plant Physiol.* 112, 1321–1330. doi: 10.1104/pp.112.3.1321

LeClere, S., Schmelz, E. A., and Chourey, P. S. (2010). Sugar levels regulate tryptophan-dependent auxin biosynthesis in developing maize kernels. *Plant Physiol.* 153, 306–318. doi: 10.1104/pp.110.155226

Liao, S., Wang, L., Li, J., and Ruan, Y.-L. (2020). Cell wall invertase is essential for ovule development through sugar signaling rather than provision of carbon nutrients. *Plant Physiol.* 183, 1126–1144. doi: 10.1104/pp.20.00400

Li, B., Liu, H., Zhang, Y., Kang, T., Zhang, L., Tong, J., et al. (2013). Constitutive expression of cell wall invertase genes increases grain yield and starch content in maize. *Plant Biotechnol. J.* 11, 1080–1091. doi: 10.1111/pbi.12102

Link, M., Rausch, T., and Greiner, S. (2004). In arabidopsis thaliana, the invertase inhibitors AtC/VIF1 and 2 exhibit distinct target enzyme specificities and expression profiles. *FEBS Lett.* 573, 105–109. doi: 10.1016/j.febslet.2004.07.062

Lin, Y., Liu, T., liu, J., Liu, X., Ou, Y., Zhang, H., et al. (2015). Subtle regulation of potato acid invertase activity by a protein complex of StvacINV1-StInvInh2B-SbSnRK1. *Plant Physiol.* 168, 1807–1819. doi: 10.1104/pp.15.00664

Liu, X., Chen, L., Shi, W., Xu, X., Li, Z., Liu, T., et al. (2021). Comparative transcriptome reveals distinct starch-sugar interconversion patterns in potato genotypes contrasting for cold-induced sweetening capacity. *Food Chem.* 334, 127550. doi: 10.1016/j.foodchem.2020.127550

Liu, X., Lin, Y., Liu, J., Song, B., Ou, Y., Zhang, H., et al. (2013). StInvInh2 as an inhibitor of StvacINV1 regulates the cold-induced sweetening of potato tubers by specifically capping vacuolar invertase activity. *Plant Biotechnol. J.* 11, 640–647. doi: 10.1111/pbi.12054

Liu, X., Shi, W., Yin, W., and Wang, J. (2017). Distinct cold responsiveness of a StInvInh2 gene promoter in transgenic potato tubers with contrasting resistance to cold-induced sweetening. *Plant Physiol. Biochem.* 111, 77–84. doi: 10.1016/j.plaphy.2016.11.021

Liu, X., Song, B., Zhang, H., Li, X.-Q., Xie, C., and Liu, J. (2010). Cloning and molecular characterization of putative invertase inhibitor genes and their possible contributions to cold-induced sweetening of potato tubers. *Mol. Genet. Genomics* 284, 147–159. doi: 10.1007/s00438-010-0554-3

Liu, J., and Xie, C. (2001). Correlation of cell division and cell expansion to potato microtuber growth *in vitro*. plant cell tiss. *Org. Cult.* 67, 159–164. doi: 10.1023/A:1011926504660

Liu, X., Zhang, C., Ou, Y., Lin, Y., Song, B., Xie, C., et al. (2011). Systematic analysis of potato acid invertase genes reveals that a cold-responsive member, StvacINV1, regulates cold-induced sweetening of tubers. *Mol. Genet. Genomics* 286, 109–118. doi: 10.1007/s00438-011-0632-1

Miller, M. E., and Chourey, P. S. (1992). The maize invertase-deficient miniature-1 seed mutation is associated with aberrant pedicel and endosperm development. *Plant Cell.* 4, 297–305. doi: 10.1105/tpc.4.3.297

Nicot, N., Hausman, J.-F., Hoffmann, L., and Evers, D. (2005). Housekeeping gene selection for real-time RT-PCR normalization in potato during biotic and abiotic stress. *J. Exp. Bot.* 56, 2907–2914. doi: 10.1093/jxb/eri285

Pham, G. M., Hamilton, J. P., Wood, J. C., Burke, J. T., Zhao, H., Vaillancourt, B., et al. (2020). Construction of a chromosome-scale long-read reference genome assembly for potato. *GigaScience* 9 (9), giaa100. doi: 10.1093/gigascience/giaa100

Pressey, R., and Shaw, R. (1966). Effect of temperature on invertase, invertase inhibitor, and sugars in potato tubers. *Plant Physiol. Biochem.* 41, 1657–1661. doi: 10.1104/pp.41.10.1657

Rausch, T., and Greiner, S. (2004). Plant protein inhibitors of invertases. *Biochim. Biophys. Acta. Protein Struct. Mol. Enzymol. B.* 1696, 253–261. doi: 10.1016/j.bbapap.2003.09.017

Rende, U., Wang, W., Gandla, M. L., Jönsson, L. J., and Niittylä, T. (2017). Cytosolic invertase contributes to the supply of substrate for cellulose biosynthesis in developing wood. *New Phytol.* 214, 796–807. doi: 10.1111/nph.14392

Ruan, Y.-L. (2014). Sucrose metabolism: Gateway to diverse carbon use and sugar signaling. *Annu. Rev. Plant Biol.* 65, 33–67. doi: 10.1146/annurev-arplant-050213-040251

Ruan, Y.-L. (2022). CWIN-sugar transporter nexus is a key component for reproductive success. *J. Plant Physiol.* 268, 153572. doi: 10.1016/j.jplph.2021.153572

Ruan, Y.-L., Jin, Y., Yang, Y.-J., Li, G.-J., and Boyer, J. S. (2010). Sugar input, metabolism, and signaling mediated by invertase: roles in development, yield potential, and response to drought and heat. *Mol. Plant* 3, 942–955. doi: 10.1093/mp/ssq044

Ru, L., Osorio, S., Wang, L., Fernie, A. R., Patrick, J. W., and Ruan, Y.-L. (2017). Transcriptomic and metabolomics responses to elevated cell wall invertase activity during tomato fruit set. *J. Exp. Bot.* 68, 4263–4279. doi: 10.1093/jxb/erx219

Schwimmer, S., Makower, R. U., and Rorem, E. S. (1961). Invertase & invertase inhibitor in potato. *Plant Physiol.* 36, 313–316. doi: 10.1104/pp.36.3.313

Sergeeva, L. I., Keurentjes, J. J., Bentsink, L., Vonk, J., van der Plas, L. H., Koornneef, M., et al. (2006). Vacuolar invertase regulates elongation of *Arabidopsis thaliana* roots as revealed by QTL and mutant analysis. *Proc. Natl. Acad. Sci.* 103, 2994–2999. doi: 10.1073/pnas.0511015103

Sonnewald, U., Hajirezaei, M.-R., Kossmann, J., Heyer, A., Trethewey, R. N., and Willmitzer, L. (1997). Increased potato tuber size resulting from apoplastic expression of a yeast invertase. *Nat. Biotechnol.* 15, 794–797. doi: 10.1038/nbt0897-794

Sturm, A. (1999). Invertases. primary structures, functions, and roles in plant development and sucrose partitioning. *Plant Physiol.* 121, 1–7. doi: 10.1104/pp.121.1.1

Su, T., Wolf, S., Han, M., Zhao, H., Wei, H., Greiner, S., et al. (2016). Reassessment of an arabidopsis cell wall invertase inhibitor AtCIF1 reveals its role in seed germination and early seedling growth. *Plant Mol. Biol.* 90, 137–155. doi: 10.1007/s11103-015-0402-2

Tang, X., Su, T., Han, M., Wei, L., Wang, W., Yu, Z., et al. (2017). Suppression of extracellular invertase inhibitor gene expression improves seed weight in soybean (*Glycine max*). *J. Exp. Bot.* 68, 469–482. doi: 10.1093/jxb/erw425

Tauberger, E., Hoffmann-Benning, S., Fleischer-Notter, H., Willmitzer, L., and Fisahn, J. (1999). Impact of invertase overexpression on cell size, starch granule formation and cell wall properties during tuber development in potatoes with modified carbon allocation patterns. *J. Exp. Bot.* 50, 477–486. doi: 10.1093/jxb/50.333.477

Vilhar, B., Kladnik, A., Blejec, A., Chourey, P. S., and Dermastia, M. (2002). Cytometrical evidence that the loss of seed weight in theminiature1 seed mutant of maize is associated with reduced mitotic activity in the developing endosperm. *Plant Physiol.* 129, 23–30. doi: 10.1104/pp.001826

Viola, R., Roberts, A. G., Haupt, S., Gazzani, S., Hancock, R. D., Marmiroli, N., et al. (2001). Tuberization in potato involves a switch from apoplastic to symplastic phloem unloading. *Plant Cell.* 13, 385–398. doi: 10.1105/tpc.13.2.385

Walter, M., Chaban, C., Schütze, K., Batistic, O., Weckermann, K., Näke, C., et al. (2014). Visualization of protein interactions in living plant cells using bimolecular fluorescence complementation. *Plant J.* 40, 428–438. doi: 10.1111/j.1365-313X.2004.02219

Wang, L., Li, X.-R., Lian, H., Ni, D.-A., He, Y.-K., Chen, X.-Y., et al. (2010). Evidence that high activity of vacuolar invertase is required for cotton fiber and arabidopsis root elongation through osmotic dependent and independent pathways, respectively. *Plant Physiol.* 154, 744–756. doi: 10.1104/pp.110.162487

Wang, E., Wang, J., Zhu, X., Hao, W., Wang, L., Li, Q., et al. (2008). Control of rice grain-filling and yield by a gene with a potential signature of domestication. *Nat. Genet.* 40, 1370–1374. doi: 10.1038/ng.220

Wan, H., Wu, L., Yang, Y., Zhou, G., and Ruan, Y.-L. (2018). Evolution of sucrose metabolism: The dichotomy of invertases and beyond. *Trends Plant Sci.* 23, 163–177. doi: 10.1016/j.tplants.2017.11.001

Weber, H., Borisjuk, L., and Wobus, U. (2005). Molecular physiology of legume seed development. *Annu. Rev. Plant Biol.* 56, 253–279. doi: 10.1146/annurev.arplant.56.032604.144201

Xiang, L., Le Roy, K., Bolouri-Moghaddam, M.-R., Vanhaecke, M., Lammens, W., Rolland, F., et al. (2011). Exploring the neutral invertase–oxidative stress defence connection in *Arabidopsis thaliana*. J. *Exp. Bot.* 62, 3849–3862. doi: 10.1093/jxb/err069

Yang, W., Chen, S., Cheng, Y., Zhang, N., Ma, Y., Wang, W., et al. (2020). Cell wall/vacuolar inhibitor of fructosidase 1 regulates ABA response and salt tolerance in *Arabidopsis. Plant Signal Behav.* 15 (4), 1744293. doi: 10.1080/15592324.2020.1744293

Zanor, M. I., Osorio, S., Nunes-Nesi, A., Carrari, F., Lohse, M., Usadel, B., et al. (2009). RNA Interference of LIN5 in tomato confirms its role in controlling brix content, uncovers the influence of sugars on the levels of fruit hormones, and demonstrates the importance of sucrose cleavage for normal fruit development and fertility. *Plant Physiol.* 150, 1204–1218. doi: 10.1104/pp.109.136598

frontiers | Frontiers in Plant Science

TYPE Original Research
PUBLISHED 07 October 2022
DOI 10.3389/fpls.2022.1021617

OPEN ACCESS

EDITED BY
Leo Sabatino,
University of Palermo, Italy

REVIEWED BY
Yuling Lin,
Fujian Agriculture and Forestry University, China
Jiabao Ye,
Yangtze University, China

*CORRESPONDENCE
Botao Song
songbotao@mail.hzau.edu.cn

SPECIALTY SECTION
This article was submitted to Crop and Product Physiology, a section of the journal Frontiers in Plant Science

RECEIVED 17 August 2022
ACCEPTED 14 September 2022
PUBLISHED 07 October 2022

CITATION
Zhang H, Zhao Y, Zhao X, Zhang Z, Liu J, Shi M and Song B (2022) Methylation level of potato gene *OMT30376* regulates tuber anthocyanin transformations. *Front. Plant Sci.* 13:1021617. doi: 10.3389/fpls.2022.1021617

Methylation level of potato gene *OMT30376* regulates tuber anthocyanin transformations

Huiling Zhang[1], Yanan Zhao[1], Xijuan Zhao[2,3], Zhonghua Zhang[1], Ju Liu[1], Minghui Shi[4] and Botao Song[2,3]*

[1]College of Horticulture and Plant Protection, Henan University of Science and Technology, Luoyang, China, [2]Key Laboratory of Horticultural Plant Biology, Ministry of Education, Huazhong Agricultural University, Wuhan, China, [3]Key Laboratory of Potato Biology and Biotechnology, Ministry of Agriculture and Rural Affairs, Huazhong Agricultural University, Wuhan, China, [4]Yichang Agricultural Technology Extension Center, Yichang, China

After anthocyanin synthesis, a variety of anthocyanin compounds are produced through further methylation, glycosylation, and acylation. However, the effect of the potato methylase gene on anthocyanin biosynthesis has not been reported. Red and purple mutation types appear in tubers of the potato cultivar 'Purple Viking' with chimeric skin phenotypes. In this study, transcriptome and anthocyanin metabolome analyses were performed on skin of Purple Viking tubers and associated mutants. According to the metabolome analysis, the transformation of delphinidin into malvidin-3-O-glucoside and petunidin 3-O-glucoside and that of cyanidin into rosinidin O-hexoside and peonidin-3-O-glucoside were hindered in red tubers. Expression of methyltransferase gene *OMT30376* was significantly lower in red tubers than in purple ones, whereas the methylation level of *OMT30376* was significantly higher in red tubers. In addition, red skin appeared in tubers from purple tuber plants treated with S-adenosylmethionine (SAM), indicating the difference between purple and red was caused by the methylation degree of the gene *OMT30376*. Thus, the results of the study suggest that the *OMT30376* gene is involved in the transformation of anthocyanins in potato tubers. The results also provide an important reference to reveal the regulatory mechanisms of anthocyanin biosynthesis and transformation.

KEYWORDS

***OMT30376* gene, methylation level, gene expression, anthocyanin transformation, potato**

Introduction

Potato (*Solanum tuberosum* L.) is the fourth largest crop after wheat, rice, and corn and is used as a grain, vegetable, feed, and industrial raw material. Pigmented potato is rich in anthocyanins, which give tuber skin and flesh color, including purple, blue, and red (Fossen and Andersen, 2000). Biosynthesis and accumulation of anthocyanins can

increase plant resistance to different biological and abiotic stresses, such as low temperature, ultraviolet radiation, drought stress, and diseases (Liu et al., 2019). Anthocyanins also benefit human health because of strong antioxidant capacity (Heim et al., 2002; Khoo et al., 2017). The antioxidant capacity of pigmented potato tubers is three to five times that of yellow and white tubers (Brown, 2005). Consuming pigmented potatoes can also significantly reduce the incidence rate of prostate cancer and colon cancer (Reddivari et al., 2007).

Anthocyanins are synthesized through the flavonoid pathway, which includes both structural and regulatory genes. Structural genes encode enzymes that primarily catalyze the formation of anthocyanin through three main synthetic pathways, namely cyanidin, pelargonidin and delphinidin pathways (Liu et al., 2018). Further modification of anthocyanins, including methylation, glycosylation, and acylation of the three aglycones, can produce a variety of anthocyanin compounds and enhance color phenotypes. Those processes are catalyzed by anthocyanin O-methyltransferase (OMT), flavonoid 3-glucosyl transferase (3GT), and acyltransferase (AT), respectively (Rausher, 2008; Wessinger and Rausher, 2012). The tissue-specific expression of structural genes is mainly regulated by the transcription factors R2R3-MYB, basic helix-loop-helix (bHLH), WD-repeats (WDR), and the MYB-bHLH-WDR (MBW) complex (Hichri et al., 2011).

Gene methylation is the process of transferring an activated methyl from S-adenosylmethionine (SAM) to N-, C-, O- or s-nucleophiles of receptor molecules, which occur widely in plants and animals (Klimasauskas and Weinhold, 2007). Methylation is an epigenetic modification that can affect many biological processes, including growth and development of fruits (Ma et al., 2018; Guo et al., 2019) and anthocyanin biosynthesis (Jiang et al., 2020). The anthocyanin content of a yellow-skinned apple mutant was lower than that of its parent because of the higher methylation level of the *MdMYB10* promoter (El-Sharkawy et al., 2015). Similar results are also observed in a red-bud apple (Xu et al., 2012). When the key regulatory gene in anthocyanin biosynthesis in red-fleshed radish, *RsMYB1*, is mutated because of a hypermethylated transposon sequence in the promoter, white-fleshed radish is produced. Methylation of the *RsMYB1* promoter leads to a decrease in gene expression and affects the biosynthesis and accumulation of anthocyanin (Wang et al., 2020).

Most methyltransferases act on hydroxyl and carboxyl groups and are called O- methyltransferases (OMTs). The OMTs can catalyze specific substrates to produce a wide variety of anthocyanin compounds that enrich color phenotypes (Wessinger and Rausher, 2012). Several OMT genes involved in the formation of O-methylated anthocyanins have been previously reported (Sakata et al., 1995; Hugueney et al., 2009). Genetic analysis of anthocyanin biosynthesis in petunia shows that *MT1/MT2* and *MF1/MF2*, two pairs of repetitive genes, are responsible for the methylation of anthocyanin molecules (Wiering and Devlaming, 1977). Owing to the action of OMTs, the content of anthocyanin components containing methoxyl and hydroxyl groups changes. In studies on tree peony petals, as the number of methoxyl groups increases, the transformation from red to purple also increases (Sakata et al., 1995). The red–purple-flowered cyclamen mutant appeared in purple-flowered cyclamen following ion-beam irradiation (Kondo et al., 2009), and the major anthocyanins in the petals of red–purple-flowers and purple-flowers were delphinidin 3, 5-diglucoside and malvidin 3, 5-diglucoside, respectively. In further research, *CkmOMT2* catalysis of the 3′ or 3′5′ O-methylation of the B-ring of anthocyanin substrates was only detected in purple-flowered cyclamen, and not in the red–purple-flowered mutant. Therefore, defective *CkmOMT2* gene expression was responsible for the change in anthocyanin composition and flower coloration in mutants (Kondo et al., 2009). Genes of O-methyltransferases are also found in purple-flowered (*PsAOMT*) and red-flowered (*PtAMOT*) paeonia plants. Owing to the difference of a single amino acid between PsAOMT and PtAMOT, there are significant differences in gene expression and enzyme activity, which ultimately affect the formation of purple (Du et al., 2015). Thus, previous results show that OMT genes have important roles in the transformation from red anthocyanin to purple anthocyanin. However, whether potato OMTs regulate tuber anthocyanin transformation remains unclear.

In the present study, the transcriptome and anthocyanin metabolic components of the potato cultivar Purple Viking and its red and purple mutant tubers were analyzed. The results showed that methylation level of the O*MT30376* gene might affect anthocyanin transformation in tubers. The study will provide a theoretical basis to reveal the molecular mechanism regulating anthocyanin biosynthesis in potato tubers.

Materials and methods

Plant materials

The potato (*Solanum tuberosum* L.) 'Purple Viking' and its mutants were grown in 24-cm-diameter plastic pots in a greenhouse with 16 h of light per day supplied by lamps. Three biological replicates were made for each material for subsequent anthocyanin content and transcriptome analysis. At 80 d after planting, tubers were harvested according to skin color. Skin (1 mm thick) of Purple Viking tubers (PurS), flesh of Purple Viking tubers (PurF), Skin (1 mm thick) of red mutant (M-R) and purple mutant (M-P) of Purple Viking were sampled respectively, and frozen immediately in liquid nitrogen and stored at -80°C until use.

Anthocyanin extraction and metabolomics analysis

Powder, 100mg, was extracted with 1.0 mL 70% aqueous methanol overnight at 4°C. Extracts were centrifuged at 10,000 ×g for 10 min and then filtrated (0.22-μm pore size). Samples were analyzed using an LC-ESI-MS/MS system (HPLC, Shim-pack UFLC SHIMADZU CBM30A system). The LC-ESI-MS/MS analysis was performed by Wuhan MetWare Biotechnology Co., Ltd., (www.mettware.cn). Metabolite content data were normalized by the range method, and accumulation patterns of metabolites among different samples were analyzed by the R package. Fold Change ≥ 2 and ≤ 0.5 were set as the threshold for significantly differential metabolites.

RNA isolation and library construction

Total RNA was isolated using a PLANTpure Universal RNA Kit (Aidlab, Beijing, China) according to the manufacturer's instructions, and then, post-treatment with a DNase Digestion Kit (Aidlab, Beijing, China) was used to remove genomic DNA contaminants. The mRNA was purified from total RNA with poly-T oligo-attached magnetic beads. First-strand cDNA was synthesized under elevated temperature in NEBNext first strand synthesis reaction buffer (5×) using random hexamer primers and M-MuLV Reverse Transcriptase. Second-strand cDNA synthesis was subsequently performed using RNase H and DNA Polymerase I. Library fragments were purified with an AMPure XP system (Beckman Coulter, Beverly, USA). Then, PCR was performed with Phusion High-Fidelity DNA polymerase, Universal PCR primers, and Index (X) Primer. The PCR products were purified (AMPure XP system), and library quality was assessed on an Agilent Bioanalyzer 2100 system. Library products were then sequenced *via* an Illumina HiSeqTM 2000 (San Diego, CA, USA).

Sequence data filtering, *de novo* assembly, and annotation

Clean reads were obtained by removing adapters, and reads containing ploy-N and those of low-quality from raw reads. Simultaneously, Q20, Q30, GC content, and sequence duplication level of clean reads were calculated. Clean reads were then mapped to the potato DM reference genome (v4.03, http://spuddb.uga.edu/pgsc_download.shtml) with HISAT2 (v2.1.0, Kim et al., 2015). Gene function was annotated based on public databases, including the National Center for Biotechnology Information (NCBI) non-redundant protein sequences (NR) and Swiss-Prot (Apweiler et al., 2004), Protein family (Pfam) (Finn et al., 2014), Clusters of Orthologous Groups of proteins (COG) (Tatusov et al., 2000), eukaryotic Orthologous Groups of proteins (KOG) (Koonin et al., 2004), and Kyoto Encyclopedia of Genes and Genomes (KEGG) (Kanehisa et al., 2004) databases.

Differentially expressed gene analyses

Fragments Per Kilobase of transcript per Million fragments mapped (FPKM) were used to estimate gene expression level. Differential gene expression among different samples was estimated by Cuffdiff (v2.0.0). Thresholds for significantly differential expression were false discovery rate (FDR) ≤ 0.05 and fold change ≥2. The KEGG pathways enrichment analysis of differentially expressed genes (DEGs) was performed by KOBAS software (Mao et al., 2005).

Reverse-transcription quantitative PCR

Isolation of RNA, reverse transcription, and reverse-transcription quantitative PCR (RT-qPCR) were conducted according to a previously method (Zhang et al., 2020). Primers were designed using the NCBI Primer-BLAST (https://www.ncbi.nlm.nih.gov/tools/primer-blast/) and are listed in Table 1. The RT-qPCR was performed on a CFX96^{TM} real-time PCR system (Bio-Rad, USA) using a TransStart Top Green qPCR SuperMix kit (Transgen, Beijing, China). The potato gene Ef1α (GenBank: AB061263) was selected as the control. The relative expression of individual gene was calculated with the $2^{-\Delta\Delta CT}$ method (Livak and Schmittgen, 2001).

Methylation assay

Methylation and demethylation treatments were applied. Potato M-P and M-R genotypes were induced to form tubers in MS medium containing 8% sucrose under a short-day photoperiod (8 h day/16 h night). In the methylation treatment, 30-μM S-adenosylmethionine (SAM) was added to sterilized MS medium, whereas in the demethylation treatment, 40-μM azacitidine (5-azaC) was added according to previous study (Ai et al., 2021). Water was used as the control. Thirty plantlets were used for each treatment. After 6 to 8 weeks, chimeric color of red and purple tubers (MPS) appeared in M-P plantlets cultured in the medium containing SAM. Three MPS tubers were planted separately to form three independent lines, named MPS-1, MPS-2, and MPS-3, respectively.

To detect methylation level, genomic DNA was isolated from leaves of M-P and M-R, red skin of Purple Viking tuber (Pur-R), purple skin of Purple Viking tuber (Pur-P), red skin of MPS-1 (MPS-1-R) and MPS-2 (MPS-2-R) tuber, and purple skin of MPS-1

10.3389/fpls.2022.1021617

TABLE 1 The primer sequences for PCR and RT-qPCR.

Primer name	Primer sequence (5′-3′)	Genbank ID
OMT10040-F	GCGCTTAACCTAACCCGAAA	PGSC0003DMG400003935[A]
OMT10040-R	TGTGGTGCAGTCAGAGTCAT	
OMT30376-F	ACGTTCAATGCGTTTGCTTC	PGSC0003DMG400011624 [A]
OMT30376-R	AGAGGTAAGGGGAACAAAGTGT	
AT26230-F	CTAACCCACCAGAAGGCTCA	PGSC0003DMG400010117 [A]
AT26230-R	ACCGTGTATTCCTCCGGTTT	
AT69755-F	TCACCGGAAACAATGGATGC	PGSC0003DMG400027127 [A]
AT69755-R	AAAATCACAAAGAGCAAAAGCTACT	
OMT44353-F	TGAAAGACACTGCCCATTGC	PGSC0003DMG400017221 [A]
OMT44353-R	TCGCCTTCCAAACCTCATCT	
FLS-F	ACACCGCGTCACTTTCCTAT	PGSC0003DMG400014093 [A]
FLS-R	TCAAGGCTGTTGTTGCACTC	
bHLH96-F	GAACAGCAGGCACAATTGGA	PGSC0003DMG400028578 [A]
bHLH96-R	TTCGTTCAACGGCAATGTGT	
nsLTP1-F	TGTTGCGGTGGAGTTAGGAA	PGSC0003DMG400001904 [A]
nsLTP1-R	GACCAGCAGCTTTGCTGTAA	
DMT03581-F	TAATTGCGCACTTTGTGCCT	PGSC0003DMG400001415 [A]
DMT03581-R	GGAGGTGATCCAGGTCAAGA	
Ef1α-F	ATTGGAAACGGATATGCTCCA	AB061263[B]
Ef1α-R	TCCTTACCTGAACGCCTGTCA	
OMT10040M-F	CCACTCCATCACTCATTGTAAGCC	
OMT10040M-R	CGATATCTGAATAAGTTCTGATGAATGTG	
AT26230M-F	TACATTGCTATTTTGGTTTCATCGT	
AT26230M-R	AAGAGAAACAGAAACATACAACATGATAA	
OMT30376M-F	TTTTCTAAAGTCAAACCCAAATCCT	
OMT30376M-R	CGATGAGCTTAACTTCAAGCCAC	

[A]Gene from the Potato Genome Sequence Consortium database.
[B]Gene from the National Center of Biotechnology Information database.

(MPS-1-P) and MPS-2 (MPS-2-P) tuber using a Plant Genomic DNA Extraction Kit (DP305; TIangen, Beijing, China) following the manufacturer's instructions. The gDNA was digested by the restriction enzyme *Hpa*II which is sensitive to the methylation of gene sequences. Then, PCR amplification was conducted with primers (MT30376M-F/R) spanning GC island sequences using gDNA before and after enzyme digestion as a template. The methylation level of target genes was determined according to the presence or absence of the target band in PCR products.

Results

Anthocyanin transformation was different between Purple Viking and its mutants

The tuber skin of Purple Viking was a chimeric color of red and purple (Figure 1A). A special tuber of Purple Viking with skin that was red on one side and purple on the other was obtained (Figure 1B), and the bud eyes of red and purple parts were planted separately. The tuber obtained by propagating buds from the purple part had pure purple skin (M-P) (Figure 1C), and the tuber obtained by propagating buds from the red part had pure red skin (M-R) (Figure 1D).

To determine differences in anthocyanin composition and content between purple and red tubers, anthocyanin metabolites of M-R and M-P were analyzed by HPLC. The skin and flesh of Purple Viking tubers (abbreviated as PurS and PurF, respectively) were used controls. Eight types of anthocyanins were detected, including rosinidin-O-hexoside, peonidin-3-O-glucoside, delphinidin, pelargonidin, malvidin-3-O-glucoside, petunidin 3-O-glucoside, pelargonidin 3-O-beta-D-glucoside, and cyaniding. Relative contents in each sample are shown in Table S1. According to cluster analysis of anthocyanin contents in each sample, contents of cyanidin, delphinidin, pelargonidin, and pelargonidin 3-O-beta-D-glucoside were higher in M-R than in M-P, whereas contents of the other four anthocyanins were higher in M-P (Figure 1E). According to the anthocyanin biosynthesis pathway, in M-R, the transformation of cyanidin into rosinidin O-hexoside and peonidin-3-O-glucoside and that of delphinidin into malvidin-3-O-glucoside and petunidin 3-O-glucoside were hindered (Figure 2).

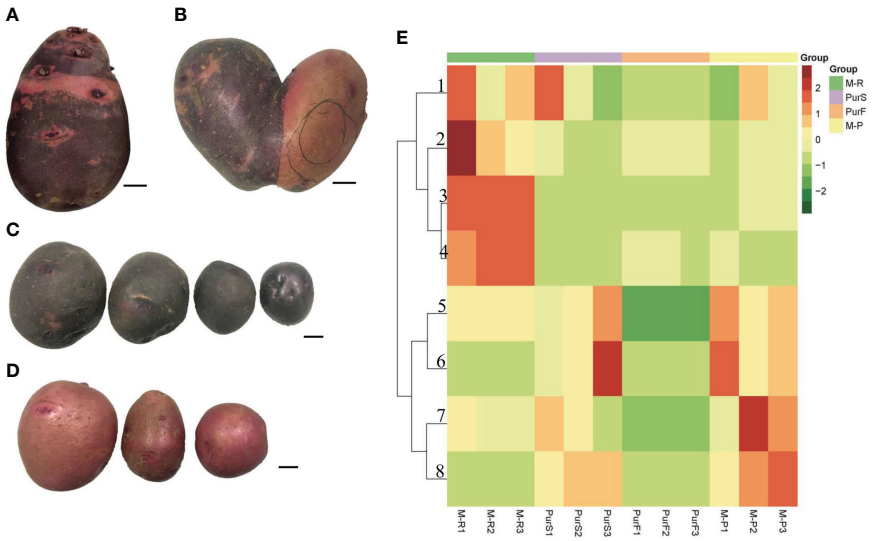

FIGURE 1
Tuber phenotype and anthocyanin content of potato cultivar Purple Viking and its mutants. **(A)** Phenotype of Purple Viking wild-type tuber. **(B)** Phenotype of Purple Viking chimeric tuber. **(C)** Tuber phenotype of Purple Viking red mutant (M-R). **(D)** Tuber phenotype of Purple Viking purple mutant (M-P). Bars=1cm. **(E)** Heat map of eight anthocyanins in tubers of Purple Viking and its mutants. 1: cyaniding; 2: delphinidin; 3: pelargonidin; 4: pelargonidin 3-O-beta-D-glucoside; 5: rosinidin-O-hexoside; 6: malvidin-3-O-glucoside; 7: rosinidin-O-hexoside; 8: petunidin 3-O-glucoside.

Differentially expressed genes in pure red skin and pure purple skin tubers

To further explore the molecular mechanisms that formed red and purple anthocyanins in tubers, the cDNA libraries of M-R, M-P, PurS, and PurF were constructed for transcriptomic analysis, with PurS and PurF used as controls. There was a strong correlation among biological repeats in the transcriptome, with Pearson's correlation coefficient (r^2) greater than 0.954 (Figure 3A). Number of clean reads per library ranged from 19,776,183 to 27,106,135, and 80.43% to 89.66% of reads mapped to the potato reference genome. At least 94.38% of reads in each library scored Q30 (0.02% error rate) or above, and the average GC content across all libraries was

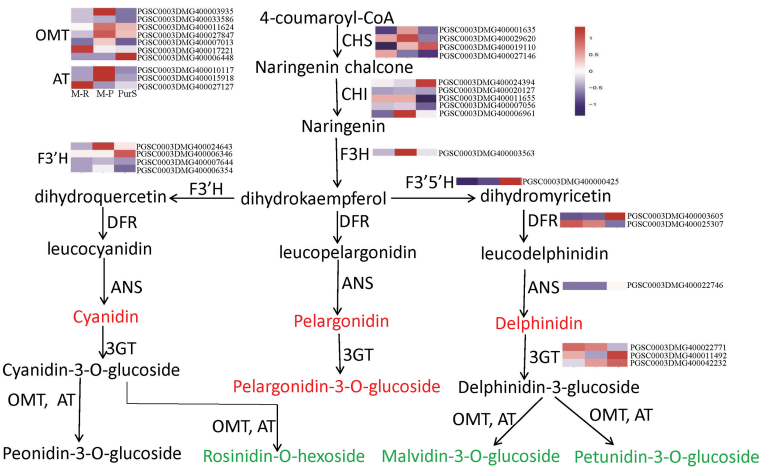

FIGURE 2
Metabolites and heat map of anthocyanin biosynthetic genes. Red font indicates that the content of anthocyanins in red tubers is higher than that in purple tubers, and green font indicates that the content of anthocyanins in red tubers is lower than that in purple tubers.

10.3389/fpls.2022.1021617

43.00% (Table S2). The data demonstrated that reads were of high quality and were suitable for further differential gene expression analysis.

Differentially expressed genes in different libraries were analyzed to identify genes likely involved in the accumulation of different anthocyanins. Based on thresholds fold change ≥ 2 and FDR < 0.01, 296, 497, and 1,058 genes were up-regulated in the comparisons M-P vs M-R, PurS vs M-R, and PurS vs M-P, respectively, and 607, 273, and 657 genes were respectively significantly down-regulated (Figure 3B). The DEGs were identified in order to analyze the differential pathways and genes controlling the formation of red and purple anthocyanins in tubers. Thus, KEGG pathways enrichment analysis was performed to analyze up-regulated and down-regulated genes in the M-P vs M-R comparison. Thirty-nine enriched pathways were associated with the 296 up-regulated genes. The first 20 pathways of the enrichment analysis are shown in Figure 4A. The most significantly enriched pathways were those associated with plant hormone signal transduction, sulfur metabolism, phenylpropanoid biosynthesis, and linoleic acid metabolism. Forty-seven enriched pathways were associated with the 607 down-regulated genes. The first 20 pathways of the enrichment analysis are shown in Figure 4B. The most significantly enriched pathways were those associated with protein processing in endoplasmic reticulum; cutin, suberine, and wax biosynthesis; arginine and proline metabolism; and arginine biosynthesis.

According to expression patterns of anthocyanin synthesis structural genes in the transcriptomes, there was no significant difference in expression of most structural genes in M-R and M-P, including *CHI*, *F3'H*, *F3'5'H*, *DFR*, *ANS* and *3GT* (Figure 2). In further analysis, 236 genes had more than a 5-fold change in expression between M-R and M-P (Table S3), including the flavonol synthase gene (PGSC0003DMG400014093), glutathione s-transferase gene (PGSC0003DMG400015726), acyltransferase gene (PGSC0003DMG400010117), bHLH (PGSC0003DMG400028578), and WRKY (PGSC0003DMG400015104) transcription factors.

Confirmation of differential gene expression by reverse-transcription quantitative PCR

According to differences in anthocyanin components between M-R and M-P, in the M-R tuber, the formation of rosinidin O-hexoside, malvidin-3-O-glucoside, and petunidin 3-O-glucoside was hindered. With consideration of the anthocyanin biosynthesis pathway (Figure 2), it was speculated that the limited formation of those compounds might be caused by functional differences in methyltransferase or acyltransferase. Of the DEGs in the transcriptome, seven genes encoded O-methyltransferase and three genes encoded acyltransferase. To verify the reliability of transcriptome data, expression patterns of the OMT and AT genes in different samples were detected by RT-qPCR. Four of the 236 genes with more than a 5-fold difference in expression between M-R and M-P were randomly selected for verification. The RT-qPCR results were consistent with the transcriptome results (Figure 5). Expression of two OMT genes (*OMT10040* (PGSC0003DMG400003935) and *OMT30376* (PGSC0003DMG400011624)) and one AT gene (*AT26230* (PGSC0003DMG400010117)) was significantly higher in M-P than in M-R (Figures 5A–C). It was speculated that their higher expression in M-P tubers might promote the rapid accumulation of rosinidin O-hexoside, malvidin-3-O-glucoside, and petunidin 3-O-glucoside.

Methylation level of the *OMT30376* gene was different between purple and red tubers

Sequences of *OMT10040*, *OMT30376*, and *AT26230* genes and promoters were cloned from M-R and M-P. There were no significant differences in sequences of the three genes between

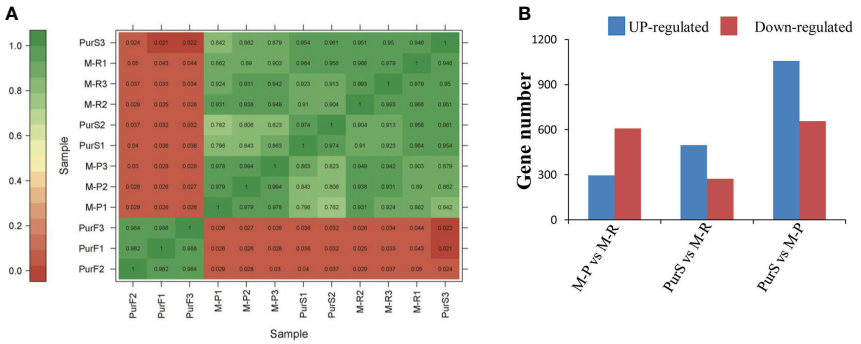

FIGURE 3
Overview of transcriptome analysis. **(A)** Correlation analysis of RNA-seq data of different tuber samples. **(B)** Number of differentially expressed genes (DEGs) in each comparison.

10.3389/fpls.2022.1021617

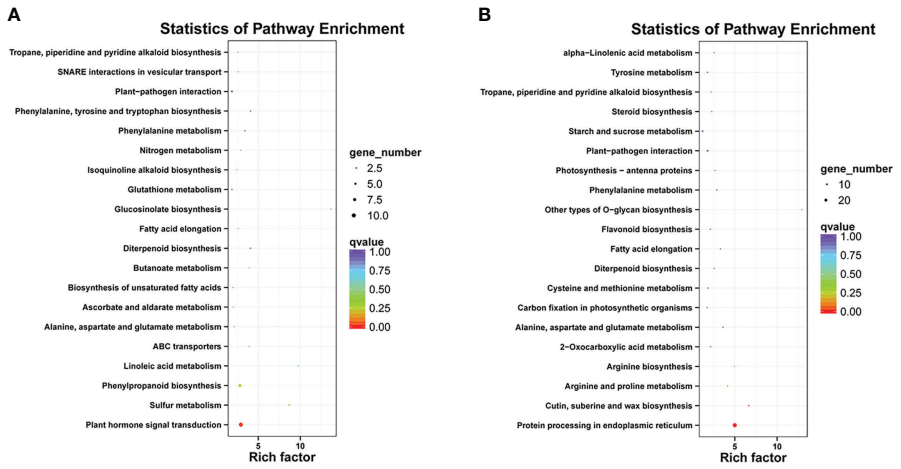

FIGURE 4
Kyoto Encyclopedia of Genes and Genomes (KEGG) enrichment analysis of **(A)** up-regulated and **(B)** down-regulated differentially expressed genes (DEGs) between red mutant (M-R) and purple mutant (M-P) tubers.

M-R and M-P. Therefore, methylation levels of the three genes and associate 3,000-bp upstream promoter sequences were predicted. All three genes contained CpG island sequences, and the positions of the CpG island in sequences of *AT26230*, *OMT10040*, and *OMT30376* genes were 1,605–2,245, –134–363, and 76–301, respectively (Figure 6A), which indicated that the three genes might be methylated.

The gDNA was extracted from the red part (Pur-R) and purple part (Pur-P) of Purple Viking tuber skin and tuber skins of M-R and M-P. The gDNA of Pur-R, Pur-P, M-R, and M-P was digested by *Hpa*II, which is a restriction enzyme sensitive to methylation. Primers spanning CpG island sequences were designed, and gDNA before and after enzyme digestion was used as a template for PCR amplification to determine whether a

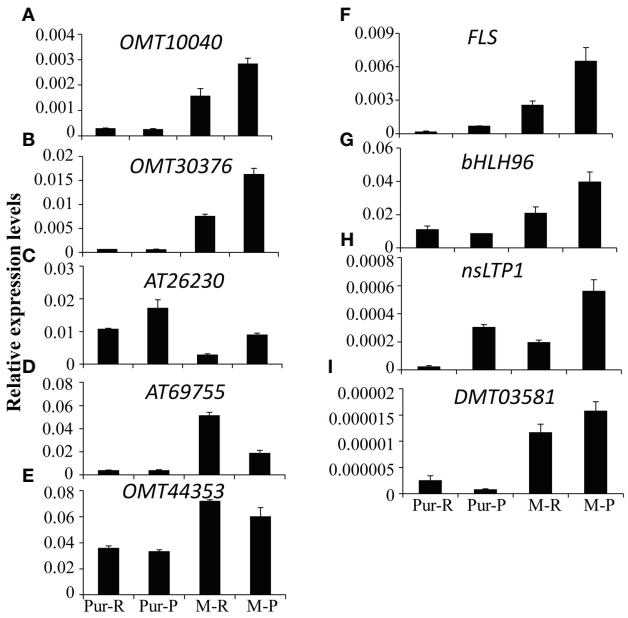

FIGURE 5
Quantitative analysis of transcript levels of differentially expressed genes (DEGs) in tubers skin of Purple Viking and its mutants. Each column represents the mean value ± standard error (n = 3).

gene sequence was methylated. Target gene fragments were amplified when gDNA before *Hpa*II digestion was used as the template. However, when digested gDNA was used as the template, the primer of the *OMT30376* gene amplified the target band in gDNA of Pur-R and M-R, but there was no target band in Pur-P and M-P (Figure 6B). However, target bands in *OMT10040* and *AT26230* genes were not amplified in any template after enzymatic digestion (Figure 6B). The results indicated that the methylation degree of the *OMT30376* gene in Pur-R and M-R was higher than that in Pur-P and M-P. Thus, the difference in degree of methylation might cause lower expression of the *OMT30376* gene in M-R than in M-P (Figure 6B).

Methylation level of the *OMT30376* gene affected the transformation of anthocyanin in tubers

The M-P tissue culture seedlings were expanded with MS medium supplemented with S-adenosylmethionine (SAM) or 5-azacytidine (5-azaC) to induce tuber formation. The phenotype of the chimeric color of red and purple (MPS) appeared in M-P potato tubers cultured in the medium containing SAM (Figure 7A). The three micro potatoes of MPS were planted in separately in plastic pots, and the tubers harvested also had the color skin phenotype (Figure 7A). However, the phenotype of the tuber cultured in the medium containing 5-azaC was purple, which was the same as that of M-P (Figure 7A). The gDNA of red skin (MPS-1-R and MPS-2-R) and purple skin (MPS-1-P and MPS-2-P) of MPS-1 and MPS-2 tubers was extracted, and digested with restriction enzyme *Hpa*II. The target gene was amplified with digested and undigested gDNA with *OMT30376* primers (MT30376M-F/R). The results of MPS-1 and MPS-2 were consistent and showed that the target fragment was amplified from gDNA without *Hpa*II treatment. After *Hpa*II treatment, the target fragment was amplified in MPS-1-R and MPS-2-R, but not in MPS-1-P and MPS-2-P (Figure 7B). Therefore, the methylation level of the *OMT30376* gene was higher in red skin of MPS than in purple skin of MPS. The expression level of *OMT30376* in MPS-1-R and MPS-2-R was similar to that in the M-R tuber, which was much lower than that in MPS-1-P, MPS-2-P and M-P (Figure 7C). Thus, an increase in the methylation level of the *OMT30376* gene led to a decrease in its expression, which then led to an increase in red anthocyanin accumulation.

Discussion

Plant anthocyanin biosynthesis is regulated by many factors, such as temperature, hormonse, microRNAs, and epigenetics (Zhang et al., 2012; Yamazaki et al., 2021). To understand the regulation of potato anthocyanin biosynthesis, research has primarily focused on analysis of key gene functions and regulation mechanisms, particularly of structural genes, including *F3'5'H*, *DFR*, *ANS*, and *3GT* (Jung et al., 2005; Wei et al., 2012; Zhang et al., 2020), and MBW transcription factors (Li et al., 2014; Liu et al., 2016). However, regulation of methylation modification in potato anthocyanin biosynthesis has not been reported. In this study, transcriptome and anthocyanin metabolome analyses were performed on Purple

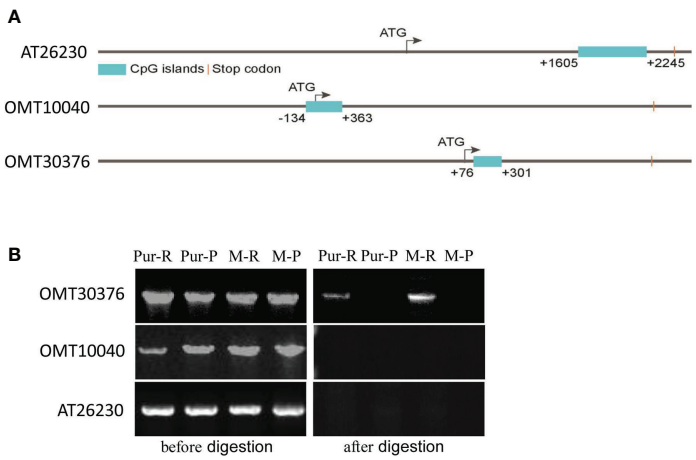

FIGURE 6
Detection of the methylation level of O-methyltransferase (OMT) and acyltransferase (AT) genes. **(A)** Distribution of CpG islands in gene sequences of *AT26230*, *OMT10040*, and *OMT30376*. **(B)** Specific primers amplified target genes in gDNA of red skin of Purple Viking tuber (Pur-R), purple skin of Purple Viking tuber (Pur-P), skin of red mutant (M-R), and skin of purple mutant (M-P) before (left) and after (right) *Hpa*II digestion.

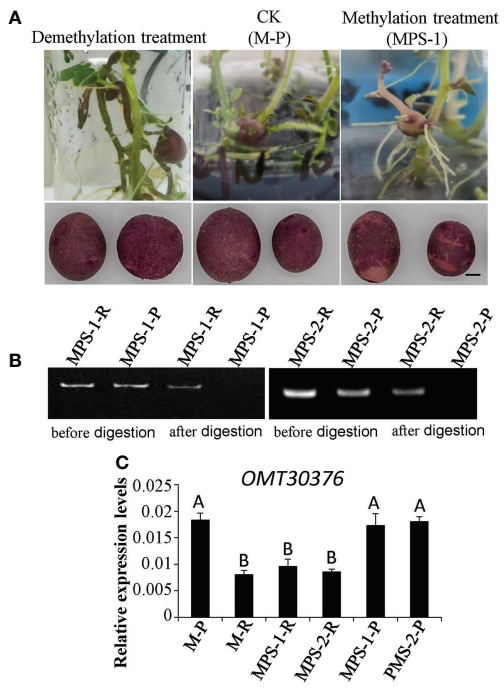

FIGURE 7
Effects of methylation treatment on transformation of anthocyanin. **(A)** Phenotypes of tubers from purple mutant (M-P) plantlets cultured on the medium containing 5-azaC (demethylation treatment), SAM (methylation treatment) (MPS), and water (CK), respectively. Bars = 1 cm. **(B)** OMT30376M-F/R primers amplified the target gene in gDNA of red skin of MPS (MPS-1-R and MPS-2-R) and purple skin of MPS (MPS-1-P and MPS-2-P) before and after *Hpa*II digestion. **(C)** Transcript levels of *OMT30376* in red and purple skin of MPS tubers. Each column represents the mean value ± standard error (n = 3). Different letters above bars indicate a significant difference between means ($P<0.01$).

Viking tubers with a chimeric skin phenotype and its associated red and purple-skin mutants. The metabolome analysis showed that the transformation of cyanidin and delphinidin was hindered in red tubers (Figure 2). Analysis of DEGs showed that expression of the *OMT30376* gene, which catalyzes the conversion of cyanidin and delphinidin, was significantly different between M-R and M-P (Figure 5). Further analysis showed a difference in the methylation degree of the *OMT30376* gene between M-R and M-P. In addition, M-P treated with SAM had the phenotype of the restored mutation (Figure 7). The results indicated that the anthocyanin difference between purple and red was caused by the methylation degree of the *OMT30376* gene. Therefore, the *OMT30376* gene is involved in the transformation of anthocyanins in potato tubers, which is consistent with the function of the grape *AOMT* gene. Transient expression of the grapevine *AOMT* gene in tobacco leaves expressing anthocyanin pigment 1 (PAP1) transcription factor from *Arabidopsis*, indicates that AOMT transforms the nonmethylated anthocyanin delphinidin 3-rutinoside induced by PAP1 into malvidin 3-rutinoside (Hugueney et al., 2009).

Epigenetic modification of anthocyanin biosynthesis regulators, especially methylation modification, is closely associated with color changes in some crops (Xu et al., 2012; Wang et al., 2013; El-Sharkawy et al., 2015). The OMT genes have key roles in methylation modification, and the multiple genes in the OMT gene family also have different effects. For example, four different OMTs isolated from petunia exhibit different kinetic properties (Jonsson et al., 1984), and of 57 candidate OMT genes identified in tomatoes, only one gene is strongly correlated with methylated anthocyanin accumulation (Roldan et al., 2014). Similar results are found in grapes. High expression of the *FAOMT* gene is detected in colored grape skin, but other OMT genes are not detected (Lucker et al., 2010). In this study, seven OMT genes were detected in the transcriptomes, and RT-qPCR results showed that only two (*OMT10040* and *OMT30376*) had lower in expression in M-R than in M-P (Figure 5). According to further analysis, only the difference in methylation level of the *OMT30376* gene (Figure 6) affected anthocyanin transformation.

The focus of most previous studies is on the effect of OMT genes on anthocyanin methylation in order to change the color performance of plants (Ageorges et al., 2006; Castellarin and Di Gaspero, 2007; Du et al., 2015). Methylation of anthocyanins was first reported in petunia at the 3′ and 5′ positions of aglycones (Jonsson et al., 1983). Subsequently, effects of OMT genes on anthocyanin methylation were determine in many species, including peony and grape (Sakata et al., 1995; Kondo et al., 2009). However, differences in regulation of different OMT genes in different phenotypes are rarely reported. In this study, the difference in methylation level of the *OMT30376* gene between M-R and M-P affected anthocyanin transformation, which is a new discovery in potato.

Methylation regulates anthocyanin synthesis primarily because of changes in methylation level of key transcription factors, which lead to changes in expression of structural genes and thus activity of those genes (El-Sharkawy et al., 2015). A decrease in the promoter methylation level of *MdMYB1*, the key transcription factor in anthocyanin biosynthesis in apples, increases the accumulation of red anthocyanin and produces a red bud sport (Xu et al., 2012). Similar results are also found in red-fleshed radish, in which methylation of the *RsMYB1* promoter leads to a decrease in gene expression and affects the synthesis and accumulation of anthocyanin (Wang et al., 2020). However, in this study, there were no significant differences in expression of key transcription factors and most key structural genes (Figure 2) between red and purple tubers. When methylation level and expression of the *OMT30576* gene in red and purple tubers (Figures 5B, 6) and effect of methylation level on anthocyanin transformation were both considered (Figure 7), the difference in anthocyanin between purple and red tubers was primarily due to difference in methylation levels of the

OMT30376 gene, which affected its expression. This is the first report on how methylation of an OMT gene affects anthocyanin biosynthesis and transformation in potato tubers. In addition, the CpG of *OMT30376*, *OMT10040*, and *AT26230* are all in the coding region (Figure 6A), and the expression level of them in the M-R and M-P is significantly different (Figure 5), indicating that the difference in methylation of gene coding regions can regulate gene expression, which is consistent with the results in rice and maize (Lu et al., 2015; Tan et al., 2016). In this study, the regulation of *OMT30376* on other new structural genes and transcription factors could not be excluded, because expression of the structural gene *FLS* and the transcription factor gene *bHLH96* was significantly different between M-R and M-P (Figure 5). Therefore, whether *OMT30376* can regulate expression of *FLS* and *bHLH96* needs to be investigated further.

In this study, part of the MPS tuber skin was red (Figure 7A), and expression of the *OMT30376* gene in the red part was lower than that in the purple part (Figure 7C), which indicated that expression of the *OMT30376* gene was site-specific. A similar phenomenon is observed in red–purple-flowered cyclamen (Akita et al., 2011). However, there was no purple on the tuber skin of M-R plants grown on medium containing 5-azaC, indicating that there might be other regulatory mechanisms in red tubers. In addition, differences in methylation levels of *OMT10040* and *AT26230* in M-R and M-P were not detected using the current method (Figure 6B). The reasons for differences expression of *OMT10040* and *AT26230* in M-R and M-P need to be studied further. The function of transcription factor *bHLH96* was not clear, although its expression in M-P and M-R was significantly different (Figure 5). Thus, whether bHLH96 regulates anthocyanin biosynthesis and whether it regulates *OMT10040* and *AT26230* also need to be investigated further.

Data availability statement

The data presented in the study are deposited in the Harvard Dataverse repository, and the original fpkm value of RNA-seq can be obtained through the website https://dataverse.harvard.edu/dataset.xhtml?persistentId=doi:10.7910/DVN/K24WV6.

Author contributions

BS and HZ designed the research. YZ and XZ analyzed the data. ZZ analyzed gene expression. YZ and JL performed the methylation treatment of samples. MS found the mutant tuber. HZ and BS wrote the article. All authors contributed to the article and approved the submitted version.

Funding

This work was supported by grants from the China Agriculture Research System of MOF and MARA (CARS-09-P07), the Natural Science Foundation of Henan (202300410152), the Training Plan for Young Backbone Teachers in the Colleges and Universities of Henan Province (2021GGJS049), and Research Funding for Young Backbone Teachers of Henan University of Science and Technology (4026-13450008).

Conflict of interest

The authors declare that the research was conducted in the absence of any commercial or financial relationships that could be construed as a potential conflict of interest.

Publisher's note

All claims expressed in this article are solely those of the authors and do not necessarily represent those of their affiliated organizations, or those of the publisher, the editors and the reviewers. Any product that may be evaluated in this article, or claim that may be made by its manufacturer, is not guaranteed or endorsed by the publisher.

Supplementary material

The Supplementary Material for this article can be found online at: https://www.frontiersin.org/articles/10.3389/fpls.2022.1021617/full#supplementary-material

References

Ageorges, A., Fernandez, L., Vialet, S., Merdinoglu, D., Terrier, N., and Romieu, C. (2006). Four specific isogenes of the anthocyanin metabolic pathway are systematically co-expressed with the red colour of grape berries. *Plant Sci.* 170, 372–383. doi: 10.1016/j.plantsci.2005.09.007

Ai, Y., Jing, S., Cheng, Z., Song, B., Xie, C., Liu, J., et al. (2021). DNA Methylation affects photoperiodic tuberization in potato (*Solanum tuberosum* l.) by mediating the expression of genes related to the photoperiod and GA pathways. *Hortic. Res.* 8, 181. doi: 10.1038/s41438-021-00619-7

Akita, Y., Kitamura, S., Hase, Y., Narumi, I., Ishizaka, H., and Kondo, E. (2011).). isolation and characterization of the fragrant cyclamen O-methyltransferase involved in flower coloration. *Planta* 234, 1127–1136. doi: 10.1007/s00425-011-1466-0

Apweiler, R., Bairoch, A., Wu, C. H., Barker, W. C., Boeckmann, B., and Ferro, S. (2004). UniProt: the universal protein knowledgebase. *Nucleic Acids Res.* 32, 115–119. doi: 10.1093/nar/gkh131

Brown, C. R. (2005). Antioxidants in potato. *Am. J. Potato Res.* 82, 163–172. doi: 10.1007/BF02853654

Castellarin, S. D., and Di Gaspero, G. (2007). Transcriptional control of anthocyanin biosynthetic genes in extreme phenotypes for berry pigmentation of naturally occurring grapevines. *BMC Plant Biol.* 7 (46). doi: 10.1186/1471-2229-7-46

Du, H., Wu, J., Ji, K. X., Zeng, Q. Y., Bhuiya, M. W., and Su, S. (2015). Methylation mediated by an anthocyanin, O-methyltransferase, is involved in purple flower coloration in paeonia. *J. Exp. Bot.* 66, 6563–6577. doi: 10.1093/jxb/erv365

El-Sharkawy, I., Liang, D., and Xu, K. (2015). Transcriptome analysis of an apple (Malus×domestica) yellow fruit somatic mutation identifies a gene network module highly associated with anthocyanin and epigenetic regulation. *J. Exp. Bot.* 66, 7359–7376. doi: 10.1093/jxb/erv433

Finn, R. D., Bateman, A., Clements, J., Coggill, P., Eberhardt, R. Y., and Eddy, S. R. (2014). Pfam: The protein families database. *Nucleic Acids Res.* 42, 222–230. doi: 10.1093/nar/gkt1223

Fossen, T., and Andersen, M. (2000). Anthocyanins from tubers and shoots of the purple potato, *Solanum tuberosum*. *J. Hortic. Sci. Biotech.* 75, 360–363. doi: 10.1080/14620316.2000.11511251

Guo, D. L., Li, Q., Zhao, H. L., Wang, Z. G., Zhang, G. H., and Yu, Y. H. (2019). The variation of berry development and DNA methylation after treatment with 5-azaC on 'Kyoho' grape. *Sci. Hortic.* 246, 265–271. doi: 10.1016/j.scienta.2018.11.006

Heim, K. E., Tagliaferro, A. R., and Bobilya, D. J. (2002). Flavonoid antioxidants: Chemistry, metabolism and structure-activity relationships. *J. Nutr. Biochem.* 13, 572–584. doi: 10.1016/S0955-2863(02)00208-5

Hichri, I., Barrieu, F., Bogs, J., Kappel, C., Delrot, S., and Lauvergeat, V. (2011). Recent advances in the transcriptional regulation of the flavonoid biosynthetic pathway. *J. Exp. Bot.* 62, 2465–2483. doi: 10.1093/jxb/erq442

Hugueney, P., Provenzano, S., Verries, C., Ferrandino, A., Meudec, E., and Batelli, G. (2009). A novel cation-dependent O-methyltransferase involved in anthocyanin methylation in grapevine. *Plant Physiol.* 150, 2057–2070. doi: 10.1104/pp.109.140376

Jiang, S. H., Wang, N., Chen, M., Zhang, R., Sun, Q. G., and Xu, H. F. (2020). Methylation of MdMYB1 locus mediated by RdDM pathway regulates anthocyanin biosynthesis in apple. *Plant Biotechnol. J.* 18, 1736–1748. doi: 10.1111/pbi.13337

Jonsson, L. M. V., Aarsman, M. E. G., Poulton, J. E., and Schram, A. W. (1984). Properties and genetic control of four methyltransferases involved in methylation of anthocyanins in flower of p*etunia hybrid*. *Planta* 160, 174–179. doi: 10.1007/BF00392867

Jonsson, L. M. V., de Vlaming, P., Wiering, H., Aarsman, M. E. G., and Schram, A. W. (1983). Genetic control of anthocyanin O-methyltransferase activity in flowers of p*etunia hybrid*. *Theor. Appl. Genet.* 66, 349–355. doi: 10.1007/BF00251170

Jung, C. S., Griffiths, H. M., De Jong, D. M., Cheng, S., Bodis, M., and De Jong, W. S. (2005). The potato p locus codes for flavonoid 3′5′-hydroxylase. *Theor. Appl. Genet.* 110, 269–275. doi: 10.1007/s00122-004-1829-z

Kanehisa, M., Goto, S., Kawashima, S., Okuno, Y., and Hattori, M. (2004). The KEGG resource for deciphering the genome. *Nucleic Acids Res.* 32, 277–280. doi: 10.1093/nar/gkh063

Khoo, H. E., Azlan, A., Tang, S. T., and Lim, S. M. (2017). Anthocyanidins and anthocyanins: colored pigments as food, pharmaceutical ingredients, and the potential health benefits. *Food Nutr. Res.* 61, 1–21. doi: 10.1080/16546628.2017.1361779

Kim, D., Langmead, B., and Salzberg, S. L. (2015). HISAT: a fast spliced aligner with low memory requirements. *Nat. Methods* 12, 357–360. doi: 10.1038/nmeth.3317

Klimasauskas, S., and Weinhold, E. (2007). A new tool for biotechnology: AdoMet-dependent methyltransferases. *Trends Biotechnol.* 25, 99–104. doi: 10.1016/j.tibtech.2007.01.006

Kondo, E., Nakayama, M., Kameari, N., Tanikawa, N., Morita, Y., Akita, Y., et al. (2009). Red-purple flower due to delphinidin 3,5-diglucoside, a novel pigment for *Cyclamen* spp., generated by ion-beam irradiation. *Plant Bio.* 26, 565–569. doi: 10.5511/plantbiotechnology.26.565

Koonin, E. V., Fedorova, N. D., Jackson, J. D., Jacobs, A. R., Krylov, D. M., and Makarova, K. S. (2004). A comprehensive evolutionary classification of proteins encoded in complete eukaryotic genomes. *Genome Biol.* 5, 7. doi: 10.1186/gb-2004-5-2-r7

Liu, Y., Lin-Wang, K., Espley, R. V., Wang, L., Li, Y., and Liu, Z. (2019). StMYB44 negatively regulates anthocyanin biosynthesis at high temperatures in tuber flesh of potato. *J. Exp. Bot.* 70, 3809–3824. doi: 10.1093/jxb/erz194

Liu, Y., Lin-Wang, K., Espley, R. V., Wang, L., Yang, H., and Yu, B. (2016). Functional diversification of the potato R2R3 MYB anthocyanin activators AN1, MYBA1, and MYB113 and their interaction with basic helix-loop-helix cofactors. *J. Exp. Bot.* 67, 2159–2176. doi: 10.1093/jxb/erw014

Liu, Y., Tikunov, Y., Schouten, R. E., Marcelis, L. F. M., Visser, R. G. F., and Bovy, A. (2018). Anthocyanin biosynthesis and degradation mechanisms in solanaceous vegetables: a review. *Front. Chem.* 6. doi: 10.3389/fchem.2018.00052

Livak, K. J., and Schmittgen, T. D. (2001). Analysis of relative gene expression data using real-time quantitative PCR and the $2^{-\Delta\Delta CT}$ method. *Methods* 25, 402–408. doi: 10.1006/meth.2001.1262

Li, W., Wang, B., Wang, M., Chen, M., Yin, J., and Kaleri, G. M. (2014). Cloning and characterization of a potato *StAN11* gene involved in anthocyanin biosynthesis regulation. *J. Integr. Plant Bio.* 56, 364–372. doi: 10.1111/jipb.12136

Lucker, J., Martens, S., and Lund, S. T. (2010). Characterization of a vitis vinifera cv. Cabernet sauvignon 3′,5′-o-methyltransferase showing strong preference for anthocyanins and glycosylated flavonols. *Phytochemistry* 71, 1474–1484. doi: 10.1016/j.phytochem.2010.05.027

Lu, X., Wang, W., Ren, W., Chai, Z., Guo, W., Chen, R., et al. (2015). Genome-wide epigenetic regulation of gene transcription in maize seeds. *PloS One* 10, e0139582. doi: 10.137/journal.pone.0139582

Ma, C. Q., Liang, B. W., Chang, B., Liu, L., Yan, J. Y., and Yang, Y. (2018). Transcriptome profiling reveals transcriptional regulation by DNA methyltransferase inhibitor 5-Aza-2'-deoxycytidine enhancing red pigmentation in bagged "Granny smith" apples (*Malus domestica*). *Int. J. Mol. Sci.* 19, 3133. doi: 10.3390/ijms19103133

Mao, X., Cai, T., Olyarchuk, J. G., and Wei, L. (2005). Automated genome annotation and pathway identification using the KEGG orthology (KO) as a controlled vocabulary. *Bioinformatics* 21, 3787–3793. doi: 10.1093/bioinformatics/bti430

Rausher, M. D. (2008). Evolutionary transitions in floral color. *Int. J. Plant Sci.* 169, 7–21. doi: 10.1086/523358

Reddivari, L., Vanamala, J., Chintharlapalli, S., Safe, S. H., and Miller, J. C. (2007). Anthocyanin fraction from potato extracts is cytotoxic to prostate cancer cells through activation of caspase-dependent and caspase-independent pathways. *Carcinogenesis* 28, 2227–2235. doi: 10.1093/carcin/bgm117

Roldan, M. V. G., Outchkourov, N., Van Houwelingen, A., Lammers, M., de la Fuente, I. R., and Ziklo, N. (2014). An O-methyltransferase modifies accumulation of methylated anthocyanins in seedlings of tomato. *Plant J.* 80, 695–708. doi: 10.1111/tpj.12664

Sakata, Y., Aoki, N., Tsunematsu, S., Nishikouri, H., and Johjima, T. (1995). Petal coloration and pigmentation of tree peony bred and selected in daikon island (Shimane prefecture). *J. Jpn. Soc Hortic. Sci.* 64, 351–357. doi: 10.2503/jjshs.64.351

Tan, F., Zhou, C., Zhou, Q., Zhou, S., Yang, W., Zhao, Y., et al. (2016). Analysis of chromatin regulators reveals specific features of rice DNA methylation pathway. *Plant Physiol.* 171, 2041–2054. doi: 10.1104/pp.16.00393

Tatusov, R. L., Galperin, M. Y., Natale, D. A., and Koonin, E. V. (2000). The COG database: a tool for genome scale analysis of protein functions and evolution. *Nucleic Acids Res.* 28, 33–36. doi: 10.1093/nar/28.1.33

Wang, Z., Meng, D., Wang, A., Li, T., Jiang, S., and Cong, P. (2013). The methylation of the PcMYB10 promoter is associated with green-skinned sport in max red bartlett pear. *Plant Physiol.* 162, 885–896. doi: 10.1104/pp.113.214700

Wang, Q. B., Wang, Y. P., Sun, H. H., Sun, L., and Zhang, L. (2020). Transposon-induced methylation of the RsMYB1 promoter disturbs anthocyanin accumulation in red-fleshed radish. *J. Exp. Bot.* 2020, 71, 2537–2550. doi: 10.1093/jxb/eraa010

Wei, Q., Wang, Q., Feng, Z., Wang, B., Zhang, Y., and Yang, Q. (2012). Increased accumulation of anthocyanins in transgenic potato tubers by overexpressing the 3GT gene. *Plant Biotechnol. Rep.* 6, 69–75. doi: 10.1007/s11816-011-0201-4

Wessinger, C. A., and Rausher, M. D. (2012). Lessons from flower colour evolution on targets of selection. *J. Exp. Bot.* 63, 5741–5749. doi: 10.1093/jxb/ers267

Wiering, H., and Devlaming, P. (1977). Glycosylation and methylation patterns of anthocyanins in petunia hybrida. II. genes Mf1 and Mf2. *Plant Breed.* 78, 113–123.

Xu, Y., Feng, S., Jiao, Q., Liu, C., Zhang, W., and Chen, W. (2012). Comparison of MdMYB1 sequences and expression of anthocyanin biosynthetic and regulatory genes between malus domestica borkh. cultivar'Ralls' and its blushed sport. *Euphytica* 185, 157–170. doi: 10.1007/s10681-011-0494-y

Yamazaki, M., Ishida, A., Suzuki, Y., Aoki, Y., Suzuki, S., and Enoki, S. (2021). Ethylene induced by sound stimulation enhances anthocyanin accumulation in grape berry skin through direct upregulation of UDP-glucose: flavonoid 3-o-glucosyltransferase. *Cells* 10, 2799. doi: 10.3390/cells10102799

Zhang, B., Hu, Z. L., Zhang, Y. J., Li, Y. L., Zhou, S., and Chen, G. P. (2012). A putative functional MYB transcription factor induced by low temperature regulates anthocyanin biosynthesis in purple kale (Brassica oleracea var. acephala f. tricolor). *Plant Cell Rep.* 31, 281–289. doi: 10.1007/s00299-011-1162-3

Zhang, H., Zhao, X., Zhang, J., Yang, B., Yu, Y., and Liu, T. (2020). Functional analysis of an anthocyanin synthase gene StANS in potato. *Sci. Hortic.* 272, 109569. doi: 10.1016/j.scienta.2020.109569

frontiers | Frontiers in Plant Science

TYPE Original Research
PUBLISHED 17 October 2022
DOI 10.3389/fpls.2022.1030138

OPEN ACCESS

EDITED BY
Botao Song,
Huazhong Agricultural University, China

REVIEWED BY
Bailin Liu,
Northwest A&F University, China
Saowapa Duangpan,
Prince of Songkla University, Thailand

*CORRESPONDENCE
Zhaoyan Lv
zhaoyanlv@ahau.edu.cn
Xiaobiao Zhu
xiaobiao11302005@163.com

†These authors have contributed equally to this work and share first authorship

SPECIALTY SECTION
This article was submitted to Crop and Product Physiology, a section of the journal Frontiers in Plant Science

RECEIVED 28 August 2022
ACCEPTED 26 September 2022
PUBLISHED 17 October 2022

CITATION
Jing Q, Hou H, Meng X, Chen A, Wang L, Zhu H, Zheng S, Lv Z and Zhu X (2022) Transcriptome analysis reveals the proline metabolic pathway and its potential regulation TF-hub genes in salt-stressed potato. *Front. Plant Sci.* 13:1030138. doi: 10.3389/fpls.2022.1030138

Transcriptome analysis reveals the proline metabolic pathway and its potential regulation TF-hub genes in salt-stressed potato

Quankai Jing†, Hualan Hou†, Xiaoke Meng†, Airu Chen, Lixia Wang, Husen Zhu, Shuang Zheng, Zhaoyan Lv* and Xiaobiao Zhu*

College of Horticulture, Anhui Agricultural University, Hefei, China

Potato (*Solanum tuberosum*) is currently the third most important food crop in the world. However, the production of potato is seriously threatened by salt stress, which often occurs in the facility cultivation environment, and the mining of salt tolerance genes in potato remains to be further studied. In this study, test-tube plantlets of DM potato were treated with 200-mM NaCl to simulate salt stress, and 15 cDNA libraries were constructed for RNA-seq analysis. A total of 8383 DEGs were identified, of which 3961 DEGs were shared among all the salt treatments, and 264 (7.15%) TF-coding genes were identified from these shared DEGs. KEGG enrichment analysis showed that most DEGs identified from the "arginine and proline metabolism" (ko00330) were enriched in the proline metabolic pathway, and their functions almost covered the whole proline metabolic process. Further analysis showed that expression levels of all the 13 structural DEGs in the pathway were significantly up-regulated and proline accumulation was also significantly increased under salt stress, and 13 TF-hub genes were discovered by WGCNA in the lightcyan and tan modules which were highly positively correlated with the proline contents. Correlation analysis revealed that the four TF-hub genes of the lightcyan module and seven structural DEGs of the proline metabolic pathway might be the potential candidate genes, especially the potential and novel regulatory gene *StGLK014720*. Furthermore, the dual-luciferase reporter assay confirmed that the key protein StGLK014720 could activate the promoters of both structural genes *StAST021010* and *StAST017480*. In conclusion, these results lay the foundation for further study on the salt tolerance mechanism of potato, and provide a theoretical basis and new genetic resources for salt tolerance breeding of potato.

KEYWORDS

potato, salt stress, proline, RNA-seq, WGCNA, transcription factor (TF)

Introduction

Potato (*Solanum tuberosum*) is the world's most important non-cereal food crop, belonging to the *Petota* section of the *Solanum* genus within the Solanaceae family (Spooner et al., 2014; Tang et al., 2022). Along with the unceasing increase in the world population, people have put forward higher requirements on crop yields. Potato is cultivated in more than 100 countries and over a billion people worldwide eat it (Dahal et al., 2019), so increasing potato productivity is crucial to global food security. However, potato production is often restricted by various abiotic stresses, among which salt stress is one of the major constraints. Soil salinization is a worldwide problem that threatens the growth and yield of crops and hinders the sustainable development of modern agriculture (Zhao et al., 2020). Crop yield loss due to soil salinization is a growing threat to agriculture worldwide.

Salinity stress imposes osmotic stress and ion toxicity, which impairs major plant processes such as photosynthesis, cellular metabolism, and plant nutrition (Joshi et al., 2022). Osmotic stress triggers signaling pathways that promote the biosynthesis and accumulation of compatible osmolytes, which is important for both short-term and long-term osmotic stress tolerance in plants (Zhao et al., 2020). Some of the osmolytes, such as proline, glycine betaine, polyamine, mannitol, glucose, fructose, and trehalose, are typically accumulated in several plant species in response to salt, heat, drought, ionic, osmotic, and heavy metal stresses (Gul et al., 2022). Recent evidence from salinity tolerance mechanisms highlights that osmolytes play a key role in quenching free radicals, inducing antioxidant machinery, and osmotic regulation (Choudhary et al., 2022). These osmolytes participate in the regulation of osmotic pressure by lowering the osmotic potential in the cytosolic compartment (Zhao et al., 2021). All crop plants contain proline, which increases as the plants are subjected to various stressors (Gul et al., 2022).

The increase of proline content in plants is usually involved in response to environmental stress. Proline is not only a signal substance, but can also improve plant resistance to abiotic stress by improving photosynthesis, antioxidant activity, osmotic pressure, and regulating the homeostasis of sodium and potassium (Hosseinifard et al., 2022). The accumulation of proline can be achieved through the activation of the proline biosynthetic pathway and the inactivation of the catabolic pathway (Kiyosue et al., 1996). In potato, PEG simulated drought stress promoted the up-regulated expression of Δ-1-pyrroline-5-carboxylate synthase (*P5CS*) and pyrroline-5-carboxylate reductase (*P5CR*) genes in the proline biosynthesis pathway, and inhibited the expression of pyrroline dehydrogenase (*PDH*) and Δ-1-pyrroline-5-carboxylate dehydrogenase (*P5CDH*) genes in the proline catabolic pathway, and the expression levels of *P5CS* and *P5CR* genes in the proline biosynthesis pathway were positively correlated with the proline contents (Liu et al., 2019). Over-expression of the *AtP5CS* gene could significantly improve the proline contents and salt tolerance of potato transgenic lines (Hmida-Sayari et al., 2005). A previous study has shown that the potato variety Desiree was more salt-tolerant than Mozart, and the expression level of the *P5CS1* gene was significantly up-regulated in Desiree under salt stress, while there was no significant change in Mozart (Jaarsma et al., 2013).

In addition, several genes, which were not involved in the proline metabolic pathway, could also enhance plant salt tolerance by promoting proline accumulation. El-Banna et al. (2010) demonstrated that transgenic suspension cells of the potato cultivar Desiree over-expressing the PR-10a protein could significantly improve the proline levels and salt tolerance compared to the wild-type cells, respectively. Transgenic Arabidopsis lines, which over-express glyceraldehyde 3-phosphate dehydrogenase (GAPDH) encoded by the *StD43* gene, showed a significantly higher proline content and salt tolerance than those in the wild-type (WT) lines (Kappachery et al., 2021). Over-expression of the *StCYS1* gene in transgenic potato plants significantly promoted their tolerance to high salinity and accumulation of proline and chlorophyll under salt stress (Liu M. et al., 2020). A previous study has found that different families of transcription factors (TFs) could activate the expressions of proline biosynthetic genes (Zarattini and Forlani, 2017). Ectopic expression of dehydration-responsive element binding proteins (StDREB2) proved that *StDREB2* might be involved in the potential response process of plants to abiotic stress by regulating the transcription level of gene *P5CS* to promote proline accumulation (Bouaziz et al., 2012).

Plants in response to different stresses are highly complex and involve changes at the transcriptome, cellular, and physiological levels, and involve the synergistic action of multiple genes, but previous studies on potato salt stress mainly focused on the physiological, biochemical, and functional verification of a few genes (Fidalgo et al., 2004; Levy and Veilleux, 2007; Chourasia et al., 2021). Moreover, transcriptome researches mostly focused on the identification of DEGs but rarely on elucidating gene regulatory networks, and transcriptome research for multiple time points (within 24 h) at the initial stress stages has not been reported. In this study, to gain further insights into the response mechanisms of potato to salt stress and mining key candidate genes that can improve potato salt tolerance, the DM test-tube plantlets treated with NaCl were used for RNA-seq analysis, and WGCNA was combined together to construct co-expression networks. Then multiple gene modules in the networks and TF-hub genes in each module were identified, respectively. Finally, the TF-hub genes with potential regulatory effects on the proline accumulation were screened according to the expression patterns of the DEGs in the proline metabolic pathway.

Materials and methods

Plant materials and salt treatment

The tissues of the doubled monoploid potato clone DM1-3 516 R44 (DM, a homozygous line, $2n = 2x = 24$) were cultured in test tubes containing 10 mL Murashige and Skoog solid medium (MS, 3% (w/v) sucrose, pH 5.6-5.8) in the light incubator with a 16-h light/8-h dark cycle, day/night temperatures of 22°C/18°C (Hardigan et al., 2016; Zeng et al., 2019).

The concentration of NaCl treatment was the same as that in previous studies (Zhou et al., 2018; Zhu et al., 2021). The transcript levels of the previously reported NaCl-responsive genes *StZFP1* (Tian et al., 2010; Liu Z. et al., 2020), *StMAPK3* (Zhu et al., 2020), and *StDWF4* (Zhou et al., 2018) were used to check the stress intensity of the test-tube plantlets to salt stress. 45-day-old test-tube plantlets were treated with 10 mL of liquid MS medium containing 400-mM NaCl (the treatment group, the final concentration of NaCl was 200 mM), and MS liquid medium as the control. After 24 h of ion balance, the treatment solutions in the test tubes were removed. At 3 h, 6 h, 12 h, and 24 h (S1, S2, S3, and S4) after the ion balance, the aboveground parts of DM test-tube plantlets were quickly cut off and put into liquid nitrogen immediately, then transferred to -80°C for cold storage, and the control group (CK, 10 mL MS) was collected at 24 h after the ion balance. The experiment was repeated three times with three biological replicates and four test-tube plantlets for each replicate.

RNA extraction and quality assessment

Total RNAs were extracted from the aboveground parts of DM test-tube plantlets from each NaCl treatment, using OmniPlant RNA Kit (DNase I) (CW2598S, CWBIO, China) following the manufacturer's instructions. RNA concentrations and purities were measured using NanoDrop 2000 (Thermo Fisher Scientific, Wilmington, DE). RNA integrities were assessed using the RNA Nano 6000 Assay Kit of the Agilent Bioanalyzer 2100 system (Agilent Technologies, CA, USA).

qRT-PCR analysis

Methods of qRT-PCR (quantitative real-time PCR) for gene expression analysis were applied according to our previously published protocols (Zhu et al., 2014; Zhu et al., 2016). The first-strand cDNA was synthesized from RNA used in RNA-seq by using PrimeScript™ RT reagent Kit with gDNA Eraser (RR047A, Takara, Japan), and then qRT-PCR was performed using TB Green® Premix Ex Taq™ I (RR820A, Takara, Japan). 16 genes were used for qRT-PCR assays to validate the reliability and accuracy of the RNA-seq data. The *StActin97* was used as the reference gene for gene expression normalization. The $2^{-\Delta\Delta Ct}$ method was used to calculate the relative expression levels of the genes. Each gene was examined in three biological replicates. The primer sequences used in this study are listed in Supplementary Table 1.

Library establishment and sequencing

A total of 1 μg RNA per sample was used as input material for the RNA sample preparations. Sequencing libraries were constructed by NEB Next UltraTM RNA Library Prep Kit for Illumina (NEB, USA). To select cDNA fragments of preferentially 240 bp in length, the library fragments were purified with the AMPure XP system (Beckman Coulter, Beverly, USA). Library quality was assessed on the Agilent Bioanalyzer 2100 system.

The clustering of the index-coded samples was performed on a cBot Cluster Generation System using TruSeq PE Cluster Kit v4-cBot-HS (Illumia) according to the manufacturer's instructions. After cluster generation, the libraries were sequenced using the Illumina platform and paired-end reads were generated.

Quality control of RNA-seq data

Raw data (raw reads) of fastq format were firstly processed through in-house Perl scripts. In this step, clean data (clean reads) were obtained by removing reads containing adapter, reads containing ploy-N and low-quality reads from raw data. At the same time, Q20, Q30, GC-content, and sequence duplication levels of the clean data were calculated. All the downstream analyses were based on clean data with high quality.

The principal component analysis (PCA) was performed using the PCAtools package in the R software (Kyritsis et al., 2021).

Alignment and annotations of new transcripts

The new transcripts were found by filtering out the sequences of short peptide chains (less than 50 amino acid residues) or single exons. The DIAMOND software was used to compare the new genes with NR, Swiss prot, COG, KOG, and KEGG databases, and then the new genes were analyzed with the GO database by InterPro (Jones et al., 2014; Buchfink et al., 2015). After predicting the new gene, HMMER software was used to compare it with the Pfam database (Eddy, 1998; Punta et al., 2011).

Quantitative gene expression, differentially expressed gene analysis, and prediction of TFs and TFBs

Raw sequences were transformed into clean reads after data processing, then these clean reads were mapped to the reference genome (DM v6.1) using the Hisat2 software. Gene expression levels were estimated by fragments per kilobase of transcript per million mapped reads (FPKM). A formula for the calculation of the FPKM was shown as follows:

FPKM=cDNA Fragments/(Mapped Fragments (Millions) * Transcript Length (kb)).

Differential expression analysis of each treatment was performed using the DESeq2 software. Genes with an adjusted *P*-value < 0.01 (FDR < 0.01) and Fold Change ≥ 2 found by DESeq2 were assigned as DEGs.

The information of TF families was predicted using Plant TFDB (http://planttfdb.cbi.pku.edu.cn/). TF binding sites (TFBs) in the promoter region were detected by using the "promoter analysis" function of the PlantPAN 2.0 database (http://plantpan.itps.ncku.edu.tw/promoter.php) (Chow et al., 2015; Zarattini and Forlani, 2017).

Enrichment analysis

Gene Ontology (GO) enrichment analysis of the differentially expressed genes (DEGs) was implemented by the GOseq R packages based on the Wallenius non-central hyper-geometric distribution (Young et al., 2010), which could adjust for gene length bias in DEGs.

Kyoto Encyclopedia of Genes and Genomes (KEGG) is a database resource for understanding high-level functions and utilities of the biological system, such as the cell, the organism, and the ecosystem, from molecular-level information, especially large-scale molecular datasets generated by genome sequencing and other high-throughput experimental technologies (http://www.genome.jp/kegg/) (Kanehisa et al., 2007). We used KOBAS software to test the statistical enrichment of DEGs in KEGG pathways (Mao et al., 2005).

Determination of proline and malondialdehyde contents

The contents of proline and malondialdehyde (MDA) in a total of 15 samples (S1, S2, S3, S4, and CK) were measured by Proline Determination Kit (colorimetry) (A107-1-1, Nanjing Jiancheng, China) and Plant Malondialdehyde Determination Kit (microplate method) (A003-3-1, Nanjing Jiancheng, China) following the manufacturer's protocols, respectively.

Weighted gene co-expression network analysis

The WGCNA package in R software was used to construct a gene co-expression network (FPKM ≥ 1, and variation of FPKM: cv ≥ 0.5), and the physiological indexes and gene expressions of the DEGs were analyzed in this study. The graphical network was created by Cytoscape 3.7.1 software for each module (weight ≥ 0.1) (Shannon et al., 2003).

Hub genes in each co-expressed module were defined according to module eigengene-based intramodular connectivity or module membership (kME) index in non-preserved modules (Panahi and Hejazi, 2021). Genes with |kME| ≥ 0.7 were considered as hub genes in the respective module (Langfelder and Horvath, 2008). The ggcor package in R software was used for correlation testing and visualization (Yang et al., 2021).

Dual luciferase reporter assay

A 711-bp full-length cDNA fragment of the potential key regulatory gene *StGLK014720* was cloned and recombined into the pGreen II 62-SK vector to generate an effector. 1,500-bp DNA fragments (upstream of TSS) of promoter regions of the seven DEGs in the proline metabolic pathway were cloned and inserted into the pGreenII 0800-LUC vector to obtain different reporters (Luo et al., 2022). The recombinant plasmids were transformed into the *Agrobacterium Tumefaciens* strain GV3101 (pMP90). The leaves of 4-week-old tobacco plants (*Nicotiana benthamiana*) were subjected to transient expression assays according to the previous methods (Cheng et al., 2022). The activities of Firefly Luciferase (LUC) and Renilla Luciferase (REN) were determined by using the Dual Luciferase Reporter Gene Assay Kit (11402ES60, Yeasen, China) according to the manufacturer's instructions. The ratio of LUC/REN showed the activity of the promoter. The tobacco leaves co-transformed with the reporter and pGreenII 62-SK vector without *StGLK014720* were used as the control, the LUC/REN ratio of which was taken as 1. Constructs for dual luciferase reporter assay were developed using primers mentioned in Supplementary Table 2.

Results

Transcriptional responses and transcriptome quality assessment

To check the transcriptional responses of the aboveground parts of DM test-tube plantlets under the 200-mM NaCl treatments, three NaCl-responsive genes previously reported as *StZFP1*, *StMAPK3*, and *StDWF4* were selected for qRT-PCR

assays. The results showed that the expression levels of the three representative genes were significantly up-regulated, and then significantly decreased at 12 h or 24 h after the NaCl treatments (Figure 1), which indicated that the 200-mM NaCl treatments were suitable for inducing salt stress to the plantlets.

To comprehensively understand the transcriptional responses to salt stress in potato, 15 cDNA libraries were constructed for RNA-seq analysis. After cleaning and quality control, a total of 140.29 Gb of sequencing data was obtained by Illumina Hi-seq 2000 platform (Supplementary Table 3). The data of all 15 samples were more than 7.31 GB, the Q30 bases accounted for greater than 91.49% of the total, and the GC contents were between 42.97% and 43.60% (Supplementary Table 3). The *S. tuberosum* DM v6.1 database was used as the reference genome, and the alignment results showed that 93.34%~96.72% of the reads were mapped to the reference genome (Supplementary Table 4). To verify the repeatability and reliability of the results, we performed principal component analysis (PCA) on the gene expression data of 15 samples. The analysis of the expression patterns showed that there were significant separations between NaCl-treated samples and the controls, and between samples at different treatment times, while the samples from biological replicates grouped together (Supplementary Figure 1).

To validate the reliability and accuracy of the RNA-seq data, and to confirm the expression patterns of the structural DEGs and their potential regulatory DEGs in the proline metabolic pathway, thirteen DEGs potentially related to proline metabolism and three NaCl-responsive genes were also selected for qRT-PCR assays. The results showed that the qRT-PCR results of the 16 genes were consistent with the RNA-seq data, demonstrating the accuracy of the RNA-seq data (Supplementary Figure 2).

Identification of novel transcripts, DEGs, and TF-encoding genes under salt stress

A total of 3716 novel transcripts were identified from the RNA-seq data, and 1920 new genes were functionally annotated (Supplementary Table 5). To identify DEGs among different treatments under salt stress, a total of 8383 DEGs were revealed by comparing and analyzing the RNA-seq data of NaCl-treated samples at different treatment times and the control. The Venn diagram indicated the numbers of the unique and shared DEGs under 200-mM NaCl treatments at different times (Figure 2A). We cross-compared the DEGs among the four different datasets *vs*. CK, which resulted in 3691 shared DEGs, comprised of 2434 up-regulated and 1257 down-regulated genes. Among the regulated genes under salt stress, 1029, 292, 337, and 253 genes were exclusively expressed at 3 h, 6 h, 12 h, and 24 h, respectively. As shown in Figure 2B, 2770, 3374, 3289, and 2899 genes were significantly up-regulated after NaCl treatment for 3 h, 6 h, 12 h, and 24 h, respectively. Among the down-regulated genes, the expressions of 3096, 2828, 2444, and 1944 genes were regulated specifically at 3 h, 6 h, 12 h, and 24 h, respectively (Figure 2C). In general, most DEGs showed up-regulated expression in samples treated with NaCl at four different time points (Figure 2D).

A total of 264 (7.15%) TF-coding genes were predicted in the 3691 DEGs, of which 198 genes were up-regulated while 66 genes were down-regulated (Figures 2E, F). These TFs mainly included AP2/ERF, WRKY, MYB, and NAC families, and the corresponding numbers of family members were 36, 35, 25, and 24, respectively. Further analysis revealed that the WRKY family had the largest number of up-regulated TF-coding genes (34) (Figure 2E), while the bHLH family had the largest number of down-regulated TF-coding genes (11) (Figure 2F).

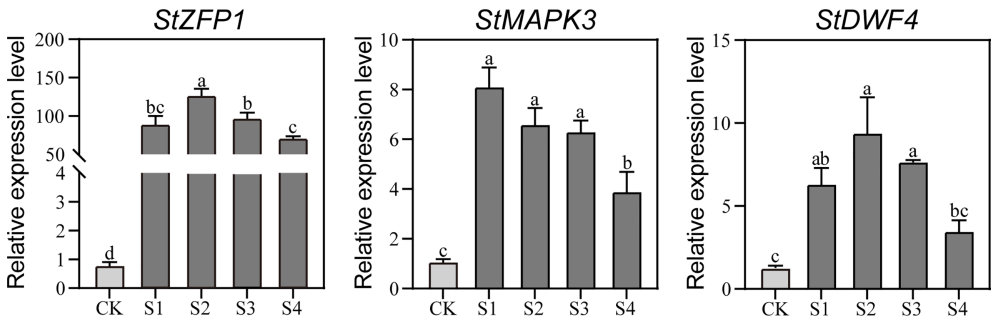

FIGURE 1
The qRT-PCR-based transcription analysis of the three NaCl-responsive genes in the DM plantlets under NaCl stress. Gene expression is normalized relative to the potato reference gene *StActin97*. Data presented as mean ± standard error from three biological replicates were tested by one-way analysis of variance (ANOVA). Different letters represent statistically significant differences ($\alpha = 0.05$). S1, S2, S3, and S4, represent the aboveground parts of DM text-tube plantlets under 200-mM NaCl treatment for 3, 6, 12, and 24 h, respectively; CK represents the aboveground parts of DM text-tube plantlets after 24 h treatment with MS liquid medium (the same below).

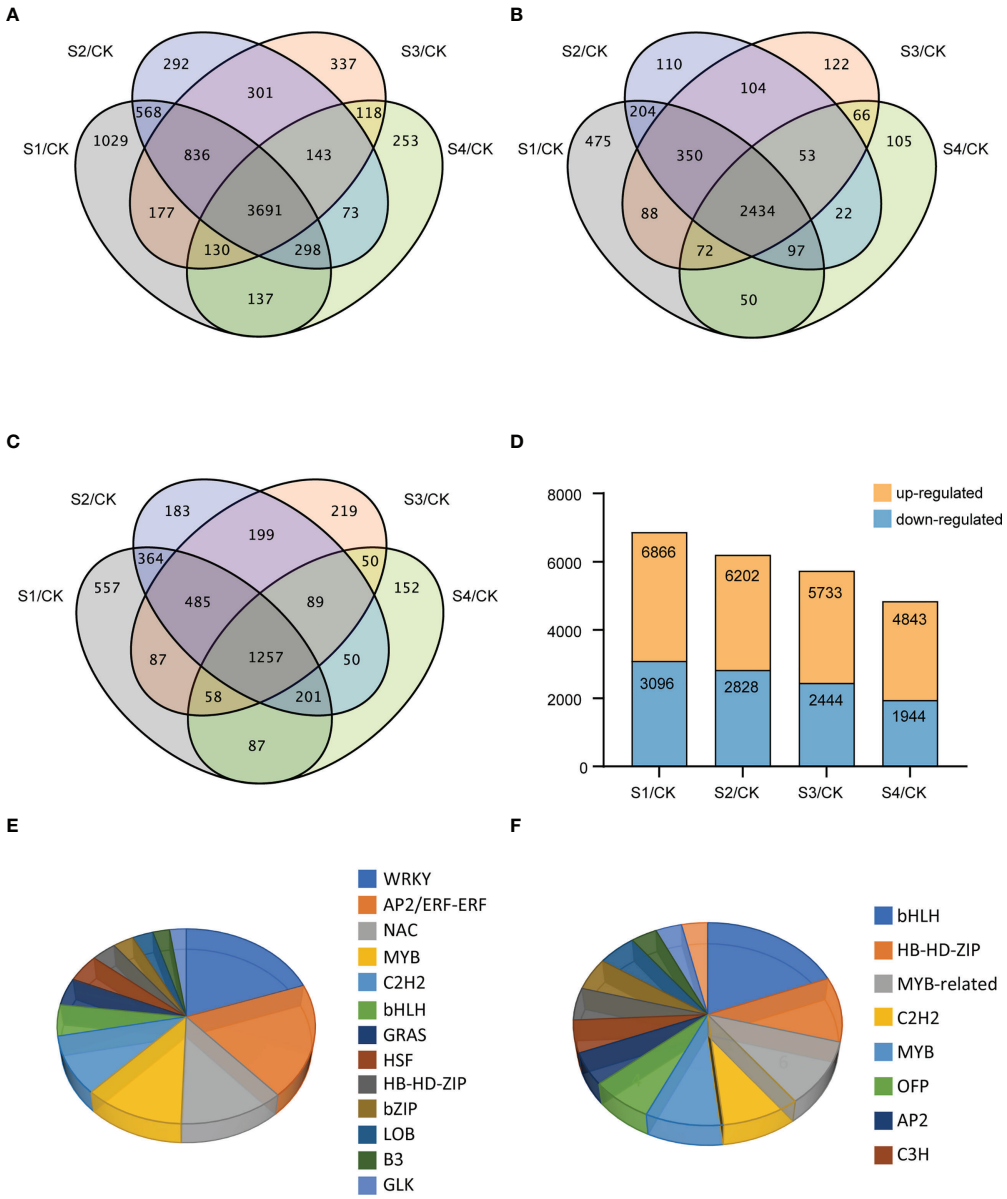

FIGURE 2
Differentially expressed genes (DEGs) and TF-coding genes after 3, 6, 12, and 24 h of NaCl stress in the DM plantlets. **(A–C)** Venn diagrams for all, up-, and down-regulated genes, respectively. **(D)** Distribution diagram for the numbers of the DEGs at different salt treatment times, and all NaCl-treated samples were compared with CK samples. **(E, F)** Pie charts for the numbers of up-regulated and down-regulated genes in different TF families of potato under salt stress, respectively.

Enrichment analysis of the DEGs

To understand the biological functions and molecular responses in metabolic pathways of potato DEGs under salt stress, enrichment analysis of the DEGs was carried out in this study based on the GO and KEGG databases. Among the shared 3691 DEGs in all differential groups, 2936 and 2500 genes could be annotated by GO and KEGG databases, respectively.

GO enrichment analysis of these annotated DEGs shows that the DEGs participated in three categories: "biological process, BP", "cell composition, CC" and "molecular function, MF" (Supplementary Figure 3). "Cell process" and "metabolic process" were the most obvious terms in the biological process category; "Binding" and "catalytic activity" were the most enriched in the metabolic process category; in the cell composition category, "membrane" had the largest number of

genes. Notably, the distribution pattern of DEGs annotated in the GO database was different from all potato genes. A higher proportion of DEGs annotated in the GO database were enriched in "detoxification, BP", "antioxidant activity, MF", and "nucleic acid binding transcription factor activity, MF".

We identified the KEGG pathway with the largest proportion of the DEGs in potato under salt stress (KEGG ontology terms, $P < 0.05$) (Chen et al., 2021). NaCl treatment significantly affected metabolic pathways in the aboveground parts of DM test-tube plantlets, including "photosynthesis-antenna proteins", "carbon fixation in photosynthetic organizations", "phenylalanine metabolism", and "glutathione metabolism" (Supplementary Figure 4).

KEGG enrichment analysis showed that a total of 19 DEGs were enriched in the "arginine and proline metabolism" (ko00330) pathway, of which up to 13 DEGs were concentrated in the proline metabolic pathway (Figure 3A). The 13 DEGs included not only main hot-spot genes in

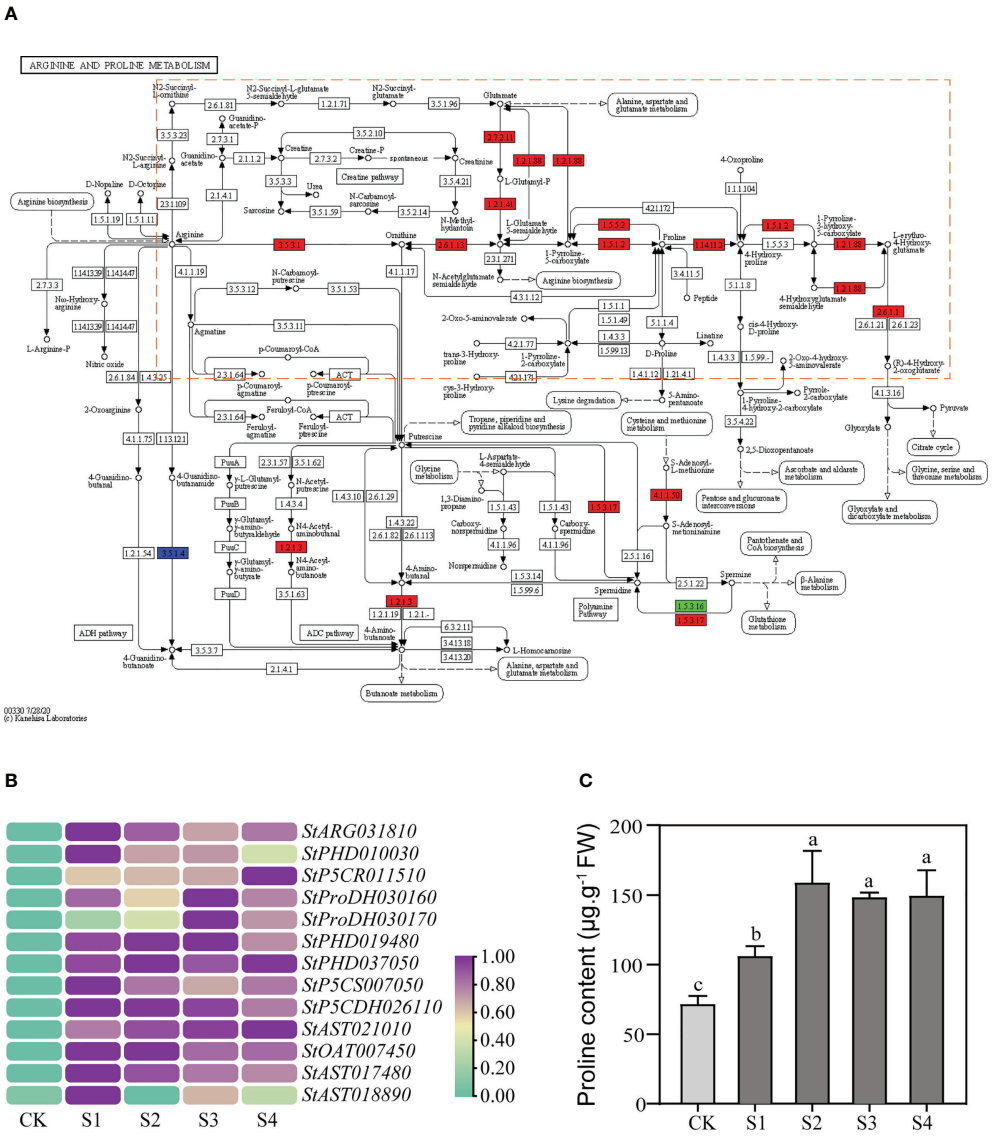

FIGURE 3
Expression levels of the structural DEGs in the proline metabolic pathway and the proline contents in the DM plantlets under salt stress. **(A)** Differential expression of the structural DEGs in KEGG enrichment analysis. The green rectangle represents the DEGs down-regulated; the red rectangle represents the DEGs up-regulated; the blue rectangle represents both up-regulated and down-regulated DEGs. The proline metabolic pathway is highlighted by orange dotted frame. **(B)** Heat map of the structural DEGs in the proline metabolic pathway. **(C)** Changes of the proline contents in aboveground parts of DM text-tube plantlets under the 200-mM NaCl treatments. Data presented as mean ± standard error from three biological replicates were tested by one-way analysis of variance (ANOVA). Different letters represent statistically significant differences ($\alpha = 0.05$).

proline research, such as *P5CS*, *P5CR*, *ProDH*, and *P5CDH*, but also many genes that have received little attention, such as *ARG* and *AST* (Supplementary Table 6). Overall, we found that many genes in the proline metabolic pathway were up-regulated under salt stress, and their functions almost covered the whole proline metabolic process (Figure 3A; Supplementary Table 6).

Salt stress changed the expression levels of the proline metabolic genes and the proline contents

Further results showed that expression levels of all the 13 structural DEGs in the proline metabolic pathway were significantly up-regulated under salt stress (Figure 3B). The expression levels of 5 (35.7%) of the 13 structural DEGs peaked at 12 h or 24 h and increased 1.96~7.66 times more than that of the controls. These structural DEGs comprised *StP5CR011510*, *StProDH030160*, *StProDH030170*, *StPHD019480*, and *StAST021010*, while the peaks of the expression levels of the remaining 8 structural DEGs appeared in advance at 3 h or 6 h and the expression levels increased 1.96~7.66 times more than that of the controls (Figure 3B).

To verify the correlation between the expression levels of the proline metabolic genes and the proline contents, we measured the proline contents in DM plantlets under salt stress, and the content of free proline can also be used as an indicator to reflect the osmotic adjustment system. Meanwhile, we also measured MDA content as the marker to measure oxidative damage. The proline contents increased gradually after 200-mM NaCl treatments and reached maximum at 6 h, which was 157.78 $\mu g \cdot g^{-1}$ and 2.22 times higher than the control, then stabilized with extension of time (Figure 3C). The results indicated that salt stress significantly promoted proline accumulation in the aboveground parts of DM test-tube plantlets. However, the MDA contents did not change significantly with the extension of time (Supplementary Figure 5).

WGCNA analysis and TF-hub genes identification

WGCNA analysis was used to identify the co-expressed gene modules and construct the interrelationship network between genes, and to reveal the hub genes in response to salt stress. A co-expression network was generated according to the expression of the DEGs in 15 samples, the genes with similar expression patterns were assigned into the same module, and finally a total of 10 different modules were identified (Figures 4A, B). The spatio-temporal specific modules lightcyan and tan were significantly positively correlated with the proline contents (R = 0.63~0.65, P = 0.008~0.01) (Figure 4C). The genes with $|kME| \geq 0.7$ were regarded as the hub genes of the module, and the hub genes represent the overall functionality of the module. Combined with gene domain analysis, the hub genes with TF domains (TF-hub genes) were identified in the modules.

A total of 44 hub genes were delimited in the lightcyan module, which were expressed at low levels in the control samples (CK), but had the highest expression levels in the NaCl-treated samples at 24 h (S4) (Supplementary Figure 6A). KEGG enrichment analysis indicated that these genes slowly responded to salt stress (24 h) and were mainly involved in the synthesis pathways of secondary metabolites such as "phenylpropanoid biosynthesis, ko00940" and "flavonoid biosynthesis, ko00941", the two most significantly enriched metabolic pathways. The lightcyan module contained five TF-hub genes: GLK family encoding gene *StGLK014720*, NAC family encoding gene *StNAC015310*, WRKY family encoding gene *StWRKY026100*, C2H2 family encoding gene *StC2H2001820*, and MADS-MIKC family encoding gene *StMADS036110* (Supplementary Table 7). The Cytoscape software (weight ≥ 0.1) was used to create a visual gene interaction network in the lightcyan module (Supplementary Figure 6B). Hub genes with more connections in the network might be the key regulatory genes. The TF-hub genes, except for *StC2H2001820*, were located in the visual gene interaction network of the lightcyan module.

A total of 68 hub genes were found in the tan module, and most of them responded to salt stress at 6 h and 12 h (Supplementary Figure 7A). GO enrichment analysis showed that the hub genes in the tan module were significantly enriched in "iron ion binding, BF". KEGG enrichment analysis found that the most significantly enriched pathways were "plant hormone signal transduction" (ko04075), suggesting that the hub genes within the module respond to salt stress perhaps *via* regulating plant hormones. There were eight TF-hub genes in the tan module, including C2C2-CO-like family encoding genes *StCOL012520* and *StCOL023800*, GARP-G2-like (GLK) family encoding genes *StGLK031660* and *StGLK003930*, bHLH family encoding gene *StbHLH026970*, bZIP family encoding gene *StbZIP015000*, HSF family encoding gene *StHSF025050* and B3-ARF family encoding gene *StARF010540* (Supplementary Table 8). To further understand the regulatory genes in the tan module, a visual gene interaction network was constructed by using Cytoscape software (weight ≥ 0.1), in which each node represents a gene and the connecting lines (edges) between genes represent co-expression correlations (Supplementary Figure 7B). The results showed that all eight TF-hub genes were located in the interaction network of the tan module.

Screening of the structural DEGs and their potential regulatory TF-hub genes

Correlation analysis showed that the expression levels of 12 (92.3%) of the 13 structural DEGs in the proline metabolic

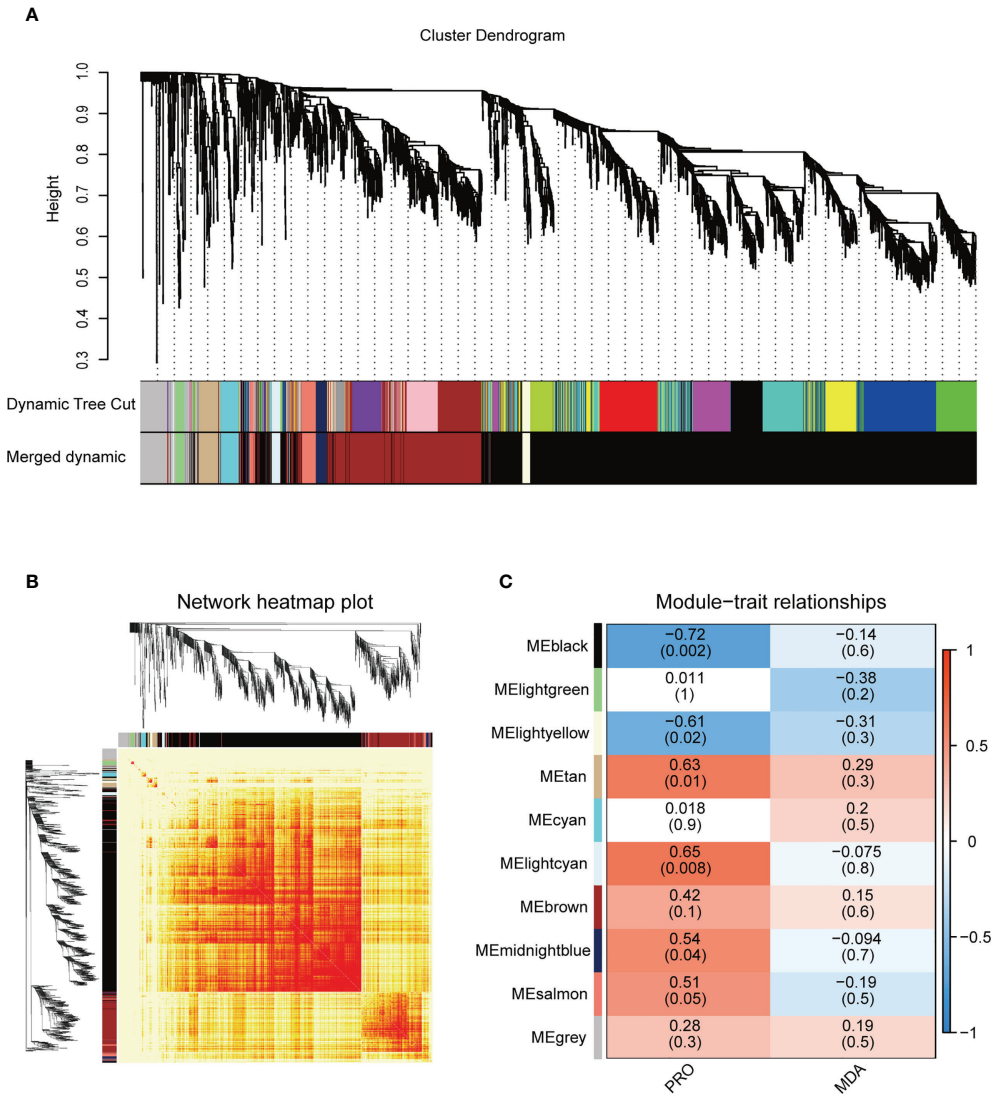

FIGURE 4
Weighted gene co-expression network analysis (WGCNA) of salt stress-responsive genes in the DM plantlets under salt stress. **(A)** Hierarchical cluster tree of the common genes between different studies. The branches and color bands represent the assigned modules; the tips of the branches represent genes. **(B)** The heat map shows the Topological Overlap Matrix (TOM) value among the proteins of the network delimited into modules by the dynamic method. Lower TOM is indicated by the yellow color and higher TOM is indicated by the progressively red color. **(C)** The thermogram showed the correlations between the modules and the contents of proline and malondialdehyde. No significant correlations are displayed in white, positive correlations and negative correlations are displayed in red and blue, respectively. PRO, proline; MDA, malondialdehyde (the same below).

pathway were significantly positively correlated with proline contents (Mantel's r = 0.33~0.82, Mantel's $p < 0.05$). Eight of them were Mantel's r ≥ 0.7, including *StARG031810*, *StP5CR011510*, *StPHD019480*, *StP5CS007050*, *StP5CDH026110*, *StAST021010*, *StOAT007450*, and *StAST017480* (Figure 5A). Meanwhile, the correlations between the proline contents and the expression levels of the 13 TF-hub genes obtained from WGCNA analysis were also analyzed (Figure 5A). The results showed that the expression levels of 7 of the 13 TF-hub genes were significantly positively correlated with the proline contents (Mantel's r = 0.29~0.75, Mantel's $p < 0.05$). These genes were comprised of GLK family encoding genes *StGLK031660* and *StGLK014720*, HSF family encoding genes *StHSF025050*, NAC family encoding genes *StNAC015310*, WRKY family encoding genes *StWRKY026100*, C2H2 family encoding gene *StC2H2001820*, and MADS-MIKC family encoding gene *StMADS036110*. There was only one gene *StGLK014720* with Mantel's r ≥ 0.7.

10.3389/fpls.2022.1030138

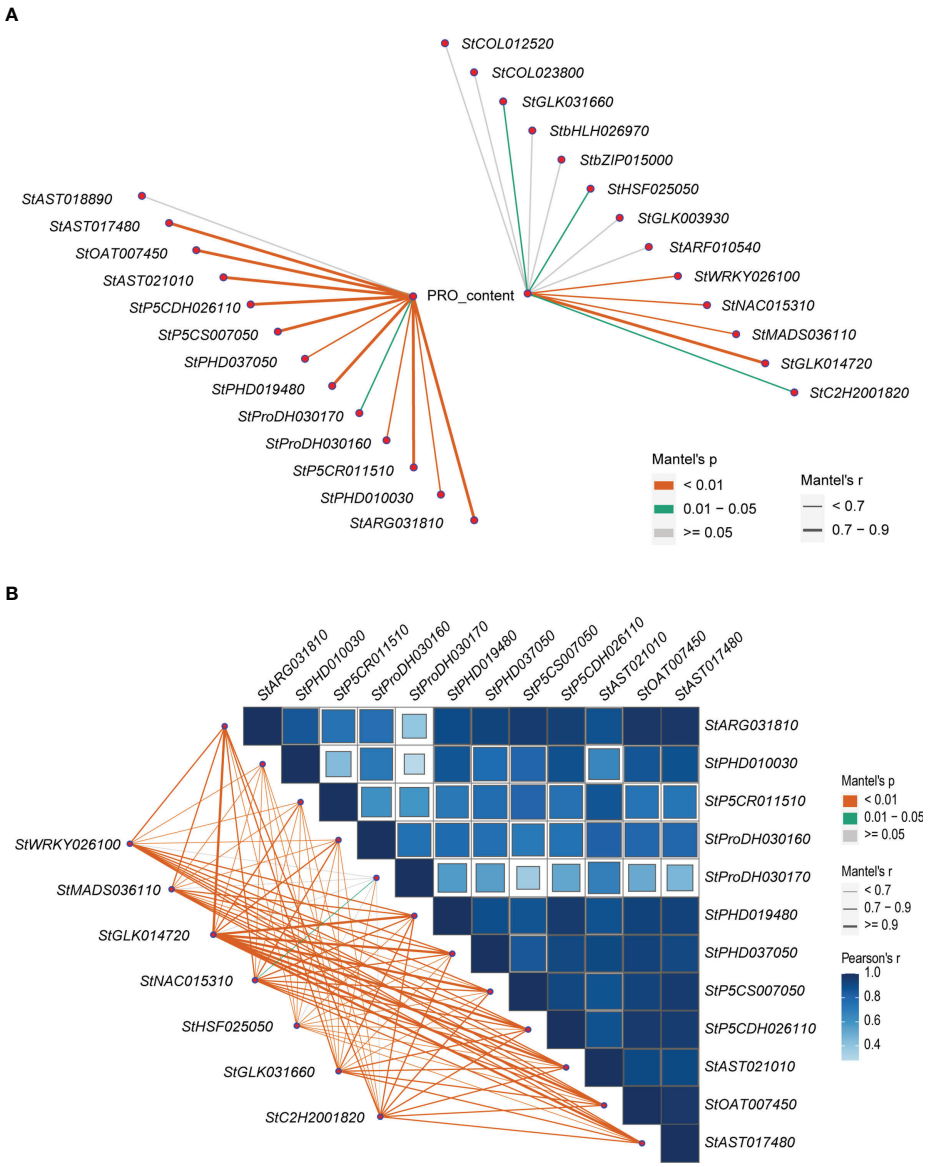

FIGURE 5
Correlation maps related to the proline contents, the expression levels of the structural DEGs and the TF-hub genes. **(A)** The correlations between the proline contents and the expression levels of the 13 structural DEGs in the proline metabolic pathway and the expression levels of the 13 TF-hub genes. **(B)** The correlations among the expression levels of the 12 structural DEGs in the proline metabolic pathway and between the expression levels of the 7 TF-hub genes and the 12 structural DEGs in the proline metabolic pathway. The lines correspond to the expression correlations between the 7 TF-hub genes and the 12 structural DEGs. The colors of the lines represent the Mantel's *p*, and the thicknesses of the lines represent the percentage of the Mantel's r. The intensity of the blue color and the size of the box indicate the degree of the expression correlation among the 12 structural DEGs.

Then, the correlations between the expression levels of the 7 TF-hub genes significantly positively correlated with the proline contents, and the 12 structural DEGs in the proline metabolic pathway were further analyzed. The results showed that among the seven TF-hub genes, except for *StHSF025050*, the expression levels of each of the other six TF-hub genes were significantly positively correlated with that of 6~10 structural DEGs in the proline metabolic pathway (Mantel's r ≥ 0.7, Mantel's p < 0.01) (Figure 5B).

Interestingly, we found that the expression levels of each of the four TF-hub genes *StGLK014720*, *StNAC015310*, *StWRKY026100*, and *StC2H2001820* were highly

significantly and positively correlated with those of eight of the same structural DEGs in the proline metabolic pathway (Mantel's r ≥ 0.7, Mantel's $p < 0.01$), and the highest correlations were found between the TF-hub gene *StGLK014720* and the eight of the same structural DEGs in the proline metabolic pathway (Mantel's r > 0.9, Supplementary Table 9), indicating that the *StGLK014720* could be used as a key regulatory gene in the proline metabolic pathway under salt stress. Meanwhile, except for the structural DEG *StPHD037050*, the expression levels of the remaining 7 structural DEGs in the proline metabolic pathway were highly positively correlated with the proline contents (Mantel's r ≥ 0.7, Mantel's $p < 0.01$) (Figure 5A).

The protein StGLK014720 could activate the promoters of both structural genes *StAST021010* and *StAST017480*

To predict the existence of TF binding sites (TFBs) in the promoter regions of the seven structural DEGs in the proline metabolic pathway, PlantPAN 2.0 database was used to analyze TFBs in gene promoter regions (1.5 Kb upstream of TSS). The results showed that the promoter regions of each of the seven structural DEGs presented multiple TFBs known to be recognized by all the four TF families. The largest number of GLK TFBs was predicted in the promoter region of the structural gene *StOAT007450*, with a total of 11 sites (Figure 6A). For the other

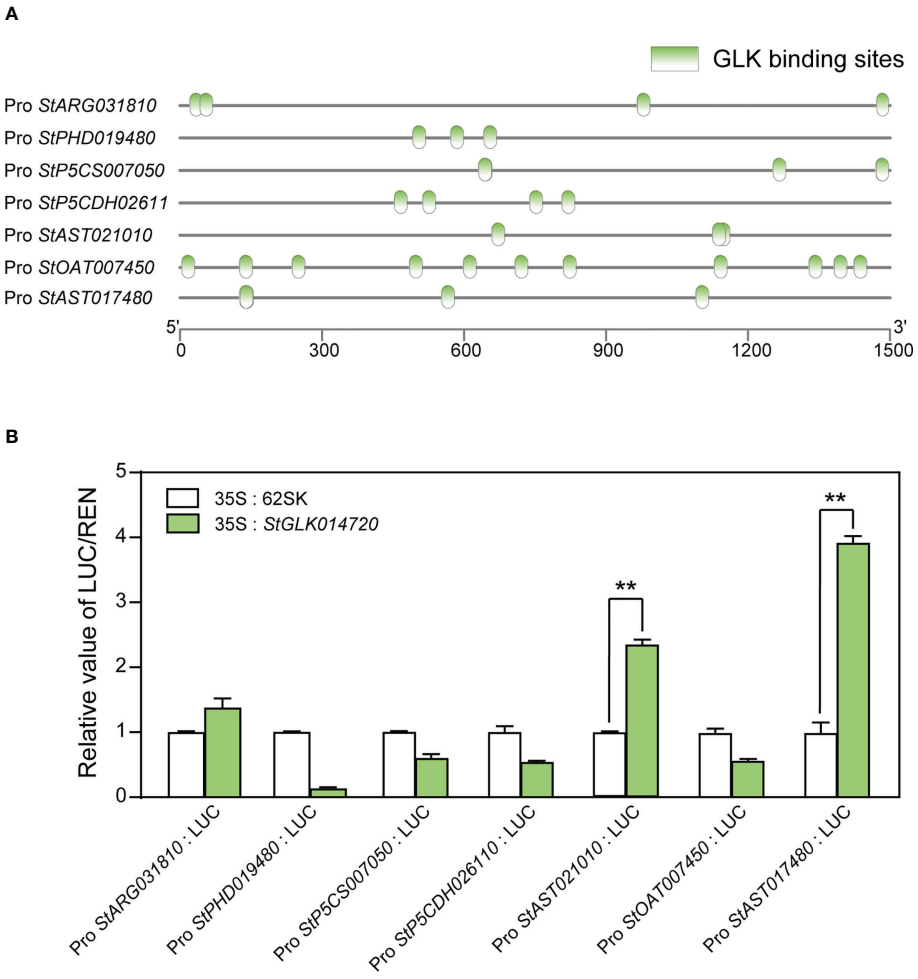

FIGURE 6
TFBs prediction and dual luciferase reporter assay between the protein StGLK014720 and the seven structural DEGs in the proline metabolic pathway. **(A)** Prediction of GLK binding sites in the promoter regions of the 7 structural DEGs in the proline metabolic pathway. **(B)** The ratios of LUC activity relative to REN activity represent the relative activities of the proline structural gene promoters. The LUC/REN ratios of the control were set to 1, to which the ratios of other groups were normalized. Data presented as means ± standard error from three biological replicates were tested by the Student *t*-test (** $P < 0.01$).

three TF families NAC, C2H2, and WRKY, the numbers of TFBs to all the seven structural genes were 2~18, 3~7, and 4~30, respectively (Supplementary Figure 8).

To determine whether the key regulatory protein StGLK014720 can activate the promoters of the seven structural DEGs, a dual luciferase (LUC) assay was performed. *StGLK014720* driven by the CaMV35S promoter was used as an effector, while the promoters of the seven structural genes fused with LUC were used as the reporters. When the tobacco leaves co-transformed with the effector and the reporters, the LUC/REN ratios of the *StAST021010* and *StAST017480* were 2.2 and 3.9, respectively, and were drastically elevated when compared to the controls ($P < 0.01$, Figure 6B). These results indicated that the regulatory protein StGLK014720 could activate the promoters of both structural genes *StAST021010* and *StAST017480*.

Discussion

Biosynthesis and degradation of proline under salt stress

Under salt stress, an increase in proline content was noted in many plants (Ghosh et al., 2022). A study in wheat supported that a high level of salt stress induced a sharp increase in the proline concentration (Hinai et al., 2022). The same type of response was noted for the rapid accumulation of free proline in salt-tolerant wild rice (Nguyen et al., 2021). In addition, the proline content was significantly increased throughout the experiment as the salt concentration increased in tomato seedlings (Shin et al., 2020). The results of our study indicated that the proline accumulation was also significantly increased in the aboveground parts of DM test-tube plantlets. Proline accumulation is achieved mainly by promoting proline biosynthesis in the cytosol and by inhibiting proline degradation in mitochondria (Lebreton et al., 2020). Proline biosynthesis can take place in different subcellular compartments such as the cytosol and chloroplast, and it is accomplished by different metabolic pathways such as the glutamate or ornithine pathway, depending on environmental conditions (Szabados and Savouré, 2010). In this study, the 13 structural DEGs identified in the proline metabolic pathway will contribute to further research on the molecular mechanism of proline accumulation in potato under salt stress (Figure 7).

Proline biosynthesis in most plant species occurs mainly from glutamate by the sequential steps of enzymes P5CS and P5CR (Furlan et al., 2020). In this study, it was found that the expression levels of genes *P5CS* and *P5CR* were significantly up-regulated in potato plantlets under salt stress, and the expression levels of the two genes were highly positively correlated with the proline contents, which was consistent with the results reported by Székely et al. (2008) in Arabidopsis, suggesting that genes *P5CS* and *P5CR* may promote the conversion of glutamate to proline. Hmida-Sayari et al. (2005) overexpressed the *P5CS* gene of *Arabidopsis Thaliana* in potato, and found that the proline accumulation and salt tolerance of transgenic potato lines were significantly enhanced. In addition, the ornithine pathway can also synthesize proline, which was initially transaminated by ornithine-delta-aminotransferase (OAT) producing GSA and P5C, and then converted to proline (Iqbal et al., 2014). We found that the expression levels of the *ornithine aminotransferase* (*OAT*) gene in the ornithine pathway and *arginase* (*ARG*) gene, which catalyzes the conversion of arginine to ornithine, were significantly up-regulated after salt treatment and highly positively correlated with the proline contents. Therefore, these results indicated that salt stress not only promoted the glutamate pathway, but also activated the ornithine pathway to achieve proline accumulation and thereby enhanced plant salt tolerance.

On the contrary, in the catabolic pathway, proline can be catalyzed by the sequential action of proline dehydrogenase (ProDH) and P5C dehydrogenase (P5CDH) to glutamate (Arabia et al., 2021). We identified several genes that promote proline decomposition in potato DEGs under salt stress, encoding ProDH, P5CDH, PHD, and AST, respectively. The house-keeping enzyme ProDH in proline degradation was inhibited in NaCl-treated wheat seedlings (Liu L. et al., 2020). However, in this study, all the structural DEGs in the proline catabolism pathway were up-regulated under salt stress. Therefore, it is speculated that the proline accumulation in the aboveground parts of DM test-tube plantlets might be achieved mainly by up-regulation of the proline biosynthesis pathway rather than by inhibition of the proline degradation pathway. In fact, activation of the proline catabolism was necessary for maintaining the growth of crop plants exposed to lengthy periods of stress (Kavi Kishor and Sreenivasulu, 2014). Although the expression patterns and functions of the structural genes in the proline metabolic pathway have been widely reported, the regulatory patterns are still unclear.

Potential transcription factors regulating proline metabolism

Transcription factors (TFs) play a key role in response to salt stress. The results of our study showed that TF-coding genes in the 3691 DEGs shared among all the salt treatments were mainly distributed in the AP2/ERF, WRKY, MYB, and NAC families, which were consistent with the previous studies in rice and bermudagrass (Zhu et al., 2019; Shao et al., 2021). The four TF-hub genes obtained by WGCNA analysis were highly positively correlated with the expression levels of several structural DEGs in the proline metabolic pathway, and several TFBs corresponding to TFs were predicted at the promoter regions of the structural DEGs. Therefore, we speculated that the four TF-hub genes, including *StNAC015310*, *StWRKY026100*, *StC2H2001820*, and *StGLK014720*, might promote proline

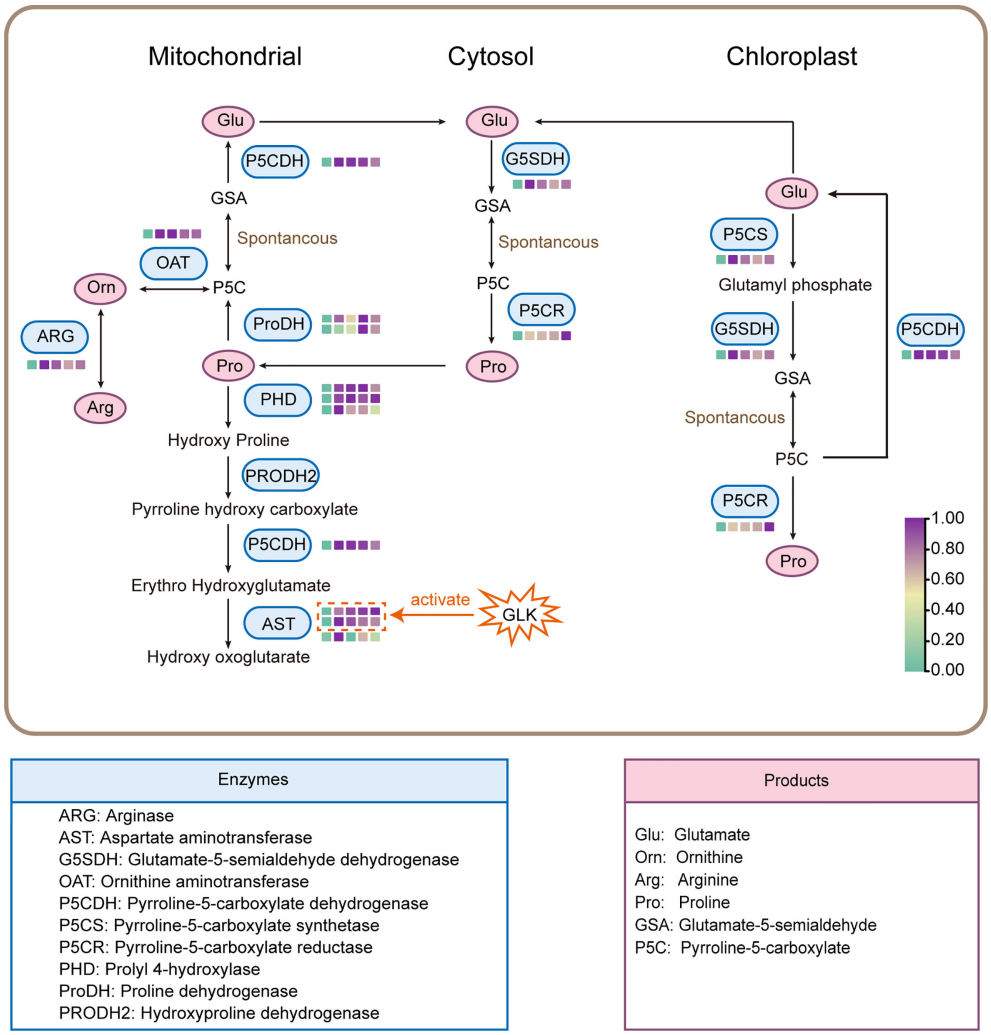

FIGURE 7
Proline biosynthesis and degradation pathway. The color of the box (□) represents the gene expression in different NaCl treatments.

accumulation under salt stress by increasing the expression levels of the proline metabolic pathway genes.

NACs [no apical meristem (NAM), *Arabidopsis thaliana* transcription activation factor (ATAF1,2), and cup-shaped cotyledon (CUC2)] proteins belong to one of the largest plant-specific TF families and play important roles in plant development processes, response to biotic and abiotic cues, and hormone signaling (Singh et al., 2013). Wang et al. (2021) found that the NAC family gene *StNAC053* (*Soltu.DM.06G017300*) in potato was in response to salt stress, and the Arabidopsis transgenic lines over-expressing this gene had significantly enhanced tolerance to salt stress. Coincidentally, the novel gene *StNAC015310* in response to salt stress in this study also belongs to the NAC family and has the potential function of regulating the expression of genes in the proline metabolic pathway, and its salt tolerance needs to be further studied.

In plants, WRKY and C2H2 are important TF families that regulate a variety of biological processes and a wide range of biotic and abiotic stresses (Ahammed et al., 2020; Luo et al., 2022). The heterologous expression of the *Dioscorea composita* gene *DcWRKY3* strongly improved the salt tolerance of Arabidopsis transgenic lines, and the yeast one-hybrid (Y1H) assay verified the interaction between transcription factor DcWRKY3 and the promoter of proline synthesis gene *AtP5CS1* (Yu et al., 2022). Y1H and dual luciferase (LUC) assays showed that the C2H2 transcription factor RmZAT10, which promoted proline accumulation under salt stress, could interact with and activate the promoter of gene *RmP5CS*, and thereby elevate the expression level of gene *RmP5CS* (Luo et al.,

2022). Therefore, the genes *StWRKY026100* and *StC2H2001820* discovered in this study might be novel genes in the regulation of the proline metabolic pathway, which had the potential function to regulate the structural gene *StP5CS007050* and yet to be confirmed in the near future.

The plant-specific GARP transcription factor family (composed of ARR-B and GLK type) contains genes with a variety of functions, including nutrient sensing, root and shoot development, floral transition, chloroplast development, circadian clock oscillation maintenance, hormone transport and signaling (Safi et al., 2017). However, GLK family proteins have not been reported in response to salt stress. Interestingly, our study found that the expression level of potato GLK family gene *StGLK014720* was highly positively correlated with that of the seven structural DEGs in the proline metabolic pathway (Mantel's $r > 0.9$), and the protein StGLK014720 could activate the promoters of both AST encoding genes *StAST021010* and *StAST017480*, but not other structural DEGs, indicating that StGLK014720 may enhance the salt tolerance of potato plantlets by directly or indirectly regulating the AST protein expression at the transcriptional level (Figure 7). Increased AST activities under salt stress have previously been reported for different crop plants (Surabhi et al., 2008; Gao et al., 2013; Naliwajski and Sklodowska, 2018; Ullah et al., 2019). The up-regulated expression of both genes *StAST021010* and *StAST017480* may enable the potato plantlets exposed to the salt stress to maintain the efficient capacity of ammonia detoxification and proline homeostasis (Surabhi et al., 2008; Gao et al., 2013; Kavi Kishor and Sreenivasulu, 2014). However, further transgenic experiment is required to confirm the regulatory role of StGLK014720 under salt stress in potato plants.

Data availability statement

The data presented in the study are deposited in the NCBI repository, accession number PRJNA882516 (https://www.ncbi.nlm.nih.gov/bioproject/PRJNA882516).

Author contributions

XZ, ZL, QJ, and HH conceived and designed the experiments. QJ, XM, AC, and HZ performed the experiments. QJ, LW, and SZ analyzed the data. QJ, XZ, and ZL prepared the manuscript. XZ, ZL, and HH revised the manuscript. All authors contributed to the article and approved the submitted version.

Funding

This research was supported by the National Natural Science Foundation of China (31771857), Anhui Provincial Natural Science Foundation (1808085MC65, 22232004), and Research Start-up Funds for High-level Personnels in Anhui Agricultural University (rc322101).

Acknowledgments

The authors gratefully acknowledge Jun Sun of Anhui Agricultural University for providing the pGreen II 62-SK and the pGreenII 0800-LUC plasmids.

Conflict of interest

The authors declare that the research was conducted in the absence of any commercial or financial relationships that could be construed as a potential conflict of interest.

Publisher's note

Supplementary material

The Supplementary Material for this article can be found online at: https://www.frontiersin.org/articles/10.3389/fpls.2022.1030138/full#supplementary-material

References

Ahammed, G. J., Li, X., Wan, H., Zhou, G., and Cheng, Y. (2020). *SlWRKY81* reduces drought tolerance by attenuating proline biosynthesis in tomato. *Sci. Hortic.* 270, 109444. doi: 10.1016/j.scienta.2020.109444

Arabia, S., Shah, M. N. A., Sami, A. A., Ghosh, A., and Islam, T. (2021). Identification and expression profiling of proline metabolizing genes in *Arabidopsis thaliana* and *Oryza sativa* to reveal their stress-specific transcript alteration. *Physiol. Mol. Biol. Plants* 27 (7), 1469–1485. doi: 10.1007/s12298-021-01023-0

Bouaziz, D., Pirrello, J., Ben Amor, H., Hammami, A., Charfeddine, M., Dhieb, A., et al. (2012). Ectopic expression of dehydration responsive element binding proteins (StDREB2) confers higher tolerance to salt stress in potato. *Plant Physiol. Biochem.* 60, 98–108. doi: 10.1016/j.plaphy.2012.07.029

Buchfink, B., Xie, C., and Huson, D. H. (2015). Fast and sensitive protein alignment using DIAMOND. *Nat. Methods* 12 (1), 59–60. doi: 10.1038/nmeth.3176

Cheng, H., Wu, W., Liu, X., Wang, Y., and Xu, P. (2022). Transcription factor CsWRKY40 regulates l-theanine hydrolysis by activating the *CsPDX2.1* promoter in tea leaves during withering. *Hortic. Res.* 9, uhac025. doi: 10.1093/hr/uhac025

Chen, Z., Niu, J., Guo, Z., Sui, X., Xu, N., Kareem, H. A., et al. (2021). Integrating transcriptome and physiological analyses to elucidate the essential biological mechanisms of graphene phytotoxicity of alfalfa (*Medicago sativa* l.). *Ecotoxicol. Environ. Saf.* 220, 112348. doi: 10.1016/j.ecoenv.2021.112348

Choudhary, S., Wani, K. I., Naeem, M., Khan, M. M. A., and Aftab, T. (2022). Cellular responses, osmotic adjustments, and role of osmolytes in providing salt stress resilience in higher plants: polyamines and nitric oxide crosstalk. *J. Plant Growth Regul.* doi: 10.1007/s00344-022-10584-7

Chourasia, K. N., Lal, M. K., Tiwari, R. K., Dev, D., Kardile, H. B., Patil, V. U., et al. (2021). Salinity stress in potato: understanding physiological, biochemical and molecular responses. *Life* 11 (6), 545. doi: 10.3390/life11060545

Chow, C. -N., Zheng, H. -Q, Wu, N. -Y, Chien, C. -H, Huang, H. -D., Lee, T. -Y., et al. (2015). PlantPAN 2.0: An update of plant promoter analysis navigator for reconstructing transcriptional regulatory networks in plants. *Nucleic Acids Res.* 4, 1154–60. doi: 10.1093/nar/gkv1035

Dahal, K., Li, X.-Q., Tai, H., Creelman, A., and Bizimungu, B. (2019). Improving potato stress tolerance and tuber yield under a climate change scenario – a current overview. *Front. Plant Sci.* 10. doi: 10.3389/fpls.2019.00563

Eddy, S. R. (1998). Profile hidden Markov models. *Bioinformatics* 14 (9), 755–763. doi: 10.1093/bioinformatics/14.9.755

El-Banna, A., Hajirezaei, M.-R., Wissing, J., Ali, Z., Vaas, L., Heine-Dobbernack, E., et al. (2010). Over-expression of PR-10a leads to increased salt and osmotic tolerance in potato cell cultures. *J. Biotechnol.* 150 (3), 277–287. doi: 10.1016/j.jbiotec.2010.09.934

Fidalgo, F., Santos, A., Santos, I., and Salema, R. (2004). Effects of long-term salt stress on antioxidant defence systems, leaf water relations and chloroplast ultrastructure of potato plants. *Ann. Appl. Biol.* 145 (2), 185–192. doi: 10.1111/j.1744-7348.2004.tb00374.x

Furlan, A. L., Bianucci, E., Giordano, W., Castro, S., and Becker, D. F. (2020). Proline metabolic dynamics and implications in drought tolerance of peanut plants. *Plant Physiol. Biochem.* 151, 566–578. doi: 10.1016/j.plaphy.2020.04.010

Gao, S., Liu, K. T., Chung, T. W., and Chen, F. (2013). The effects of NaCl stress on *Jatropha* cotyledon growth and nitrogen metabolism. *J. Soil Sci. Plant Nutr.* 13 (1), 99–113. doi: 10.4067/s0718-95162013005000010

Ghosh, U., Islam, M., Siddiqui, M., Cao, X., and Khan, M. (2022). Proline, a multifaceted signalling molecule in plant responses to abiotic stress: understanding the physiological mechanisms. *Plant Biol.* 24 (2), 227–239. doi: 10.1111/plb.13363

Gul, Z., Tang, Z.-H., Arif, M., and Ye, Z. (2022). An insight into abiotic stress and influx tolerance mechanisms in plants to cope in saline environments. *Biology* 11 (4), 597. doi: 10.3390/biology11040597

Hardigan, M. A., Crisovan, E., Hamilton, J. P., Kim, J., Laimbeer, P., Leisner, C. P., et al. (2016). Genome reduction uncovers a large dispensable genome and adaptive role for copy number variation in asexually propagated *Solanum tuberosum*. *Plant Cell.* 28 (2), 388–405. doi: 10.1105/tpc.15.00538

Hinai, M. S. A., Ullah, A., Al-Rajhi, R. S., and Farooq, M. (2022). Proline accumulation, ion homeostasis and antioxidant defence system alleviate salt stress and protect carbon assimilation in bread wheat genotypes of omani origin. *Environ. Exp. Bot.* 193, 104687. doi: 10.1016/j.envexpbot.2021.104687

Hmida-Sayari, A., Gargouri-Bouzid, R., Bidani, A., Jaoua, L., Savouré, A., and Jaoua, S. (2005). Overexpression of Δ1-pyrroline-5-carboxylate synthetase increases proline production and confers salt tolerance in transgenic potato plants. *Plant Sci.* 169 (4), 746–752. doi: 10.1016/j.plantsci.2005.05.025

Hosseinifard, M., Stefaniak, S., Ghorbani Javid, M., Soltani, E., Wojtyla, Ł. , and Garnczarska, M. (2022). Contribution of exogenous proline to abiotic stresses tolerance in plants: A review. *Int. J. Mol. Sci.* 23 (9), 5186. doi: 10.3390/ijms23095186

Iqbal, N., Umar, S., Khan, N. A., and Khan, M. I. R. (2014). A new perspective of phytohormones in salinity tolerance: Regulation of proline metabolism. *Environ. Exp. Bot.* 100, 34–42. doi: 10.1016/j.envexpbot.2013.12.006

Jaarsma, R., de Vries, R. S., and de Boer, A. H. (2013). Effect of salt stress on growth, na$^+$ accumulation and proline metabolism in potato (*Solanum tuberosum*) cultivars. *PloS One* 8 (3), e60183. doi: 10.1371/journal.pone.0060183

Jones, P., Binns, D., Chang, H.-Y., Fraser, M., Li, W., McAnulla, C., et al. (2014). InterProScan 5: genome-scale protein function classification. *Bioinformatics* 30 (9), 1236–1240. doi: 10.1093/bioinformatics/btu031

Joshi, S., Nath, J., Singh, A. K., Pareek, A., and Joshi, R. (2022). Ion transporters and their regulatory signal transduction mechanisms for salinity tolerance in plants. *Physiol. Plant* 174 (3), e13702. doi: 10.1111/ppl.13702

Kanehisa, M., Araki, M., Goto, S., Hattori, M., Hirakawa, M., Itoh, M., et al. (2007). KEGG for linking genomes to life and the environment. *Nucleic Acids Res.* 36 (suppl_1), D480–D484. doi: 10.1093/nar/gkm882

Kappachery, S., Sasi, S., Alyammahi, O., Alyassi, A., Venkatesh, J., and Gururani, M. A. (2021). Overexpression of cytoplasmic *Solanum tuberosum* glyceraldehyde 3-phosphate dehydrogenase (GAPDH) gene improves PSII efficiency and alleviates salinity stress in *Arabidopsis*. *J. Plant Interact.* 16 (1), 398–410. doi: 10.1080/17429145.2021.1962420

Kavi Kishor, P. B., and Sreenivasulu, N. (2014). Is proline accumulation per se correlated with stress tolerance or is proline homeostasis a more critical issue? *Plant Cell Environ.* 37 (2), 300–311. doi: 10.1111/pce.12157

Kiyosue, T., Yoshiba, Y., Yamaguchi-Shinozaki, K., and Shinozaki, K. (1996). A nuclear gene encoding mitochondrial proline dehydrogenase, an enzyme involved in proline metabolism, is upregulated by proline but downregulated by dehydration in arabidopsis. *Plant Cell.* 8 (8), 1323–1335. doi: 10.1105/tpc.8.8.1323

Kyritsis, N., Torres-Espín, A., Schupp, P. G., Huie, J. R., Chou, A., Duong-Fernandez, X., et al. (2021). Diagnostic blood RNA profiles for human acute spinal cord injury. *J. Exp. Med.* 218 (3), e20201795. doi: 10.1084/jem.20201795

Langfelder, P., and Horvath, S. (2008). WGCNA: an r package for weighted correlation network analysis. *BMC Bioinf.* 9 (1), 559. doi: 10.1186/1471-2105-9-559

Lebreton, S., Cabassa-Hourton, C., Savouré, A., Funck, D., and Forlani, G. (2020). Appropriate activity assays are crucial for the specific determination of proline dehydrogenase and pyrroline-5-carboxylate reductase activities. *Front. Plant Sci.* 11. doi: 10.3389/fpls.2020.602939

Levy, D., and Veilleux, R. E. (2007). Adaptation of potato to high temperatures and salinity-a review. *Am. J. Potato Res.* 84 (6), 487–506. doi: 10.1007/BF02987885

Liu, Z., Coulter, J. A., Li, Y., Zhang, X., Meng, J., Zhang, J., et al. (2020). Genome-wide identification and analysis of the q-type C2H2 gene family in potato (*Solanum tuberosum* l.). *Int. J. Biol. Macromol.* 153, 327–340. doi: 10.1016/j.ijbiomac.2020.03.022

Liu, L., Huang, L., Lin, X., and Sun, C. (2020). Hydrogen peroxide alleviates salinity-induced damage through enhancing proline accumulation in wheat seedlings. *Plant Cell Rep.* 39 (5), 567–575. doi: 10.1007/s00299-020-02513-3

Liu, M., Li, Y., Li, G., Dong, T., Liu, S., Liu, P., et al. (2020). Overexpression of *StCYS1* gene enhances tolerance to salt stress in the transgenic potato (*Solanum tuberosum* l.) plant. *J. Integr. Agric.* 19 (9), 2239–2246. doi: 10.1016/S2095-3119(20)63262-2

Liu, Y., Wang, L., Li, Y., Li, X., and Zhang, J. (2019). Proline metabolism-related gene expression in four potato genotypes in response to drought stress. *Biol. Plant* 63 (1), 757–764. doi: 10.32615/bp.2019.153

Luo, P., Chen, L., Chen, Y., Shen, Y., and Cui, Y. (2022). *RmZAT10*, a novel Cys2/His2 zinc finger transcription factor of *Rosa multiflora*, functions in cold tolerance through modulation of proline biosynthesis and ROS homeostasis. *Environ. Exp. Bot.* 198, 104845. doi: 10.1016/j.envexpbot.2022.104845

Mao, X., Cai, T., Olyarchuk, J. G., and Wei, L. (2005). Automated genome annotation and pathway identification using the KEGG orthology (KO) as a controlled vocabulary. *Bioinformatics* 21 (19), 3787–3793. doi: 10.1093/bioinformatics/bti430

Naliwajski, M. R., and Sklodowska, M. (2018). The relationship between carbon and nitrogen metabolism in cucumber leaves acclimated to salt stress. *PeerJ* 6, e6043. doi: 10.7717/peerj.6043

Nguyen, H. T. T., Das Bhowmik, S., Long, H., Cheng, Y., Mundree, S., and Hoang, L. T. M. (2021). Rapid accumulation of proline enhances salinity tolerance in australian wild rice *Oryza australiensis* domin. *Plants* 10 (10), 2044. doi: 10.3390/plants10102044

Panahi, B., and Hejazi, M. A. (2021). Weighted gene co-expression network analysis of the salt-responsive transcriptomes reveals novel hub genes in green halophytic microalgae *Dunaliella salina*. *Sci. Rep.* 11 (1), 1607. doi: 10.1038/s41598-020-80945-3

Punta, M., Coggill, P. C., Eberhardt, R. Y., Mistry, J., Tate, J., Boursnell, C., et al. (2011). The pfam protein families database. *Nucleic Acids Res.* 40 (D1), D290–D301. doi: 10.1093/nar/gkr1065

Safi, A., Medici, A., Szponarski, W., Ruffel, S., Lacombe, B., and Krouk, G. (2017). The world according to GARP transcription factors. *Curr. Opin. Plant Biol.* 39, 159–167. doi: 10.1016/j.pbi.2017.07.006

Shannon, P., Markiel, A., Ozier, O., Baliga, N. S., Wang, J. T., Ramage, D., et al. (2003). Cytoscape: a software environment for integrated models of biomolecular interaction networks. *Genome Res.* 13 (11), 2498–2504. doi: 10.1101/gr.1239303

Shao, A., Wang, W., Fan, S., Xu, X., Yin, Y., Erick, A., et al. (2021). Comprehensive transcriptional analysis reveals salt stress-regulated key pathways, hub genes and time-specific responsive gene categories in common bermudagrass (*Cynodon dactylon* (L.) pers.) roots. *BMC Plant Biol.* 21 (1), 175. doi: 10.1186/s12870-021-02939-1

Shin, Y. K., Bhandari, S. R., Cho, M. C., and Lee, J. G. (2020). Evaluation of chlorophyll fluorescence parameters and proline content in tomato seedlings grown under different salt stress conditions. *Hortic. Environ. Biotechnol.* 61 (3), 433–443. doi: 10.1007/s13580-020-00231-z

Singh, A. K., Sharma, V., Pal, A. K., Acharya, V., and Ahuja, P. S. (2013). Genome-wide organization and expression profiling of the NAC transcription factor family in potato (*Solanum tuberosum* l.). *DNA Res.* 20 (4), 403–423. doi: 10.1093/dnares/dst019

Spooner, D. M., Ghislain, M., Simon, R., Jansky, S. H., and Gavrilenko, T. (2014). Systematics, diversity, genetics, and evolution of wild and cultivated potatoes. *Bot. Rev.* 80 (4), 283–383. doi: 10.1007/s12229-014-9146-y

Surabhi, G.-K., Reddy, A. M., Kumari, G. J., and Sudhakar, C. (2008). Modulations in key enzymes of nitrogen metabolism in two high yielding genotypes of mulberry (*Morus alba* l.) with differential sensitivity to salt stress. *Environ. Exp. Bot.* 64 (2), 171–179. doi: 10.1016/j.envexpbot.2008.04.006

Szabados, L., and Savouré, A. (2010). Proline: a multifunctional amino acid. *Trends Plant Sci.* 15 (2), 89–97. doi: 10.1016/j.tplants.2009.11.009

Székely, G., Ábrahám, E., Cséplő, Á., Rigó, G., Zsigmond, L., Csiszár, J., et al. (2008). Duplicated *P5CS* genes of arabidopsis play distinct roles in stress regulation and developmental control of proline biosynthesis. *Plant J.* 53 (1), 11–28. doi: 10.1111/j.1365-313X.2007.03318.x

Tang, D., Jia, Y., Zhang, J., Li, H., Cheng, L., Wang, P., et al. (2022). Genome evolution and diversity of wild and cultivated potatoes. *Nature* 606 (7914), 535–541. doi: 10.1038/s41586-022-04822-x

Tian, Z.-D.., Zhang, Y., Liu, J., and Xie, C.-H. (2010). Novel potato C2H2-type zinc finger protein gene, StZFP1, which responds to biotic and abiotic stress, plays a role in salt tolerance. *Plant Biol.* 12(5), 689–697. doi: 10.1111/j.1438-8677.2009.00276.x

Ullah, A., Li, M. X., Noor, J., Tariq, A., Liu, Y., and Shi, L. X. (2019). Effects of salinity on photosynthetic traits, ion homeostasis and nitrogen metabolism in wild and cultivated soybean. *PeerJ* 7, e8191. doi: 10.7717/peerj.8191

Wang, Q., Guo, C., Li, Z., Sun, J., Deng, Z., Wen, L., et al. (2021). Potato NAC transcription factor StNAC053 enhances salt and drought tolerance in transgenic *Arabidopsis*. *Int. J. Mol. Sci.* 22 (5), 2568. doi: 10.3390/ijms22052568

Yang, F., Liu, B., Zhu, Y., Wyckhuys, K. A. G., van der Werf, W., and Lu, Y. (2021). Species diversity and food web structure jointly shape natural biological control in agricultural landscapes. *Commun. Biol.* 4 (1), 979. doi: 10.1038/s42003-021-02509-z

Young, M. D., Wakefield, M. J., Smyth, G. K., and Oshlack, A. (2010). Gene ontology analysis for RNA-seq: accounting for selection bias. *Genome Biol.* 11 (2), R14. doi: 10.1186/gb-2010-11-2-r14

Yu, S., Lan, X., Zhou, J., Gao, K., Zhong, C., and Xie, J. (2022). *Dioscorea composita* WRKY3 positively regulates salt-stress tolerance in transgenic *Arabidopsis thaliana*. *J. Plant Physiol.* 269, 153592. doi: 10.1016/j.jplph.2021.153592

Zarattini, M., and Forlani, G. (2017). Toward unveiling the mechanisms for transcriptional regulation of proline biosynthesis in the plant cell response to biotic and abiotic stress conditions. *Front. Plant Sci.* 8. doi: 10.3389/fpls.2017.00927

Zeng, Z., Zhang, W., Marand, A. P., Zhu, B., Buell, C. R., and Jiang, J. (2019). Cold stress induces enhanced chromatin accessibility and bivalent histone modifications H3K4me3 and H3K27me3 of active genes in potato. *Genome Biol.* 20 (1), 123. doi: 10.1186/s13059-019-1731-2

Zhao, S. S., Zhang, Q. K., Liu, M. Y., Zhou, H. P., Ma, C. L., and Wang, P. P. (2021). Regulation of plant responses to salt stress. *Int. J. Mol. Sci.* 22 (9), 16. doi: 10.3390/ijms22094609

Zhao, C., Zhang, H., Song, C., Zhu, J.-K., and Shabala, S. (2020). Mechanisms of plant responses and adaptation to soil salinity. *Innovation-Amsterdam* 1 (1), 100017. doi: 10.1016/j.xinn.2020.100017

Zhou, X., Zhang, N., Yang, J., Tang, X., Wen, Y., and Si, H. (2018). Functional analysis of *StDWF4* gene in response to salt stress in potato. *Plant Physiol. Biochem.* 125, 63–73. doi: 10.1016/j.plaphy.2018.01.027

Zhu, X., Gong, H., He, Q., Zeng, Z., Busse, J. S., Jin, W., et al. (2016). Silencing of vacuolar invertase and asparagine synthetase genes and its impact on acrylamide formation of fried potato products. *Plant Biotechnol. J.* 14 (2), 709–718. doi: 10.1111/pbi.12421

Zhu, X., Hong, X., Liu, X., Li, S., Yang, J., Wang, F., et al. (2021). Calcium-dependent protein kinase 32 gene maintains photosynthesis and tolerance of potato in response to salt stress. *Sci. Hortic.* 285, 110179. doi: 10.1016/j.scienta.2021.110179

Zhu, X., Richael, C., Chamberlain, P., Busse, J. S., Bussan, A. J., Jiang, J., et al. (2014). Vacuolar invertase gene silencing in potato (*Solanum tuberosum* l.) improves processing quality by decreasing the frequency of sugar-end defects. *PloS One* 9 (4), e93381. doi: 10.1371/journal.pone.0093381

Zhu, M., Xie, H., Wei, X., Dossa, K., Yu, Y., Hui, S., et al. (2019). WGCNA analysis of salt-responsive core transcriptome identifies novel hub genes in rice. *Genes* 10 (9), 719. doi: 10.3390/genes10090719

Zhu, X., Zhang, N., Liu, X., Wang, S., Li, S., Yang, J., et al. (2020). *StMAPK3* controls oxidase activity, photosynthesis and stomatal aperture under salinity and osmosis stress in potato. *Plant Physiol. Biochem.* 156, 167–177. doi: 10.1016/j.plaphy.2020.09.012

frontiers | Frontiers in Plant Science

TYPE Original Research
PUBLISHED 10 November 2022
DOI 10.3389/fpls.2022.1046287

OPEN ACCESS

EDITED BY
Pietro Gramazio,
University of Tsukuba, Japan

REVIEWED BY
Hengyou Zhang,
Northeast Institute of Geography and Agroecology (CAS), China
Fa Cui,
Ludong University, China

*CORRESPONDENCE
Jingcai Li
lijingcai@hgnu.edu.cn
Botao Song
songbotao@mail.hzau.edu.cn

SPECIALTY SECTION
This article was submitted to Crop and Product Physiology, a section of the journal Frontiers in Plant Science

RECEIVED 16 September 2022
ACCEPTED 20 October 2022
PUBLISHED 10 November 2022

CITATION
Huang W, Dong J, Zhao X, Zhao Z, Li C, Li J and Song B (2022) QTL analysis of tuber shape in a diploid potato population.
Front. Plant Sci. 13:1046287.
doi: 10.3389/fpls.2022.1046287

QTL analysis of tuber shape in a diploid potato population

Wei Huang[1,2], Jianke Dong[1], Xijuan Zhao[1], Zhiyuan Zhao[1], Chunyan Li[1], Jingcai Li[3]* and Botao Song[1]*

[1]Key Laboratory of Horticultural Plant Biology, Ministry of Education/Key Laboratory of Potato Biology and Biotechnology, Ministry of Agriculture and Rural Affairs/College of Horticulture and Forestry Sciences, Huazhong Agricultural University, Wuhan, Hubei, China, [2]Forestry and Fruit Research Institute, Wuhan Academy of Agricultural Sciences, Wuhan, Hubei, China, [3]College of Biology and Agricultural Resources, Huanggang Normal University/Hubei Key Laboratory of Economic Forest Germplasm Improvement and Resources Comprehensive Utilization, Huanggang, Hubei, China

Tuber shape is one of the most important traits for potato breeding. Since poor or irregular shape increases the difficulty of handling and processing, researching the inheritance of potato tuber shape for potato breeding is highly important. To efficiently identify QTL for tuber shape, a diploid potato population (PM7) was generated by self-pollinated M6 (*S. chacoense*). A QTL TScha6 for tuber shape was identified by the QTL-seq approach at 50.91-59.93 Mb on chromosome 6 in the potato DM reference genome. To confirm TScha6, four SSR and twenty CAPS markers around the QTL were developed and the TScha6 was narrowed down to an interval of ~ 1.85 Mb. The CAPS marker C6-58.27_665 linked to TScha6 was then used to screen 86 potato cultivars and advanced breeding lines. The tuber length/width (LW) ratio was significantly correlated with the presence/absence of C6-58.27_665, and the correlation coefficient was r = 0.55 ($p < 0.01$). These results showed that C6-58.27_665 could be applied in marker-assisted selection (MAS) for tuber shape breeding in the future. Our research sets the important stage for the future cloning of the tuber shape gene and utilities of the marker in the breeding program.

KEYWORDS

tuber shape, QTL-seq, self-pollinated, potato, marker development

Introduction

Potato (*Solanum tuberosum* L.) is the most important non-cereal food crop in the world, grown on 16.49 million hectares and consumed daily by more than one billion people (FAOSTAT, 2020). Tuber shape is one of the important morphological traits for the potato processing industry and fresh market use (Si et al., 2016; Stark et al., 2020). Poor and irregular shape increases the loss of peeling and leads to higher costs in the processing industry (Fan et al., 2022). Usually, the chipping industry tends to select

round potato tubers, while French fries prefer long tubers (Bryan, 2011; Vreugdenhil et al., 2011). For consumers, the irregular tuber shape makes peeling difficult (Prashar et al., 2014). Thus, as the tuber shape influences the development of the processing industries and markets, breeding new potato varieties with uniform shapes is critical.

The variability in potato tuber appearance ranged from compressed to elongated, especially in the wild diploid potato (Lindqvist-Kreuze et al., 2015; Fan et al., 2022). Previous genetic studies have also shown that potato tuber shape was a quantitative trait in nature (De Jong and Burns, 1993). It has been long recognized that the tuber shape QTL (quantitative trait locus) included one major locus and some minor loci. The major shape QTL, termed *Ro*, was first reported by Van Eck et al. (1994) and identified on chromosome 10, explaining 75% of the observed variance for tuber shape. Similar mapping results were also reported in different potato germplasms in subsequent studies (ŚLiwka et al., 2008; Prashar et al., 2014; Endelman and Jansky, 2016; Fan et al., 2022; Pandey et al., 2022). The *Ro* gene was first mapped in the region 48.2-51.9 Mb on chromosome 10 of the potato DM reference genome (Endelman and Jansky, 2016), and the gene *StOFP20* was speculated to be the encoding gene of the *Ro* locus (Wu et al., 2018). In addition to the *Ro* locus, other genetic loci related to tuber shape have been reported. For example, Prashar et al. (2014) identified a major QTL for tuber shape on chromosome 2 by constructing a dense SNP (single nucleotide polymorphism) map and explaining 20% of the shape variation. Lindqvist-Kreuze et al. (2015) mapped a major QTL for tuber shape on chromosome 10, and two minor QTLs also associated with the trait on chromosomes 5 and 12, respectively. In cultivated Superior, tuber shape QTLs were reported on chromosomes 4, 6, 10, and 11 (Manrique-Carpintero et al., 2018).

Potato are polyploidy and self-incompatibility, which greatly limit the development of genetic studies in potato (Visser et al., 2009; Lindhout et al., 2011). It has long been recognized that cultivated potato is highly heterozygous autotetraploid (2n = 4x = 48) and the genetic ratios are complex because of reduced doubling in crosses (Zhou et al., 2014). Hence, most genetic analysis is conducted by using diploid potato populations (Li et al., 2005; Prashar et al., 2014; Torrance et al., 2020). Although progress was made at the diploid level, the F_1 progeny segregated for potato traits due to two heterozygous diploid parents (Endelman and Jansky, 2016). It was difficult that produce an inbred line in the diploid potato population because of self-incompatibility (Pushkarnath, 1953; Pandey, 1962). However, Endelman and Jansky (2016) reported that a diploid inbred line F_2 population was used for mapping tuber traits in potato. The F_2 population was created by crossing between the double monoploid potato, DM1-3, and the S_7 inbred line, M6 (Endelman and Jansky, 2016). This was the first report of the creation and application of an inbred line in potato, which indicates that the recombinant inbred line can also be developed in the future. Nonetheless, the genome sequence of M6 revealed that some loci were still heterozygous and two haplotypes are present (Jansky et al., 2014; Leisner et al., 2018). In addition, M6 till retained some excellent agronomic characteristics, including producing tubers, resistance PVA and PVY, and high dry matter content (Jansky et al., 2014; Huang et al., 2021).

In this study, a diploid potato population (PM7) was used to map potato tuber shape. The inbred parent of the population, designated M6, was inbred for seven generations (Jansky et al., 2014; Leisner et al., 2018). The PM7 population was constructed by self-crossing the M6. Then, we found that the population was segregated for tuber length/width (LW), and the QTL-seq approach was used to map the tuber shape in the population. The major QTL TScha6 for tuber shape was located on the distal long arm of potato chromosome 6 and delimited to a 1.85 Mb genomic region. Moreover, a CAPS marker linked to TScha6 was developed and evaluated for the capacity applied in marker-assisted selection (MAS) for tuber shape.

Materials and methods

Plant materials

The mapping population (PM7) was derived from self-pollinated diploid individual M6 (*S. chacoense*) which was inbred for seven generations and still retained some excellent agronomic characteristics (Jansky et al., 2014). The M6 genome revealed that some localized regions still maintained residual heterozygosity (Leisner et al., 2018).

The diploid self-cross population PM7 consists of a total of 180 individuals, 164 of which were used to construct the genetic map. The progeny was grown at Wuhan (30.5°N, 114.4°E) in three environments: spring 2016 (environment I), 2016 autumn (environment II), and 2017 spring (environment III). The field management ensured normal crop growth through standard agronomic practices and pesticide applications.

Assessment of tuber shape

Tubers were harvested when most plants had become foliage senescence and phenotypic evaluation was carried out for tuber shape. All potato tubers were washed and five fully developed tubers per plot were selected for subsequent evaluation. Two methods were used for tuber shape assessment. On the one hand, tuber shape was assessed by visual evaluation from the total

individuals on a 1-7 scale (Lindqvist-Kreuze et al., 2015). The 1-7 were represented as compressed (1), round (2), obovate (3), elliptic (4), oblong (5), long-oblong (6), and elongate (7). On the other hand, tuber shape was also evaluated by length/width (LW) ratio (Van Eck et al., 1994). For each PM7 progeny, the average of LW from five tubers was used as the trait value.

Additional 86 potato cultivars and advanced breeding lines constructed the natural population and were used to evaluate the effect of tuber shape QTL. These clones were also assessed the LW ratio as mentioned above. Generally, when the LW value is <1.4, the tuber shape is round; when the LW value is ≥1.4, the tuber shape is long (Ortiz and Huaman, 1994). The heritability of these traits were estimated according to Hara-Skrzypiec et al. (2018).

QTL-seq analysis

Genomic DNA were isolated from frozen 500 mg of fresh leaves of the PM7 population using the cetyltrimethyl ammonium bromide (CTAB) method (Saghai-Maroof et al., 1985) and quantified using a Nanodrop 1000 spectrophotometer (Thermo Scientific).

For QTL-seq (Takagi et al., 2013), two pools, Round-pool and Long-pool were constructed by mixing an equal ratio of DNA. Each pool includes 24 individuals with extreme phenotype for tuber shape. The sequencing libraries were constructed using the NEBNext Ultra DNA Library Prep Kit (New England Biolabs, MA, USA) and subjected to 150 bp paired-end sequencing using an Illumina HiSeq 2500 platform in Tianjin Sequencing Center (Novegene Co., Ltd., Tianjin, China).

The quality of raw reads from Illumina HiSeq 2500 platform was first assessed by the FASTQC tool (http://www.bioinformatics.babraham.ac.uk/projects/fastqc/). Low-quality reads were discarded by the Trimmomatic tool (Lohse et al., 2012) with default settings and a Phred score cut-off of 20. High-quality clean reads were then aligned to the DM potato reference genome (Xu et al., 2011) using the BWA software with default settings (Li and Durbin, 2009). SAM files were converted to BAM files utilizing the SAMtools (Li et al., 2009). BAM files were then sorted and indexed by the Picard tool (http://broadinstitute.github.io/picard/). SNP calling was performed by the GATK software (McKenna et al., 2010; DePristo et al., 2011). Δ(SNP-index) and G' were calculated by QTLseqr (Mansfeld and Grumet, 2018). The number of reads harboring SNPs that are different from the reference sequence is divided by the total reads as the SNP-index. The SNP-index of the Round-pool subtracted from the SNP-index of the Long-pool is Δ(SNP-index). The G statistic (G') is calculated for each SNP based on the Nadaraya-Watson or tricube smoothing kernel (Nadaraya, 1964; Watson, 1964). The G' and Δ(SNP-index) distribution were visualized by the sliding window method with 2 Mb window size and 10 kb increment (Takagi et al., 2013).

Mapping QTL with SSR and CAPS markers

The simple sequence repeat (SSR) markers located in the candidate region (Xiao et al., 2018) were employed for polymorphism screening between the parental M6 and two pools (Round-pool and Long-pool). The polymorphic markers were then applied to all progeny. PCR mixtures (total 20 μl) containing 10 μl 2×Utaq PCR mix (Vazyme Co., Ltd., Nanjing, China), 1 μl of genomic DNA (50 ng/μl), 0.5 μl each forward and reverse primers (10 μmol/L), and 8 μl ddH_2O were used for the following program: 3 min at 95 °C;35 cycles of 30 s at 95 °C, Tm ° C at 30 s and 72 °C 30 s; finally, 10 min at 72 °C. The PCR products were checked on 6% polyacrylamide gel electrophoresis followed by silver staining (Xiao et al., 2018).

Based on filtered SNPs, the additional CAPS (cleaved amplified polymorphic sequences) markers were developed. Primers for the CAPS markers were designed with Snap Gene 4.1.6 program. SNPs were included within the restriction enzyme recognition site. The primers of CAPS markers were used for polymorphism screening between the parental M6 and two pools (Round-pool and Long-pool). PCR mixture and program were as same as SSR primers. After PCR amplification, PCR products were cleaved using restriction enzymes. The enzyme cleavage reaction system was as follows: 5 μl of PCR products; 0.05 U of restriction enzymes; 1μl of 10×reaction buffer; ddH_2O for the rest. The enzyme cleavage mixtures were incubated at 37°C for 1 h. The reaction products were detected by agarose gel electrophoresis with a concentration of 0.8%. The size of the restriction fragment for each marker was visualized and recorded *via* the Bio-Rad Imaging System (Bio-Rad Laboratories). The linkage map was conducted with Joinmap® 4 (Van Ooijen, 2006) and the parameter settings were referred to by Xiao et al. (2018). QTL analysis was conducted by MapQTL®6.0 based on the multiple-QTL models (MQM) (Van Ooijen, 2009). CAPS markers C6-57.1_554, C6-58.27_665, and C6_58.95_587 in MAS for tuber shape were dectected as mentioned above.

Results

Tuber shape analysis

Tuber shape was assessed from the field-grown tubers of the PM7 population in 2016 and 2017 using the 1-7 scale and the LW method. The phenotypic data were provided in Supplementary Table 1. The mean LW of the parent M6 was 1.48, corresponding to elliptic tubers in all environments (Figure 1A). In the population PM7, seven different shapes were included in three environments (Figure 1A), of which the most prevalent categories were round, obovate, oblong, and

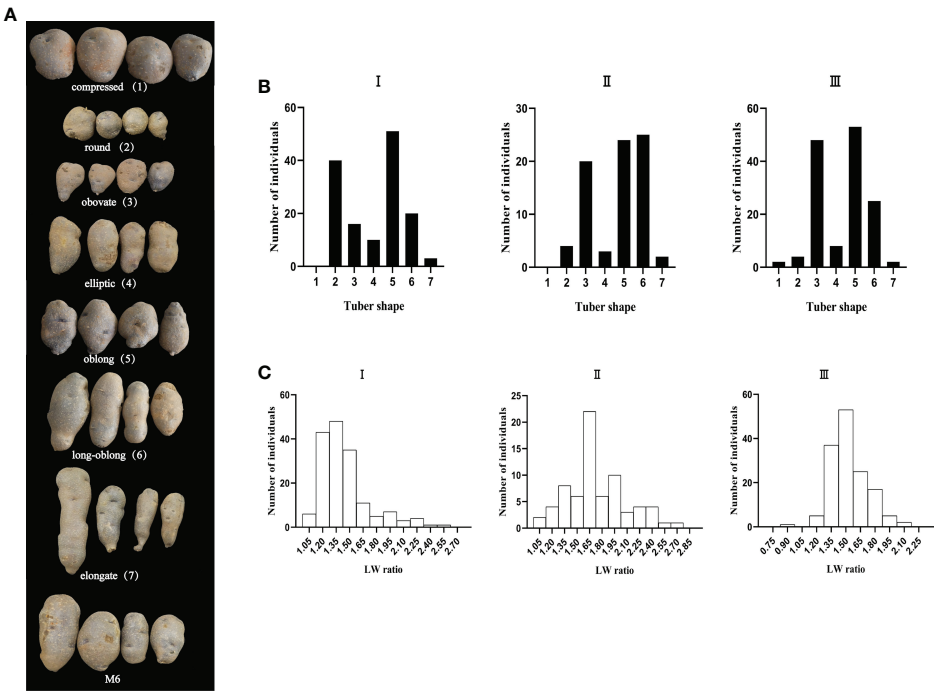

FIGURE 1
Phenotype of tuber shape in the PM7 population, and frequency distribution of tuber shape category and LW ratio in tree environment (environment I–III). **(A)** Photograph illustrating tuber shape variation in the PM7 population and the phenotype of the parent M6. Tuber shape was assessed on a 1-7 scale, where 1-7 were represented as compressed (1), round (2), obovate (3), elliptic (4), oblong (5), long-oblong (6), and elongate (7). **(B)** The frequency distribution of tuber shape category in the PM7 population in environment I–III. **(C)** The frequency distribution of LW ratio (the ratio of tuber length to width) in the PM7 population in environment I–III.

long-oblong (Figure 1B). The range of potato LW is 1.06-2.57 in environment I, 1.06-2.71 in environment II, and 0.89-2.11 in environment III (Figure 1C). The basic statistical data of the LW values in the PM7 population was shown in Table 1. The LW ratio shows a continuous distribution with skewness ranging from 0.53-1.49 and kurtosis from -0.11-2.26 in the three environments (Table 1). The LW values of environment I-III skewed positively and the tuber shape distributions in the three environments were concentrated to be round. The two assessing methods were significantly correlated ($p < 0.01$), and the Pearson correlation coefficients for the environment I-III were 0.588, 0.871, and 0.796, respectively (Table 2). The tuber shape in the PM7 population was demonstrated as a quantitative trait based on these phenotyping data in environment I-III. These phenotyping data were used for QTL analysis of tuber shape.

QTL-seq analysis for potato tuber shape

Twenty-four individuals with the extreme long trait (LW ranged from 1.64-2.57) and 24 individuals with the extreme round trait (LW ranged from 1.06-1.23) were selected to prepare the Long-pool and Round-pool, respectively (Figure 2). After sequencing, 83,444,586 and 89,087,617 clean sequences were yielded from Round-pool and Long-pool, respectively. The mean value of Q20 and Q30 was 95.49% and 89.28%,

TABLE 1 Variance analysis of the LW values in three environments.

Trait	Environment	Mean	SD[a]	Variance	Heritability[b]	Skewness	Kurtosis
LW	I	1.44	0.29	0.08	0.69	1.49	2.26
	II	1.74	0.35	0.12	0.84	0.60	-0.11
	III	1.53	0.18	0.03	0.61	0.53	1.08

[a]the standard deviation in each environment.
[b]The broad-sense heritability estimated according to Hara-Skrzypiec et al. (2018).

10.3389/fpls.2022.1046287

TABLE 2 Correlation coefficients of the tuber shape traits in three environments.

Trait	Trait	LW			Tuber shape scale		
	Environment	I	II	III	I	II	III
LW	I	1	-0.05	0.08	.588**	0.03	0.07
	II		1	.238**	-0.08	.871**	.269**
	III			1	0.12	.287**	.796**
Tuber shape category	I				1	0.01	0.15
	II					1	.279**
	III						1

**p < 0.01.

respectively (Supplementary Figure 1). By BWA/SAM software, these sequences were aligned to the DM potato reference genome with an average alignment rate of 80.71%. The average genome coverage and depth were 95.56% and 32.67×, respectively.

The two statistical methods of Δ(SNP-index) and G' (Mansfeld and Grumet, 2018) were used to identify the QTL associated with tuber shape. According to the results of sequencing and reference sequence alignment, SNPs were detected by the GATK software and yielded 3,938,300 SNPs between the Long-pool and Round-pool. Supplementary Figure 2 showed the distribution of all SNPs on the potato whole genome. The SNP-index of the Long-pool and Round-pool were calculated for each identified SNP and showed relationships with genomic positions by the sliding window method (Figures 3A, B). We found that SNP-index graphs of the Long-pool and Round-pool showed contrasting patterns at the end of chromosome 6. Further, the Δ(SNP-index) was calculated by combining the information of the SNP-index from the Long-pool and Round-pool and showed the distribution on chromosomes 1-12 by the sliding window method (Figure 3C). The G' of each identified SNP was calculated with the observed and expected allele depths and the value trends were plotted in Figure 3D. By combining the information of Δ(SNP-index) and the G', we found that the chromosomal region of 50.91-59.53 Mb was associated with the tuber shape. Hence, the 8.62 Mb region of chromosome 6 distinguished by QTL-seq was considered as the candidate region for tuber shape, suggesting a tuber shape QTL across the 8.62 Mb region. The QTL was designated as TScha6 (tuber shape QTL on chromosome 6 of *S. chacoense* parent M6).

Linkage mapping of TScha6

To verify TScha6 detected by QTL-seq, a traditional method (linkage mapping) was applied to map the tuber shape in the PM7 population. The 11 sets of SSR primers (Supplementary

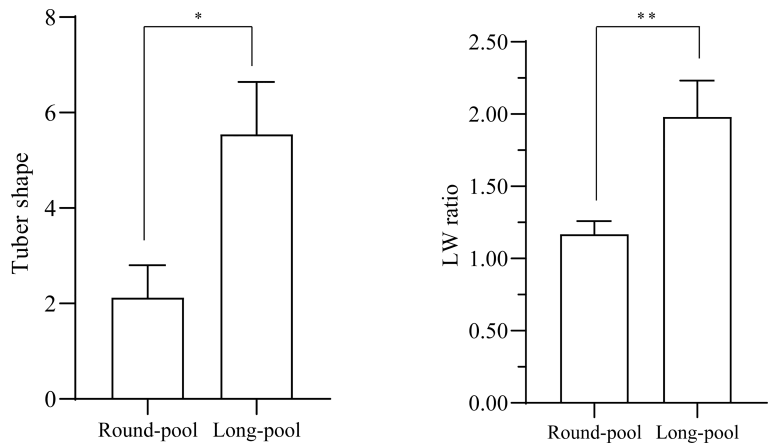

FIGURE 2
The difference analysis of tuber shape performance between Round-pool and Long-pool. **(A)** The mean value of the tuber shape category in the Round-pool was significantly lower than in the Long-pool (*p < 0.05 in the *t* test). **(B)** The mean value of the LW ratio in the Round-pool was very significantly lower than in the Long-pool (**p < 0.01 in Student *t* test).

Table 2) located around the candidate region were used to screen polymorphism between the Long-pool and Round-pool, and four polymorphic markers were obtained. To further define the interval on the linkage map of chromosome 6, SNPs were converted into CAPS markers. A total of 20 polymorphic CAPS markers (Supplementary Table 3) were obtained. These polymorphic markers were used to screen the population PM7, and a linkage map including four SSR markers and 19 CAPS markers was constructed. The total length of the map was 68.6 cM, with an average marker interval of 2.98 cM and a maximum distance between markers of 22.8 cM (Figure 4).

To narrow down the candidate region of tuber shape gene further, the traditional QTL analysis was performed based on the linkage map and the phenotypic data. QTL for the LW ratio was detected in all experiments and explained 10.2-17.5% of the phenotypic variation (Table 3). QTL for the tuber shape category was detected in only experiment I and explained 16.7% of the variation (Table 3 and Figure 4). QTLs for the phenotypic variation were considered as the same QTL based on two-LOD support intervals. Hence, the tuber shape QTL was mapped between marker C6-57.1_554 and C6-58.95_587 (Figure 4), which was consistent with the 8.62 Mb region of TScha6 distinguished by QTL-seq and narrowed down the candidate region to a 1.85 Mb region.

Tuber shape marker for MAS

A natural population, including 86 potato cultivars and advanced breeding lines, was used to verify TScha6. The LW ranged from 0.83 to 2.58 in the natural population. The tuber shape of seventeen clones with LW values (<1.4) was considered round, and the tuber shape of sixty-nine clones with high LW values (≥1.4) was considered long. According to the results of QTL mapping, CAPS markers C6-57.1_554, C6-58.27_665, and C6_58.95_587 were closely linked to the tuber shape gene. Therefore, the three markers were screened in natural populations. The correlation analysis showed that only the marker C6-58.27_665 was extremely significantly correlated with the LW in the natural population, and the correlation coefficient was 0.55 ($p < 0.01$). Further, the effect of the tuber shape QTL was analyzed by the occurrence of the QTL peak marker C6-58.27_665 in the natural population (Figure 5). The LW values of genotypes with the marker C6-58.27_665 were significantly higher than these of genotypes without the marker ($p < 0.01$). The coincidence of the phenotypic identification (round or long) and the marker C6-58.27_665 detection results reached 91.86% (Table 4). These results suggested that the marker C6-58.27_665 can be applied to molecular marker-assisted breeding for potato tuber shape.

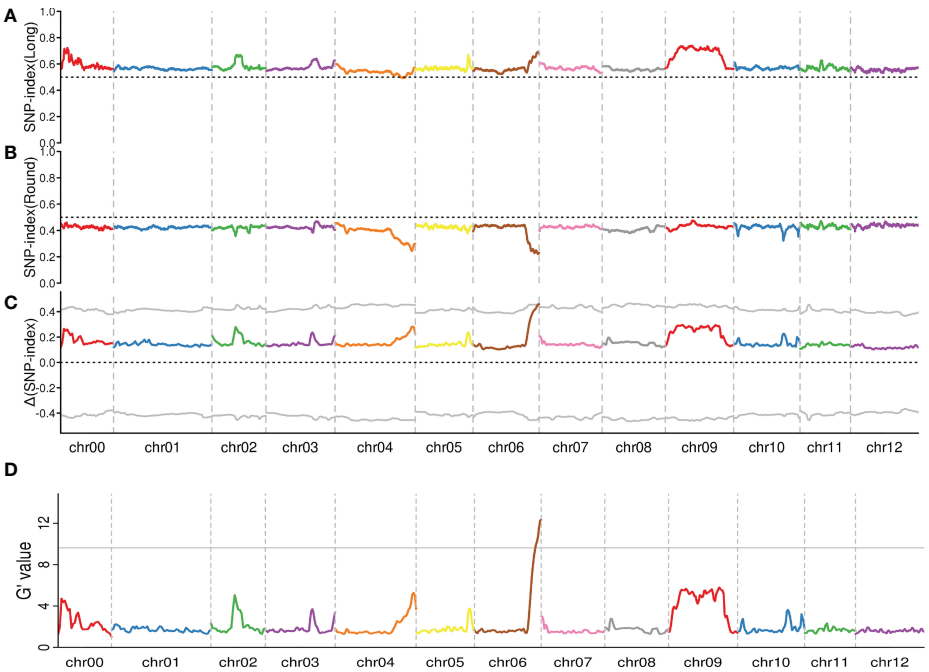

FIGURE 3
Identification of a genomic region corresponding to tuber shape by calculating the SNP-index and the G' value. The x-axis represents the position of 12 chromosomes of the potato genome and the y-axis corresponds to the average SNP-index or G' within a 2 Mb interval. **(A)** The SNP-index graph of the Long-pool. **(B)** The SNP-index of the Round-pool. **(C)** The Δ (SNP-index) graph, the grey dotted line represents that Δ (SNP-index) plot with 95% statistical two-sided confidence intervals under the null hypothesis of no QTL. **(D)** G' graph, the grey line represents the p-values (0.01).

10.3389/fpls.2022.1046287

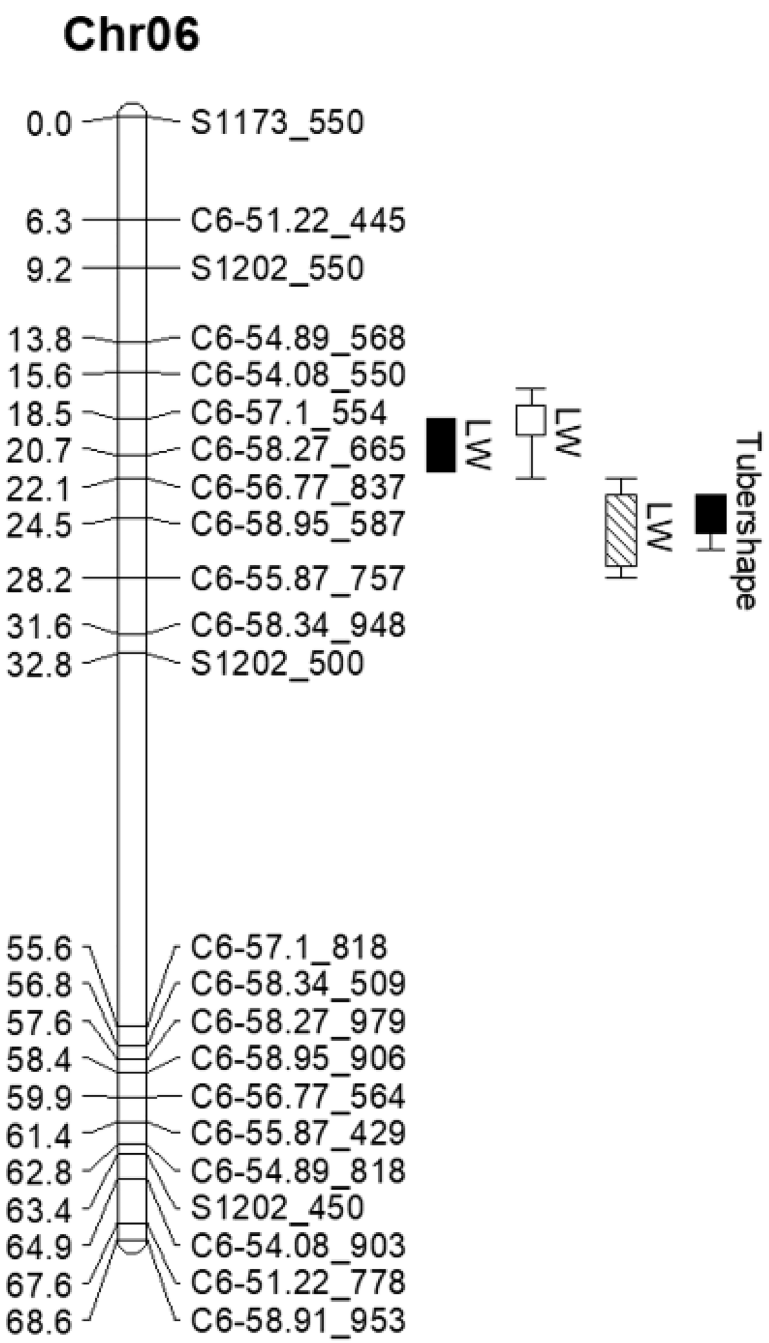

FIGURE 4
Identification and validation of the QTL Tscha6 for tuber shape in potato chromosome 6. On the linkage map, the maker locations are shown as cumulative distances in cM. The right side of the map shows the tuber shape QTL. Bars with different fill styles represent the tuber shape QTL in different environments. The solid bars represent environment I, the empty bar represents environment II, and the lower diagonal fill bar represents environment III).

Discussion

Potato is the most important non-cereal food crop in the world and is consumed daily by more than one billion people. Tuber shape is one of the major breeding objectives of breeders because poor and irregular shape increases the difficulty of handling and processing. Hence, it is necessary to research the inheritance of potato tuber shape. In this study, we employed the

TABLE 3 The QTL Tscha6 detecting for tuber shape by Multiple-QTL Models.

Trait	Environment	LOD	PVE (%)[a]	2-LOD interval (cM)	Peak (cM)	Peak Marker
LW	I	3.82	10.2	18.53-21.65	20.65	C6-58.27_665
	II	3.23	17.5	16.56-21.65	18.53	C6-57.1_554
	III	4.11	12.2	20.65-25.53	25.53	C6-58.95_587
Tuber shape category	I	5.54	16.7	23.11-26.53	24.53	C6-58.95_587

[a]The percentage of phenotypic variance explained by QTL.

TABLE 4 Evaluation of molecular markers C6-58.27_665 in the natural population.

Molecular marker C6-58.27_665[a]	Tuber shape	Clones	Total	Percentage (%)
0	Round (LW ≤ 1.4)	15	79	91.86
1	Long (LW > 1.4)	64		
0	Long (LW > 1.4)	5	7	8.14
1	Round (LW ≤ 1.4)	2		

[a]0,The clones lacked the marker C6-58.27_665; 1, the clones carried the marker C6-58.27_665.

diploid population (PM7) derived from self-pollinated M6 with the elliptic tuber to conduct a genetic analysis. The progeny in the PM7 showed segregation in tuber shape. Using the strategy of traditional QTL mapping combined QTL-seq, we mapped a major QTL TScha6 for tuber shape in the population PM7 between 57.1 -58.95 Mb on chromosome 6 in the DM reference genome. Further, the effect of TScha6 was confirmed by a natural population.

QTL-seq (Takagi et al., 2013) could identify rapidly the candidate genomic region, which overcomes the difficulties of traditional methods in terms of labor, time and cost required. It has been successfully applied to mapping the QTL in cucumber, rice, and tomato (Takagi et al., 2013; Lu et al., 2014; Illa-Berenguer et al., 2015; Sun et al., 2018). In this study, we employed the method to identify a major QTL for tuber shape (Figure 3), which is consistent with the results of Manrique-Carpintero et al. (2018).

Tuber shape is quantitatively inherited and the trait was controlled by major or minor loci. The major QTL *Ro* on chromosome X was reported to control tuber shape (Chen et al., 2019). In addition, several minor QTLs have been identified, including QTLs on chromosome II (ŚLiwka et al., 2008; Prashar et al., 2014), chromosome V (Lindqvist-Kreuze et al., 2015), chromosome VI (Manrique-Carpintero et al., 2018) and chromosome XII (D'hoop et al., 2008). Manrique-Carpintero et al. (2018) identified four QTLs for tuber shape, one of which was also located at the end of chromosome 6 and the genetic distance between two flanking markers was 18 cM. In this study, TScha6 was mapped in a genetic interval of 6 cM, corresponding to a physical interval of ~ 1.85 Mb (Figure 4). We confirm that the candidate interval of TScha6 was smaller than that reported by Manrique-Carpintero et al. (2018). This is the first step towards the cloning of the tuber shape gene. In the future, the work will focus on fine mapping by expanding the population and developing additional markers.

Although most of the recent studies reported that the major genetic interval for tuber shape was mapped on chromosome 10, which hasn't been detected by the QTL-seq in this study. This may be due to the following reasons. (1) The parent (M6) of the PM7 population is an S_7 inbred clone but still has 0.26-2.10% heterozygous positions on the 12 chromosomes (Leisner et al., 2018). Thus, it was suggested that there may be a heterozygous segment related to tuber shape on the distal long arm of potato chromosome 6 in the M6 genome. (2) The tuber shape was controlled by the *Ro* locus on the chromosome X in the F_2 population that was created by crossing between M6 × DM1-3 (Endelman and Jansky, 2016). In the F_2 population, the female DM1-3 was long and the male M6 was elliptic while the F_1 hybrid was oblong (Endelman and Jansky, 2016). The tuber shape trait in the F_2 population was associated with the *StOFP20* marker (Wu et al., 2018). Hence, we speculated that the *Ro* locus in the M6 genome was homozygous and the locus for tuber shape on the chromosome couldn't be detected in the PM7 population.

Marker-assisted selection (MAS) for the selection of plant breeding has been validated to be efficient in labor, time, and cost required (Xu and Crouch, 2008). This technology has been applied to select different traits in potato breeding, such as late blight resistance, PVY resistance, cold-induced sweetening, etc. (Nie et al., 2016; Chen et al., 2018; Xiao et al., 2018). However, although many QTLs of tuber shape was identified, there were few reports for tuber shape marker application. In this study, the CAPS marker C6-58.27_665 exhibited a high coincidence rate of 91.86% with the phenotypes of 86 potato breeding clones, indicating this marker is qualified for MAS of tuber shape.

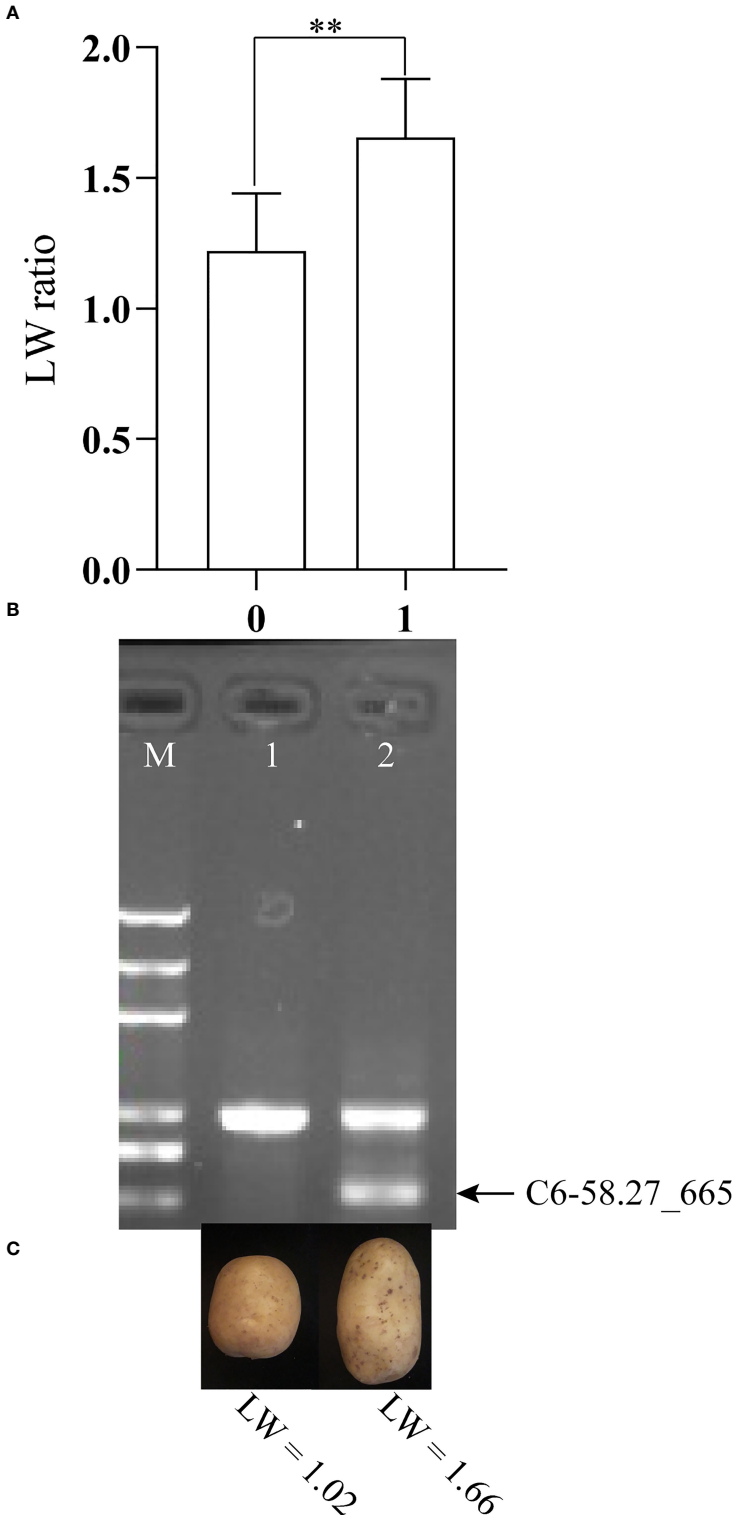

FIGURE 5
The effect of the tuber shape QTL was analyzed further by the occurrence of the QTL peak marker C6-58.27_665 in a natural population. **(A)** The difference analysis of LW value between 0 and 1. 0, the individuals lacked the marker C6-58.27_665; 1, the individuals carried the marker C6-58.27_665. **p < 0.01 in Student *t* test. **(B)** Detection of the CAPS marker C6-58.27_665 in natural polation. The PCR products were electrophoresed on 0.8% agarose gel. Lane M, 2 kb plus DNA ladder (Trans, China), and sizes of the ladders are 5000, 3000, 2000, 1000, 750, 500 bp, respectively. **(C)** The tuber shape of potato lines with (right) and without (left) C6-58.27_665.

Conclusions

QTL for tuber shape was analyzed by the QTL-seq in diploid potato population PM7. A major QTL TScha6, explaining 10.2-17.5% of the variation of tuber shape, was identified on chromosome 6, and a CAPS marker linked to TScha6 was applied in marker-assisted selection (MAS) for tuber shape.

Data availability statement

The data presented in the study are deposited in the BioProject database (ID PRJNA884166, http://www.ncbi.nlm.nih.gov/bioproject/884166).

Author contributions

Conceived and designed the experiments: BS, JL, WH, JD. Performed the experiments: WH, JD, XZ, ZZ. Analyzed the data: WH, JD, CL. Prepared the manuscript: WH, BS, JL. Revised the manuscript: WH, JL, BS, JD. All authors contributed to the article and approved the submitted version.

Funding

This project was funded by the Key Area Research and Development Program of Guangdong Province (2020B020219002) and the China Agriculture Research System of MOF and MARA (CARS-09-P07).

Acknowledgments

The authors thank Ming Luo and Zhengnan Cheng for their technical support in the analysis of sequencing data.

Conflict of interest

The authors declare that the research was conducted in the absence of any commercial or financial relationships that could be construed as a potential conflict of interest.

Publisher's note

All claims expressed in this article are solely those of the authors and do not necessarily represent those of their affiliated organizations, or those of the publisher, the editors and the reviewers. Any product that may be evaluated in this article, or claim that may be made by its manufacturer, is not guaranteed or endorsed by the publisher.

Supplementary material

The Supplementary Material for this article can be found online at: https://www.frontiersin.org/articles/10.3389/fpls.2022.1046287/full#supplementary-material

References

Bryan, G. J. (2011). "Mapping complex potato traits," in *The genetics, genomics, and breeding of potato*. Eds. J. M. Bradeen and C. Kole (New York, USA: CRC Press), 113–129.

Chen, X., Lewandowska, D., Armstrong, M. R., Baker, K., Lim, T. Y., Bayer, M., et al. (2018). Identification and rapid mapping of a gene conferring broad-spectrum late blight resistance in the diploid potato species *Solanum verrucosum* through DNA capture technologies. *Theor. Appl. Genet.* 131 (6), 1287–1297. doi: 10.1007/s00122-018-3078-6

Chen, N., Zhu, W., Xu, J., Duan, S., Bian, C., Hu, J., et al. (2019). Molecular marker development and primary physical map construction for the tuber shape *Ro* gene locus in diploid potato (*Solanum tuberosum* l.). *Mol. Breed.* 39 (1), 6. doi: 10.1007/s11032-018-0913-z

De Jong, H., and Burns, V. J. (1993). Inheritance of tuber shape in cultivated diploid potatoes. *Am. Potato J.* 70 (3), 267–284. doi: 10.1007/bf02849314

DePristo, M. A., Banks, E., Poplin, R., Garimella, K. V., Maguire, J. R., Hartl, C., et al. (2011). A framework for variation discovery and genotyping using next-generation DNA sequencing data. *Nat. Genet.* 43 (5), 491–498. doi: 10.1038/ng.806

D'hoop, B. B., Paulo, M. J., Mank, R. A., van Eck, H. J., and van Eeuwijk, F. A. (2008). Association mapping of quality traits in potato (*Solanum tuberosum* l.). *Euphytica* 161 (1-2), 47–60. doi: 10.1007/s10681-007-9565-5

Endelman, J. B., and Jansky, S. H. (2016). Genetic mapping with an inbred line-derived F_2 population in potato. *Theor. Appl. Genet.* 129 (5), 935–943. doi: 10.1007/s00122-016-2673-7

Fan, G., Wang, Q., Xu, J., Chen, N., Zhu, W., Duan, S., et al. (2022). Fine mapping and candidate gene prediction of tuber shape controlling *Ro* locus based on integrating genetic and transcriptomic analyses in potato. *Int. J. Mol. Sci.* 23 (3), 1470. doi: 10.3390/ijms23031470

FAOSTAT. (2020). Available at: https://crops.extension.iastate.edu/faostat.

Hara-Skrzypiec, A., Śliwka, J., Jakuczun, H., and Zimnoch-Guzowska, E. (2018). QTL for tuber morphology traits in diploid potato. *J. Appl. Genet.* 59, 123–132. doi: 10.1007/s13353-018-0433-x

Huang, W., Nie, B., Tu, Z., Li, C., Murphy, A. M., Singh, M., et al. (2021). Extreme resistance to potato virus a in potato cultivar Barbara is independently mediated by *Ra* and Ry_{sto}. *Plant Dis.* 105, 3344–3348. doi: 10.1094/PDIS-02-21-0233-SC

Illa-Berenguer, E., Van Houten, J., Huang, Z., and van der Knaap, E. (2015). Rapid and reliable identification of tomato fruit weight and locule number loci by QTL-seq. *Theor. Appl. Genet.* 128 (7), 1329–1342. doi: 10.1007/s00122-015-2509-x

Jansky, S. H., Chung, Y. S., and Kittipadukal, P. (2014). M6: A diploid potato inbred line for use in breeding and genetics research. *J. Plant Regist.* 8 (2), 195–199. doi: 10.3198/jpr2013.05.0024crg

Leisner, C. P., Hamilton, J. P., Crisovan, E., Manrique-Carpintero, N. C., Marand, A. P., Newton, L., et al. (2018). Genome sequence of M6, a diploid inbred clone of the high-glycoalkaloid-producing tuber-bearing potato species *solanum chacoense*, reveals residual heterozygosity. *Plant J.* 94 (3), 562–570. doi: 10.1111/tpj.13857

Li, X. Q., De Jong, H., De Jong, D. M., and De Jong, W. S. (2005). Inheritance and genetic mapping of tuber eye depth in cultivated diploid potatoes. *Theor. Appl. Genet.* 110 (6), 1068–1073. doi: 10.1007/s00122-005-1927-6

Li, H., and Durbin, R. (2009). Fast and accurate short read alignment with burrows-wheeler transform. *Bioinformatics* 25 (14), 1754–1760. doi: 10.1093/bioinformatics/btp324

Li, H., Handsaker, B., Wysoker, A., Fennell, T., Ruan, J., Homer, N., et al. (2009). The sequence alignment/map format and samtools. *Bioinformatics* 25 (16), 2078–2079. doi: 10.1093/bioinformatics/btp352

Lindhout, P., Meijer, D., Schotte, T., Hutten, R. C. B., Visser, R. G. F., and van Eck, H. J. (2011). Towards F_1 hybrid seed potato breeding. *Potato Res.* 54 (4), 301–312. doi: 10.1007/s11540-011-9196-z

Lindqvist-Kreuze, H., Khan, A., Salas, E., Meiyalaghan, S., Thomson, S., Gomez, R., et al. (2015). Tuber shape and eye depth variation in a diploid family of Andean potatoes. *BMC Genet.* 16, 57. doi: 10.1186/s12863-015-0213-0

Lohse, M., Bolger, A. M., Nagel, A., Fernie, A. R., Lunn, J. E., Stitt, M., et al. (2012). RobiNA: a user-friendly, integrated software solution for RNA-seq-based transcriptomics. *Nucleic. Acids Res.* 40 (Web Server issue), W622–W627. doi: 10.1093/nar/gks540

Lu, H., Lin, T., Klein, J., Wang, S., Qi, J., Zhou, Q., et al. (2014). QTL-seq identifies an early flowering QTL located near *Flowering locus t* in cucumber. *Theor. Appl. Genet.* 127 (7), 1491–1499. doi: 10.1007/s00122-014-2313-z

Manrique-Carpintero, N. C., Coombs, J. J., Pham, G. M., Laimbeer, F. P. E., Braz, G. T., Jiang, J., et al. (2018). Genome reduction in tetraploid potato reveals genetic load, haplotype variation, and loci associated with agronomic traits. *Front. Plant Sci.* 9. doi: 10.3389/fpls.2018.00944

Mansfeld, B. N., and Grumet, R. (2018). QTLseqr: An r package for bulk segregant analysis with next-generation sequencing. *Plant Genome* 11 (2), 180006. doi: 10.3835/plantgenome2018.01.0006

McKenna, A., Hanna, M., Banks, E., Sivachenko, A., Cibulskis, K., Kernytsky, A., et al. (2010). The genome analysis toolkit: A MapReduce framework for analyzing next-generation DNA sequencing data. *Genome Res.* 20, 1297–1303. doi: 10.1101/gr.107524.110

Nadaraya, E. A. (1964). On estimating regression. *Theory. Probab. Appl.* 10, 186–190. doi: 10.1137/1110024

Nie, X., Sutherland, D., Dickison, V., Singh, M., Murphy, A. M., and De Koeyer, D. (2016). Development and validation of high-resolution melting markers derived from Ry_{sto} STS markers for high-throughput marker-assisted selection of potato carrying Ry_{sto}. *Phytopathology* 106 (11), 1366–1375. doi: 10.1094/PHYTO-05-16-0204-R

Ortiz, R., and Huaman, Z. (1994). "Inheritance of morphological and tuber characteristics," in *Potato genetics*. Eds. J. E. Bradshaw and G. R. Mackay (Wallingford, United Kingdom: CAB International), 263–283.

Pandey, K. K. (1962). Interspecific incompatibility in *Solanum* species. *Am. J. Bot.* 49, 874–882. doi: 10.1002/j.1537-2197.1962.tb15023.x

Pandey, J., Vales, M. I., Scheuring, D. C., and Koym, J. W. (2022). Genomic regions associated with tuber traits in tetraploid potatoes and identification of superior clones for breeding purposes. *Front. Plant Sci* 13, 952263. doi: 10.3389/fpls.2022.952263

Prashar, A., Hornyik, C., Young, V., McLean, K., Sharma, S. K., Dale, M. F., et al. (2014). Construction of a dense SNP map of a highly heterozygous diploid potato population and QTL analysis of tuber shape and eye depth. *Theor. Appl. Genet.* 127 (10), 2159–2171. doi: 10.1007/s00122-014-2369-9

Pushkarnath, (1953). Studies on sterility in potato. *Euphytica* 2 (1), 49–58. doi: 10.1007/BF00035742

Saghai-Maroof, M. A., Soliman, K. M., Jorgensen, R. A., and Allard, R. W. (1985). Ribosomal DNA spacer-length polymorphisms in barley: Mendelian inheritance, chromosomal location, and population dynamics. *Proc Natl Acad Sci U.S.A.* 81(24), 8014–8018. doi: 10.1073/pnas.81.24.8014

Si, Y., Sankaran, S., Knowles, N. R., and Pavek, M. J. (2016). Potato tuber length-width ratio assessment using image analysis. *Am. J. Potato Res.* 94 (1), 88–93. doi: 10.1007/s12230-016-9545-1

ŚLiwka, J., Wasilewicz-Flis, I., Jakuczun, H., and Gebhardt, C. (2008). Tagging quantitative trait loci for dormancy, tuber shape, regularity of tuber shape, eye depth and flesh colour in diploid potato originated from six *Solanum* species. *Plant Breed.* 127 (1), 49–55. doi: 10.1111/j.1439-0523.2008.01420.x

Stark, J. C., Love, S. L., and Knowles, N. R. (2020). "Tuber quality," in *Potato production systems*. Eds. J. C. Stark, M. Thornton and P. Nolte (United States: Springer International Publishing), 479–497.

Sun, J., Yang, L., Wang, J., Liu, H., Zheng, H., Xie, D., et al. (2018). Identification of a cold-tolerant locus in rice (*Oryza sativa* l.) using bulked segregant analysis with a next-generation sequencing strategy. *Rice (N Y)* 11 (1), 24. doi: 10.1186/s12284-018-0218-1

Takagi, H., Abe, A., Yoshida, K., Kosugi, S., Natsume, S., Mitsuoka, C., et al. (2013). QTL-seq: rapid mapping of quantitative trait loci in rice by whole genome resequencing of DNA from two bulked populations. *Plant J.* 74 (1), 174–183. doi: 10.1111/tpj.12105

Torrance, L., Cowan, G. H., McLean, K., MacFarlane, S., Al-Abedy, A. N., Armstrong, M., et al. (2020). Natural resistance to potato virus y in *Solanum tuberosum* group phureja. *Theor. Appl. Genet.* 133 (3), 967–980. doi: 10.1007/s00122-019-03521-y

Van Eck, H. J., Jacobs, J. M., Stam, P., Ton, J., Stiekema, W. J., and Jacobsen, E. (1994). Multiple alleles for tuber shape in diploid potato detected by qualitative and quantitative genetic analysis using RFLPs. *Genetics* 137 (1), 303–309. doi: 10.1093/genetics/137.1.303

Van Ooijen, J. W. (2006). *JoinMap 4, software for the calculation of genetic linkage maps in experimental populations* (Wageningen: Kyazma B V).

Van Ooijen, J. W. (2009). *MapQTL6, software for the mapping of quantitative trait in experiment populations of diploid species* (Wageningen: Kyazma B V).

Visser, R. G. F., Bachem, C. W. B., de Boer, J. M., Bryan, G. J., Chakrabati, S. K., Feingold, S., et al. (2009). Sequencing the potato genome: Outline and first results to come from the elucidation of the sequence of the world's third most important food crop. *Am. J. Potato Res.* 86 (6), 417–429. doi: 10.1007/s12230-009-9097-8

Vreugdenhil, D., Bradshaw, J., Gebhardt, C., Govers, F., Taylor, M. A., MacKerron, D. K., et al. (2011). *Potato biology and biotechnology: advances and perspectives* (Amsterdam: Elsevier Press).

Watson, G. (1964). Smooth regression analysis. *Sankhy=a: Indian J. Statistics Ser. A* 26, 359–372. Available at: https://pub.uni-bielefeld.de/record/2715511.

Wu, S., Zhang, B., Keyhaninejad, N., Rodriguez, G. R., Kim, H. J., Chakrabarti, M., et al. (2018). A common genetic mechanism underlies morphological diversity in fruits and other plant organs. *Nat. Commun.* 9 (1), 4734. doi: 10.1038/s41467-018-07216-8

Xiao, G., Huang, W., Cao, H., Tu, W., Wang, H., Zheng, X., et al. (2018). Genetic loci conferring reducing sugar accumulation and conversion of cold-stored potato tubers revealed by QTL analysis in a diploid population. *Front. Plant Sci.* 9. doi: 10.3389/fpls.2018.00315

Xu, Y., and Crouch, J. H. (2008). Marker-assisted selection in plant breeding: From publications to practice. *Crop Sci.* 48 (2), 391–407. doi: 10.2135/cropsci2007.04.0191

Xu, X., Pan, S., Cheng, S., Zhang, B., Mu, D., Ni, P., et al. (2011). Genome sequence and analysis of the tuber crop potato. *Nature* 475 (7355), 189–195. doi: 10.1038/nature10158

Zhou, J., Fang, H., Shan, J., Gao, X., Chen, L., Xie, C., et al. (2014). A major QTL located on chromosome V associates with *in vitro* tuberization in a tetraploid potato population. *Mol. Genet. Genomics* 289 (4), 575–587. doi: 10.1007/s00438-014-0832-6

frontiers | Frontiers in Plant Science

TYPE Original Research
PUBLISHED 18 November 2022
DOI 10.3389/fpls.2022.1036637

OPEN ACCESS

EDITED BY
V. Mohan Murali Achary,
International Centre for Genetic Engineering and Biotechnology, India

REVIEWED BY
Xiaobiao Zhu,
Anhui Agricultural University, China
Gang Yu,
Shanghai Jiao Tong University, China

*CORRESPONDENCE
Juan Du
juandu@mail.hzau.edu.cn

†PRESENT ADDRESS
Lin Chen,
College of Horticulture, South China Agricultural University,
Guangzhou, China

‡These authors have contributed equally to this work

SPECIALTY SECTION
This article was submitted to Crop and Product Physiology, a section of the journal Frontiers in Plant Science

RECEIVED 04 September 2022
ACCEPTED 31 October 2022
PUBLISHED 18 November 2022

CITATION
Mu Y, Guo X, Yu J, Wang R, Liu Z, Hu K, Song J, Chen L, Song B and Du J (2022) SWATH-MS based quantitative proteomics analysis reveals novel proteins involved in PAMP triggered immunity against potato late blight pathogen *Phytophthora infestans*. *Front. Plant Sci.* 13:1036637. doi: 10.3389/fpls.2022.1036637

SWATH-MS based quantitative proteomics analysis reveals novel proteins involved in PAMP triggered immunity against potato late blight pathogen *Phytophthora infestans*

Yang Mu[1,2,3‡], Xiao Guo[1,2,3‡], Jian Yu[1,2,3‡], Ruxun Wang[1,2,3], Zeng Liu[1,2,3], Kefan Hu[1,2,3], Jingyi Song[1,2,3], Lin Chen[1,2†], Botao Song[1,2] and Juan Du[1,2,3*]

[1]Key Laboratory of Horticultural Plant Biology, Ministry of Education, Huazhong Agricultural University, Wuhan, China, [2]Key Laboratory of Potato Biology and Biotechnology, Ministry of Agriculture and Rural Affairs, Huazhong Agricultural University, Wuhan, China, [3]College of Life Science and Technology, Huazhong Agricultural University, Wuhan, China

Potato is the most important non-grain food in the world, while late blight caused by *Phytophthora infestans* seriously threatens the production of potato. Since pathogen-associated molecular patterns (PAMPs) are relatively conserved, PAMP-triggered immunity (PTI) can provide durable resistance to late blight for potato. However, knowledge of the regulatory mechanisms of PTI against oomycete pathogens at protein levels remains limited due to the small number of identified proteins. In the present work, changes in the proteome profile of *Nicotiana benthamiana* leaves upon *P. infestans* PAMP induction were examined using the SWATH-MS (sequential windowed acquisition of all theoretical mass spectra) approach, which provides quantification of protein abundances and large-scale identification of PTI-related proteins. A total of 4401 proteins have been identified, of which 1429 proteins were differentially expressed at least at one time point of 8, 12, 24 and 48 h after PAMP induction, compared with the expression at 0 h when immediately after PAMP induction. They were further analyzed by expression clustering and gene ontology (GO) enrichment analysis. Through functional verification, six novel DEPs of 19 candidates were proved to be involved in PTI responses, including mitochondrial phosphate carrier protein (MPT) 3, vesicle-associated membrane protein (VAMP) 714, lysophospholipase (LysoPL) 2, ascorbate peroxidase (APX) 1, heat shock 70 kDa protein (HSP) 2 and peptidyl-prolyl cis-trans isomerase FKBP (FKBP) 15-1. Taken together, the

time course approach and the resulting large-scale proteomic analyses have enlarged our understanding of PTI mechanisms and provided a valuable resource for the discovery of complex protein networks involved in the resistance response of potato to late blight.

KEYWORDS

Nicotiana benthamiana, *Phytophthora infestans*, pathogen-associated molecular pattern, immunity, SWATH-MS

Introduction

Potato is the most important non-grain food in the world. However, it severely suffers from late blight, which is caused by the devastating oomycete pathogen *Phytophthora infestans*. Enhancing the resistance of potato to *P. infestans* is the most economical and environmentally friendly approach to control late blight. Plant immune systems rely on membrane-resident pattern recognition receptors (PRRs) and intracellular nucleotide-binding oligomerization domain-like receptors (NLRs) to recognize and prevent pathogen invasion (Couto and Zipfel, 2016; Jones et al., 2016). PRR-mediated resistance is considered to be relatively more durable.

Plant PRRs can recognize conserved pathogen-associated molecular patterns (PAMPs), such as bacterial flagellin or its derived peptide, flg22, to provide broad-spectrum pathogen resistance (Zipfel, 2008; Couto and Zipfel, 2016). The experiment system of flg22-triggered reactive oxygen species (ROS) bursts has been well established and widely used for the study of PAMP-triggered immunity (PTI) (Sang and Macho, 2017). Elicitins are the most well-characterized oomycete PAMPs specifically secreted by *Phytophthora* and *Pythium* species, which share a highly conserved 98-amino-acid domain (Pfam PF00964) (Ponchet et al., 1999; Jiang et al., 2006; Lévesque et al., 2010; Derevnina et al., 2016). The receptor and co-receptors of elicitins have previously been identified, namely elicitin response (ELR), somatic embryogenesis receptor kinase (SERK) 3/brassinosteroid-associated kinase (BAK) 1 and suppressor of bir1-1 (SOBIR1) (Du et al., 2015; Domazakis et al., 2018). Besides, some other genes such as *SGT1* (Shibata et al., 2011), *SIPK/NTF6* (Asai et al., 2008), *WRKY7/8/9/11* (Adachi et al., 2015), *NbMKK1* (Takahashi et al., 2007), *Nbrboh* (Yoshioka et al., 2003) and *HSP90* and *HSP70* (Kanzaki et al., 2003) have been proved important for elicitin-triggered immunity. Moreover, we have identified 32 differentially expressed proteins (DEPs) in *Nicotiana benthamiana* induced by elicitin through iTRAQ proteomics approach and proved two DEPs namely, ATP dependent transporter and 60S ribosomal protein L15, are essential for PAMP-triggered immunity (Du et al., 2017). However, the mechanism of PTI against *P. infestans* still needs further exploration.

Compared with iTRAQ, another recently developed label-free quantitative proteomics approach named SWATH-MS (sequential windowed acquisition of all theoretical fragment ions - mass spectra) is based on a data-independent acquisition (DIA) strategy for consistent and reproducible quantification of peptides with high complexity, and thus has high coverage, unlimited sample size and can quantify more low abundance proteins (Huang et al., 2015). In this study, SWATH-MS approach was used to screen proteins involved in PTI against *P. infestans*. The culture filtrate (CF) of *P. infestans* contains a variety of PAMPs including elicitins and so on (McLellan et al., 2013; Saubeau et al., 2014). We did a time course analysis of protein abundance in *N. benthamiana* leaves at 0, 8, 12, 24 and 48 h after CF infiltration. A total of 4401 proteins were quantitatively identified by SWATH-MS in *N. benthamiana* leaves, 1429 of which were found to be differentially expressed by comparing the amount of identified proteins at the later four time points with that of 0 h post infiltration (hpi) at a fold change of 1.5 with a p-value <0.05. According to bioinformatic analysis results, 19 DEPs belonging to the gene ontology (GO) term of "response to stress" were selected for further functional verification by virus-induced gene silencing (VIGS) and PAMP-triggered reactive oxygen species (ROS) burst analysis. As a result, six novel genes were found involved in PTI responses.

Methods

Phytophthora infestans culture filtrate preparation

For preparing culture filtrate (CF), the mycelia and sporangia of a *P. infestans* isolate 88069 were cultured in the Plich liquid medium (0.5 g KH_2PO_4, 0.25 g $MgSO_4{\cdot}7H_2O$, 1 g Asparagine, 1 mg Thiamine, 0.5 g Yeast extract, 10 mg β-

sitosterol and 25 g Glucose in 1l) for four weeks at 16°C in dark. Then the liquid was used for plant treatment.

Plant materials and treatments

N. benthamiana plants were grown from seeds and maintained in the controlled climate chamber under a 16h/8 h light and dark cycle at 24°C. The fully expanded leaves of 4-5-week-old plants were used for CF infiltration with a needleless syringe. And samples were taken at 0 h (immediately after CF infiltration), 8 h, 12 h, 24 h, and 48 h, respectively. Three infiltrated leaves were taken at each time point as three biological replicates.

Protein and peptide preparation

Approximately 1.5 g of *N. benthamiana* leaves for each sample was ground in a mortar with liquid nitrogen. The tissues were homogenized by 10 ml of SDS Lysis Buffer (60 g sucrose, 4 g SDS and 3.084 g DTT in 200 ml) containing protease inhibitor and centrifuged at 20 000 rpm at 4°C for 10 min. The supernatant was taken to a freshly pre-cooled 50 ml centrifuge tube and mixed with an equal volume of Tris saturated phenol (pH 8.0). Afterward, the mixture was incubated at 37°C on a shaker for 5 min. After centrifugation at 20 000 rpm at 4°C for 10 min, the mixture was divided into three layers, with protein in the upper layer. It was then carefully taken out and mixed with 5× volumes of pre-cooled 0.1 M ammonium acetate in methanol for overnight protein precipitation at -20°C. After centrifuged at 12 000 rpm for 10 min at 4°C, the supernatants were removed, and the pellets were washed with 10 ml of pre-cooled methanol, and then further washed with 10 ml of pre-cooled acetone. Finally, the protein pellets were dissolved in the 4 ml urea buffer (8 M urea in 0.05 M ammonium bicarbonate) with ultrasonic for 6 min (ultrasonic for 2 s, stop for 3 s). After centrifugation at 20 000 rpm for 10 min at 4°C, the supernatant was carefully aspirated into a freshly pre-cooled 15 ml centrifuge tube for subsequent protein quantification. Protein concentration was determined using the Pierce™ bicinchoninic acid (BCA) Protein Assay Kit (Thermo Scientific, USA) with bovine serum albumin (BSA; 2mg/ml) as a standard for quantification.

Then each protein sample (5 mg) was reduced by 20 µl of 1 M dithiothreitol (DTT) at 56°C for 30 min and alkylated by 120 µl of 0.5 M iodoacetamide at room temperature in dark for 40 min. Then 40 µl of 1 M DTT was added into the protein materials in dark for 20 min to quench the extra iodoacetamide. Afterward, each sample was diluted into 8× volumes of 50 mM ammonium bicarbonate solution including 1 M urea and 400 µl of trypsin (enzyme/protein, 1:25 w/w) for protein digestion overnight at 37°C. Peptides were generated by specific trypsin cleavage at the C-terminal at the arginine and lysine sites of proteins. The acquired peptides were acidified by 10% trifluoroacetic acid (TCA) and desalted using oasis® HLB solid-phase extraction (SPE; Agilent, USA). Finally, the desalted peptide samples were dried in a speed-vacuum concentrator and stored at -80°C or directly dissolved in 0.1% formic acid for LC-MS/MS analysis.

SWATH-MS measurement and analysis

SCX peptide fractionation was performed according to previously reported (Lu et al., 2019). Analysis of SCX peptide fractions was performed on a Nanospray III source and a TripleTOF 5600+ (AB SCIEX) mass spectrometer (Andrews et al., 2011). The peptide fractions (2µg each) were resuspended in 0.1% formic acid (FA) and trapped separately into an Ekspert TM nanoLC 415 (AB SCIEX) with a nanoLC trap (ChromXP C18-CL 3 µm 120 Å, 350µm × 0.5 mm) at 2 µL/min for 7 min. Then, the pump flow was split to obtain a flow rate of 300 nL/min on the nanoLC trap and the nanoLC column (75 µm × 15 cm, 3C18-CL-120, 3 µm, 120 Å) was used for separation. The mobile phases consisted of solvent A containing water: acetonitrile: formic acid at a ratio of 98:2:0.1 (V/V/V), and solvent B containing water: acetonitrile: formic acid at a ratio of 2:98:0.1 (V/V/V). A nonlinear gradient of 5% to 12% B for 0.5 min, 12% to 24% B for 59.5 min, 24% to 35% B for 35 min, 35% to 50% B for10 min, 50% to 80% B for 1 min, 80% B for 5min, 80% to 5% B in 1 min, and 5% B for 8 min was employed. The mass tolerance was set to 50mDa, The spray voltage was set to 2.5 kV, and the temperature of the heated capillary was set to 275°C. The mass spectrometer was operated in positive ion mode with a nanoion spray voltage of 2.5 kV.

Data-dependent acquisition (DDA) was first performed to obtain the SWATH-MS spectral ion library. A survey scan of 0.248 s in the range 350–1250 m/z was performed to collect the MS1 spectra. The top 50 precursor ions with charge state from +2 to +5 were selected for fragmentation with an accumulation time of 50 ms per MS/MS experiment for a total cycle time of 2.3 s, and MS/MS spectra were collected in the range 100–1500 m/z. Selected ions and their isotopes were dynamically excluded from further MS/MS fragmentation for 18 s.

In the SWATH analysis, the same peptide samples were analyzed by the cyclic data-independent acquisition (DIA) mode using similar methods as described above. For DIA analysis, MS/MS proteome profiling was analyzed by the same LC-MS/MS system. A survey scan of 50 ms was performed and all precursors were subjected to fragmentation. MS/MS experiments were conducted with an accumulation time of 100 ms per 25 Da swath (total swath 36) for a total cycle time of 3.6 s.

All DDA mass spectrometry data were used to generate a reference spectral library by searching against the *Nicotiana benthamiana* protein database v04.4 (36151 proteins, 2010 release, Sol Genomics Network) using the ProteinPilot 4.5 software (Sciex). The parameters included digestion, alkylation,

and biological modification. A false discovery rate of < 1% was accepted as the criteria for the peptide assignments and protein identification. Subsequently, the DIA data and spectral library were loaded into PeakView v.1.2 software (Sciex) under restricted criteria and settings: six peptides, six transitions, 99% peptide confidence and ion library mass tolerance (75 ppm). The output of quantified proteins and corresponding peptides by the MarkerView (Sciex) generated three quantitative files including the extracted peak area for individual fragment ions, the sum of the fragment ion areas for each peptide and the sum of peptide areas for each protein. Differentially expressed proteins (DEPs) were analyzed by ANOVA analysis and Tukey's HSD multiple comparison ($P \leq 0.05$) and then were updated from reference genome Niben v0.44 to Niben v1.01. Information of the identified DEPs were shown in Table S1.

Gene ontology enrichment analysis

TBtools (Chen et al., 2020) was used to perform gene ontology (GO) enrichment for DEPs of cluster 7. GO background data was downloaded from the AgriGO website. E-value cut-off: 1.0E-3, and GO terms of Biological Process with a false discovery rate (FDR) 0.05 were obtained and included in Table S2. They were ranked according to their *P*-values (ascending), and the top 15 terms for Biological Process belonging to level 3 were then selected to draw a bubble diagram by R package ggplot2 (https://github.com/tidyverse/ggplot2).

Tobacco rattle virus-induced gene silencing

Virus-induced gene silencing (VIGS) constructs were made by cloning ~300 bp PCR fragments from candidate genes into the TRV2 vector, respectively (Ratcliff et al., 2001). The inserted fragments were selected with the help of a VIGS tool in the genome website of Solanaceae (https://vigs.solgenomics.net/). Primers for VIGS of candidate genes shown in Table S3. A TRV2 construct expressing GFP was used as a control (Du et al., 2017). *Agrobacterium tumefaciens* strains GV3101 containing TRV1 and each candidate gene VIGS construct at an OD600 of 0.3 were mixed at a 1:1 ratio and then infiltrated into the leaves of the four-leaf-stage *N. benthamiana* plant. Systemic leaves were detached and analyzed by qRT-PCR.

Quantitative RT-PCR analysis

Total RNA was extracted from the leaves of *N. benthamiana* plants after infiltration of CF and VIGS using a Total RNApure Kit (Zoman Biotechnology Co. Ltd.) according to the manufacturer's instructions. First-strand cDNA was synthesized using the 5X All-in-One RT MasterMix Reverse Transcription Kit (ABM). qRT-PCR was carried out using SYBR green as described previously (Du et al., 2017). Primers for qRT-PCR are shown in Table S3 and *Actin* was used as an internal control. For VIGS experiment, at least one primer was designed outside the region of cDNA targeted for silencing.

ROS analysis

Luminol-based assays were used to evaluate ROS bursts. After three weeks of VIGS, at least nine leaves of *N. benthamiana* plants for each candidate gene were excised into leaf discs of 0.09 cm^2. To eliminate the wounding effect, leaf discs were incubated in the 96-well plate with 200 µl of ddH_2O overnight, which was replaced by 100 µl of reaction solution as previously described with a difference in the concentration of flg22 (Sang and Macho, 2017). Instead of 5 µl flg22 stock solution (100 µM) added to 10 ml of ultra-pure distilled H_2O, 10 µl flg22 stock solution (100 µM) was added in this study. Measurements were taken immediately after adding the solution with a 1 min interval reading time for a period of 60 min with a luminometer. The measurement values for ROS production from 24 leaf discs per treatment were indicated as means of RLU (Relative Light Units).

Results

Phytophthora infestans culture filtrate induces cell death in *Nicotiana benthamiana* within 48 h

To test the PAMP-triggered immune responses by *P. infestans* culture filtrate (CF), it as well as a negative control culture medium (CM) were infiltrated into the same *N. benthamiana* leaves, respectively. Then the infiltrated leaves were observed and sampled at 0 (immediately after CF infiltration), 8, 12, 24 and 48 hpi. Under natural light, no obvious phenotypes were observed at 0, 8, 12 and 24 hpi, while at 48 hpi, a cell death was visible at the CF-infiltrated site but not at the CM-infiltrated site (Figure 1A). Interestingly, under UV light, little cell death responses could be observed as early as at 24 hpi at the CF-infiltrated site but not at the CM-infiltrated site (Figure 1A). Then samples taken at 0, 8, 12, 24 and 48 hpi were analyzed for the expression of three PTI marker genes *WRKY8, PTI5* and *ACRE31* (Nguyen et al., 2010; Wang et al., 2018) by qPCR. The expression of all three genes was significantly upregulated at 8 h after CF infiltration, however, their expression changes were diverse during 48 hpi (Figure 1B). After 8 hpi, the expression of *WRKY8* kept steady until 48 hpi,

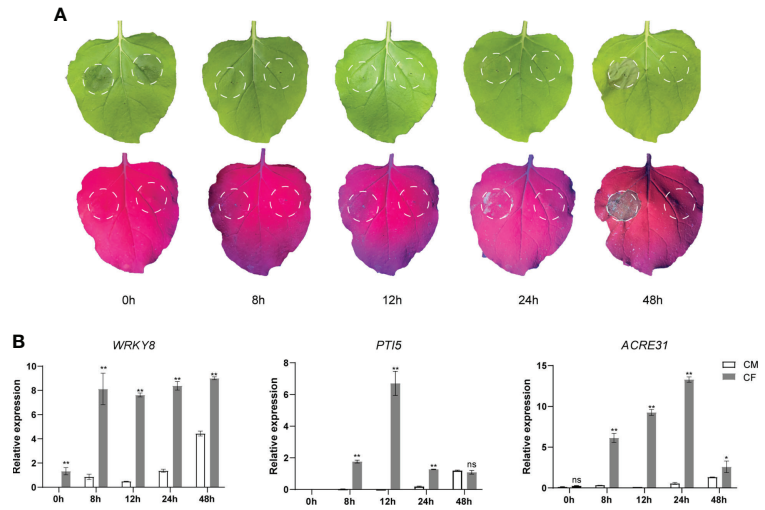

FIGURE 1
The culture filtrate (CF) of *Phytophthora infestans* induced PAMP triggered immunity responses in *Nicotiana benthamiana*. **(A)** CF was infiltrated within a white line circle on the left panel of the mid vein while culture medium (CM) was on the right panel. **(B)** CF-induced upregulation of PTI marker genes *WRKY8*, *PTI5* and *ACRE31*. Independent experiments have been conducted three times with similar results. Student's *t*-test was used for the statistical analysis. Error bars stand for SEM, ns, not significant, $*P < 0.05$ and $**P < 0.01$.

while the expression of *PTI5* and *ACRE31* peaked at 12 and 24 hpi, respectively, and then fell down (Figure 1B).

CF induced a total of 4401 proteins at five time points

In order to identify novel differentially expressed proteins (DEPs) induced by CF in *N. benthamiana*, only CF-infiltrated leaves taken at 0, 8, 12, 24 and 48 h were sent for the subsequent SWATH-MS analysis (Figure 2). For each time point, three infiltrated leaves were taken for independent tests and each sample was also tested three times for SWATH-MS as technical repeats. As a result, nine data sets were obtained for each time point. With data from all the five time points, a reference database containing a total of 38,683 unique peptides corresponding to 5714 proteins was generated using the data-dependent acquisition (DDA) model, with a false discovery rate (FDR) less than 1%. Compared with our reference database, a total of 4401 proteins were identified at all five time points with the Process in SWATH 2.0 software analysis based on important information including retention time, precursor ion mass, and fragment ion mass-to-charge ratio.

A total of 1429 DEPs were identified

Then principal component analysis (PCA) was performed to evaluate the data by R package factominer. The idensity of all 4401 proteins identified at five time points were taken as observation values, and samples at different time points and their biological replicates were taken as variables. The PCA biplot shows that they were distinctly separate in two principal components (Figure 3A), which means that proteins has experienced a significant change in *N. benthamiana* after CF induction. Among the above identified 4401 proteins, we compared the amount of identified proteins at the later four time points with that of 0 hpi. A total of 1429 DEPs were identified at a fold change of 1.5 with a *p*-value <0.05 (Table S1). Specifically, 331 DEPs were identified with 129 up-regulated and 202 down-regulated at 8 hpi, 837 DEPs were identified with 343 up-regulated and 494 down-regulated at 12 hpi, 944 DEPs were identified with 515 up-regulated and 429 down-regulated at 24 hpi, 1193 DEPs were identified with 731 up-regulated and 462 down-regulated at 48 hpi (Figure 3B).

Defense-related terms were found in Cluster 7

We used Mfuzz to cluster all 1429 DEPs according to their protein expression profiles and obtained mainly nine types of temporal patterns, which generally show four expression trends (Figure 4A). The first trend is overall down-regulated shown in clusters 1, 2, 3 and 8. The second trend is overall upregulated shown in clusters 4, 6 and 7. The third trend is first down-regulated then up-regulated shown only in cluster 5. The fourth trend is first up-regulated then down-regulated shown only in

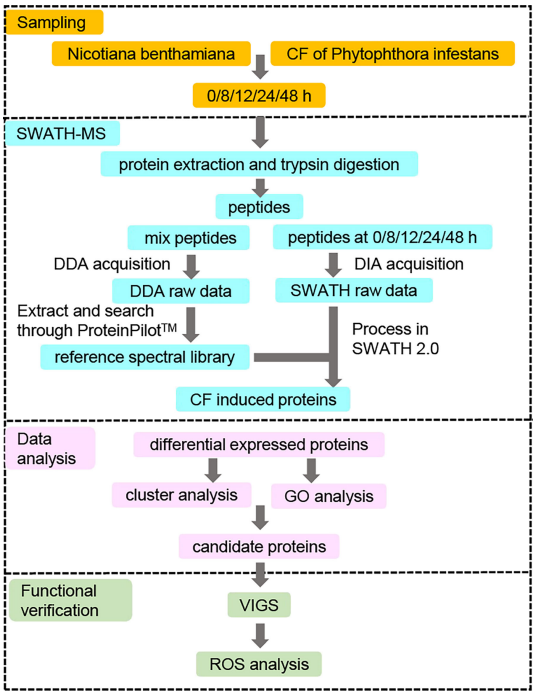

FIGURE 2
Strategy for identifying novel differentially expressed proteins (DEPs) involved in PAMP triggered immunity against *Phytophthora infestans*. *N. benthamiana* leaves were infiltrated with culture filtrate (CF) of *P. infestans*, and samples were collected at 0 (immediately after infiltration), 8, 12, 24 and 48 hpi. Proteins were extracted from the samples at five time points and digested by trypsin for the SWATH-MS analysis. The resulting peptides were first mixed and measured by a data-dependent acquisition (DDA) model to generate a reference spectral library. At the same time, the resulting peptides at each of the five time points were also measured by a data-independent acquisition (DIA) model to obtain SWATH raw data, which were compared to the reference spectral library to get the CF-induced proteins. Differentially expressed proteins (DEPs) were identified by comparing the expression of CF-induced proteins at 8, 12, 24 and 48 hpi to that at 0 hpi at a fold change of 1.5 with a *p*-value <0.05. Then protein expression clustering and GO enrichment analysis were performed to get the candidate proteins for the functional verification by virus-induced gene silencing (VIGS) and reactive oxygen species (ROS) assays.

cluster 9. Among the upregulated clusters, the trend of cluster 7 maintains the best continuity, which may be more correlated to PTI defenses. To further analyze the function of DEPs in cluster 7, we performed GO enrichment analysis of them (Figure 4B). Among the top 15 GO terms for Biological Process belonging to level 3, defense-related terms were found such as response to stress, immune response, response to biotic stimulus, etc. Interestingly, some well-known PTI-related proteins such as SGT1 and BAK1 were also found in cluster 7. This indicates that more PTI-related proteins may be involved in cluster 7 since they have similar expression patterns.

Six novel candidate DEPs were identified to be involved in PTI responses

To test the above hypothesis, we selected 19 DEPs belonging to "response to stress" for functional verifications by VIGS and ROS assays, including mitochondrial phosphate carrier protein (MPT) 3, protein disulfide-isomerase like (PDIL) 2, peroxisomal (S)-2-hydroxy-acid oxidase (GOX) 3, cysteine-rich receptor-like protein kinase (CRK) 2, thioredoxin reductase (NTRA) 2, heat shock 70 kDa protein BIP2 (HSP70-12), chaperone protein dnaJ (DJA) 2, calnexin homolog (CNX) 1, lysophospholipase (LysoPL) 2, PLAT domain-containing protein (PLAT) 1, ascorbate peroxidase (APX) 1, 2-hydroxyacyl-CoA lyase (HPCL), ABC transporter G family member (ABCG) 40, acidic endochitinase (CHIA), early responsive to dehydration (ERD) 9, peptidyl-prolyl cis-trans isomerase FKBP (FKBP) 15-1, vesicle-associated membrane protein (VAMP) 714, heat shock 70 kDa protein (HSP) 2, nucleosome assembly protein (NAP) 1;3 (Table 1).

For VIGS, ~300 bp PCR fragments from 19 candidate genes were amplified using the cDNA of *N. benthamiana* as a template. Leaves of four-leaf-stage plants were treated with TRV-candidate genes and the control TRV-*GFP*, respectively. After three weeks, three leaves from different plants of *N. benthamiana* for each candidate gene were excised, and flg22 was used to determine the ROS intensity. Compared to the control TRV-GFP, we found

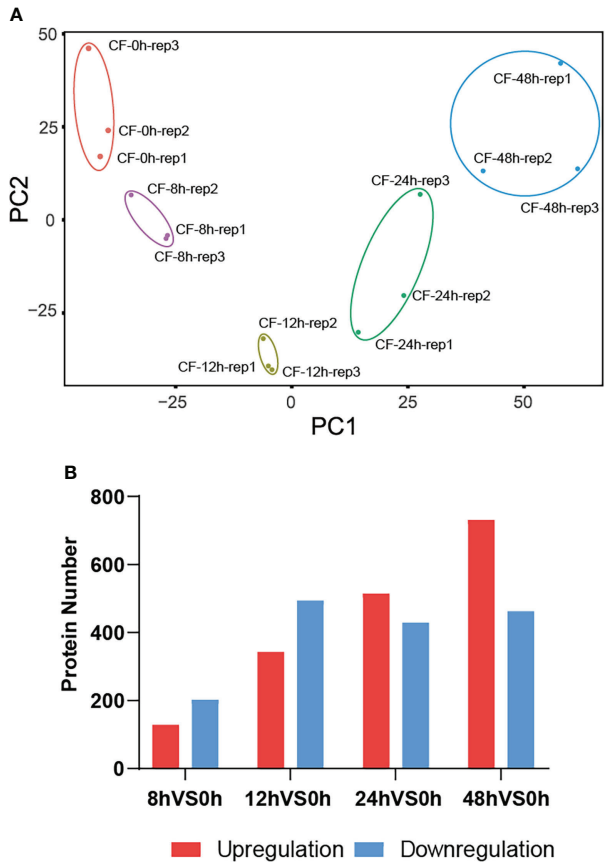

FIGURE 3
A total of 1429 DEPs were identified. The principal component analysis (PCA) biplot shows that CF-induced proteins at five time points 0, 8, 12, 24, 48 hpi were distinctly separate in two principal components **(A)**, and they were differentially expressed at 8, 12, 24, 48 hpi compared to their expression at 0 hpi **(B)**.

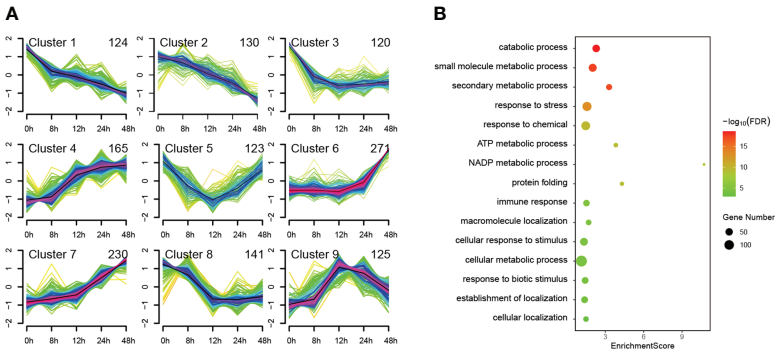

FIGURE 4
Cluster and GO enrichment analysis of 1429 differentially expressed proteins (DEPs). The identified 1429 DEPs were clustered in mainly nine types of temporal patterns according to their protein expression profiles **(A)** and GO enrichment analysis was performed on the DEPs of cluster 7, of which the top 15 GO terms for Biological Process belonging to level 3 are presented **(B)**.

10.3389/fpls.2022.1036637

TABLE 1 Information of 19 candidate proteins in cluster 7.

Accession no.	Name	Length (aa)	Annotation
Niben101Scf00109g00017.1	MPT3	366	Mitochondrial phosphate carrier protein 3
Niben101Scf00332g04004.1	PDIL2	359	Protein disulfide-isomerase like 2-1
Niben101Scf00622g00006.1	GOX3	368	Peroxisomal (S)-2-hydroxy-acid oxidase
Niben101Scf01230g01011.1	CRK2	604	Cysteine-rich receptor-like protein kinase 2
Niben101Scf01677g04003.1	NTRA	330	Thioredoxin reductase 2
Niben101Scf02030g04003.1	HSP70-12	583	Heat shock 70 kDa protein BIP2
Niben101Scf03138g01010.1	DJA2	420	Chaperone protein dnaJ 2
Niben101Scf03777g00002.1	CNX1	539	Calnexin homolog 1
Niben101Scf04820g01003.1	LysoPL2	327	Lysophospholipase 2
Niben101Scf05326g00012.1	PLAT1	183	PLAT domain-containing protein 1
Niben101Scf06195g00002.1	APX1	250	Ascorbate peroxidase 1
Niben101Scf06394g00009.1	HPCL	513	2-hydroxyacyl-CoA lyase
Niben101Scf06583g03008.1	ABCG40	1422	ABC transporter G family member 40
Niben101Scf06684g03003.1	CHIA	295	Acidic endochitinase
Niben101Scf06958g02005.1	ERD9	216	Protein early responsive to dehydration 9
Niben101Scf08447g01002.1	FKBP15-1	117	Peptidyl-prolyl cis-trans isomerase FKBP15-1
Niben101Scf08515g00019.1	VAMP714	217	Vesicle-associated membrane protein 714
Niben101Scf08590g00005.1	HSP70-2	706	Heat shock 70 kDa protein 2
Niben101Scf11512g01019.1	NAP1;3	384	Nucleosome assembly protein 1;3

that the ROS production was significantly changed after plants were treated with six TRV-candidate genes. After VIGS of a candidate gene *MPT3*, the ROS production was significantly up-regulated, while after VIGS of five other candidate genes including *VAMP714*, *LysoPL2*, *APX1*, *HSP70-2* and *FKBP15-1*, the ROS production was significantly down-regulated (Figure 5). Their silencing efficiency was tested by qRT-PCR with the transcript level of candidate genes reduced below 50% (Figure 5).

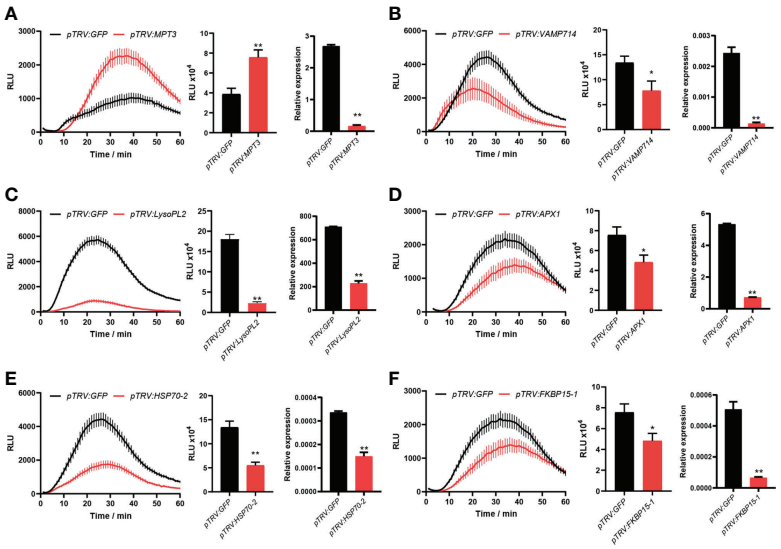

FIGURE 5
Six novel candidate DEPs were found involved in PTI responses. After virus-induced gene silencing (VIGS) of *MPT3* **(A)**, the ROS production was significantly up-regulated, while after VIGS of *VAMP714* **(B)**, *LysoPL2* **(C)**, *APX1* **(D)**, *HSP70-2* **(E)** and *FKBP15-1* **(F)**, the ROS production was significantly down-regulated. The bar charts show the total count of ROS accumulation and silencing efficiency of VIGS. Independent experiments have been conducted three times with similar results. Student's *t*-test was used for the statistical analysis. Error bars stand for SEM, $*P < 0.05$ and $**P < 0.01$.

Discussion

The mechanism of PAMP triggered immunity (PTI) against oomycete pathogens is largely unknown. In this study, we have performed a label-free quantitative proteomics approach named SWATH-MS to screen proteins involved in PTI against *P. infestans* (Figure 2). The culture filtrate (CF) of *P. infestans* was used to provide PAMPs (McLellan et al., 2013; Saubeau et al., 2014). A total of 4401 proteins were induced in *Nicotiana benthamiana* at 0, 8, 12, 24 and 48 hpi. And 1429 proteins were differentially expressed at least at one time point of 8, 12, 24 and 48 hpi (Figure 3; Table S1). With the time course expression profiles, they could be divided into nine clusters (Figure 4A). Cluster 7 contains some defense-related GO terms including "response to stress" (Figure 4B). Then 19 DEPs in this term were selected as candidates for functional verification by VIGS and ROS assay. As a result, six DEPs were proved to be involved in PTI responses (Figure 5).

Previously, we used another proteomics approach iTRAQ to identify proteins involved in PTI against *P. infestans* in *N. benthamiana*, which resulted in only 32 DEPs induced by INF1 elicitin (Du et al., 2017). Compared with iTRAQ, SWATH-MS has higher coverage and better repeatability, no limit on sample size, and can quantify more low-abundance proteins (Huang et al., 2015). Thus, here we could detect samples at five time points, while only one time point at 8 hpi was available by iTRAQ. Besides, the inducers used in the two proteomics approaches are different. The INF1 elicitin was used for iTRAQ, while CF was used for SWATH-MS, which contains a variety of PAMPs including at least three elicitins e.g. INF1, INF4, INF5, and a galactan-based complex polysaccharide (Saubeau et al., 2014). Thus, CF could induce much more DEPs and complex PTI responses.

We validated the involvement of candidate DEPs with bacterial flg22-triggered ROS burst, which is not from *P. infestans* CF. However, they may trigger similar PTI signaling. Actually, CF infiltration and agroinfiltration of INF1 have also been performed on the VIGS plants of candidate DEPs. However, there was no obvious attenuation of cell death mediated by CF or INF1 (data not shown). We guess that they may play a negative role or have redundancy in the PTI response. The well-established flg22-triggered ROS bursts system on the VIGS plants could better quantify their influences on the PTI responses. Indeed, among the six identified DEPs, one plays a negative role and the other five partially affect the ROS bursts after treated with their corresponding TRV vectors compared with the controls.

The six identified DEPs include mitochondrial phosphate carrier protein (MPT) 3, vesicle-associated membrane protein (VAMP) 714, lysophospholipase (LysoPL) 2, ascorbate peroxidase (APX) 1, heat shock 70 kDa protein (HSP) 2 and peptidyl-prolyl cis-trans isomerase FKBP15-1. MPT3 plays a crucial role in ATP production in plant cells. In eukaryotes, N-ethylmaleimide-sensitive factor adaptor protein (SNAP) receptors, also known as SNAREs, have evolved as mediators of fusion of membranes between vesicles and targets. Arabidopsis AtVAMP714 is essential for the polarisation of PIN proteins and auxin responses (Gu et al., 2021), while rice OsVAMP714-mediated trafficking pathway was indicated to play an important role in rice blast resistance (Sugano et al., 2016). LysoPL2 is involved in tolerance to cadmium-induced oxidative stress and also reported to function as Caffeoyl shikimate esterase (CSE) that is an enzyme in the lignin biosynthetic pathway in Arabidopsis (Vanholme et al., 2013). CSE converts caffeoyl shikimate to caffiate and its mutants have reduced lignin content and collapsed vessel elements. APX1 plays an important role in the regulation of the steady-state level of ROS in plant cells (Mittler et al., 2004). HSP70 is an essential protein regulator involved in maintaining internal stability such as proper folding of proteins and breakdown of unfolded proteins. NbHSP70c-1 (GenBank no. AB105430) was previously reported to be essential for INF1-triggered cell death response (Kanzaki et al., 2003). HSP70-2 identified in this study shares ~50% similarities of amino acids with NbHSP70c-1, which could play similar roles as NbHSP70c-1. FKBP15-2 was shown to be required for ER stress-mediated plant immunity (Fan et al., 2018). However, the mechanisms of them involved in PTI responses still needs further exploration.

Overall, our study sets an example to use SWATH-MS approach to study plant immunity. The six identified DEPs provide new clues to make a further deep study of the molecular mechanism of PTI. Moreover, the identified 1429 DEPs also provide a valuable resource for the discovery of complex protein networks involved in the resistance response of potato to late blight.

Data availability statement

All data supporting the findings of this research are available within the paper and within its supplementary data published online.

Author contributions

YM, XG, JY, RW, ZL, KH, JS, LC and JD performed experiments and analyzed data. YM, XG, JY, RW, ZL, KH, JS, BS and JD designed experiments. BS and JD supervised. YM, XG, LC and JD wrote the manuscript. All authors contributed to the article and approved the submitted version.

Funding

The work was partially supported by the National Science Foundation of China (31401436), the Fundamental Research

Funds for the Central Universities (2662016QD042) and the Key-Area Research and Development Program of Guangdong Province (2020B020219002).

Acknowledgments

We thank Qiansi Chen for providing the SWATH-MS proteomics platform and guidance.

Conflict of interest

The authors declare that the research was conducted in the absence of any commercial or financial relationships that could be construed as a potential conflict of interest.

Publisher's note

Supplementary material

The Supplementary Material for this article can be found online at: https://www.frontiersin.org/articles/10.3389/fpls.2022.1036637/full#supplementary-material

References

Adachi, H., Nakano, T., Miyagawa, N., Ishihama, N., Yoshioka, M., Katou, Y., et al. (2015). WRKY transcription factors phosphorylated by MAPK regulate a plant immune NADPH oxidase in *Nicotiana benthamiana*. *Plant Cell* 27, 2645–2663. doi: 10.1105/tpc.15.00213

Andrews, G. L., Simons, B. L., Young, J. B., Hawkridge, A. M., and Muddiman, D. C. (2011). Performance characteristics of a new hybrid quadrupole time-of-flight tandem mass spectrometer (TripleTOF 5600). *Anal. Chem.* 83, 5442–5446. doi: 10.1021/ac200812d

Asai, S., Ohta, K., and Yoshioka, H. (2008). MAPK signaling regulates nitric oxide and NADPH oxidase-dependent oxidative bursts in *Nicotiana benthamiana*. *Plant Cell* 20, 1390–1406. doi: 10.1105/tpc.107.055855

Chen, C., Chen, H., Zhang, Y., Thomas, H. R., Frank, M. H., He, Y., et al. (2020). TBtools: An integrative toolkit developed for interactive analyses of big biological data. *Mol. Plant* 13, 1194–1202. doi: 10.1016/j.molp.2020.06.009

Couto, D., and Zipfel, C. (2016). Regulation of pattern recognition receptor signalling in plants. *Nat. Rev. Immunol.* 16, 537–552. doi: 10.1038/nri.2016.77

Derevnina, L., Dagdas, Y. F., de la Concepcion, J. C., Bialas, A., Kellner, R., Petre, B., et al. (2016). Nine things to know about elicitins. *N. Phytol.* 212, 888–895. doi: 10.1111/nph.14137

Domazakis, E., Wouters, D., Visser, R., Kamoun, S., Joosten, M. H., and Vleeshouwers, V. (2018). The ELR-SOBIR1 complex functions as a two-component RLK to mount defense against *Phytophthora infestans*. *Mol. Plant-Microbe In* 31, 795–802. doi: 10.1094/MPMI-09-17-0217-R

Du, J., Guo, X., Chen, L., Xie, C., and Liu, J. (2017). Proteomic analysis of differentially expressed proteins of *Nicotiana benthamiana* triggered by INF1 elicitin from *Phytophthora infestans*. *J. Gen. Plant Pathol.* 83, 66–77. doi: 10.1007/s10327-017-0699-6

Du, J., Verzaux, E., Chaparro-Garcia, A., Bijsterbosch, G., Keizer, L. C. P., Zhou, J., et al. (2015). Elicitin recognition confers enhanced resistance to *Phytophthora infestans* in potato. *Nat. Plants* 1, 15034. doi: 10.1038/nplants.2015.34

Fan, G., Yang, Y., Li, T., Lu, W., Du, Y., Qiang, X., et al. (2018). A *Phytophthora capsici* RXLR effector targets and inhibits a plant PPIase to suppress endoplasmic reticulum-mediated immunity. *Mol. Plant* 11, 1067–1083. doi: 10.1016/j.molp.2018.05.009

Gu, X., Fonseka, K., Agneessens, J., Casson, S. A., Smertenko, A., Guo, G., et al. (2021). The Arabidopsis R-SNARE VAMP714 is essential for polarisation of PIN proteins and auxin responses. *N. Phytol.* 230, 550–566. doi: 10.1111/nph.17205

Huang, Q., Yang, L., Luo, J., Guo, L., Wang, Z., Yang, X., et al. (2015). SWATH enables precise label-free quantification on proteome scale. *Proteomics* 15, 1215–1223. doi: 10.1002/pmic.201400270

Jiang, R. H. Y., Tyler, B. M., Whisson, S. C., Hardham, A. R., and Govers, F. (2006). Ancient origin of elicitin gene clusters in *Phytophthora* genomes. *Mol. Biol. Evol.* 23, 338–351. doi: 10.1093/molbev/msj039

Jones, J. D., Vance, R. E., and Dangl, J. L. (2016). Intracellular innate immune surveillance devices in plants and animals. *Science* 354, aaf639. doi: 10.1126/science.aaf6395

Kanzaki, H., Saitoh, H., Ito, A., Fujisawa, S., Kamoun, S., Katou, S., et al. (2003). Cytosolic HSP90 and HSP70 are essential components of INF1-mediated hypersensitive response and non-host resistance to pseudomonas cichorii in *Nicotiana benthamiana*. *Mol. Plant Pathol.* 4, 383–391. doi: 10.1046/j.1364-3703.2003.00186.x

Lévesque, C. A., Brouwer, H., Cano, L., Hamilton, J. P., Holt, C., Huitema, E., et al. (2010). Genome sequence of the necrotrophic plant pathogen *Pythium ultimum* reveals original pathogenicity mechanisms and effector repertoire. *Genome Biol.* 11, 1–22. doi: 10.1007/s000180050491

Lu, Z. S., Chen, Q. S., Zheng, Q. X., Shen, J. J., Luo, Z. P., Fan, K., et al. (2019). Proteomic and phosphoproteomic analysis in tobacco mosaic virus-infected tobacco (*Nicotiana tabacum*). *Biomolecules* 9, 39. doi: 10.3390/biom9020039

McLellan, H., Boevink, P. C., Armstrong, M. R., Pritchard, L., Gomez, S., Morales, J., et al. (2013). An RxLR effector from *Phytophthora infestans* prevents re-localisation of two plant NAC transcription factors from the endoplasmic reticulum to the nucleus. *PloS Pathog.* 9, e1003670. doi: 10.1371/journal.ppat.1003670

Mittler, R., Vanderauwera, S., Gollery, M., and Van Breusegem, F. (2004). Reactive oxygen gene network of plants. *Trends Plant Sci.* 9, 490–498. doi: 10.1016/j.tplants.2004.08.009

Nguyen, H. P., Chakravarthy, S., Velasquez, A. C., McLane, H. L., Zeng, L. R., Nakayashiki, H., et al. (2010). Methods to study PAMP-triggered immunity using tomato and *Nicotiana benthamiana*. *Mol. Plant-Microbe In* 23, 991–999. doi: 10.1094/MPMI-23-8-0991

Ponchet, M., Panabieres, F., Milat, M. L., Mikes, V., Montillet, J. L., Suty, L., et al. (1999). Are elicitins cryptograms in plant-oomycete communications? *Cell Mol. Life Sci.* 56, 1020–1047. doi: 10.1186/gb-2010-11-7-r73

Ratcliff, F., Martin-Hernandez, A. M., and Baulcombe, D. C. (2001). Technical advance tobacco rattle virus as a vector for analysis of gene function by silencing. *Plant J.* 25, 237–245. doi: 10.1046/j.0960-7412.2000.00942.x

Sang, Y., and Macho, A. P. (2017). Analysis of PAMP-triggered ROS burst in plant immunity. *Methods Mol. Biol.* 1578, 143–153. doi: 10.1007/978-1-4939-6859-6_11

Saubeau, G., Gaillard, F., Legentil, L., Nugier-Chauvin, C., Ferrieres, V., Andrivon, D., et al. (2014). Identification of three elicitins and a galactan-based complex polysaccharide from a concentrated culture filtrate of *Phytophthora infestans* efficient against *Pectobacterium atrosepticum*. *Molecules* 19, 15374–15390. doi: 10.3390/molecules191015374

Shibata, Y., Kawakita, K., and Takemoto, D. (2011). SGT1 and HSP90 are essential for age-related non-host resistance of *Nicotiana benthamiana* against the oomycete pathogen *Phytophthora infestans*. *Physiol. Mol. Plant P* 75, 120–128. doi: 10.1016/j.pmpp.2010.10.001

Sugano, S., Hayashi, N., Kawagoe, Y., Mochizuki, S., Inoue, H., Mori, M., et al. (2016). Rice OsVAMP714, a membrane-trafficking protein localized to the chloroplast and vacuolar membrane, is involved in resistance to rice blast disease. *Plant Mol. Biol.* 91, 81–95. doi: 10.1007/s11103-016-0444-0

Takahashi, Y., Nasir, K. H. B., Ito, A., Kanzaki, H., Matsumura, H., Saitoh, H., et al. (2007). A high-throughput screen of cell-death-inducing factors in *Nicotiana benthamiana* identifies a novel MAPKK that mediates INF1-induced cell death signaling and non-host resistance to *Pseudomonas cichorii*. *Plant J.* 49, 1030–1040. doi: 10.1111/j.1365-313X.2006.03022.x

Vanholme, R., Cesarino, I., Rataj, K., Xiao, Y., Sundin, L., Goeminne, G., et al. (2013). Caffeoyl shikimate esterase (CSE) is an enzyme in the lignin biosynthetic pathway in arabidopsis. *Science* 341, 1103–1106. doi: 10.1126/science.1241602

Wang, H., He, H., Qi, Y., McLellan, H., Tian, Z., Birch, P. R. J., et al. (2018). The oomycete microbe-associated molecular pattern pep-13 triggers SERK3/BAK1-independent plant immunity. *Plant Cell Rep.* 38, 173–182. doi: 10.1007/s00299-018-2359-5

Yoshioka, H., Numata, N., Nakajima, K., Katou, S., Kawakita, K., Rowland, O., et al. (2003). *Nicotiana benthamiana* gp91phox homologs *Nbrboha* and *Nbrbohb* participate in H2O2 accumulation and resistance to *Phytophthora infestans*. *Plant Cell* 15, 706–718. doi: 10.1105/tpc.008680

Zipfel, C. (2008). Pattern-recognition receptors in plant innate immunity. *Curr. Opin. Immunol.* 20, 10–16. doi: 10.1016/j.coi.2007.11.003

frontiers | Frontiers in Plant Science

TYPE Original Research
PUBLISHED 12 January 2023
DOI 10.3389/fpls.2022.1037030

OPEN ACCESS

EDITED BY
Bourlaye Fofana,
Agriculture and Agri-Food Canada (AAFC), Canada

REVIEWED BY
William Underwood,
Agricultural Research Service, (USDA), United States
Yasuhiro Kadota,
RIKEN Center for Sustainable Resource Science (CSRS), Japan

*CORRESPONDENCE
Vivianne G. A. A. Vleeshouwers
vivianne.vleeshouwers@wur.nl

SPECIALTY SECTION
This article was submitted to Crop and Product Physiology, a section of the journal Frontiers in Plant Science

RECEIVED 05 September 2022
ACCEPTED 09 December 2022
PUBLISHED 12 January 2023

CITATION
Lin X, Torres Ascurra YC, Fillianti H, Dethier L, de Rond L, Domazakis E, Aguilera-Galvez C, Kiros AY, Jacobsen E, Visser RGF, Nürnberger T and Vleeshouwers VGAA (2023) Recognition of Pep-13/25 MAMPs of *Phytophthora* localizes to an *RLK* locus in *Solanum microdontum*. *Front. Plant Sci.* 13:1037030. doi: 10.3389/fpls.2022.1037030

Recognition of Pep-13/25 MAMPs of *Phytophthora* localizes to an *RLK* locus in *Solanum microdontum*

Xiao Lin[1], Yerisf Carla Torres Ascurra[1], Happyka Fillianti[1], Laura Dethier[1], Laura de Rond[1], Emmanouil Domazakis[1], Carolina Aguilera-Galvez[1], Afewerki Yohannes Kiros[1], Evert Jacobsen[1], Richard G. F. Visser[1], Thorsten Nürnberger[2,3] and Vivianne G. A. A. Vleeshouwers[1*]

[1]Plant Breeding, Wageningen University and Research, Wageningen, Netherlands, [2]Department of Plant Biochemistry, Centre of Plant Molecular Biology (ZMBP), University of Tübingen, Tübingen, Germany, [3]Department of Biochemistry, University of Johannesburg, Johannesburg, South Africa

Pattern-triggered immunity (PTI) in plants is mediated by cell surface-localized pattern recognition receptors (PRRs) upon perception of microbe-associated molecular pattern (MAMPs). MAMPs are conserved molecules across microbe species, or even kingdoms, and PRRs can confer broad-spectrum disease resistance. Pep-13/25 are well-characterized MAMPs in *Phytophthora* species, which are renowned devastating oomycete pathogens of potato and other plants, and for which genetic resistance is highly wanted. Pep-13/25 are derived from a 42 kDa transglutaminase GP42, but their cognate PRR has remained unknown. Here, we genetically mapped a novel surface immune receptor that recognizes Pep-25. By using effectoromics screening, we characterized the recognition spectrum of Pep-13/25 in diverse Solanaceae species. Response to Pep-13/25 was predominantly found in potato and related wild tuber-bearing Solanum species. Bulk-segregant RNA sequencing (BSR-Seq) and genetic mapping the response to Pep-25 led to a 0.081 cM region on the top of chromosome 3 in the wild potato species *Solanum microdontum* subsp. *gigantophyllum*. Some BAC clones in this region were isolated and sequenced, and we found the Pep-25 receptor locates in a complex receptor-like kinase (*RLK*) locus. This study is an important step toward the identification of the Pep-13/25 receptor, which can potentially lead to broad application in potato and various other hosts of *Phytophthora* species

KEYWORDS

Potato late blight, *Phytophthora infestans*, MAMP, RLK, Pep-13/25, BSR-Seq

Introduction

Plants have evolved two layers of innate immune system to perceive non-self molecules and elicit immune responses. Plasma membrane-localized immune receptors, typically receptor-like proteins (RLPs) and receptor-like kinases (RLKs), form the first layer of defense. These surface receptors recognize microbial-associated molecular patterns (MAMPs) or apoplastic effectors and induce pattern-triggered immunity (PTI). Inside the plant cells, nucleotide-binding domain and leucine-rich repeat-containing receptors (NLRs) recognize pathogen intracellular effectors and mediate effector-triggered immunity (ETI) (Jones and Dangl, 2006).

Phytophthora species are renown as notorious plant pathogens that trigger pandemics in many important crops, like potato late blight, sudden oak death, soybean root rot, and tobacco black shank disease, caused by *Phytophthora infestans*, *P. ramorum*, *P. sojae* and *P. parasitica* respectively. Various MAMPs of oomycetes, such as Pep-13, nlp20, INF1, XEG1 PcF and CBEL (Ricci et al., 1989; Orsomando et al., 2001; Brunner et al., 2002; Liu et al., 2005; Gaulin et al., 2006; Ma et al., 2015) have been characterized. Yet for only a few oomycete PAMPS, the matching surface immune receptors have been cloned so far, namely ELR, RLP23 and RXEG1, that recognize INF1, nlp20 and XEG1 respectively (Albert et al., 2015; Du et al., 2015; Wang et al., 2018), all the three characterized PRRs are LRR-RLPs, and these PRRs have shown to enhance resistance to the respective oomycete pathogen. Remarkably, the structure of XEG1-BAK1-RXEG1 (LRR) complex was resolved recently, it revealed the mechanism of LRR-RLP activation upon ligand recognition (Sun et al., 2022).

Pep-13 is derived from GP42, a 42 kDa transglutaminase (TGase) that was firstly isolated from *Phytophthora sojae* culture filtrates (Parker et al., 1991). To find the minimal peptide of the elicitor, various endo- and exopeptidases were used to digest GP42, and a peptide of 13 amino acid residues (Pep-13) was found sufficient for the elicitor activity in parsley cell cultures (Nürnberger et al., 1994). Pep-25 is a longer peptide that shows a similar activity as Pep-13. Pep-13/25 are highly conserved among *Phytophthora* species. In parsley cell culture, Pep-13 induces defense responses including, oxidative burst, ion fluxes, phytoalexin formation, and defense-related gene activation (Nürnberger et al., 1994). In potato, infiltration of Pep-13 and Pep-25 into the leaves can induce hypersensitive response (HR) and expression of the defense-related genes (Brunner et al., 2002). The Pep-13 triggered immunity was reported to be SERK3A/B (BAK1)-dependent in potato (Nietzschmann et al., 2019). However, the Pep-13/25 receptor has not been cloned so far.

Map-based cloning is a traditional strategy for gene mapping and cloning, however it is time-consuming and laborious. With the fast evolving of next and third generations of sequencing technology, genetic mapping becomes easier and faster than ever before. For potato, many reference genomes are available now, like *Solanum tuberosum* group Phureja DM1-3 516 R44, RH89-039-16, Solyntus, *Solanum verrucosum*, *Solanum chacoense*, and recently a tetraploid potato cultivar was also assembled into chromosome level (Xu et al., 2011; Leisner et al., 2018; Paajanen et al., 2019; van Lieshout et al., 2020; Zhou et al., 2020; Sun et al., 2022). Additionally, target enrichment sequencing and bulk segregant analysis (BSA) like Resistance gene enrichment sequencing (RenSeq), RLP/K enrichment sequencing, and BSA-Seq can also help to clone new resistance genes (Witek et al., 2016; Zou et al., 2016; Lin et al., 2020a; Witek et al., 2021).

Here, we performed a large-scale infiltration of Pep-13 and Pep-25 peptides in different Solanaceae species. We found that Pep-13/25 recognition is relatively common in potato cultivars, less prevalent in wild potatoes, and absent in other Solanaceae families. Then, we generated a segregating population of Pep-25 responsiveness by several rounds of crossings of diverse diploid wild potato genotypes. By using BSR-Seq and map-based cloning strategy, the Pep-25 receptor was finally fine-mapped to a 0.081 cM *LRR-RLK* gene locus on the top of chromosome 3. Our findings will lead to the identification of the Pep-13/25 receptor.

Materials and methods

Peptide synthesis

Pep13 (VWNQPVRGFKVYE) and Pep25 (DVTAG AEVWNQ4PVRGFKYEQTEMTE) were synthesized by GenScript (USA). The peptides were dissolved in MQ to a concentration of 1-3 μM. The peptides Pep-13 and Pep-25 were infiltrated into the abaxial side of plant leaves by a needleless syringe, and the cell death phenotype was scored 3 days after infiltration.

Plant materials

Seeds of 24 tomato, 7 eggplant, and 10 pepper accessions were obtained from the Centre for Genetic Resources, the Netherlands (CGN). They were sown in the greenhouse, and the peptides infiltration was performed 6 weeks after germination. In addition, seeds from *Nicotiana benthamiana*, *N. glutinosa*, and 6 cultivars of *Nicotiana tabacum*, including cv. Rustica, cv. White burley, cv. Cleveland, cv. Samsun, cv. Xanthii, cv. SR1 were obtained from Unifarm of Wageningen University and Research. Six weeks-old plants were used for peptides infiltration. Wild species and potato cultivars were obtained from the *in vitro* collection of Plant Breeding, Wageningen University and Research. These plants are maintained *in vitro* on MS20 medium at 25°C. Top shoots of plants were cut and

clonally propagated 2 weeks before transfer to the soil. All plants were grown in a climate-controlled greenhouse compartment at 22°C/18°C day/night temperature regime under long-day conditions. In all cases, three leaves per plant, and three plants per accession were used.

Mapping population

The crossings between selected lines were made in different years. Seedlings were propagated and grown *in vitro* on MS20 medium for 2 weeks, and then transferred to the greenhouse. The female parental line was emasculated before anthesis, and 3 days later was pollinated with the donor. Ripe berries were collected, and the seeds were recovered, cleaned with water, and air-dried on filter paper before packaging.

The seeds were sterilized before germination. They were rinsed in 70% ethanol and soaked in a solution of 1.5% hypochlorite and Tween 20, then they were washed with autoclaved water to remove the hypochlorite. For the recombinant screening, the seeds were sown on MS20 medium (with 1000 ppm GA3, if the seeds were new for breaking the dormancy) or in the greenhouse directly. For the plants in greenhouse, after genotyping, the selected recombinants were sterilized and moved into the *in vitro* collection for later analyses.

Sample preparation and RNA isolation for BSR-Seq

One hundred seeds from population 3521 were sown in the greenhouse, when they were 6 weeks old, Pep-25 peptides and water (negative control) were infiltrated for phenotyping. The infiltration was performed on 3 leaves and was repeated at least 3 times on the same plant. The cell death phenotype was scored 3-4 days after infiltration, then the leaves from 34 Pep-25 responding (R bulk) and 34 Pep-25 non-responsive progenies (NR bulk), as well as the parental line 3341-15 were collected for inoculation with *P. infestans*. Forty-eight hours after inoculation, two 1 cm-leaf discs from the same plant were collected into 2 ml tubes containing 2 small metal beads and immediately frozen with liquid nitrogen. Six samples were collected in total, i.e. R bulk mock, R bulk inoculated with *P. infestans* isolate Dinteloord, NR bulk mock, NR inoculated with *P. infestans* isolate Dinteloord, 3341-15 mock, and 3341-15 inoculated with *P. infestans* Dinteloord. The 6 samples were ground by TissueLyser II (QIAGEN). Then 100 mg samples were used for RNA isolation by Rneasy Plus Mini Kit from QIAGEN following industrial instructions. The gDNA eliminator spin column from the kit was used to remove the gDNA. The six RNA samples were tested by agarose electrophoresis, quantified by Nanodrop (ThermoFisher) and sent to Novogene (Beijing, China) with dry ice for RNA sequencing. The RNAseq data from Pep-25 non-responsive parent MCD360-1 were obtained from previous studies (Lin et al., 2020b).

Bioinformatic analysis

Paired-end Illumina HiSeq reads were first checked with FastQC (v0.10.0; http://www.bioinformatics.babraham.ac.uk/projects/fastqc/) and the adapters were trimmed with trimmomatic v0.36 (Bolger et al., 2014). The trimmed reads were then mapped to the potato DM reference genome (v4.03) using STAR v2.5 (Dobin et al., 2013). Pileup files were generated for the bulk and parents using SAMtools mpileup with default settings and piped into VarScan mpileup2snp (v2.3.7) (Koboldt et al., 2012). SNPs were filtered using a custom Java code (Lin et al., 2020a) to retain informative SNPs present in both bulks and both parents. SNPs were filtered based on expected allele ratios in responsive (Rr)/non-responsive (rr) samples. To be retained, each SNP had a minimum read depth of 50 and alternate allele ratios reflecting the expected genotype: 0-10% or 90-100% alternate allele for rr and 40-60% alternate allele for Rr. BEDTools intersect (v2.20.1) (Quinlan and Hall, 2010) was used to extract SNPs present in both bulks and parents (informative SNPs) and to relate the informative SNP locations to transcripts of the reference genome. The number of SNPs were plotted in 1 Mb bins across each chromosome and visualized using R (Lin et al., 2020a).

High resolution melting (HRM) marker development and analysis

The BAM and VCF files (filtered informative SNPs) were imported into Geneious R10 for visualization (Kearse et al., 2012) (http://www.geneious.com). The primers were designed in Geneious R10, ideally, the PCR product should only contain one informative SNP and the size should be between 80-150bp. Primers flanking the informative SNPs were manually selected on the conserved sequences of both parents, R and NR bulks. The protocols for DNA isolation and HRM markers were described previously (Lin et al., 2020a).

BAC library screening

The BAC library of GIG362-6 was generated as described previously (Lin et al., 2020a). PCR primers were designed in the mapping interval based on the DM genome for detecting the positive BAC clones.

Candidate gene cloning and agroinfiltration

The coding region of the candidate genes was PCR-amplified and firstly cloned into the Gateway entry vector, then shuffled into destination vector pK7WG2 with 35S promoter. Then the constructs were transformed into *Agrobacterium tumefaciens* strain AGL1 for transiently overexpression assay in plants. The agroinfiltration was performed in 4 –weeks-old *N. benthamiana* leaves, Pep-25 peptides (2 μM) were infiltrated into the same leaves two days later.

P. infestans inoculation

P. infestans isolate Dinteloord were propagated on rye medium for 14 days in a climate chamber (18°C). The zoospores were collected in cold water, 10 μL zoospore suspension (5 x 10^4 zoospores/ml) was used to inoculate detached leaves. The leaves were sampled from 10 weeks-old Pep-25 responsive and non-responding progenies of population 3341-15 x MCD360-1.

Phylogenetic analysis

The kinase domains of 365 potato RLK proteins and 12 candidate RLK proteins from GIG362-6 were included (Lin et al., 2020a). I3 from tomato was used as an outgroup, 21 known RLK proteins were also included as reference. The kinase domains were aligned in Geneious (Kearse et al., 2012), Maximum likelihood (ML) tree was made by iqtree (v1.6.10), LG+F+R7 was selected as the best-fit model, 1000 samples were generated for the ultrafast bootstrap analysis (Kalyaanamoorthy et al., 2017; Hoang et al., 2018; Minh et al., 2020).

Data availability

The raw sequencing data were deposited in GenBank SRA under project number PRJNA893349. The BAC sequence was deposited in GenBank (OP716690).

Results

Pep-13/25 trigger HR on cultivated and wild potatoes

Pep-13/25 are conserved regions in the cell wall-associated, Ca^{2+}-dependent transglutaminase (GP42), the structure of GP42 (PDF code 3TW5) from *Phytophthora sojae* was solved (Reiss et al., 2011), and is visualized in Figure S1A, Pep-13 peptides are highlighted by cyan. Pep-13 and Pep-25 were found among ten *Phytophthora* species (Brunner et al., 2002). The Pep-13 and Pep-25 sequences from *P. infestans*, *P. sojae*, *P. palmivora*, *P. parasitica*, *P. cactorum*, *P. ramorum*, *P. cinnamomi*, and *P. capsici* are visualized in Figure S1B.

Pep-13 was reported to elicit defense responses or cell death in parsley and potato cv. Désirée (Hahlbrock et al., 1995; Halim et al., 2004). However, whether both Pep-13/25 could be widely recognized in different plant families remains unknown. Here, we performed a large-scale screening of a collection of Solanaceae plants by Pep-13 and Pep-25 peptides infiltration. Firstly, we tested 19 potato cultivars, including the previous reported potato cultivar Désirée as a positive control, and some progenitor species of cultivated potato, i.e., *S. tuberosum andigena* (ADG240-2), PHU372-8 and PHU200-4, *S. stenotomum* (STN829-3), and *S. candolleanum* (CND531-3). We found Pep-13/25 recognition is common in potato cultivars, thirteen out of nineteen potato cultivars recognize both Pep-13/25, and five do not recognize any, or only show a weaker cell death phenotype to Pep-25 (Figure 1A). All five tested landraces recognize both Pep-13/25, however, the proposed progenitor of cultivated potato *S. candolleanum* (CND531-3) does not (Figure 1B).

To test if Pep-13/25 can trigger cell death in wild potatoes, peptide infiltration was performed in 146 wild potato genotypes belonging to 56 species. Among the 146 genotypes, 14 genotypes that belong to at least 8 different tuber-bearing *Solanum* species/sub-species showed cell death after infiltration of Pep-13 and/or Pep-25 (Figures 1B, C, Table S1). These 8 wild potato species/sub-species include *Solanum doddsii* (DDS), *Solanum demissum* (DMS), *Solanum edinense* (EDN), *Solanum hondelmannii* (HDM), *Solanum leptophyes* (LPH), *Solanum microdontum* (MCD), *Solanum microdontum* subsp. *gigantophyllum* (GIG), *Solanum chacoense* (CHC), *Solanum ehrenbergii* (I), and two unclassified species (SPEC) (Jacobs et al., 2008). We found that 36% of the responsive wild potatoes only showed response to Pep-25, but not Pep-13, which may be explained by a lower stability of Pep-13 in the harsh conditions in the apoplast, or, could point to other receptors in potatoes with different recognition specificity to Pep-13 versus Pep-25

To further determine whether Pep-13 and Pep-25 recognition is common in other members of the Solanaceae family, we screened the peptides in twenty-four tomato accessions, seven eggplant accessions, ten pepper accessions, and eight *Nicotiana* accessions. However, none of them recognize either Pep-13 or Pep-25 (Figure 1; Table S1). These results indicate Pep-13/25 recognition might be limited to a subset of *Solanum* species.

10.3389/fpls.2022.1037030

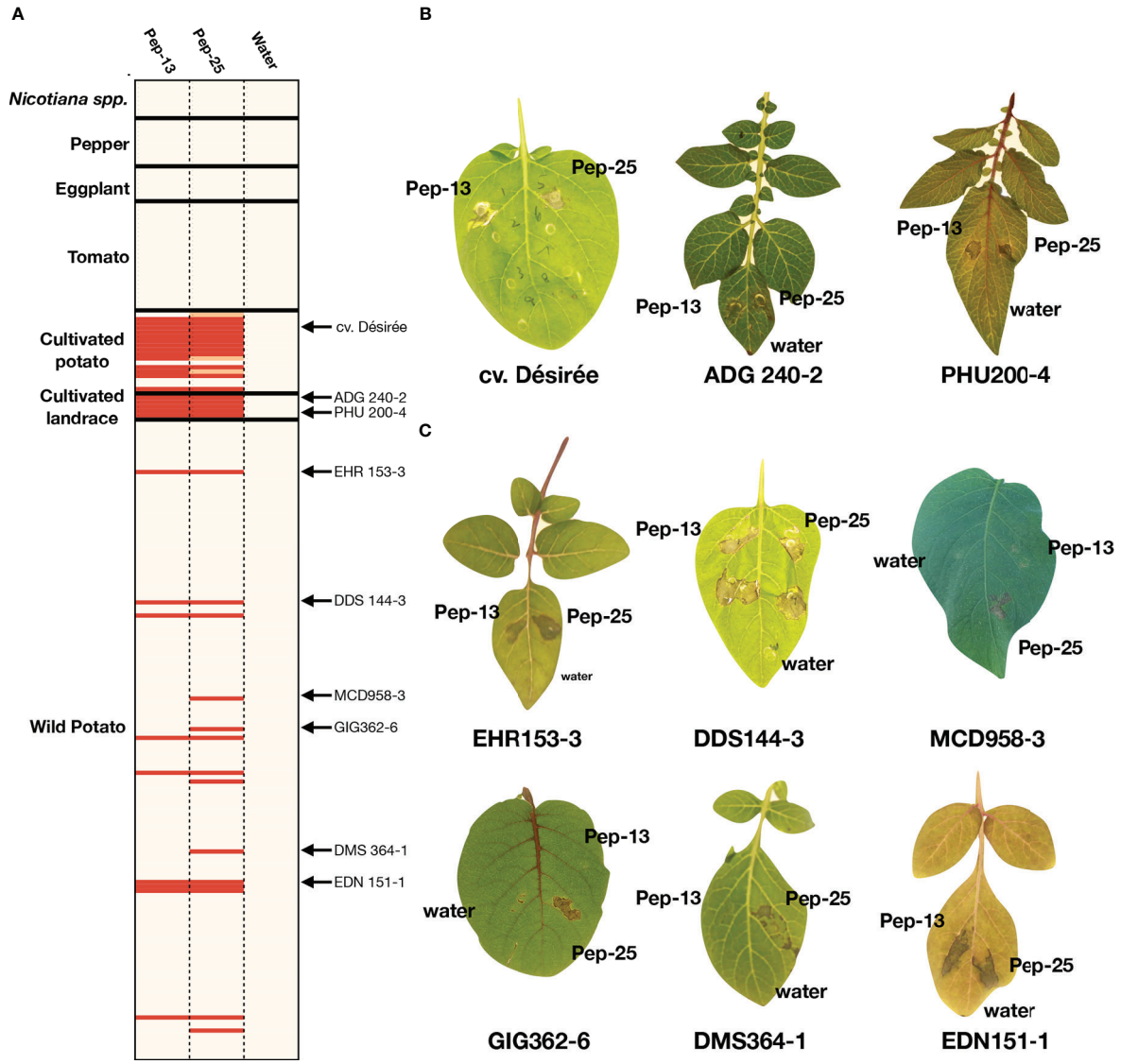

FIGURE 1
Screening for Pep-13/25 recognition in multiple Solanaceae species **(A)**. Heatmap of Pep-13 and Pep-25 recognition in different Solanaceae species and genotypes. The HR severity was scored. Strong HRs after Pep-13/25 infiltration are highlighted by red, weak HRs are highlighted by orange, beige indicates no HR. The genotypes with arrows are shown in **(B, C)**. The detailed scoring table is shown in Supplementary Table 1. **(B)**. Examples of Pep-13/25 recognition in cultivated potatoes and landraces. *Solanum tuberosum* Group tuberosum cv Désirée, *S. tuberosum* Group andigena (ADG 240-2) and *S. phureja* (PHU200-4) respond to both Pep-13 and Pep-25. **(C)** Examples of Pep-13/25 recognition in wild *Solanum* spp. Genotypes of *S. ehrenbergii* (EHR), *S. doddsii* (DDS), *S. microdontum* (MCD), *S. microdontum* subsp. *gigantophyllum* (GIG), *S. demissum* (DMS) and *S. edinense* (EDN) are shown. EHR153-3, DDS144-3 and EDN151-1 respond to both Pep-13 and Pep-25, but MCD958-3, GIG362-6, DMS364-1 respond only to Pep-25.

Genetic mapping of Pep-25 receptor by BSR-Seq

Although the responses of Pep-13 and Pep-25 in plants were well characterized, the corresponding plant receptor remains unknown. The Pep-13/25 screening has revealed that there is genetic variation for response to Pep-13 and/or Pep-25. For instance, *Solanum microdontum* subsp. *gigantophyllum* (GIG362-6), a diploid species that responds to Pep-25, but not Pep-13; and *Solanum microdontum* (MCD360-1), which shows no response to Pep-13/25. To generate a mapping population of Pep-25, population 7026 was generated by crossing GIG362-6 and MCD360-1, and subsequently tested for segregation of Pep-25 response (Figure 2A). However, all the F1 progenies of 7026 respond to Pep-25 after peptides infiltration. Similarly, crossing GIG362-6 with the Pep-13/25 non-responsive *Solanum*

10.3389/fpls.2022.1037030

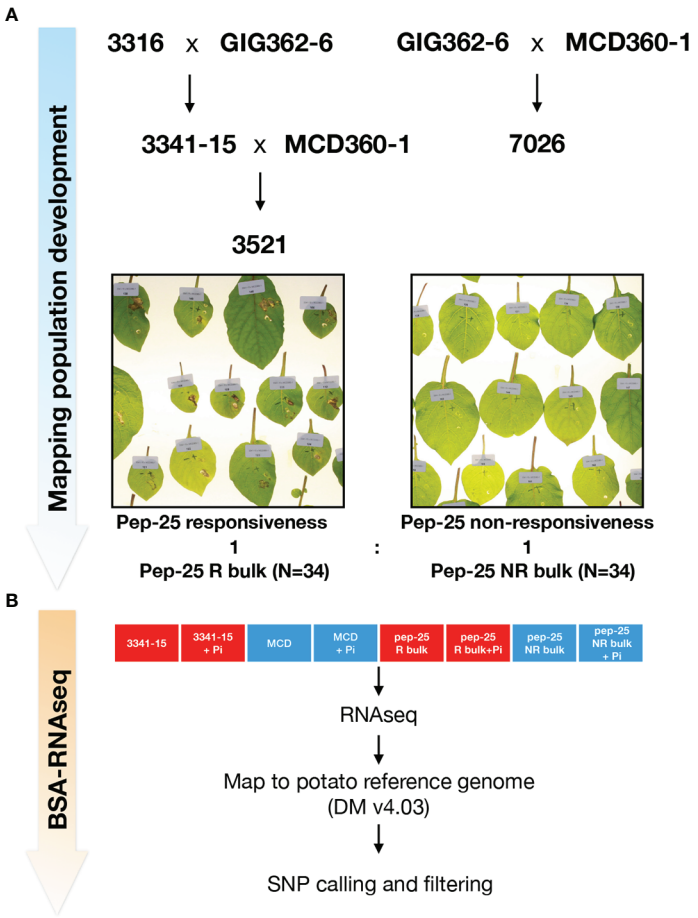

FIGURE 2
Mapping Pep-25 receptor to the top of Chromosome 3 by BSR-Seq **(A)** Mapping population development for mapping Pep-25 receptor. *S. microdontum* subsp. *gigantophyllum* GIG362-6 (R) was crossed with *S. verrucosum* 3316-17 (NR) and all progenies of the F1 population (3341) respond to Pep-25. Then, the segregating population 3521 was generated by crossing 3341-15 (R) with *S. microdontum* MCD360-1 (NR). The 34 R and 34 NR progenies were bulked for the BSR-Seq. R, respond to Pep-25; NR, not respond to Pep-25 **(B)** Two parental lines 3341-15 and MCD360-1, and two bulks (Pep-25 R and NR bulks) were treated with water (mock) or *Phytophthora infestans* zoospores followed by RNA extraction and RNA-seq. The reads were mapped to the potato reference genome (DMv403), and the SNPs were called, the informative SNPs were filtered.

verrucosum 3316-17, also led to a population (3341) in which all F1 progeny plants respond to Pep-25 (Figure 2A). These data indicate that the Pep-25 locus is likely homozygous in GIG362-6.

To generate a segregating population of Pep-25 response, we crossed the responsive 3341-15 with the non-responsive MCD360-1 to generate population 3521. One hundred and ten progeny plants of population 3521 were tested, 49 of them were responsive to Pep-25, 61 were non-responsive. This segregating ratio is close to 1:1 ($\chi 2$ p=0.252), suggesting that the Pep-25 response is determined by a single dominant gene that is homozygous in GIG362-6.

To genetically map the potential Pep-25 receptor, 34 Pep-25 responsive and 34 Pep-25 non-responsive individuals from population 3521 were pooled for BSR-Seq (Figure 2A). The parental lines 3341-15 and MCD360-1 were included for the RNAseq, to allow identification of high-quality SNPs in the downstream bioinformatics analysis. In addition, we included samples with *P. infestans* infection and mock control (water) to be able to explore up-regulated defense-related genes. The BSR-Seq bioinformatics pipeline are shown in Figure 2B.

Fine mapping of Pep-25 receptor to an *RLK* gene locus on chromosome 3

To identify the causal SNPs of Pep-25 responsiveness, the BSR-Seq reads were mapped to the potato reference genome (DMv403), and SNPs were called and filtered. The most informative SNPs linked to the Pep-25 responsiveness are located on the top of Chromosome 3 (Figure 3A and

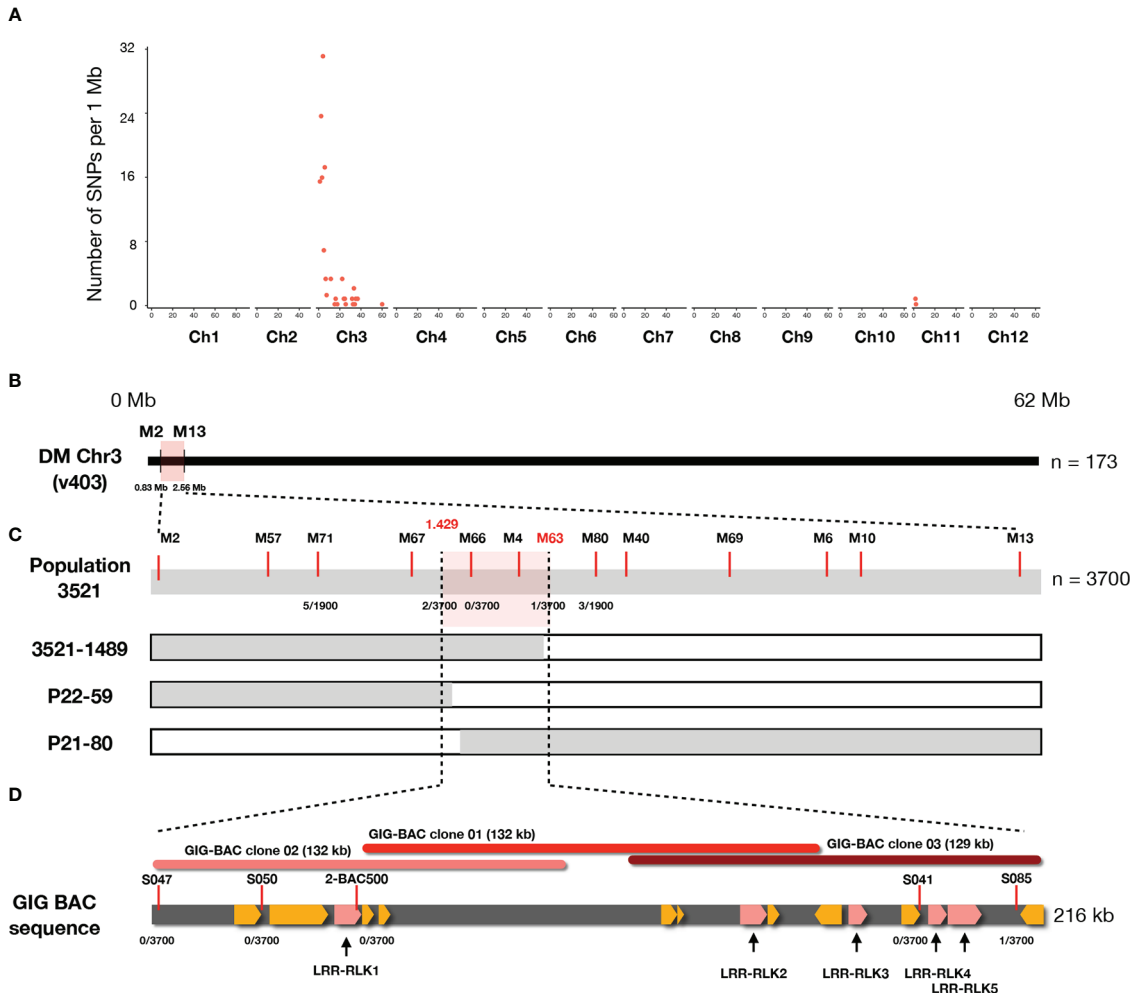

FIGURE 3
The Pep-25 receptor is fine-mapped to an *RLK* gene locus in *Solanum microdontum*. **(A)** The number of filtered SNPs per 1 Mb interval are visualized (*y* axis), the chromosome IDs are shown in *x* axis. Most of the informative SNPs are located on the top of chromosome 3, based on the potato reference genome (DM v4.03). **(B)** The Pep-25 receptor is mapped to a 1.73 Mb interval, between markers M2 and M13. **(C)** Fine-mapping of Pep-25 receptor in population 3521 (n=3700) to a 0.081 cM interval, between markers 1.429 and S085. Markers are shown with red lines, markers M66 and M4 are co-segregating with the Pep-25 response, the number of recombination/total plants are shown below the markers. **(D)**. A 216 kb contig generated from three BAC clones (01-03) from GIG362-6 shows 15 predicted *RLK* genes (highlighted yellow), five of these *RLK* are up-regulated upon *P. infestans* infection (highlighted by pink).

Table S2). To verify these informative SNPs, we designed high-resolution melting (HRM) markers and firstly tested them in a small population (n=173). We obtained two flanking markers (M2 and M13) and located the candidate Pep-25 receptor in a 1.73 Mb region (Figure 3B).

Then we developed a rapid-genotyping pipeline. In brief, the seeds were sown *in-vitro* and grown in MS20 medium, some leaf samples were cut from the *in-vitro* plants and used for DNA isolation, then the two flanking markers were used for genotyping. The recombinants were maintained *in-vitro* and propagated for phenotyping of Pep-25 response (Torres Ascurra et al., 2021). Molecular markers were designed based on the potato reference genome DM v4.03 (Figure S3 and Table S2). In total, 3700 progenies individual were genotyped, and three recombinants were identified, which allowed us to fine-map Pep-25 receptor to a small interval between markers 1.429 and M63 (1.528) (Figures 3C; S3 and Table S2). The genetic distance of this interval is ~0.081 cM (3/3700).

To obtain the physical map of this region, three BAC clones were isolated from a BAC library of GIG362-6 (Lin et al., 2020b), and they were sequenced. These three BAC clones cover 216 kb region, marker S085 locates at the end of the BAC sequence (Figure 3D), however, all other markers (S047, S050, 2-BAC500, S041) are co-segregating with Pep-25 responsiveness (Figure 3D).

Candidate genes of Pep-25 receptor

The genes in the BAC contig (Figure 3D) were annotated, many leucine-rich repeat receptor-like kinase (*LRR-RLK*) genes locate in this region, and they mainly belong to two *FLS2* and *MDIS2* clades (Figure S2). In this mapping interval, the gene architecture of the DM (v4.03) genome is similar as the GIG BAC contig. To obtain the expression profile of these candidate genes, we mapped the RNA-seq reads from the parental lines to the BAC sequence, and five *LRR-RLK* genes (*LRR-RLK1, LRR-RLK2*, *LRR-RLK3*, *LRR-RLK4*, and *LRR-RLK5*) (Figure 3D) were up-regulated after *P. infestans* inoculation, and we considered these as candidate genes. We cloned the five *LRR-RLK* genes into overexpression vectors with 35S promoter and transformed them into *Agrobacterium tumefaciens* strain AGL1, these constructs were transiently expressed in *N. benthamiana* leaves followed by Pep-25 infiltration. However, none of the five tested candidate *RLK* genes is responsible for Pep-25 responsiveness (Figure 4). Therefore, we speculate that the Pep-25 receptor likely locates in the un-sequenced region of the mapping interval.

Discussion

Surface immune receptors, such as the receptor of Pep13/25, are believed to confer broad-spectrum and more durable resistance against *Phytophthora* pathogens by recognizing conserved MAMPs, in line with earlier findings with ELR and RLP23 (Albert et al., 2015; Du et al., 2015). The conserved peptides Pep-13/25 are well studied MAMPs (Brunner et al., 2002), and the TGase activity of the *Phytophthora* GP42 protein suggests that this protein is important to the fitness of these pathogens. The Pep-13/25 induced immune responses were reported in the potato cultivar Désirée and parsley cell cultures in the past (Nürnberger et al., 1994; Brunner et al., 2002; Halim et al., 2004), and a potential Pep-13 receptor in parsley was suggested to be a monomeric 100 kDa protein on the plasma membrane (Nurnberger et al., 1995; Nennstiel et al., 1998). However, the gene encoding the Pep-13 receptor in parsley or potato has remained unknown to date.

This study aimed to gain a better understanding of Pep-13/25 triggered immunity in a broad range of plant species and we performed a large-scale investigation on Solanaceae, including wild and cultivated potatoes, tomato, eggplant, pepper, and *Nicotiana* genotypes. Surprisingly, we found the Pep-13/25-induced cell death limited to tuber-bearing *Solanum* species (Figure 1), but not in other Solanaceae, which suggests that a Pep-13/25 receptor might have evolved independently in the ancestor of potato. The cell-death phenotype is restricted to potatoes as well. In sum, our data suggest that Pep-13 and Pep-25 recognition capacity from parsley and potato might have evolved independently, however, we cannot rule out that homologues of an ancient Pep-13/25 receptor are present in many different plant species.

We mapped the candidate Pep-25 receptor to a small interval (~0.081 cM) on the top of chromosome 3 in an *RLK* cluster that contains at least 15 full-length or partial *RLK* genes. Five candidate *RLK* genes were cloned and tested transiently in *N. benthamiana*, but none of them gave cell death activity with Pep-13/25, however, we cannot rule out that *N. benthamiana* lacks downstream signalling components for Pep-13/25 recognition. Unfortunately, we were unable to isolate more BAC clones to cover the whole mapping interval, but nonetheless, this work lay the groundwork for the cloning of Pep-13/25 receptor from potato.

Wild tuber-bearing *Solanum* species are renowned as a great resource of resistance genes encoding NLR immune receptors

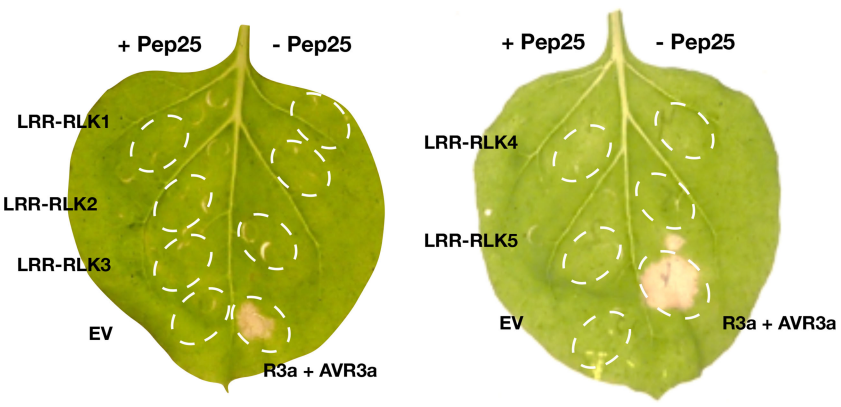

FIGURE 4
Complementation study of candidate genes. The five candidate genes of the Pep-25 receptor (*LRR-RLK1, LRR-RLK2, LRR-RLK3, LRR-RLK4, LRR-RLK5*) were agroinfiltated in *N. benthamiana* leaves, OD_{600} = 1.0, and Pep-25 peptides (2 μM) were infiltrated 2 days later. The photos were taken 3 days after the peptides infiltration. Co-agroinfiltration of *R3a* and *AVR3a* were used as a positive control, empty vector and Pep-25 were used as a negative control.

that can be detected by expressing avirulence genes in plants, so-called effectoromics screens. These wild *Solanum* accessions show higher frequency of responses to *Avr* genes than potato cultivars, yet. In contrast, the response to Pep-13/25 was much more prominent in cultivars (*S. tuberosum* Group Tubersum) and landraces (*S. tuberosum* Group andigena, *S. tuberosum* Group Phureja and *S. stenotomum*) (Figure 1). This suggests that the Pep-13/25 receptor may have evolved from an ancestor of the *S. tuberosum* clade and then was selected during potato domestication. However, most potato cultivars are not resistant to *P. infestans*, why it was kept during selection? One possible explanation could be that *P. infestans* has evolved effectors which inhibit Pep13/25 receptor-triggered immunity. Similar findings are reported the a well-studied *P. infestans* RXLR effector Avr3a^{KI} that can inhibit cell death response induced by INF1 (Bos et al., 2006). Alternatively, the Pep-13/25 receptor might be closely linked to domestication traits or has other unknown functions which are important for potato cultivars.

Recently, mutual potentiation of PTI and ETI was reported (Ngou et al., 2021; Yuan et al., 2021), therefore, we can argue that combining the PRR, such as the Pep-13/25 receptor, with *NLR* genes from wild potatoes might help to achieve stronger and more durable resistance against oomycete pathogens. Thus, it remains important to identify PRR that recognize *Phytophthora*, and tools to efficiently identify these genes in the genetically complicated *Solanum* germplasm are most welcome. In this study, we also developed a pipeline to swiftly map potato genes by BSR-Seq (Figure 2). It is the first time that BSR-Seq was applied to potato, and our result demonstrated that this approach can dramatically accelerates the speed of map-based cloning. Once the segregating population is generated, the BSR-Seq can be used to rapidly map the gene in weeks. It is noteworthy that all the markers needed for fine mapping can be developed directly based in the filtered SNPs. Meantime, the differential expression data would also facilitate to narrow down the list of candidate genes.

In summary, this work reveals that the receptor of Pep-13/25 is widely distributed in wild and cultivated potatoes. Our development of a BSR-Seq pipeline for rapid mapping of potato genes, and subsequent fine-mapping of Pep-25 receptor to the *RLK* locus is an important step towards the identification of Pep-13/25 receptor in wild and cultivated potatoes.

Data availability statement

The data presented in the study are deposited in the NCBI SRA and GenBank repository, project number PRJNA893349; accession number OP716690.

Author contributions

XL and VV conceived and designed the project. XL and YT wrote the first draft with inputs from all the authors. VV and EJ reviewed and edited the manuscript. XL, YT, HF, LD, LR, ED, CA-G, and AK performed the experiments. XL performed the bioinformatics analyses. RV, TN, and VV contributed resources. All authors contributed to the article and approved the submitted version.

Funding

This work was supported by an NWO-VIDI grant 12378 (XL, ED, and VV), China Scholarship Council (CSC) (XL), Peruvian Council for science, technology and technological innovation (CONCYTEC) and FONDECYT contract 129-2017 (YT).

Acknowledgments

We thank Isolde Bertram-Pereira for culturing *Solanum* plants, Henk Smid and Harm Wiegersma for their help in the greenhouse. We thank the center for genetic resources, the Netherlands (CGN) for providing the seeds of *Solanaceae* plants used in this study. We thank Dr. Helene Berges and Caroline Callot from the French Plant Genomic Resource Center (INRA-CNRGV) for their help to sequence the BAC clones.

Conflict of interest

The authors declare that the research was conducted in the absence of any commercial or financial relationships that could be construed as a potential conflict of interest.

Publisher's note

Supplementary material

The Supplementary Material for this article can be found online at: https://www.frontiersin.org/articles/10.3389/fpls.2022.1037030/full#supplementary-material

SUPPLEMENTARY FIGURE 1
Pep-13/25 are conserved patterns among oomycete pathogens. **(A)** The structure of the cell-wall associated transglutaminases (TGases) GP42 from *Phytophthora sojae* is visualized by web3dmol (Reiss et al., 2011).

The Pep-13 peptides are highlighted by cyan (PDB: 3TW5). **(B)** Alignment of Pep-13 and Pep-25 peptides from 8 *Phytophthora* species.

SUPPLEMENTARY FIGURE 2
Phylogeny of potato LRR-RLKs and the candidate proteins The kinase domains of 365 potato RLK proteins, 12 candidate RLK proteins from GIG362-6 and 21 known RLK proteins were included (blue). I3 from tomato was used as an outgroup The candidate RLK proteins from *Solanum microdontum* subsp. *gigantophyllum* are highlighted by red. The scale bar indicates the number of amino acid substitutions per site.

SUPPLEMENTARY FIGURE 3
Fine mapping of Pep-25 receptor The molecular markers were designed based on the potato reference genome (DM v4.03), the physical positions (Mb) of the markers on Chromosome 3 are shown in the first line. The polymorphism of each SNPs is shown by "NR" (MCD360-1 allele) or "R" (3341-15 allele). The IDs of recombinants are shown on the left. Pep-25 responsiveness phenotype are noted by "NR" (non-responsiveness) or "R" (responsiveness). The haploid from responsive parent (3341-15) are highlighted by red, and the haploid from the non-responsive parent (MCD360-1) are highlighted by blue.

References

Albert, I., Böhm, H., Albert, M., Feiler, C. E., Imkampe, J., Wallmeroth, N., et al. (2015). An RLP23–SOBIR1–BAK1 complex mediates NLP-triggered immunity. *NPLANTS* 1, 15140. doi: 10.1038/nplants.2015.140

Bolger, A. M., Lohse, M., and Usadel, B. (2014). Trimmomatic: a flexible trimmer for illumina sequence data. *Bioinformatics* 30, 2114–2120. doi: 10.1093/bioinformatics/btu170

Bos, J. I. B., Kanneganti, T.-D., Young, C., Cakir, C., Huitema, E., Win, J., et al. (2006). The c-terminal half of *Phytophthora infestans* RXLR effector AVR3a is sufficient to trigger R3a-mediated hypersensitivity and suppress INF1-induced cell death in *Nicotiana benthamiana*. *Plant J.* 48, 165–176. doi: 10.1111/j.1365-313X.2006.02866.x

Brunner, F., Rosahl, S., Lee, J., Rudd, J. J., Geiler, C., Kauppinen, S., et al. (2002). Pep-13, a plant defense-inducing pathogen-associated pattern from *Phytophthora* transglutaminases. *EMBO J.* 21, 6681–6688. doi: 10.1093/emboj/cdf667

Dobin, A., Davis, C. A., Schlesinger, F., Drenkow, J., Zaleski, C., Jha, S., et al. (2013). STAR: ultrafast universal RNA-seq aligner. *Bioinformatics* 29, 15–21. doi: 10.1093/bioinformatics/bts635

Du, J., Verzaux, E., Chaparro-Garcia, A., Bijsterbosch, G., Keizer, L. C. P., Zhou, J., et al. (2015). Elicitin recognition confers enhanced resistance to *Phytophthora infestans* in potato. *NPLANTS* 4, 19–27. doi: 10.1038/nplants.2015.34

Gaulin, E., Dramé, N., Lafitte, C., Torto-Alalibo, T., Martinez, Y., Ameline-Torregrosa, C., et al. (2006). Cellulose binding domains of a Phytophthora cell wall protein are novel pathogen-associated molecular patterns. *The Plant Cell* 18, 1766–1777. doi: 10.1105/tpc.105.038687.

Hahlbrock, K., Scheel, D., Logemann, E., Nurnberger, T., Parniske, M., Reinold, S., et al. (1995). Oligopeptide elicitor-mediated defense gene activation in cultured parsley cells. *Proc. Natl. Acad. Sci.* 92, 4150–4157. doi: 10.1073/pnas.92.10.4150

Halim, V. A., Hunger, A., Macioszek, V., Landgraf, P., Nürnberger, T., Scheel, D., et al. (2004). The oligopeptide elicitor pep-13 induces salicylic acid-dependent and -independent defense reactions in potato. *Physiol. Mol. Plant Pathol.* 64, 311–318. doi: 10.1016/j.pmpp.2004.10.003

Hoang, D. T., Chernomor, O., Haeseler, von, A., Minh, B. Q., and Vinh, L. S. (2018). UFBoot2: improving the ultrafast bootstrap approximation. *Mol. Biol. Evol.* 35, 518–522. doi: 10.1093/molbev/msx281

Jacobs, M. M., van den Berg, R. G., Vleeshouwers, V. G., Visser, M., Mank, R., Sengers, M., et al. (2008). AFLP analysis reveals a lack of phylogenetic structure within *Solanum* section *Petota*. *BMC Evol. Biol.* 8, 1–12. doi: 10.1186/1471-2148-8-145

Jones, J. D. G., and Dangl, J. L. (2006). The plant immune system. *Nature* 444, 323–329. doi: 10.1038/nature05286

Kalyaanamoorthy, S., Minh, B. Q., Wong, T. K. F., Haeseler, von, A., and Jermiin, L. S. (2017). ModelFinder: fast model selection for accurate phylogenetic estimates. *Nat. Meth* 14, 587–589. doi: 10.1038/nmeth.4285

Kearse, M., Moir, R., Wilson, A., Stones-Havas, S., Cheung, M., Sturrock, S., et al. (2012). Geneious Basic: An integrated and extendable desktop software platform for the organization and analysis of sequence data. *Bioinformatics* 28, 1647–1649. doi: 10.1093/bioinformatics/bts199.

Koboldt, D. C., Zhang, Q., Larson, D. E., Shen, D., McLellan, M. D., Lin, L., et al. (2012). VarScan 2: somatic mutation and copy number alteration discovery in cancer by exome sequencing. *Genome Research* 22, 568–576. doi: 10.1101/gr.129684.111.

Leisner, C. P., Hamilton, J. P., Crisovan, E., Carpintero, N. C.M., Marand, A. P., Newton, L., et al. (2018). Genome sequence of M6, a diploid inbred clone of the high-glycoalkaloid-producing tuber-bearing potato species Solanum chacoense, reveals residual heterozygosity. *The Plant Journal* 94, 562–570. doi: 10.1111/tpj.13857.

Lin, X., Armstrong, M., Baker, K., Wouters, D., Visser, R. G. F., Wolters, P. J., et al. (2020a). RLP/K enrichment sequencing; a novel method to identify receptor-like protein (RLP) and receptor-like kinase (RLK) genes. *New Phytol.* 227, 1264–1276. doi: 10.1111/nph.16608

Lin, X., Wang, S., de Rond, L., Bertolin, N., Wouters, R. H. M., Wouters, D., et al. (2020b). Divergent evolution of PcF/SCR74 effectors in oomycetes is associated with distinct recognition patterns in solanaceous plants. *MBio* 11, 380. doi: 10.1128/mBio.00947-20

Liu, Z., Bos, J. I.B., Armstrong, M., Whisson, S. C., da Cunha, L., Torto-Alalibo, T., et al. (2005). Patterns of diversifying selection in the phytotoxin-like scr74 gene family of Phytophthora infestans. *Mol Biol Evol* 22, 659–672. doi: 10.1093/molbev/msi049.

Ma, Z., Song, T., Zhu, L., Ye, W., Wang, Y., Shao, Y., et al. (2015). A Phytophthora sojae glycoside hydrolase 12 protein is a major virulence factor during soybean infection and is recognized as a PAMP. *The Plant Cell* 27, 2057–2072. doi: 10.1105/tpc.15.00390.

Minh, B. Q., Schmidt, H. A., Chernomor, O., Schrempf, D., Woodhams, M. D., Haeseler, von, A., et al. (2020). IQ-TREE 2: new models and efficient methods for phylogenetic inference in the genomic era. *Mol. Biol. Evol.* 37, 1530–1534. doi: 10.1093/molbev/msaa015

Nennstiel, D., Scheel, D., and Nürnberger, T. (1998). Characterization and partial purification of an oligopeptide elicitor receptor from parsley (*Petroselinum crispum*). *FEBS Lett.* 431, 405–410. doi: 10.1016/S0014-5793(98)00800-X

Ngou, B. P. M., Ahn, H. K., Ding, P., and Jones, J. D. G. (2021). Mutual potentiation of plant immunity by cell-surface and intracellular receptors. *Nature* 592, 110–115. doi: 10.1038/s41586-021-03315-7

Nietzschmann, L., Gorzolka, K., Smolka, U., Matern, A., Eschen Lippold, L., Scheel, D., et al. (2019). Early pep-13-induced immune responses are SERK3A/B-dependent in potato. *Sci. Rep.* 9, 18380. doi: 10.1038/s41598-019-54944-y

Nurnberger, T., Nennstiel, D., Hahlbrock, K., and Scheel, D. (1995). Covalent cross-linking of the *Phytophthora megasperma* oligopeptide elicitor to its receptor in parsley membranes. *Proc. Natl. Acad. Sci.* 92, 2338–2342. doi: 10.1073/pnas.92.6.2338

Nürnberger, T., Nennstiel, D., Jabs, T., Sacks, W. R., Hahlbrock, K., and Scheel, D. (1994). High affinity binding of a fungal oligopeptide elicitor to parsley plasma membranes triggers multiple defense responses. *Cell* 78, 449–460. doi: 10.1016/0092-8674(94)90423-5

Orsomando, G., Lorenzi, M., Raffaelli, N., Dalla Rizza, M., Mezzetti, B., and Ruggieri, S. (2001). Phytotoxic protein PcF, purification, characterization, and cDNA sequencing of a novel hydroxyproline-containing factor secreted by the strawberry pathogen Phytophthora cactorum. *Journal of Biological Chemistry* 276, 21578–21584. doi: 10.1074/jbc.M101377200.

Paajanen, P., Kettleborough, G., López-Girona, E., Giolai, M., Heavens, D., Baker, D., et al. (2019). A critical comparison of technologies for a plant genome sequencing project. *Gigascience* 8, 56. doi: 10.1093/gigascience/giy163.

Parker, J. E., Schulte, W., and Hahlbrock, K. (1991). An extracellular glycoprotein from *Phytophthora megasperma* f. sp. *glycinea* elicits phytoalexin synthesis in cultured parsley cells and protoplasts. *MPMI* 4, 19–27. doi: 10.1094/MPMI-4-019

Quinlan, A. R., and Hall, I. M. (2010). BEDTools: a flexible suite of utilities for comparing genomic features. *Bioinformatics* 26, 841–842. doi: 10.1093/bioinformatics/btq033.

Reiss, K., Kirchner, E., Gijzen, M., Zocher, G., Löffelhardt, B., Nürnberger, T., et al. (2011). Structural and phylogenetic analyses of the GP42 transglutaminase from *Phytophthora sojae* reveal an evolutionary relationship between oomycetes and marine *Vibrio* bacteria. *J. Biol. Chem.* 286, 42585–42593. doi: 10.1074/jbc.M111.290544

Ricci, P., Bonnet, P., Huet, J. C., Sallantin, M., Beauvais-Cante, F., Bruneteau, M., et al. (1989). Structure and activity of proteins from pathogenic fungi Phytophthora

eliciting necrosis and acquired resistance in tobacco. *Eur J Biochem* 183, 555–563. doi: 10.1111/j.1432-1033.1989.tb21084.x.

Sun, Y., Wang, Y., Zhang, X., Chen, Z., Xia, Y., Wang, L., et al. (2022). Plant receptor-like protein activation by a microbial glycoside hydrolase. *Nature* 610, 335–342. doi: 10.1038/s41586-022-05214-x

Torres Ascurra, Y., Lin, X., Wolters, P. J., and Vleeshouwers, V. G. A. A. (2021). Identification of solanum immune receptors by bulked segregant RNA-seq and high-throughput recombinant screening. *Methods Mol. Biol.* 2354, 315–330. doi: 10.1007/978-1-0716-1609-3_15

van Lieshout, N., van der Burgt, A., de Vries, M. E., Maat Ter, M., Eickholt, D., Esselink, D., et al. (2020). Solyntus, the new highly contiguous reference genome for potato (Solanum tuberosum). *G3* 10, 3489–3495. doi: 10.1534/g3.120.401550.

Wang, Y., Xu, Y., Sun, Y., Wang, H., Qi, J., Wan, B., et al. (2018). Leucine-rich repeat receptor-like gene screen reveals that *Nicotiana* RXEG1 regulates glycoside hydrolase 12 MAMP detection. *Nat. Commun.* 9, 594–512. doi: 10.1038/s41467-018-03010-8

Witek, K., Jupe, F., Witek, A. I., Baker, D., Clark, M. D., and Jones, J. D. G. (2016). Accelerated cloning of a potato late blight–resistance gene using RenSeq and SMRT sequencing. *Nat. Biotechnol.* 34, 656–660. doi: 10.1038/nbt.3540

Witek, K., Lin, X., Karki, H. S., Jupe, F., Witek, A. I., Steuernagel, B., et al. (2021). A complex resistance locus in *Solanum americanum* recognizes a conserved *Phytophthora* effector. *NPLANTS* 7, 198–208. doi: 10.1038/s41477-021-00854-9

Xu, X., Pan, S., Cheng, S., Zhang, B., Mu, D., Ni, P., et al. (2011). Genome sequence and analysis of the tuber crop potato. *Nature* 475, 189–195. doi: 10.1038/nature10158.

Yuan, M., Jiang, Z., Bi, G., Nomura, K., Liu, M., Wang, Y., et al. (2021). Pattern-recognition receptors are required for NLR-mediated plant immunity. *Nature* 592, 105–109. doi: 10.1038/s41586-021-03316-6

Zhou, Q., Tang, D., Huang, W., Yang, Z., Zhang, Y., Hamilton, J. P., et al. (2020). Haplotype-resolved genome analyses of a heterozygous diploid potato. *Nature Genetics* 52, 1018–1023. doi: 10.1038/s41588-020-0699-x.

Zou, C., Wang, P., and Xu, Y. (2016). Bulked sample analysis in genetics, genomics and crop improvement. *Plant Biotechnol. J.* 14, 1941–1955. doi: 10.1111/pbi.12559

frontiers | Frontiers in Plant Science

TYPE Original Research
PUBLISHED 20 January 2023
DOI 10.3389/fpls.2023.1087121

OPEN ACCESS

EDITED BY
Carlos R. Figueroa,
University of Talca, Chile

REVIEWED BY
Lihui Zeng,
Fujian Agriculture and Forestry University, China
Claudio Inostroza-Blancheteau,
Temuco Catholic University, Chile

*CORRESPONDENCE
Botao Song
songbotao@mail.hzau.edu.cn
Changzheng He
hecz@hotmail.com

SPECIALTY SECTION
This article was submitted to Crop and Product Physiology, a section of the journal Frontiers in Plant Science

RECEIVED 02 November 2022
ACCEPTED 04 January 2023
PUBLISHED 20 January 2023

CITATION
Zhao X, Zhang H, Liu T, Zhao Y, Hu X, Liu S, Lin Y, Song B and He C (2023) Transcriptome analysis provides *StMYBA1* gene that regulates potato anthocyanin biosynthesis by activating structural genes. *Front. Plant Sci.* 14:1087121. doi: 10.3389/fpls.2023.1087121

Transcriptome analysis provides *StMYBA1* gene that regulates potato anthocyanin biosynthesis by activating structural genes

Xijuan Zhao[1,2], Huiling Zhang[3], Tengfei Liu[2], Yanan Zhao[3], Xinxi Hu[1], Shengxuan Liu[2], Yuan Lin[1], Botao Song[2]* and Changzheng He[1]*

[1]Engineering Research Center for Germplasm Innovation and New Variety Breeding of Horticultural Crops, Key Laboratory for Vegetable Biology of Hunan Province, Hunan Agricultural University, Changsha, China, [2]Key Laboratory of Potato Biology and Biotechnology, Ministry of Agriculture and Rural Affairs, National Key Laboratory for Germplasm Innovation and Utilization of Horticultural Crops, College of Horticulture and Forestry Sciences, Huazhong Agricultural University, Wuhan, China, [3]College of Horticulture and Plant Protection, Henan University of Science and Technology, Luoyang, China

Anthocyanin biosynthesis is affected by light, temperature, and other environmental factors. The regulation mode of light on anthocyanin synthesis in apple, pear, tomato and other species has been reported, while not clear in potato. In this study, potato RM-210 tubers whose peel will turn purple gradually after exposure to light were selected. Transcriptome analysis was performed on RM-210 tubers during anthocyanin accumulation. The expression of *StMYBA1* gene continued to increase during the anthocyanin accumulation in RM-210 tubers. Moreover, co-expression cluster analysis of differentially expressed genes showed that the expression patterns of *StMYBA1* gene were highly correlated with structural genes *CHS* and *CHI*. The promoter activity of *StMYBA1* was significantly higher in light conditions, and StMYBA1 could activate the promoter activity of structural genes *StCHS*, *StCHI*, and *StF3H*. Further gene function analysis found that overexpression of *StMYBA1* gene could promote anthocyanin accumulation and structural gene expression in potato leaves. These results demonstrated that *StMYBA1* gene promoted potato anthocyanin biosynthesis by activating the expression of structural genes under light conditions. These findings provide a theoretical basis and genetic resources for the regulatory mechanism of potato anthocyanin synthesis.

KEYWORDS

potato, anthocyanin biosynthesis, light-induced, *StMYBA1*, transcriptional activation

1 Introduction

Potato (*Solanum tuberosum* L.) is the most important non-cereal crop worldwide. It has been found that pigmented potato cultivars are rich in anthocyanin (Fossen and Andersen, 2000) addition to their colorful appearance and enhanced flavor, pigmented potato tubers also exhibit high antioxidant activity. It was found that the oxidation activity of red and

purple potato tubers was 2–3 times higher than that of white tubers (Brown, 2005). Therefore, consuming pigmented potatoes can also protect against some cancers and cardiovascular diseases (He and Giusti, 2010; Crowe et al., 2011).

Anthocyanins are synthesized through the flavonoid pathway, which includes both regulatory and structural genes. The structural genes can be divided into two groups, early biosynthetic genes (EBGs) and late biosynthetic genes (LBGs), based on the catalytic substrate. The EBGs include chalcone synthase (*CHS*), chalcone isomerase (*CHI*), and flavanone 3-hydroxylase (*F3H*) which catalyze the formation of colorless dihydroflavonol compounds. The LBGs consist of flavonoid 3′-hydroxylase (*F3′H*), flavonoid 3′,5′-hydroxylase (*F3′5′H*), dihydroflavonol 4-reductase (*DFR*), anthocyanin synthase (*ANS*), and flavonoid 3-O-glucosyltransferase (*3GT*), usually catalyzing the formation of colored anthocyanins (Baudry et al., 2004; Liu et al., 2018). The regulatory genes modulating anthocyanin biosynthesis are mainly through the well-documented MBW complexes which formed by MYB, bHLH, and WD40 (Allan et al., 2008; Lloyd et al., 2017). MYB transcription factors (TFs) are believed to play crucial roles in regulating anthocyanin biosynthetic genes (Lai et al., 2013), as well as, many MYB TFs have been demonstrated to be activators of the anthocyanin accumulation from many species, such as Arabidopsis (Borevitz et al., 2000; Gonzalez et al., 2008), apple (Espley et al., 2007; Jiang et al., 2021), and pear (Yao et al., 2017). In potato, the MYB gene *StAN2* can promote anthocyanin accumulation in tubers by regulating the structural genes (Jung et al., 2009; Liu et al., 2016). Another two MYB genes, *StMYBA1* and *StMYB113*, could promote anthocyanin biosynthesis in tobacco leaves (Liu et al., 2016; Liu et al., 2017), and *StMYBA1* promoted anthocyanin synthesis, which requires light (Liu et al., 2017). However, it is unclear whether they can promote anthocyanin biosynthesis in potato.

Anthocyanins biosynthesis is not only affected by genes, but also regulated by many environmental factors, such as low temperatures, salt, drought, and light (Cominelli et al., 2008; Catala et al., 2011; Li et al., 2017). In purple kale, the anthocyanin accumulation is induced by low temperature, the total content of anthocyanin under low temperature was about 50-fold higher than that of the plants grown in the greenhouse (Zhang et al., 2012). Light is an important environmental factor affecting anthocyanin biosynthesis according to light quality and light intensity. Also, the effect of light on anthocyanin accumulation has been reported in tomato (Wang et al., 2021), eggplant (Li et al., 2017), apple (Li et al., 2012; Chen et al., 2019), pear (Liu et al., 2019), grape (Azuma et al., 2012) and many other species. The light regulation mechanism of anthocyanin biosynthesis is that the light response proteins such as COP1, and HY5, inhibit or promote anthocyanin biosynthesis by degrading or activating MBW members, mainly MYB TFs. *PAP1* and *PAP2*, two members of MYB genes, are required for anthocyanin accumulation in arabidopsis. In dark-grown plants, the photoresponsive protein COP1 interacts with PAP1 and PAP2 and degrades them, so there is no accumulation of anthocyanin. However, anthocyanin is biosynthesized when COP1 is degraded under light conditions (Maier et al., 2013). In apples, PdHY5 regulates the *MdMYB10* gene at transcriptional and post-transcriptional levels under light conditions, thereby activating the expression of structural genes to promote anthocyanin synthesis (Espley et al., 2007; An et al., 2017). Moreover, MYB genes related to light-stimulated anthocyanin synthesis were identified in pear (Wang et al., 2020), buckwheat (Yao et al., 2020) and other species.

In our previous study, we found that the tubers of potato population F_1RM are yellow peel yellow flesh, but the peel of the tubers will turn purple gradually after exposure to light. In this study, the tuber anthocyanin content and transcriptome sequencing analyze were further applied to these light-sensitive F_1RM tubers, to explore the key regulatory genes of light-induced potato anthocyanin biosynthesis and reveal its regulatory mechanism.

2 Methods

2.1 Plant materials

The potato population F_1RM was obtained by crossing with the heterozygous diploid yellow peel yellow flesh potato RH (*S. tuberosum*) as the female parent and the yellow peel yellow flesh diploid inbred clone M6 (*S. chacoense*) as the male parent. F_1RM tubers are also yellow peel yellow flesh, but the peel of the tubers will turn purple gradually after exposure to light. Among them, the tubers of line RM-210 were selected to study the regulation of anthocyanin accumulation during light exposure. The RM-210 plants were grown in 24-cm-diameter plastic pots in greenhouse with 16 h light per day supplied by lamps. For about 80 days after planting, the mature tubers were harvested and dark storage for 10 days at 20°C. Then they were incubated under the continuous light intensity of 2000 LX, and samples were collected at 0, 6, 12, 36, 48, and 120 h. Five tubers were used for sampling at each time point, and the peels (1 mm thick) were collected and stored at −70°C for molecular and biochemical analyses.

Nicotiana benthamiana L. for dual luciferase assays was grown under greenhouse conditions until 5–6 leaves were available for *Agrobacterium* infiltration.

2.2 Anthocyanin extraction and content analysis

Anthocyanin mixtures were extracted according to the agricultural standard of China (NY/T 2640-2014). 100mg powder was extracted with 1.0 ml 1% formic acid methanol overnight at 4°C. Extracts were centrifuged at 10,000 ×g for 10 min and filtrated with 0.22-μm microporous membrane. Anthocyanin quantification was measured by High Performance Liquid Chromatography (HPLC) as a previous description (Zhou et al., 2008). The anthocyanin standard consisted of peonidin, delphinidin, malvidin, petunidin, pelargonidin, and cyanidin dissolved in methanol.

2.3 RNA isolation and library construction

Total RNA was isolated according to previous description (Zhang et al., 2022). The RNA integrity was assessed using the Fragment Analyzer 5400 (Agilent Technologies, CA, USA). Sequencing libraries were generated using NEBNext® Ultra™ RNA Library Prep Kit for

Illumina® (NEB, USA) in accordance with the manufacturer's recommendations and index codes were added to attribute sequences to each sample.

2.4 Sequence data filtering, *de novo* assembly, and annotation

The original files obtained from the Illumina platform are transformed into raw data by base calling. The raw reads were trimmed by removing adapters, reads containing ploy-N more than 5% and low-quality sequences. Raw sequences were transformed into clean reads after processing. Then the clean reads were mapped to the transcriptome of the potato DM reference genomes (6.1 version, http://spuddb.uga.edu/dm_v6_1_download.shtml) with Salmon software, version 1.3.0 (Patro et al., 2017).

2.5 Differentially expressed gene analyses

Transcripts Per Kilobase Million (TPM) were used to estimate gene expression level. The R package DESeq2 was used to perform the differential gene expression among different samples. Thresholds for significantly differential expression were false discovery rate (FDR) ≤ 0.05 and fold change ≥2 or ≤ 0.5. The KEGG pathway enrichment analysis of differentially expressed genes (DEGs) was performed by TBtools at the adjusted $p < 0.05$ by using a hypergeometric test (Chen et al., 2020). The cluster analysis was performed as described previously (Guo et al., 2016).

2.6 Reverse transcription quantitative real-time PCR

Reverse transcription quantitative real-time PCR (RT-qPCR) primers were designed with the NCBI Primer-BLAST and listed in Table 1. The RT-qPCR was performed on a CFX96™ real-time PCR system (Bio-Rad, USA) with the TransStart Top Green qPCR SuperMix kit (Transgen, Beijing, China). The potato housekeeping genes *ef1α* (GenBank: AB061263) and *actin* (GenBank: XM_006345899.2) were selected as internal reference genes. Relative expression of the individual gene was calculated with calculated multiple internal control method (Vandesompele et al., 2002).

2.7 Construction of expression vectors and transient assays

According to the Soltu.DM.10G020840.1 sequence from the Potato Genome Database, the open reading frame (ORF) of the *StMYBA1* was amplified from the cDNA of RM-210 tuber peel. The ORF of *StMYBA1* was cloned into the pSAK-277 vector through *Eco*RI restriction sites, and the recombinant plasmid pSAK-StMYBA1 was sequenced (Sangon Biotech, Shanghai, China). The primer sequences pSAK-StMYBA1-F/R were listed in Table 1.

The promoter sequences of *StMYBA1*, *StCHS*, *StCHI*, *StF3H*, *StF3'H*, *StDFR*, *StF3'5'H*, *StANS* and *StGST* were isolated from M6 (the tubers peel will turn purple gradually after exposure to light) and cloned into the pGreenII0800-LUC vector with the *Kpn*I and *Nco*I restriction sites. The primer sequences were listed in Table 1. Dual-luciferase assays were performed in tobacco, as previously described (Liu et al., 2016; Zhang et al., 2022), and the pGreenII0800-LUC vector without a promoter was used as a negative control. pSAK-StMYBA1 was infiltrated into tobacco leaves with pGreenII0800-StCHS, pGreenII0800-StCHI, pGreenII0800-StF3H, pGreenII0800-StF3'H, pGreenII0800-StF3'5'H, pGreenII0800-StDFR, pGreenII0800-StGST and pGreenII0800-StANS in a second *Agrobacterium* strain, respectively. To analyze the light response of the *StMYBA1* gene promoter, tobacco leaves were infected with *Agrobacterium* containing fusion vectors pGreenII0800-StMYBA1, and the pGreenII0800-LUC vector without a promoter was selected as a negative control. After infiltration, the tobacco plants were kept in the dark for 12 h. Then some of the plants were moved to the culture chamber with 16 h of light per day, and the other plants were still in the dark. The leaves were sampled after three days of infiltration and stored at −70°C. The LUC and REN activities were tested using the Dual-Luciferase® reporter Assay System (Promega, USA).

2.8 Transformation of potato

The overexpression (OE) vector pSAK-StMYBA1 was transformed into the potato diploid clone AC142 as previously (Si et al., 2003; Zhang et al., 2014). The transgenic plants and untransformed control were grown in 12-cm-diameter plastic pots in the greenhouse. For one month after planting, the leaves were sampled, frozen in liquid nitrogen, and stored at −70°C until use.

3 Results

3.1 Light-induced anthocyanin accumulation in tuber peel of potato

Tubers of potato population F_1RM are yellow peel yellow flesh, while the peel of the tubers will turn purple gradually after exposure to light (Figure 1A). Among them, the tubers of line RM-210 were selected to study the regulation of anthocyanin accumulation during light exposure. Purple can be seen at the top of the RM-210 tubers at 48 h light exposure (Figure 1B), and the whole tuber peels appear to be purple at 120 h (Figure 1A). Thus, the time points of sampling for anthocyanin content and RNA-seq analysis were 0, 6, 12, 36, 48, and 120 h.

The HPLC chromatograms of the extracts from the peel of tubers are shown in Figure S1, and one peak was detected at approximately 0.91 min. According to the comparison analysis with the standard, the component represented by the spectrogram is delphinium. The results showed that delphinium could not be detected in the tuber peel with 0 and 12 h light exposure, and the content of delphinium in the tuber peel for 36, 48, and 120 h was 6.36, 34.08, and 43.07 mg/kg, respectively (Figure 1C). This indicates that light can promote the accumulation of delphinium in RM-210 tuber peel and show purple.

TABLE 1 The primer sequences for qPCR and constructing vectors.

Primer name	Gene ID	Forward primer (5′-3′)	Reverse primer (5′-3′)	Used for
StMYBA1	Soltu.DM.10G020840.1	CCTCAACCTCGGAACTTCTCA	TCCTTGCAACGTTTGTCGTC	qRT-PCR
StCHS1	Soltu.DM.09G028560.1	CGGCCGCTATCATTATGGGT	TCCATCGATAGCACCTTCGC	
StCHS2	Soltu.DM.05G023610.1	ACTTTTCGTGGCCCAAGTGA	AAGGCCTTTCGACTTCTGGT	
StCHI1	Soltu.DM.05G001950.1	ATGCAGAGAGGGAGGCCATT	CGTCAATGATCCAAGCGGTG	
StCHI2	Soltu.DM.07G023150.1	GCCGTCTTTCAAGGGAAACC	ACGTCGAAGAGAGCTGATGC	
StPAL1	Soltu.DM.09G005700.1	CAGCTGCACCTACCCTTTGA	ACAGGGTTGCCACTTTCAAGA	
StPAL2	Soltu.DM.10G020990.1	TGGCAGGCCTAATTCCAAGG	TACCGCGAGCACATTAGCAT	
StC4H1	Soltu.DM.06G032850.1	AAGCTTCCGTACCTTCAGGC	AGGTTTCTTCCAGTGAGCGG	
StC4H2	Soltu.DM.06G032860.1	AAGCTTCCGTACCTTCAGGC	AGGTTTCTTCCAGTGAGCGG	
St4CL	Soltu.DM.03G020790.1	GCTTGATTACAGGGGTGGCT	AGCTCCAACAGCGCACTAAT	
StMYB48	Soltu.DM.11G026620.2	ACCAGGGCGTACTGATAACG	AAGAGCTTGATTCCACCCGT	
StB3	Soltu.DM.09G002750.1	GAGCAATGCCGAACCAAACA	ATCCTGGTTGTGGCTCGATG	
StHSF2	Soltu.DM.07G011880.1	TAACAGCAGCCCAGAGATGG	GCACTCGGATGGGTTTGAGA	
pSAK-StMYBA1	Soltu.DM.10G020840.1	TAGTGGATCCAAAGAATTCCGTTGGGAGTTAGGAAAGG	CGAGAAGCTTTTTGAATTCTTAATTAAGTAGATTCCATAAG	Construction vector
Prom-StMYBA1	Soltu.DM.10G020840.1	TAGTGGATCCAAAGAATTCCGTTGGGAGTTAGGAAAGG	CGAGAAGCTTTTTGAATTCTTAATTAAGTAGATTCCATAAG	
Prom-StCHS	Soltu.DM.05G023610.1	ATAGGGCGAATTGGGTACCCCTACTTAACAATCAAACACAACAA	TTTTTGGCGTCTTCCATGGCGTGTTTTTTTTTTTTACTAAGATTT	
Prom-StCHI	Soltu.DM.07G023150.1	ATAGGGCGAATTGGGTACCTCACTAACCTGAGAAGTAGGACGAG	TTTTTGGCGTCTTCCATGGATCAGTTGTATTATTACCAGAAGAGGAG	
Prom-StF3H	Soltu.DM.02G023850.1	ATAGGGCGAATTGGGTACCTTGACATGTTTTTTTTTTAGCTAGG	TTTTTGGCGTCTTCCATGGGTTCAAAAGAGTTATGAGGTGCC	
Prom-StF3’H	Soltu.DM.03G029340.1	ATAGGGCGAATTGGGTACCAAAAAAGGCTAGTCAAATGGGATAA	TTTTTGGCGTCTTCCATGGCGGGCCATTGATGCAGTG	
Prom-StF3’5’H	Soltu.DM.11G020990.1	ATAGGGCGAATTGGGTACCATGTAAAAAATACGATAACAAAAAGT	TTTTTGGCGTCTTCCATGGCAACATGTGGCATTGAACCT	
Prom-StANS	Soltu.DM.08G026700.1	ATAGGGCGAATTGGGTACCTATTGTGACTTTAGCTTTCATGATC	TTTTTGGCGTCTTCCATGGTGTTACGCGGAGTACTTATTTAGA	
Prom-StDFR	Soltu.DM.02G024900.2	ATAGGGCGAATTGGGTACCCGCTATGTTATTGTTAAGGGTG	TTTTTGGCGTCTTCCATGGCAGAAATGAGAGGAAAAAAGAGTC	
Prom-StGST	Soltu.DM.02G020850.1	ATAGGGCGAATTGGGTACCCTTCAGTTCAAAAATAGTTTCCTCT	TTTTTGGCGTCTTCCATGGCTTTTTTTTTTCTTGTGAAATCC	

10.3389/fpls.2023.1087121

10.3389/fpls.2023.1087121

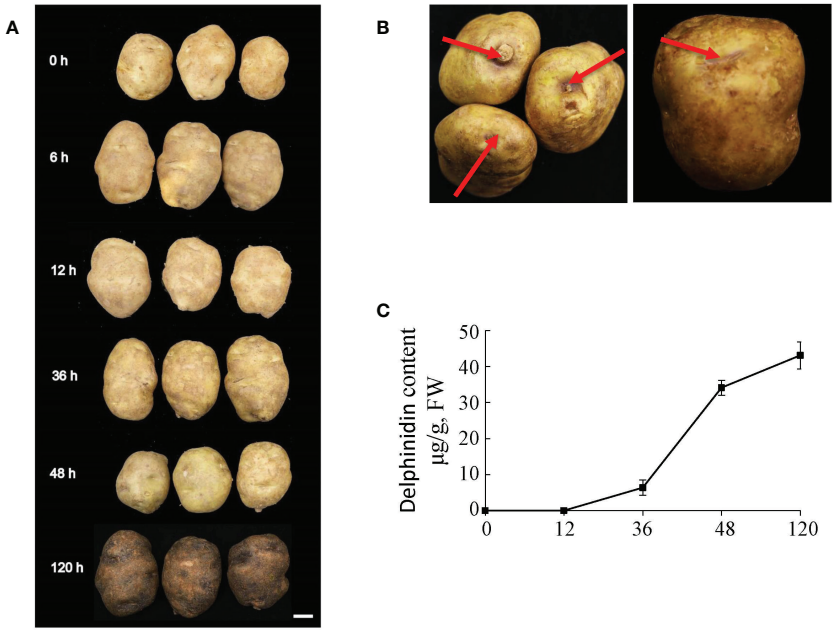

FIGURE 1
Tuber phenotype and anthocyanin content of RM-210 tubers. **(A)** The phenotype of RM-210 tubers during light treatment. **(B)** The phenotype of the RM-210 tubers exposed to light 48 h. **(C)** Delphinidin content of RM-210 tubers.

3.2 Analysis of differentially expressed genes during anthocyanin accumulation

To understand the key pathways and regulatory genes in light regulation of anthocyanin biosynthesis, transcriptomics based on RNA-seq was performed on RM-210 tuber peel response to light. mRNA-sequencing libraries were generated from tuber peel samples obtained at 0, 6, 36, and 48 h light exposure, respectively, and except for two replicates from samples obtained at 36 h, all other samples had three replicates. The relationship among the samples was analyzed by the Principle Component Analysis (PCA) approach, which shows that the three replicates of the same sample are polymerized together with good repeatability (Figure 2A). Therefore, it was suggested that the RNA-seq data was suitable for further differential gene expression (DGE) analysis. To better understand the overall expression patterns of the transcripts in four samples, clustering analysis of the expression patterns in different samples was performed using the R package "TCseq". There were six clusters in total from the four samples (Figure 3). Interesting, the expression levels of genes from cluster 2 were higher at 6h than other samples, indicating that the genes in this cluster were the early light response. The expression of genes from class 6 increased with the light duration and anthocyanin accumulation, indicates that the function of these genes may related to anthocyanin accumulation.

To explore the genes contributing to anthocyanin biosynthesis in response to light, comparisons 6h vs 0h, 36h vs 0h, and 48h vs 0h were made. Based on fold change ≥ 2 and FDR < 0.01 criteria, 3224, 3976, and 3701 genes up-regulated were identified in comparisons 6h vs 0h, 36h vs 0h, and 48h vs 0h respectively, and 2642, 2969, and 2602 genes respectively were significantly down-regulated (Figure 2B). The list of DEGs in each comparison is shown in Table S1, and the KEGG pathway enrichment analysis was performed. There were 26 pathways enriched in 6h vs 0h, the top 5 of which were photosynthesis-antenna proteins, photosynthesis, porphyrin and chlorophyll metabolism, ubiquinone and other terpenoid-quinone biosynthesis, and glutathione metabolism. There were 37 pathways enriched in 36h vs 0h, the top 5 of which were photosynthesis, photosynthesis-antenna proteins, phenylalanine metabolism, oxidative phosphorylation, and porphyrin and chlorophyll metabolism. In 48h vs 0h, there were 34 pathways enriched, of which the first 5 were photosynthesis, photosynthesis-antenna proteins, porphyrin and chlorophyll metabolism, phenylalanine metabolism, and carbon fixation in photosynthetic organisms (Figure 2C).

3.3 Identification of transcription factors related to anthocyanin biosynthesis

Delphinidin in potato is mainly synthesized by structural genes (Figure 4A) and regulated transcription factors. The expression levels of most structural genes in the four samples were different. For example, the expression of most *PAL* genes were high at 0h or 6h, *C4H* and *4CL* genes were high at 6h, *CHS* and *CHI* genes were high at 36h or 48h, and the expression of *F3H*, *F3'5'H*, *DFR*, and *ANS* were high at 48h (Figure 4A). This result indicated that the expression of these early biosynthesis genes of anthocyanin is earlier than that of late biosynthesis genes.

To further explore the key transcription factors regulating structural genes, 114 differentially expressed structural genes, and TFs (Table S2) were subjected to co-expression cluster analysis. The results showed that there were three clusters with a strong correlation between major structural genes and TFs (Figure 4B). The structural genes *PAL* (Soltu.DM.09G005700.1, Soltu.DM.10G020990.1), *C4H* (Soltu.DM.06G032850.1,

10.3389/fpls.2023.1087121

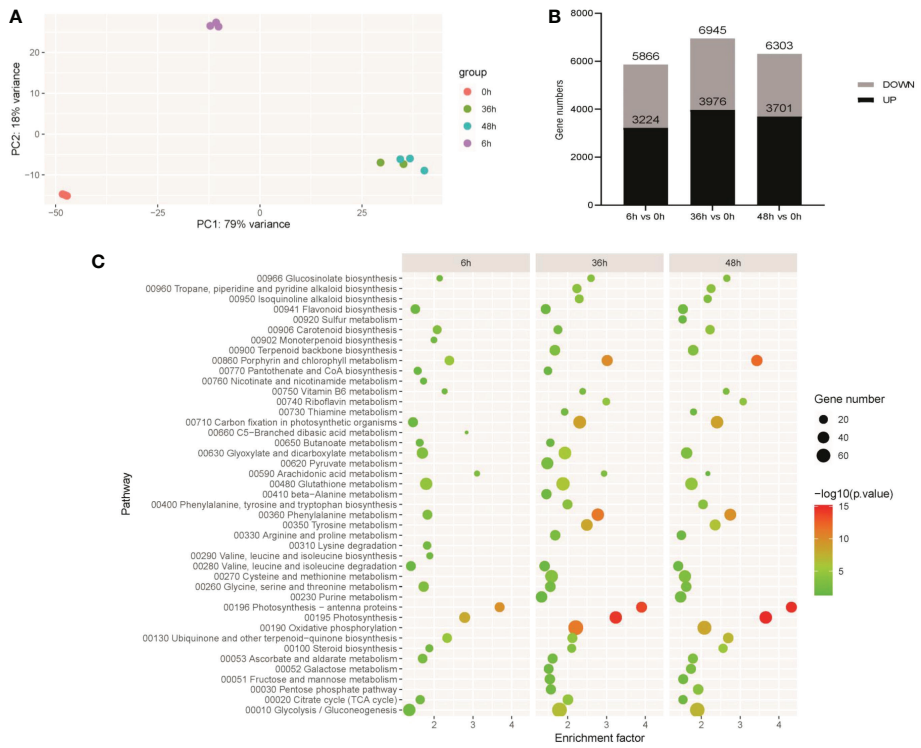

FIGURE 2
Overview of transcriptome analysis. **(A)** Correlation analysis of RNA-seq data of different treatments. **(B)** The number of differentially expressed genes (DEGs) in each comparison. **(C)** Kyoto Encyclopedia of Genes and Genomes (KEGG) enrichment analysis of DEGs in each comparison.

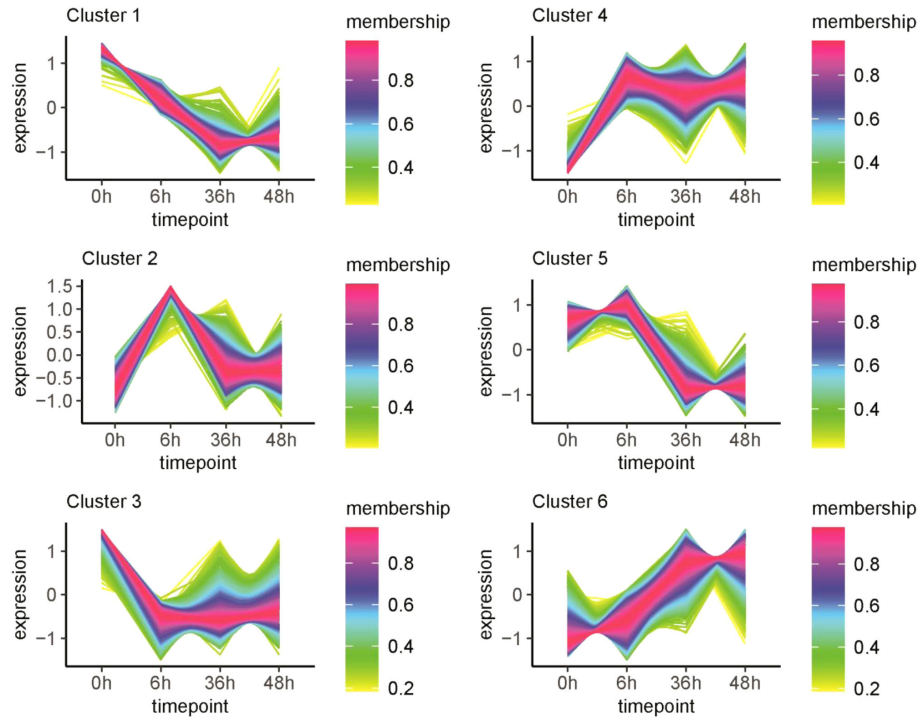

FIGURE 3
Cluster analysis of gene expression patterns in RM-210 tubers at different time points of light treatment. The Y-axis represents the deviation of the gene expression. The X-axis represents the sampling time points.

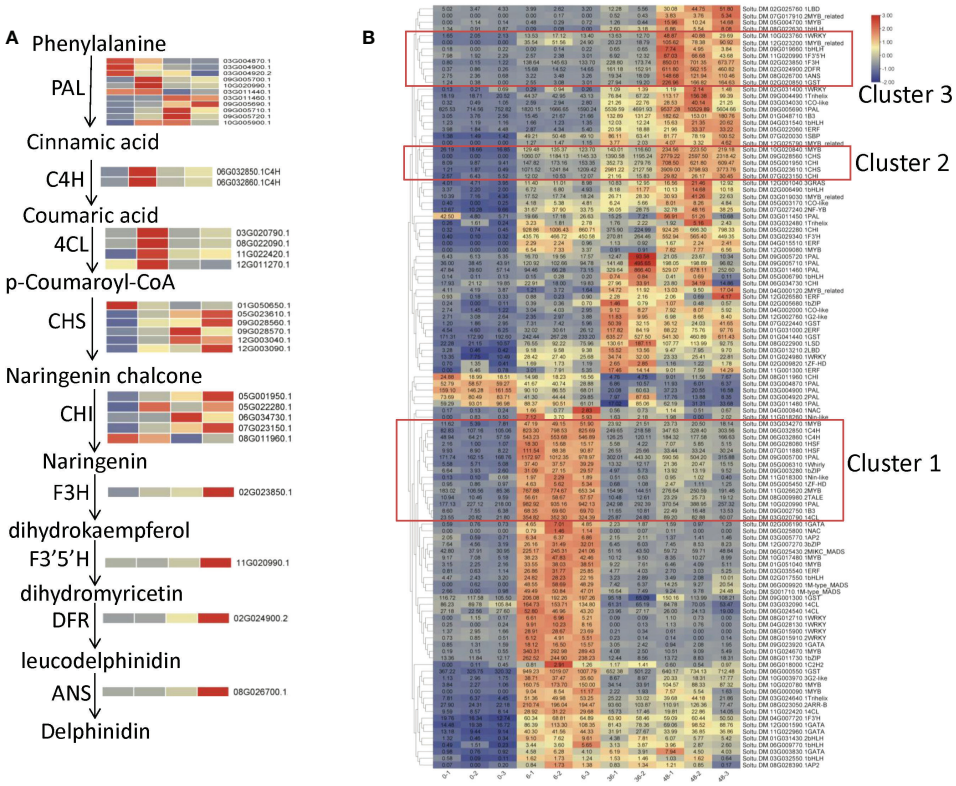

FIGURE 4
Co-expression analysis of structural genes and transcription factors in DEGs. **(A)** Anthocyanin biosynthesis pathway. **(B)** Co-expression cluster analysis of structural genes and transcription factors. The red boxes mark transcription factors that have a high correlation with the expression of key structural genes.

Soltu.DM.06G032860.1), *4CL* (Soltu.DM.03G020790.1) and MYB transcription factors (Soltu.DM.03G034270.1, Soltu.DM.11G026620.2), bZIP (Soltu.DM.09G003280.1) and B3 (Soltu.DM.09G002750.1) transcription factors were included in cluster 1. Above structural genes, *PAL*, *C4H* and *4CL* had the highest expression in the sample exposed to light for 6 h, so it was speculated that the transcription factors in cluster 1 might be early light response factors. Cluster 2 included two *CHS* genes (Soltu.DM.09G028560.1, Soltu.DM.05G023610.1), two *CHI* genes (Soltu.DM.05G001950.1, Soltu.DM.07G023150.1) and one *MYB* gene (Soltu.DM.10G020840.1, *StMYBA1*), whose expression level is gradually increased with the extension of treatment time. And structural genes *F3H* (Soltu.DM.02G023850.1), *F3'5'H* (Soltu.DM.11G020990.1), *DFR* (Soltu.DM.02G024900.2), *ANS* (Soltu.DM.08G026700.1), *GST* (Soltu.DM.02G020850.1), and MYB (Soltu.DM.12G023200.1), bHLH (Soltu.DM.09G019660.1, *StAN1*), and WRKY (Soltu.DM.10G023760.1, *StWRKY13*) transcription factors were included in cluster 3. Expression levels of all the five structural genes in cluster 3 increased rapidly in the sample exposed to light for 48 h, indicating that the transcriptional factors associated with them may also function at the late stage of anthocyanin biosynthesis. To assess the repeatability of the sequencing data, the genes in cluster1 and cluster2 were selected to determine their expression levels using RT-qPCR. The results showed that most of them had a similar expression trend with transcriptome analysis results (Figure S2).

3.4 Regulation of *StMYBA1* gene on structural genes

The *StMYBA1* gene in cluster 2 was previously confirmed to promote anthocyanin accumulation in tobacco leaves, and light is required for its function on anthocyanin accumulation (Liu et al., 2017). Analysis of the promoter sequences of *StMYBA1* showed that it contained multiple cis-acting regulatory elements involved in light responsiveness, such as Box4 (ATTAAT) and G-box (CACGTC/CACGTC/TACGTG) (Figure 5A, Table S3). To further analyze the response of the *StMYBA1* promoter to light, tobacco leaves were infected with *Agrobacterium* containing fusion vectors pGreenII0800-StMYBA1. The dual luciferase activity in tobacco leaves was evaluated after 3d incubation in darkness or light. The result showed that the promoter activity of *StMYBA1* in light conditions was significantly higher than that in dark, and no differences were observed in control (Figure 5B), suggesting that the activity of *StMYBA1* promoter could be induced by light.

The 2Kb promoter sequences of key structural genes in potato anthocyanin biosynthesis (*StCHS*, Soltu.DM.05G023610.1; *StCHI*, Soltu.DM.07G023150.1; *StF3H*, Soltu.DM.02G023850.1; *StF3'H*, Soltu.DM.03G029340.1; *StF3'5'H*, Soltu.DM.11G020990.1; *StDFR*, Soltu.DM.02G024900.2; *StANS*, Soltu.DM.08G026700.1; *StGST*, Soltu.DM.02G020850.1) were selected. The sequence analyzing showed that each of the structural gene promoter sequences contained at least one MYB binding elements (Figure 5A,

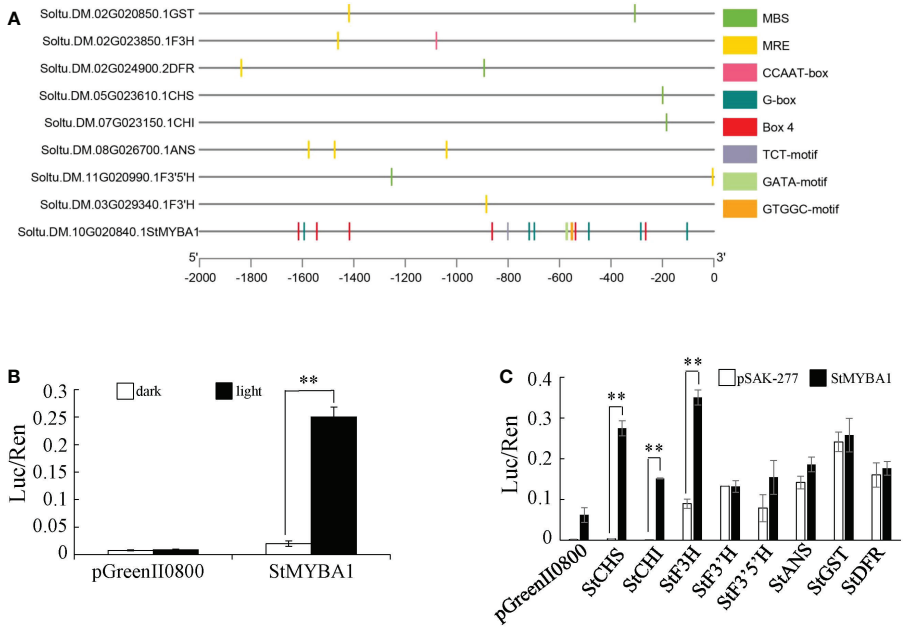

FIGURE 5
Light Response analysis of *StMYBA1* Gene and its regulation on structural genes. **(A)** Distribution of main core elements of *StMYBA1* and structural gene promoters. **(B)** Activity analysis of *StMYBA1* promoter under light and dark conditions. **(C)** Regulation of *StMYBA1* on structural genes related to anthocyanin biosynthesis. Significant differences (LSD) between means of the dark and light treatments, and pSAK-277 and StMYBA1 are indicated by asterisks (** $p < 0.01$).

Table S3). Therefore, transient luciferase assays in tobacco were used to test the activation of these structural gene promoters by StMYBA1. The results showed that compared to the negative control, StMYBA1 can significantly activate the promoters of *StCHS*, *StCHI*, and *StF3H*, but not the promoters of the other five structural genes (Figure 5C).

3.5 Regulation of *StMYBA1* gene on anthocyanin biosynthesis in potato

To explore the function of *StMYBA1* in potato anthocyanin biosynthesis, the potato genotype AC142 was transformed with expression vector pSAK-StMYBA1 (Figure S3A). After rooting screening (Figure S3B) and gene expression analysis, nineteen overexpression transgenic lines with increased *StMYBA1* transcripts were generated (Figure S3C). Three independent transgenic lines (OE-7, OE-8, and OE-10) were selected for function analysis. The transgenic lines showed normal plant morphology under greenhouse growing conditions comparing to wild type (Figure S3D). The leaf phenotype of transgenic lines was observed after 30 days of planting. Leaves of transgenic lines were purple, whereas those of wild-type were green (Figure 6A). Anthocyanin content in transgenic leaves was analyzed. The contents of delphinidin, pelargonidin, and cyanidin in the leaves of the transgenic lines were 5.37–6.15, 2.01–2.74, and 3.98–5.05 times than those in AC142 leaves, respectively (Figure 6B). These results strongly demonstrated that *StMYBA1* could promote the accumulation of anthocyanin in potato leaves. The regulatory role of *StMYBA1* was further investigated by analyzing the expression of the structural genes. The results showed that overexpression of the *StMYBA1* gene could increase the expression of structural genes (*StCHS*, *StCHI*, *StF3H*, *StF3'H*, *StF3'5'H*, *StDFR*, *StANS*, and *StGST*) significantly (Figures 6C–K), implying that the *StMYBA1* gene promotes anthocyanin biosynthesis in potato leaves by upregulating the expression of structural genes.

4 Discussion

Anthocyanins not only have a strong antioxidant capacity, but also can protect plants against various biotic and abiotic stresses (Sivankalyani et al., 2016; Liu et al., 2019). The structural genes in the anthocyanin synthesis pathway are mainly regulated by the members of the MBW complex (Lloyd et al., 2017; Cui et al., 2021), especially the MYB TFs (Lai et al., 2013). In this study, the transcriptome analysis of light sensitive tuber samples in potato showed that the expression level of a MYB gene, *StMYBA1*, gradually increased during the anthocyanin biosynthesis (Figure 4B, Table S1), and the promoter activity of the *StMYBA1* in light conditions was significantly higher than that in dark (Figure 5B). These results indicated that *StMYBA1* gene was a light-induced transcription factor associated with anthocyanin biosynthesis. Previous studies also showed that the promotion of anthocyanin biosynthesis in tobacco leaves by *StMYBA1* gene was light dependent (Liu et al., 2017). MYB genes which regulate anthocyanin biosynthesis induced by light also exist in many species such as *Arabidopsis*, apple, and so on (Maier et al., 2013; Yao et al., 2020). When dark-grown fruit was exposed to sunlight, transcript levels of *MdMYB1* in apple increased correlating with anthocyanin biosynthesis in the skin (Takos et al., 2006).

So far, studies on structural genes of potato anthocyanin biosynthesis mainly focuses on the late synthesis genes, such as *StF3'5'H*, *StDFR*, *StANS* and *3GT* (Jung et al., 2005; Zhang et al., 2009; Zhang et al., 2020). In this study, the expression level of the

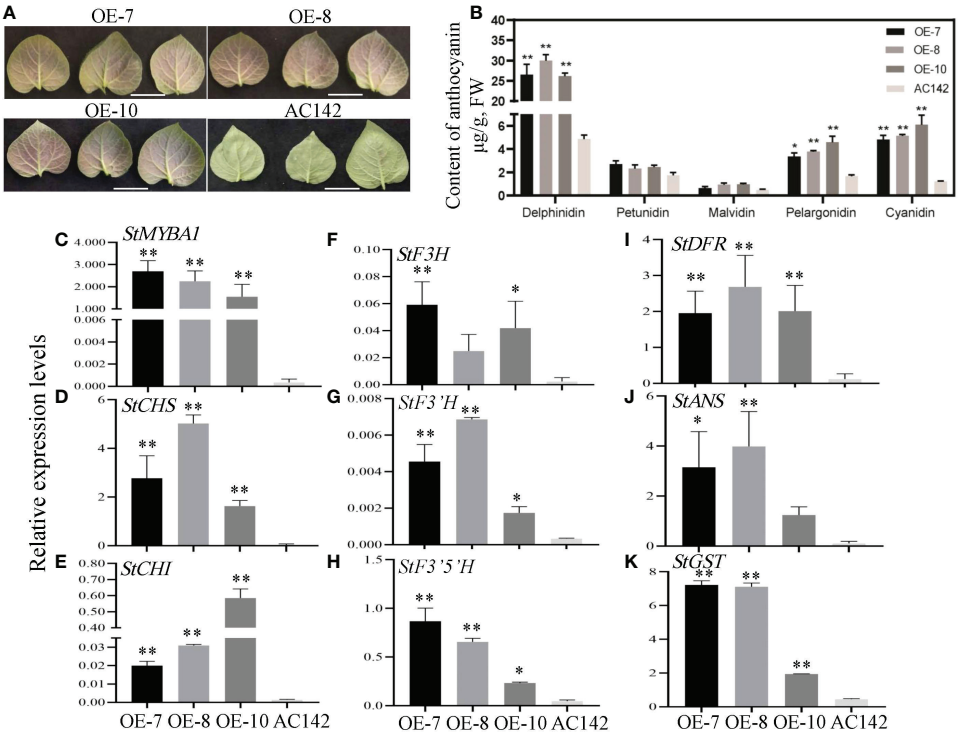

FIGURE 6
Regulation of *StMYBA1* gene on anthocyanin biosynthesis in potato. **(A)** Representative leaves images of StMYBA1-overexpressed transgenic lines (OE-7, OE-8, and OE-10) and the wild type (AC142). Bars=2 cm. **(B)** The anthocyanin content in the *StMYBA1* transgenic leaves. **(C–K)** The relative expression of *StMYBA1* and structural genes in the transgenic leaves. Significant differences (LSD) between means of the transgenic lines and wild type are indicated by asterisks (* $p < 0.05$, ** $p < 0.01$).

light-induced *StMYBA1* was highly correlated with the expression trend of early synthesis genes *CHS* and *CHI* (Figure 4), and the promoter activity of early synthesis genes *StCHS*, *StCHI*, and *StF3H* could be activated by StMYBA1 under light conditions (Figure 5), these results showed that *StMYBA1* has a direct regulatory effect on late synthetic genes. Further gene function analysis found that the anthocyanin accumulation and expression of structural genes in transgenic leaves that overexpressed *StMYBA1* was significantly higher than that of the control (Figure 6). All of these results demonstrate that the *StMYBA1* gene promoted anthocyanins biosynthesis in potato by activating the expression of structural genes under light conditions (Figure 7). These findings provide a theoretical basis and genetic resources for the regulatory mechanism of anthocyanin biosynthesis in potato.

StMYBA1 can activate the expression of early biosynthetic genes of anthocyanin biosynthesis *StCHS*, *StCHI*, and *StF3H*, while the expression of late synthesis gene *StF3'5'H* has no significant difference in the early stage of light induction, and its expression increases rapidly at 48 hours (Table S2). It is speculated that StMYBA1 activates the expression of the early synthesis gene, resulting in the accumulation of dihydrokaempferol, and further generating delphinidin from dihydrokaempferol with the participation of StF3'5'H. The expression of the late synthetic gene *StF3'H* increased at 6 hours of light induction, and then the expression was relatively stable (Table S2), but the purple anthocyanin cyanidin controlled by StF3'H did not accumulate. This indicates that the anthocyanins accumulation in tubers induced by light requires the regulation of other transcription factors on late synthetic genes besides the *StMYBA1* gene. Therefore, the transcription factors in cluster 3 which are highly correlated with the expression of *StF3'5'H* may be involved in the regulation of anthocyanin biosynthesis. Previous studies showed that the *StWRKY13* gene (Soltu.DM.10G023760.1) and *StbHLH1* (Soltu.DM.09G019660.1) gene in cluster 3 could indeed regulate anthocyanin biosynthesis in potato (Liu et al., 2016; Zhang et al., 2022).

During light induction, RM-210 tuber peel turned into purple gradually, and anthocyanin content showed that only delphinidin content increased, but other components did not (Figure 1 and Figure

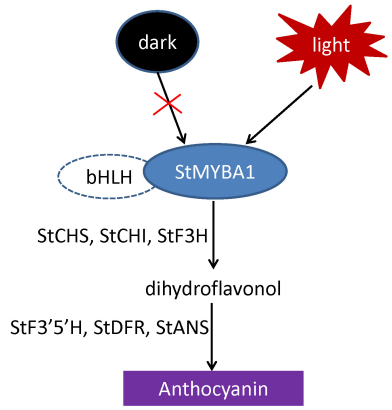

FIGURE 7
The regulatory model of *StMYBA1* gene on potato anthocyanin biosynthesis.

S1). This is consistent with the results in apple, which showed low intensity would change the color of apple peel, only the content of cyanidin increased. The content of other anthocyanins did not change (Chen et al., 2019). Most of the key genes in transcriptome data are mined using multiple analysis methods (Qi et al., 2021; Zheng et al., 2021). In this study, we used the similar approach. The co-expression cluster analysis indicated that the expression of *StMYBA1* strongly correlated with that of the structural genes *StCHS* and *StCHI* (Figure 4B). Therefore, it is speculated that the *StMYBA1* gene may be the key factor in regulating light-induced anthocyanin synthesis in potato.

Different from RM-210 tubers, the contents of pelargonidin and cyanidin in potato leaves overexpressing *StMYBA1* also increased significantly (Figure 6B). It may be that the different genetic backgrounds of RM-210 and AC142 lead to the different regulation modes of *StMYBA1*. The promoter activity of late synthetic genes could not be activated by StMYBA1, but their expression in transgenic leaves increased (Figures 6H–K), indicating that StMYBA1 is an indirect regulator of late synthetic genes or might need to be regulated together with bHLH in the form of complexes. Previous studies also showed that most MYB genes regulate anthocyanin biosynthesis in the form of complexes (Liu et al., 2016; Liu et al., 2021; Qin et al., 2022). However, the specific regulation mode of the *StMYBA1* gene needs to be further studied.

Data availability statement

The data presented in the study are deposited in the Harvard Dataverse repository, and the original fpkm value of RNA-seq can be obtained through the website https://dataverse.harvard.edu/dataset.xhtml?persistentId=doi:10.7910/DVN/PYOK2T.

Author contributions

BS and CH designed the research. SL performed anthocyanin content determination. YZ performed transient assays. XZ performed the potato transformation. XH and TL analyzed the data. XZ analyzed gene expression. XZ, HZ and YL wrote the article. All authors contributed to the article and approved the submitted version.

Funding

This work was supported by grants from the China Agriculture Research System of MOF and MARA (CARS-09), the Training Plan for Young Backbone Teachers in the Colleges and Universities of Henan Province (2021GGJS049).

Conflict of interest

The authors declare that the research was conducted in the absence of any commercial or financial relationships that could be construed as a potential conflict of interest.

Publisher's note

Supplementary material

The Supplementary Material for this article can be found online at: https://www.frontiersin.org/articles/10.3389/fpls.2023.1087121/full#supplementary-material

SUPPLEMENTARY FIGURE 1
The HPLC chromatograms of 6 anthocyanins in RM-210 tubers.

SUPPLEMENTARY FIGURE 2
Quantitative analysis of transcript levels of differentially expressed genes (DEGs) in RM-210 tubers light-induced. Each column represents the mean value ± standard error (n = 3).

SUPPLEMENTARY FIGURE 3
Screening of StMYBA1-overexpressed transgenic lines. **(A)** Regeneration bud from the microtuber of potato. **(B)** Rooting screening of transgenic lines. **(C)** The relative expression of the *StMYBA1* gene in the transgenic lines. Each column represents the mean value ± standard error (n = 3). **(D)** Growth status of transgenic plants and the untransformed control. Bars=2 cm.

References

Allan, A. C., Hellens, R. P., and Laing, W. A. (2008). MYB transcription factors that colour our fruit. *Trends Plant Sci.* 13, 99–102. doi: 10.1016/j.tplants.2007.11.012

An, J., Qu, F., Yao, J., Wang, X., You, C., Wang, X., et al. (2017). The bZIP transcription factor MdHY5 regulates anthocyanin accumulation and nitrate assimilation in apple. *Hortic. Res.* 4, 17056. doi: 10.1038/hortres.2017.23

Azuma, A., Yakushiji, H., Koshita, Y., and Kobayashi, S. (2012). Flavonoid biosynthesis-related genes in grape skin are differentially regulated by temperature and light conditions. *Planta* 236, 1067–1080. doi: 10.1007/s00425-012-1650-x

Baudry, A., Heim, M., Dubreucq, B., Caboche, M., Weisshaar, B., and Lepiniec, L. (2004). TT2, TT8, and TTG1 synergistically specify the expression of BANYULS and proanthocyanidin biosynthesis in arabidopsis thaliana. *Plant J.* 39, 366–380. doi: 10.1111/j.1365-313X.2004.0213

Borevitz, J. O., Xia, Y., Blount, J., Dixon, R. A., and Lamb, C. (2000). Activation tagging identifies a conserved MYB regulator of phenylpropanoid biosynthesis. *Plant Cell.* 12, 2383–2394. doi: 10.1105/tpc.12.12.2383

Brown, C. R. (2005). Antioxidants in potato. *Am. J. Potato Res.* 82, 163–172. doi: 10.1007/BF02853654

Catala, R., Medina, J., and Salinas, J. (2011). Integration of low temperature and light signaling during cold acclimation response in arabidopsis. *P. Natl. A. Sci. India. B.* 108, 16475–16480. doi: 10.1073/pnas.1107161108

Chen, C., Chen, H., Zhang, Y., Thomas, H., Frank, M., He, Y., et al. (2020). TBtools: An integrative toolkit developed for interactive analyses of big biological data. *Mol. Plant* 13, 1194–1202. doi: 10.1016/j.molp.2020.06.009

Chen, W., Zhang, M., Zhang, G., Li, P., and Ma, F. (2019). Differential regulation of anthocyanin synthesis in apple peel under different sunlight intensities. *Int. J. Mol. Sci.* 20, 6060. doi: 10.3390/ijms20236060

Cominelli, E., Gusmaroli, G., Allegra, D., Galbiati, M., Wade, H. K., Jenkins, G. I., et al. (2008). Expression analysis of anthocyanin regulatory genes in response to different light qualities in arabidopsis thaliana. *J. Plant Physiol.* 165, 886–894. doi: 10.1016/j.jplph.2007.06.010

Crowe, F., Roddam, A., Key, T., Appleby, P., Overvad, K., Jakobsen, M., et al. (2011). Fruit and vegetable intake and mortality from ischaemic heart disease: Results from the European prospective investigation into cancer and nutrition (EPIC)-heart study. *Eur. Heart J.* 32, 1235–1243. doi: 10.1093/eurheartj/ehq465

Cui, D., Zhao, S., Xu, H., Allan, A., Zhang, X., Fan, L., et al. (2021). The interaction of MYB, bHLH and WD40 transcription factors in red pear (Pyrus pyrifolia) peel. *Plant Mol. Biol.* 106, 407–417. doi: 10.1007/s11103-021-01160-w

Espley, R., Hellens, R., Putterill, J., Stevenson, D., Kutty-Amma, S., and Allan, A. (2007). Red colouration in apple fruit is due to the activity of the MYB transcription factor, MdMYB10. *Plant J.* 49, 414–427. doi: 10.1111/j.1365-313X.2006.02964.x

Fossen, T., and Andersen, M. (2000). Anthocyanins from tubers and shoots of the purple potato, solanum tuberosum. *J. Hortic. Sci. Biotech.* 75, 360–363. doi: 10.1080/14620316.2000.11511251

Gonzalez, A., Zhao, M., Leavitt, J. M., and Lloyd, A. M. (2008). Regulation of the anthocyanin biosynthetic pathway by the TTG1/bHLH/Myb transcriptional complex in arabidopsis seedlings. *Plant J.* 53, 814–827. doi: 10.1111/j.1365-313X.2007.03373.x

Guo, D., Yu, Y., Xi, F., Shi, Y., and Zhang, G. (2016). Histological and molecular characterization of grape early ripening bud mutant. *Int. J. Genomics* 56, 20106. doi: 10.1155/2016/5620106

He, J., and Giusti, M. M. (2010). Anthocyanins: Natural colorants with health-promoting properties. *Annu. Rev. Food Sci. Technol.* 1, 163–187. doi: 10.1146/annurev.food.080708.100754

Jiang, S., Sun, Q., Zhang, T., Liu, W., Wang, N., and Chen, X. (2021). MdMYB114 regulates anthocyanin biosynthesis and functions downstream of MdbZIP4-like in apple fruit. *J. Plant Physiol.* 257, 153353. doi: 10.1016/j.jplph.2020.153353

Jung, C., Griffiths, H., De Jong, D., Cheng, S., Bodis, M., and De Jong, W. (2005). The potato p locus codes for flavonoid 3′5′-hydroxylase. *Theor. Appl. Genet.* 110, 269–275. doi: 10.1007/s00122-004-1829-z

Jung, C. S., Griffiths, H. M., De Jong, D. M., Cheng, S., Bodis, M., Kim, T. S., et al. (2009). The potato developer (D) locus encodes an R2R3 MYB transcription factor that regulates expression of multiple anthocyanin structural genes in tuber skin. *Theor. Appl. Genet.* 120, 45–57. doi: 10.1007/s00122-009-1158-3

Lai, Y., Li, H., and Yamagishi, M. (2013). A review of target gene specificity of flavonoid R2R3-MYB transcription factors and a discussion of factors contributing to the target gene selectivity. *Front. Biol.* 8, 577–598. doi: 10.1007/s11515-013-1281-z

Li, Y., Mao, K., Zhao, C., Zhao, X., Zhang, H., Shu, H., et al. (2012). MdCOP1 ubiquitin E3 ligases interact with MdMYB1 to regulate light-induced anthocyanin biosynthesis and red fruit coloration in apple. *Plant Physiol.* 160, 1011–1022. doi: 10.1104/pp.112.199703

Li, J., Ren, L., Gao, Z., Jiang, M., Liu, Y., Zhou, L., et al. (2017). Combined transcriptomic and proteomic analysis constructs a new model for light-induced anthocyanin biosynthesis in eggplant (Solanum melongena l.). *Plant Cell Environ.* 40, 3069–3087. doi: 10.1111/pce.13074

Liu, Y., Lin-Wang, K., Espley, R. V., Wang, L., Yang, H., Yu, B., et al. (2016). Functional diversification of the potato R2R3 MYB anthocyanin activators AN1, MYBA1, and MYB113 and their interaction with basic helix-loop-helix cofactors. *J. Exp. Bot.* 67, 2159–2176. doi: 10.1093/jxb/erw014

Liu, Y., Ma, K., Qi, Y., Lv, G., Ren, X., Liu, Z., et al. (2021). Transcriptional regulation of anthocyanin synthesis by MYB-bHLH-WDR complexes in kiwifruit (Actinidia chinensis). *J. Agr. Food Chem.* 69, 3677–3691. doi: 10.1021/acs.jafc.0c07037

Liu, H., Su, J., Zhu, Y., Yao, G., Allan, A., Ampomah-Dwamena, C., et al. (2019). The involvement of PybZIPa in light-induced anthocyanin accumulation *via* the activation of PyUFGT through binding to tandem G-boxes in its promoter. *Hortic. Res.* 6, 134. doi: 10.1038/s41438-019-0217-4

Liu, Y., Tikunov, Y., Schouten, R. E., Marcelis, L. F. M., Visser, R. G. F., and Bovy, A. (2018). Anthocyanin biosynthesis and degradation mechanisms in solanaceous vegetables: A review. *Front. Chem.* 6. doi: 10.3389/fchem.2018.00052

Liu, Y., Wang, L., Zhang, J., Yu, B., Wang, J., and Wang, D. (2017). The MYB transcription factor StMYBA1 from potato requires light to activate anthocyanin biosynthesis in transgenic tobacco. *J. Plant Biol.* 60, 93–101. doi: 10.1007/s12374-016-0199-9

Lloyd, A., Brockman, A., Aguirre, L., Campbell, A., Bean, A., Cantero, A., et al. (2017). Advances in the MYB-bHLH-WD repeat (MBW) pigment regulatory model: Addition of a WRKY factor and co-option of an anthocyanin MYB for betalain regulation. *Plant Cell Physiol.* 58, 1431–1441. doi: 10.1093/pcp/pcx075

Maier, A., Schrader, A., Kokkelink, L., Falke, C., Welter, B., Iniesto, E., et al. (2013). Light and the E3 ubiquitin ligase COP1/SPA control the protein stability of the MYB transcription factors PAP1 and PAP2 involved in anthocyanin accumulation in arabidopsis. *Plant J.* 74, 638–651. doi: 10.1111/tpj.12153

Patro, R., Duggal, G., Love, M., Irizarry, R., and Kingsford, C. (2017). Salmon provides fast and bias-aware quantification of transcript expression. *Nat. Methods* 14, 417–419. doi: 10.1038/nmeth.4197

Qi, Y., Li, C., Duan, C., Gu, C., and Zhang, Q. (2021). Integrated metabolomic and transcriptomic analysis reveals the flavonoid regulatory network by eutrema EsMYB90. *Int. J. Mol. Sci.* 22, 8751. doi: 10.3390/ijms22168751

Qin, J., Zhao, C., Wang, S., Gao, N., Wang, X., Na, X., et al. (2022). PIF4-PAP1 interaction affects MYB-bHLH-WD40 complex formation and anthocyanin accumulation in arabidopsis. *J. Plant Physiol.* 268, 153558. doi: 10.1016/j.jplph.2021.153558

Sivankalyani, V., Feygenberg, O., Diskin, S., Wright, B., and Alkan, N. (2016). Increased anthocyanin and flavonoids in mango fruit peel are associated with cold and pathogen resistance. *Postharvest Biol. Technol.* 11, 132–139. doi: 10.1016/j.postharvbio.2015.08.001

Si, H., Xie, C., and Liu, J. (2003). An efficient protocol for agrobacterium-mediated transformation with microtuber and the introduction of an antisense class I patatin gene into potato. *Acta Agronomica Sinica.* 29, 801–805. doi: 10.4141/cjps07031

Takos, A. M., Jaffe, F. W., Jacob, S. R., Bogs, J., Robinson, S. P., and Walker, A. R. (2006). Light-induced expression of a MYB gene regulates anthocyanin biosynthesis in red apples. *Plant Physiol.* 142, 1216–1232. doi: 10.1104/pp.106.088104

Vandesompele, J., De Preter, K., Pattyn, F., Poppe, B., Van Roy, N., De Paepe, A., et al. (2002). Accurate normalization of real-time quantitative RT-PCR data by geometric averaging of multiple internal control genes. *Genome Biol.* 3, 34. doi: 10.1186/gb-2002-3-7-research0034

Wang, W., Wang, P., Li, X., Wang, Y., Tian, S., and Qin, G. (2021). The transcription factor SlHY5 regulates the ripening of tomato fruit at both the transcriptional and translational levels. *Hortic. Res.* 8, 83. doi: 10.1038/s41438-021-00523-0

Wang, Y., Zhang, X., Zhao, Y., Yang, J., He, Y., Li, G., et al. (2020). Transcription factor PyHY5 binds to the promoters of PyWD40 and PyMYB10 and regulates its expression in red pear 'Yunhongli no. 1'. *Plant Physiol. Biochem.* 154, 665–674. doi: 10.1016/j.plaphy.2020.07.008

Yao, P., Huang, Y., Dong, Q., Wan, M., Wang, A., Chen, Y., et al. (2020). FtMYB6, a light-induced SG7 R2R3-MYB transcription factor, promotes flavonol biosynthesis in tartary buckwheat (Fagopyrum tataricum). *J. Agric. Food Chem.* 68, 13685–13696. doi: 10.1021/acs.jafc.0c03037

Yao, G., Ming, M., Allan, A. C., Gu, C., Li, L., Wu, X., et al. (2017). Map-based cloning of the pear gene MYB114 identifies an interaction with other transcription factors to coordinately regulate fruit anthocyanin biosynthesis. *Plant J.* 92, 437–451. doi: 10.1111/tpj.13666

Zhang, Y., Cheng, S., De Jong, D., Griffiths, H., Halitschke, R., and De Jong, W. (2009). The potato r locus codes for dihydroflavonol 4-reductase. *Theor. Appl. Genet.* 119, 931–937. doi: 10.1007/s00122-009-1100-8

Zhang, B., Hu, Z. L., Zhang, Y. J., Li, Y. L., Zhou, S., and Chen, G. P. (2012). A putative functional MYB transcription factor induced by low temperature regulates anthocyanin biosynthesis in purple kale (Brassica oleracea var. acephala f. tricolor). *Plant Cell Rep.* 31, 281–289. doi: 10.1007/s00299-011-1162-3

Zhang, H., Liu, J., Hou, J., Yao, Y., Lin, Y., Ou, Y., et al. (2014). The potato amylase inhibitor gene SbAI regulates cold-induced sweetening in potato tubers by modulating amylase activity. *Plant Biotechnol. J.* 12, 984–993. doi: 10.1111/pbi.12221

Zhang, H., Zhang, Z., Zhao, Y., Guo, D., Zhao, X., Gao, W., et al. (2022). StWRKY13 promotes anthocyanin biosynthesis in potato (Solanum tuberosum) tubers. *Funct. Plant Biol.* 49, 102–114. doi: 10.1071/FP21109

Zhang, H., Zhao, X., Zhang, J., Yang, B., Yu, Y., Liu, T., et al. (2020). Functional analysis of an anthocyanin synthase gene StANS in potato. *Sci. Hortic.* 272, 109569. doi: 10.1016/j.scienta.2020.109569

Zheng, Q., Chen, W., Luo, M., Xu, L., Zhang, Q., and Luo, Z. (2021). Comparative transcriptome analysis reveals regulatory network and regulators associated with proanthocyanidin accumulation in persimmon. *BMC Plant Biol.* 21, 356. doi: 10.1186/s12870-021-03133-z

Zhou, L., Zeng, H., Shi, M., and Xie, D. (2008). Development of tobacco callus cultures over expressing arabidopsis PAP1/MYB75 transcription factor and characterization of anthocyanin biosynthesis. *Planta* 229, 825–837. doi: 10.1007/s00425-008-0809-y

frontiers | Frontiers in Plant Science

TYPE Original Research
PUBLISHED 23 February 2023
DOI 10.3389/fpls.2023.1075042

OPEN ACCESS

EDITED BY
Tong Chen,
Institute of Botany (CAS), China

REVIEWED BY
Gang Yu,
Shanghai Jiao Tong University, China
Doron Teper,
Agricultural Research Organization (ARO), Israel

*CORRESPONDENCE
Bingsen Wang
wangbingsen@webmail.hzau.edu.cn
Huilan Chen
chenhuilan@mail.hzau.edu.cn

†These authors have contributed equally to this work and share first authorship

SPECIALTY SECTION
This article was submitted to Crop and Product Physiology, a section of the journal Frontiers in Plant Science

RECEIVED 20 October 2022
ACCEPTED 13 February 2023
PUBLISHED 23 February 2023

CITATION
Huang M, Tan X, Song B, Wang Y, Cheng D, Wang B and Chen H (2023) Comparative genomic analysis of *Ralstonia solanacearum* reveals candidate avirulence effectors in HA4-1 triggering wild potato immunity. *Front. Plant Sci.* 14:1075042. doi: 10.3389/fpls.2023.1075042

Comparative genomic analysis of *Ralstonia solanacearum* reveals candidate avirulence effectors in HA4-1 triggering wild potato immunity

Mengshu Huang[1,2,3†], Xiaodan Tan[1,2,3,4†], Botao Song[1,2,3], Yuqi Wang[1,2,3], Dong Cheng[1,2,3], Bingsen Wang[1,2,3*] and Huilan Chen[1,2,3*]

[1]National Key Laboratory for Germplasm Innovation & Utilization of Horticultural Crops, Huazhong Agricultural University, Wuhan, Hubei, China, [2]Key Laboratory of Potato Biology and Biotechnology (HZAU), Ministry of Agriculture and Rural Affairs, Wuhan, Hubei, China, [3]College of Horticulture and Forestry Science, Huazhong Agricultural University, Wuhan, Hubei, China, [4]Guangdong University Key Laboratory for Sustainable Control of Fruit and Vegetable Diseases and Pests & Key Laboratory of Green Prevention and Control on Fruits and Vegetables in South China, Ministry of Agriculture and Rural Affairs, Zhongkai University of Agriculture and Engineering, Guangzhou, China

Ralstonia solanacearum is the causal agent of potato bacterial wilt, a major potato bacterial disease. Among the pathogenicity determinants, the Type III Secretion System Effectors (T3Es) play a vital role in the interaction. Investigating the avirulent T3Es recognized by host resistance proteins is an effective method to uncover the resistance mechanism of potato against *R. solanacearum*. Two closely related *R. solanacearum* strains HA4-1 and HZAU091 were found to be avirulent and highly virulent to the wild potato *Solanum albicans* 28-1, respectively. The complete genome of HZAU091 was sequenced in this study. HZAU091 and HA4-1 shared over 99.9% nucleotide identity with each other. Comparing genomics of closely related strains provides deeper insights into the interaction between hosts and pathogens, especially the mechanism of virulence. The comparison of type III effector repertoires between HA4-1 and HZAU091 uncovered seven distinct effectors. Two predicted effectors RipA5 and the novel effector RipBS in HA4-1 could significantly reduce the virulence of HZAU091 when they were transformed into HZAU091. Furthermore, the pathogenicity assays of mutated strains HA4-1 ΔRipS6, HA4-1 ΔRipO1, HA4-1 ΔRipBS, and HA4-1 ΔHyp6 uncovered that the absence of these T3Es enhanced the HA4-1 virulence to wild potato *S. albicans* 28-1. This result indicated that these T3Es may be recognized by *S. albicans* 28-1 as avirulence proteins to trigger the resistance. In summary, this study provides a foundation to unravel the *R. solanacearum*-potato interaction and facilitates the development of resistance potato against bacterial wilt.

KEYWORDS

***Ralstonia solanacearum*-potato interaction, bacterial resistance, avirulence effector, comparative genomics, type III effectors**

Introduction

Bacterial wilt disease, previously known as brown rot, is caused by the Gram-negative bacteria *Ralstonia solanacearum*. The *R. solanacearum* species complex (RSSC), one of the most harmful bacterial diseases that affect the production of many important crops worldwide, has a broad range of hosts varying from dicots to monocots. A report showed that RSSC could infect more than 250 plant species from 54 families in the world (Prior et al., 2016). According to the survey of the International Potato Center, bacterial wilt is one of the five biggest challenges affecting potato (*Solanum tuberosum* L.) yield in tropical and subtropical regions, which can account for up to 75% yield of losses (Rich, 1983; Wale et al., 2008; Patil et al., 2012). Some wild potato species and cultivated varieties are resistant or highly tolerant to bacterial wilt, such as *S. chacoense*, *S. microdontum*, *S. phureja*, *S. stenotonum*, and BR clones (the hybrid offspring containing the germplasms of *S. phuerja* and *S. demissum* are resistant to both bacterial wilt disease and late blight disease) and varieties (Machida-Hirano, 2015). The poor adaptability to various regions and the ineffectiveness against all strains of the pathogen hinder the wide application of these resistance resources (Prior et al., 1998; Wang et al., 2017). Taxonomists classified the RSSC into three species: *R. solanacearum* (phylotype II), *R. pseuosolanacearum* (phylotype I and III), and *R. syzygii* (phylotype IV) based on their phylotype and the geographical distribution (Genin and Denny, 2012; Safni et al., 2014).

Comparative genomics is a powerful tool for researchers to explore biological problems and explain biological phenomena. With the rapid increase in high-quality genomes, the application of comparative genomics is more and more extensive and in-depth (Setubal et al., 2018). So far, comparative genomics has been used in various species such as the Zoonotic pathogen *Ehrlichia chaffeensis*, revealing candidate effectors and putative host cell targets (Noroy and Meyer, 2017). The complete genome of seven highly virulent *Xanthomonas. translucens* strains have been obtained, and the T3Es were identified, giving an insight into the pathovar-specific population structure (Shah et al., 2021). The comparative genome analysis of *Clavibacter michiganensis*, the causal agent of bacterial canker in tomatoes, shows the distinct gene contents in the plasmids (Oh et al., 2022). The first *R. solanacearum* genome GMI1000 was sequenced in 2002 and has been widely utilized in *R. solanacearum* studies (Salanoubat et al., 2002). Up to now, over 300 *R. solanacearum* genomes have been sequenced and uploaded to NCBI (Genome List - Genome - NCBI), giving enriched information to uncover the similarities and differences among the strains. The comparative genome research of *R. solanacearum* has been divided into two ways: 1. A few genomes of the strains possess different pathogenicity to the host, such as PeaFJ1 and HA4-1 (Wan and Yang, 2022); 2. Meta-analysis of multiple genomes to discover the evolutionary relationships, phylogeny, and populations since individual strains vary in multiple conditions. For example, 100 RSSC genomes have been analyzed to highlight the evolution and diversity of *R. solanacearum* (Sharma et al., 2022). As many as 150 sequenced *R. solanacearum* strains have been used to analyze the T3Es repertoires, and the comparative genomics strategy has been proven to be useful with the identification of eight new T3Es and two new hypothetical T3Es (Sabbagh et al., 2019).

R. solanacearum possesses many kinds of virulent factors, such as the pili, exopolysaccharide (EPS), and genes that can express compounds to overcome host stress (Genin and Denny, 2012). Type III secretion system (T3SS) is one of the most important and generally acknowledged virulence factors utilized in plant-microbe interactions. T3SS is a syringe-like structure that delivers effectors into the cytoplasm or the plasma membrane of a plant cell (Deng et al., 2017). The proteins secreted from T3SS are called type III secretion system effectors (T3Es). *R. solanacearum* has more than 100 T3Es that can affect plant immunity by suppressing or triggering the plant defense response, targeting and modulating the plant metabolism by various molecular mechanisms (Landry et al., 2020). The methods of identifying T3Es are as followed: 1. Homology search using amino acid sequences of previously reported effectors; 2. Identification of the *hrpII* box (TTCGn16TTCG) or PIP (plant-induced promoter) box in the promoters (Cunnac et al., 2004); 3. Based on gene expression, such as the experiment using a Calmodulin-dependent adenylate cyclase (Cya) reporter system (Mukaihara et al., 2010); 4. Bioinformatics prediction approaches with gradually improved databases, such as "Ralsto T3E" (Peeters et al., 2013). Plant resistance against bacterial disease usually depends on the hosts successfully perceiving the avirulent effectors (Flor, 1971). More and more research on *R. solanacearum* avirulent effectors has been reported in *Solanum* species, such as RipJ, RipAX2, and RipAZ1 in tomato, eggplant, and black nightshade. The first avirulent gene to trigger bacterial resistance in tomato *Solanum pimpinellifolium* LA2093 was RipJ (Pandey et al., 2021). RipAZ1 confers avirulence in black nightshade *S. americanum* and triggers cell death on the leaves (Moon et al., 2021). RipAX2 is a highly prevalent effector avirulent in eggplant AG91-25, which possesses a major resistance locus *EBWR9* (Morel et al., 2018). However, the effectors of *R. solanacearum* that regulate and trigger potato resistance remain unclear.

Our previous study sequenced the genome of *R. solanacearum* strain HA4-1 and found that HA4-1 and another *R. solanacearum* strain, GMI1000, were avirulent and highly virulent to the wild potato species *Solanum albicans* 28-1 (ALB28-1), respectively (Tan et al., 2019). This result indicated that HA4-1 may contain avirulence effectors that could be recognized by resistant proteins in ALB28-1. In this study, we found that a novel *R. solanacearum* strain HZAU091 isolated from potato also displayed strong virulence to *Solanum albicans* 28-1. HZAU091 is more closely related to HA4-1 (PeaHuB4) than GMI1000 based on the genetic and pathogenic diversity analysis (Wang et al., 2017). To reveal the avirulence effectors triggering potato immunity, the complete genome of HZAU091 was sequenced to perform comparative genomic analysis and T3E repertoire analysis with HA4-1. Mutant strains and the virulent strain HZAU091 carrying effectors from HA4-1 were constructed to verify the candidate avirulence effectors by inoculation experiments.

Materials and methods

Plant materials and bacterial strains

The potato seedlings of *Solanum albicans* 28-1 (ALB28-1) were cultivated in Murashige-Skoog (MS) medium (supplemented with 4% sucrose and 0.75% agar) and grown for approximately 3 weeks

in vitro at 20 ± 1°C with a 16 h/8 h (day/night) regime. The seedlings were then transferred into pots containing nutritional soil (ShangDao DB37/T1142-2008) and grown in a greenhouse at 22 ± 2°C. After 3-4 weeks, the seedlings having 5-7 full-grown leaves were transferred to an inoculation room and grown at 28°C. All the experiments were performed according to the experiment security regulations of Huazhong Agricultural University (HZAU) and approved by the biosafety committee in HZAU.

Ralstonia solanacearum strains were incubated on BG medium [10 g/L peptone, 2.5 g/L glucose, and 1 g/L casamino acids] and BGT medium [BG, 50 mg/L triphenyltetrazolium chloride (TTC), and 15 g/L agar], 200 revolutions per minute overnight according to Tan (Tan et al., 2019). All strains used in this study are listed in Table S1 (see supporting information). The HZAU091 transformed strains were created by 2.5KV, 6.0 ms electroporation, which introduced the plasmids containing the candidate effectors with their native promoters into the HZAU091 competent cells. Two days later, the clones were tested and confirmed by polymerase chain reaction.

Genome sequencing of HZAU091 and prediction methods of T3Es in *R. solanacearum*

The genome sequencing was performed by combined technologies including PacBio RS II and Illumina HiSeq2000. The single molecule real-time (SMRT) sequencing was performed on the PacBio RS II platform with a 20 kb library. A paired-end library with an insert size of 400 bp was sequenced using an Illumina HiSeq2000 using PE150 strategy.

The platform and bioinformatics methods were listed in Table S2 (see supporting information). Since "Ralsto T3E" was the website specially developed for *R. solanacearum* strains, it was chosen for the main prediction. Three other prediction software platforms MAUVE, BRIG-0.95 (BLAST options is -evalue $1e^{-5}$), FastANI (fastANI -q genome1.fa -r genome2.fa -o output.txt -FragLen), and the representative genome GMI1000 were utilized to predict and rectify the prediction result of the T3Es in HA4-1 and HZAU091. Each predicted T3E gene of HZAU091 was then amplified by polymerase chain reaction and confirmed or corrected by sanger sequencing.

Pathogenicity analysis

After the ALB28-1 seedlings experienced 2 days of adaptation to the higher temperature, ALB28-1 wild potato plants were inoculated with fresh *R. solanacearum* strain suspensions at OD_{600} = 0.1 (≈1 × 10^8 CFU/mL). For the inoculation assay, 10 mL of prepared bacterial suspension was added into the soil matrix around the roots, cutting with a sterile knife beside the stem (about 4cm) to the 5cm depth. Negative controls were roots wounded as above mentioned and inoculated with sterile water. These pathogenicity assays were repeated at least three times in a 28°C inoculation room in HZAU.

The virulence of the strains was evaluated using the Disease Index (DI) and Area under Disease Progress Curve (AUDPC) according to Wang (Wang et al., 2017). The disease index of each plant was then recorded every 2 days consecutively for 3 weeks after infection, using the scales as previously reported (Tan et al., 2019). More than six plants from each potato line were inoculated. The significance treatments of DI values were identified using the method of student's *t* test by GraphPad Prism 9.0.0. AUDPC values were estimated by SPSS 22.0. Means were compared through student's *t* test (p = 0.05).

For the virulence/hypersensitive response assay of the strains on wild potato leaves, fresh *R. solanacearum* strain suspensions at OD600 = 0.1 (≈1 × 10^8CFU/mL) were infiltrated into 12 well-expanded 4 weeks-old ALB28-1 leaves.

Colony morphological observation and growth curve measurement of the *R. solanacearum* strains

The morphology of the bacterial clones used in this study (Table S1) was determined using bacterial suspension in the exponential phase, which was diluted, spread onto the TTC medium, and then incubated at 28 °C overnight. To measure the growth curve, 20 mL of BG liquid medium with the bacterial suspension at the starting OD_{600} = 0.05 in a conical flask was cultured under shaking conditions at 200 rpm and 28°C. Every two hours, 100 µL of bacterial growing culture was pipetted out and added to 900 µL BG liquid to measure the absorbance value at 600 nm. This experiment was repeated four times.

cAMP concentration assay

The adenylate cyclase assay was performed as previously described with minor modifications (Mukaihara et al., 2010; Zheng et al., 2019). Five µL of bacterial culture at 1×10^8CFU/mL density of strain HA4-1 and derivatives harboring plasmids were infiltrated into the cutting surface of potato tubers freshly harvested from the field at Huazhong Agriculture University. The tissues were sampled after 28 days of injection. cAMP levels were monitored with a cAMP enzyme immunoassay kit 523 (New east biosciences, PA, USA) according to the instruction.

Mutagenesis and complementation of *R. solanacearum*

The mutagenesis of effectors in HA4-1 strain was performed as previously described (Cheng et al., 2021). To generate a mutant of the *R. solanacearum* target effector gene, the effector gene was replaced with a cassette harboring spectinomycin resistance. The genome fragment containing the target gene and its two flanking regions was amplified from the strain HA4-1 genome and then was cloned into pCE2-TA-Blunt-Zero vector (Vazyme 5min™ TA/Blunt-Zero Cloning Kit C601-01/02). A reverse amplification of the above recombinant vector was performed to delete the target gene and generate a linear vector only with the flanking region of the effector. A spectinomycin resistance gene (Spe) was connected

with the linear to replace the target gene. The mutant plasmid was successfully constructed. Then the spectinomycin cassette with the effector flanking regions was generated, which was used to be transformed into *R. solanacearum* competent cells to replace the target effector gene.

To generate the effector complementation strain, the coding sequences with their native promoters and a Km^r cassette were cloned into the plasmid pH7C and then the fragments containing the coding sequences with the effector promoters and the antibiotic gene were amplified and inserted into a permissive chromosome site by transferred into the mutant competent cell, as described previously (Monteiro et al., 2012).

Results

HA4-1 and HZAU091 were closely-related and exhibited different virulence levels

The phylotype I strain of HA4-1 has been identified as an avirulent strain to *Solanum albicans* 28-1 (ALB28-1) which showed a close relationship to the strain HZAU091 (Wang et al., 2017; Tan et al., 2019). To test the resistance of ALB28-1 to HZAU091, we performed the inoculation parallel to HA4-1 and GMI1000. As shown in Figure 1A, ALB28-1 inoculated with HA4-1 grew healthy, while plants inoculated with either HZAU091 or GMI1000 showed wilting symptoms after 12 days of inoculation (Figure 1A). The disease index also illustrated that HZAU091 was a virulent strain to ALB28-1 (Figure 1B). The disease index of the ALB28-1 after 20 days of the inoculation indicated that ALB28-1 was susceptible to HZAU091 and GMI1000 while resistant to HA4-1 (Figure 1C). Considering that HZAU091 has a closer genetic relationship with HA4-1 than GMI1000, HZAU091 was selected for an in-depth comparison with HA4-1 to explore the avirulence factors for wild potato. To reveal the mechanism triggering potato immunity, leaves of ALB28-1 plants were inoculated with *R. solanacearum* strains HA4-1 and HZAU091, and resulted in a hypersensitive response (HR) reaction with the former one, while not with the latter. When *hrpB* gene, the core component of the type III secretion system of HA4-1 was mutated, HR was no longer triggered (Figure S1). These results also indicated that resistance of ALB28-1 caused by HA4-1 inoculation may be mediated by HA4-1 effector proteins.

The genome of HZAU091 was sequenced and deposited at GenBank under BioSample and Bioproject accession number SAMN28868074 and PRJNA846088, respectively. HZAU091 was composed of a circular chromosome and a megaplasmid. The whole-genome size of HZAU091 was 5,757,034 bp. A total of 5,092 CDS (coding sequence) genes were predicted. Compared to HA4-1, the genome size of HZAU091 was smaller (Table S3, see supporting information). HA4-1 had been proven previously to have a closer relationship with HZAU091 than GMI1000 based on the alignment of the partial endoglucanase (*egl*) sequence (Wang et al., 2017). However, the similarity of these three strains on the genome level remained unclear. To carry out the alignment, Mauve, BRIG, and FastANI were applied (Alikhan et al., 2011; Jain et al., 2018). The collinearity analysis indicated that HZAU091 had fewer gaps in both chromosome and plasmid levels than GMI1000. Apart from the gaps, HZAU091 didn't possess the two inverted regions as GMI1000 possessed (Figures 2A, B). Average Nucleotide Identity (ANI) is an indicator of the comparison of two genomic similarities at nucleotide levels. If the ANI of organisms remarkably presents ≥95%, they belong to the same species (Konstantinidis and Tiedje, 2005). The ANI analysis of the chromosome and plasmid among the three genomes showed that the HA4-1 chromosome sequence had 99.90% nucleotide identity with HZAU091 chromosome while with only 98.85% nucleotide identity with GMI1000. As for megaplasmid comparison, HA4-1 had 99.94% nucleotide identity with HZAU091 while 98.87% with GMI1000 (Figure 2C). Thus, HZAU091 presented a more closely related relationship with HA4-1 than GMI1000 at the genome level.

Comparison of T3Es between HA4-1 and HZAU091 identified seven distinct effectors

With the genomes of an avirulent strain and a virulent strain, we used comparative genomics to identify the core effectors. The

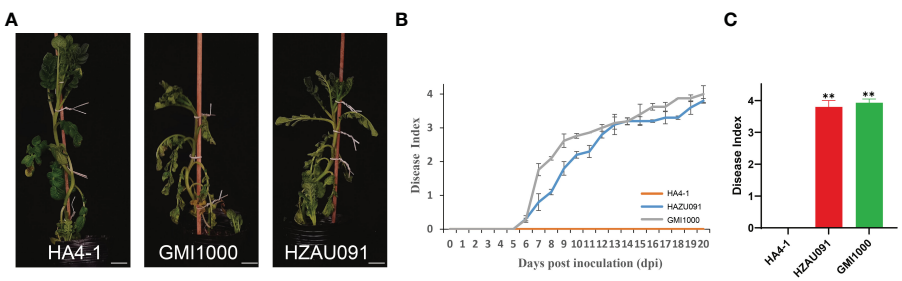

FIGURE 1
Ralstonia solanacearum strains HA4-1, HZAU091, and GMI1000 exhibit significantly different disease progression in the wild potato *Solanum albicans* 28-1 (ALB28-1). **(A)** Photos of ALB28-1 plants 12 days after inoculation with HA4-1, HZAU091, and GMI1000. ALB28-1 inoculated with HA4-1 grew healthy, while plants inoculated with either GMI1000 or HZAU091 showed wilting symptoms. The white scale bar indicates 5 cm. **(B, C)** The disease index of ALB28-1 inoculated with HZAU091, GMI1000, and the avirulent control HA4-1. The concentration of the bacterial suspension was 1×10^8 CFU/mL. **(C)** The disease index of HZAU091, GMI1000, and HA4-1 were quantified at 20 days post inoculation. The asterisks indicate significant differences between virulent strains and the wild-type HA4-1 (Student's *t* test, $^{**}p < 0.01$). All data are presented as mean ± SD for three replicates. The DI values of healthy plants were presented with zero value.

10.3389/fpls.2023.1075042

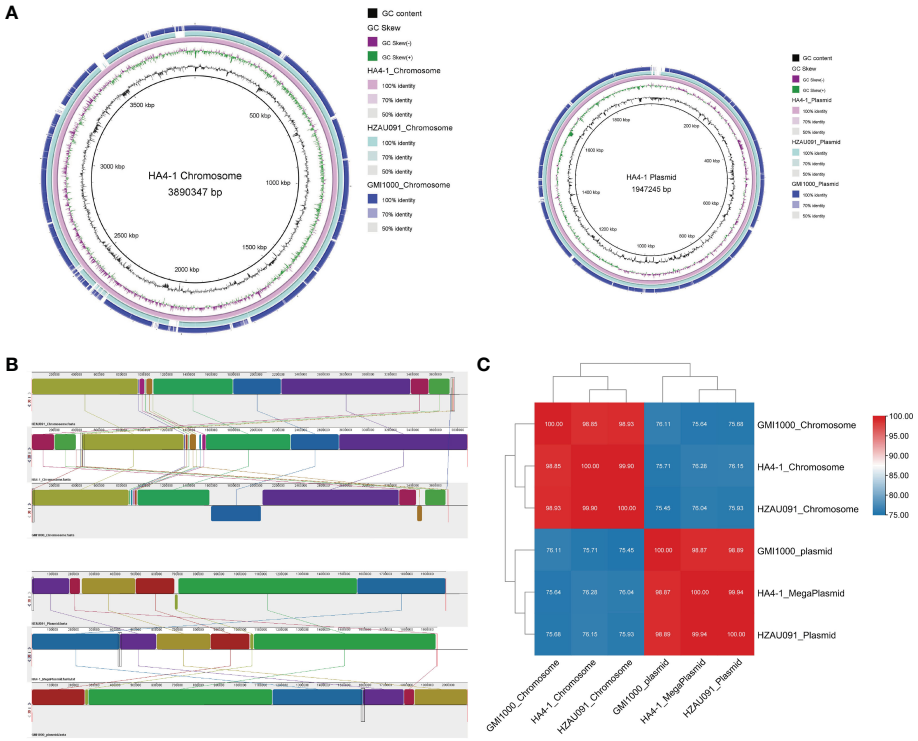

FIGURE 2
Comparative genomics analyses reveal higher similarity of HA4-1 to HZAU091 than to GMI1000. Genome comparisons between HA4-1, HZAU091, and GMI1000 according to the bioinformatics tools BRIG **(A)**, MAUVE **(B)**, and FastANI **(C)**. **(A)** HZAU091 presented a better alignment with HA4-1 than GMI1000 with HA4-1. The circles from inside to the outside represent GC content, GC Skew, HA4-1, HZAU091, and GMI1000. Left, the chromosome comparison among the three genomes. Right, the plasmid comparison among the three genomes. **(B)** Chromosome comparison is shown above, plasmid comparison is shown down. Upper sequence, HZAU091. Medium sequence, HA4-1. Lower sequence, GMI1000. Boxes with the same color indicate the syntenic regions. Boxes below the horizontal line indicate inverted regions. **(C)** The ANI analysis result of HA4-1, HZAU091, and GMI1000.

first step was to identify the T3Es in these two strains. Four prediction software platforms and a representative genome were utilized to predict and rectify the prediction result of the T3Es in HA4-1 and HZAU091. Since "Ralsto T3E" was the website specially developed for *R. Solanacearum* strains, it was chosen for the main prediction (Table S2). The result showed that HA4-1, HZAU091, and GMI1000 possessed 77, 74, and 78 effectors, respectively (Figure 3A). Of them, 71 effectors coexisted in all three genomes. No unique effectors were identified for HZAU091. Each predicted T3E gene of HZAU091 was amplified using polymerase chain reaction and confirmed or corrected by Sanger sequencing. All effectors of HZAU091 were present in the HA4-1 genome. Correspondingly, HA4-1 owned three effectors absent in HZAU091.

Since Hyp6 presented only in HA4-1, it was chosen as a candidate avirulence effector first. Both HA4-1 and HZAU091 had several genes with multiple copies or pseudogenes in the genome. RipO1 and RipBS were chosen among the three genomes based on the different copy numbers in HA4-1 and HZAU091. RipO1 was predicted to have two copies in HA4-1 genome, one copy CFM90_21005 was identical to RipO1^{GMI1000}. Compared with CFM90_21005, RipO1^{HZAU091} had an 1194 bp insertion fragment containing a transposase. We judged the other one CFM90_10880 to be a pseudogene since this copy was <5% similar to RipO1^{GMI1000}, it possessed many mismatches and gaps. Thus, we choose the first copy CFM90_21005 to conduct the following virulence/HR assay of RipO1. RipBS, which possessed three copies in HA4-1, was absent in GMI1000 and presented only identical copy in HZAU091. RipBS had three identical copies in HA4-1 genome positioned in CFM90_18115, CFM90_26330, and CFM90_26510. RipBS was absence in GMI1000, and possessed only one identical copy gene2801 in HZAU091. These three copies were surrounded by the transposases, mobile element proteins, and hypothetical proteins. RipA5, RipO1, and RipS6 both had a transposon in the gene CDS and were identified to be pseudogenes in HZAU091 while functional in HA4-1 (Figure 3B). Apart from the insertion of the transposon, RipA5 also had a 99 bp deletion in HZAU091. The DNA sequences of common effectors in HZAU091 and HA4-1 were aligned, then the difference between RipH1 and RipAO was detected. In summary, we identified seven distinct effectors as candidates. The basic information of the seven candidates was listed in Table S4 (see supporting information).

Several candidate effectors introduced into HZAU091 could boost the immunity of ALB28-1

Virulence assays were carried out with seven candidate effectors from HA4-1 which were driven under their native promoters and then transferred into the virulent strain HZAU091. As shown in

10.3389/fpls.2023.1075042

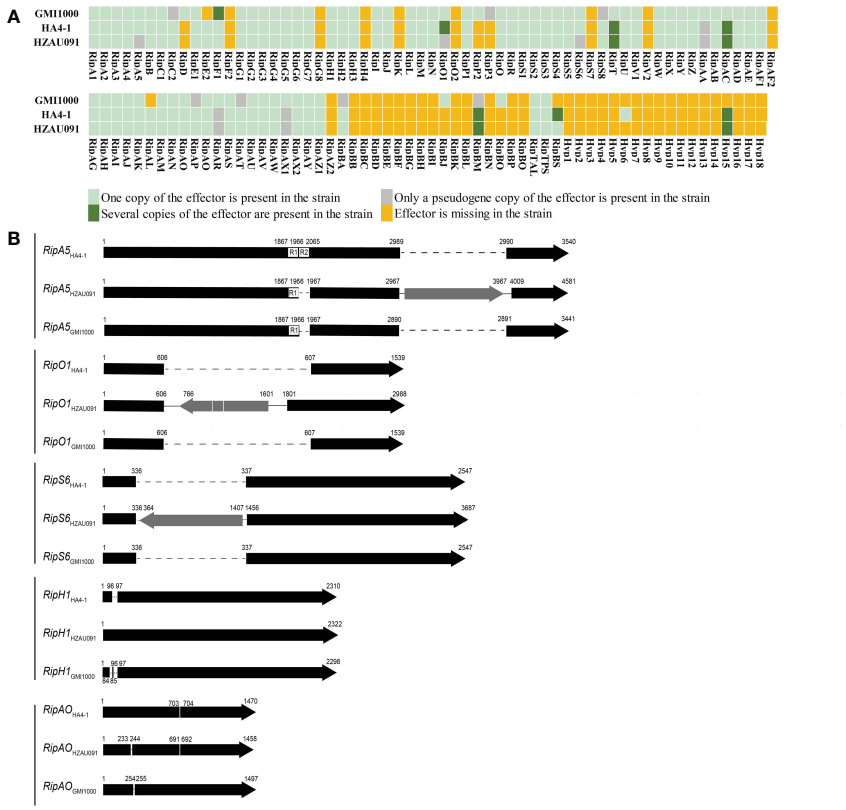

FIGURE 3
HA4-1 and HZAU091 exhibit differences in their T3Es repertoires. **(A)** Distributions of repertoires of T3Es in HA4-1 and HZAU091. GMI1000 is a representative T3Es repertoire. Different colors of the boxes indicate different copy numbers in the genome. Light green boxes indicate the effector is present in the strain with only one copy. Dark green boxes indicate several copies of the effector are present in the strain. Grey boxes indicate pseudo-effectors in the strain. Yellow boxes indicate the effector is missing in the strain. Five effectors RipA5, RipO1, RipS6, RipBS, and Hyp6 have different copy numbers in HA4-1 and HZAU091. **(B)** Sketch structure maps of T3Es different between HA4-1 and HZAU091. Grey arrows indicate the insertion. Dotted lines indicate the absence of a region in the gene. RipA5, RipO1, and RipS6 in HZAU091 exhibit large fragment insertions than HA4-1. RipH1 and RipAO in HZAU091 exhibit 12 base pair insertion and deletion.

Figure 4A, the virulence of HZAU091 carrying the candidate effectors was offset to different degrees. ALB28-1 exhibited better resistance against HZAU091::RipBS than wild-type HZAU091 and other virulent strains of HZAU091 carrying effectors from HA4-1 after 12 days of inoculation. To evaluate the ability of each candidate effector to reduce the virulence of HZAU091, all DI progression curves had been shown in Figures 4B–O. With HZAU091::Hyp6 inoculation, a higher disease index was observed than HZAU091 (Figure 4C). As for HZAU091::RipH1, the development trend showed a trade-off with HZAU091 (Figure 4D). ALB28-1 exhibited more susceptibility against *R. solanacearum* strain HZAU091 carrying RipH1 at the early stage (Figure 4E). HZAU091::RipA5, HZAU091::RipS6, and HZAU091::RipAO significantly depressed the virulence at the early stage (Figures 4F–K). HZAU091::RipBS significantly reduced the virulence of HZAU091 throughout the inoculation progression (Figures 4L, M). HZAU091::RipO1 significantly reduced the virulence at the late stage (Figures 4N, O). The significant difference analysis of HAZU091 carrying candidate effectors with wild-type HZAU091 was shown beside the corresponding disease index curve. Apart from the disease index, the AUDPC assay should also be taken into consideration to assess the overall pathogenicity of the strains. According to the area under the disease progress curve (AUDPC) caused by the eight strains (Figure 4P) and the above DI results, we demonstrated that the introduction of RipBS and RipA5 could significantly reduce the pathogenicity of HZAU091.

Even though no candidate effectors with the ability to induce complete loss of pathogenicity were discovered, the result of the experiment to evaluate the virulence of HZAU091 carrying effectors from HA4-1 still yielded useful information. The delivery of RipBS and RipA5 by HZAU091 significantly reduced the virulence. ALB28-1 leaves infiltrated with HA4-1 caused HR while HA4-1 ΔhrpB and HZAU091 failed. To investigate whether the HR was related to these candidate effectors, all chosen effectors introduced into HZAU091 were infiltrated into ALB28-1 leaves. Except for HZAU091::RipS6 and HZAU091::RipBS triggering cell death, the ALB28-1 phenotypes infiltrated with other HZAU091 complementation strains were consistent with HZAU091 (Figure 5). RipBS and RipS6 were recognized by ALB28-1 during the infiltration in the leaf.

10.3389/fpls.2023.1075042

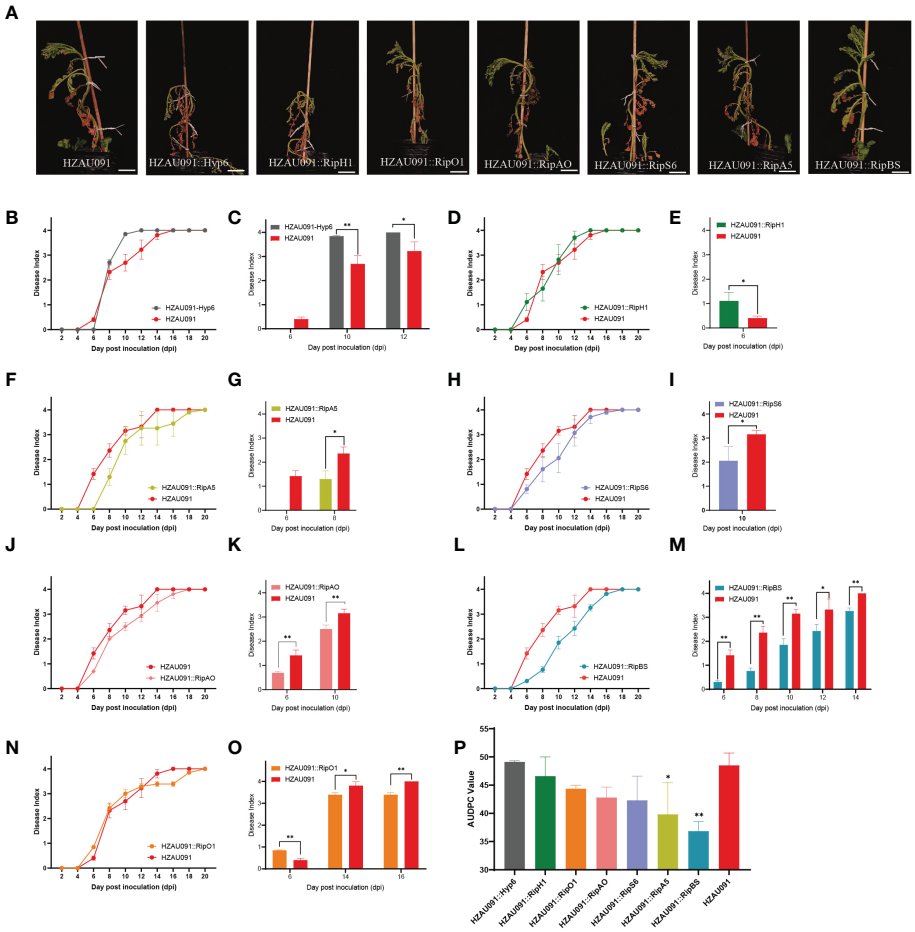

FIGURE 4
HZAU091 virulence is compromised in different degrees when carrying each of the seven candidate effector proteins. **(A)** The phenotypes of *Solanum albicans* 28-1 (ALB28-1) at 12 dpi. The white scale bar indicates 10 cm. The concentration of the bacterial suspension was 1×10^8 CFU/mL. **(B, D, F, H, J, L, N)** The disease index of ALB28-1 inoculated with the virulent strain HZAU091 carrying effectors from HA4-1 for 20 days. **(C, E, G, I, K, M, O)** The corresponding significant differences of DI were compared between the material ALB28-1 inoculated with HZAU091 carrying each of the seven candidate effector proteins and the virulent control HZAU091 at depicted time points. **(P)** The area under the disease progress curve (AUDPC) value of pathogenicity of eight strains. The virulence of HZAU091 carrying effectors in HA4-1 was compared with HZAU091. Data are presented as mean ± SD for three representative experimental replicates. Asterisks indicate significant differences of results (Student's *t* test, $*p < 0.05$, $**p < 0.01$). The DI values of healthy plants were presented with zero value. The experiments were repeated at least three times with similar results.

Mutation of candidate effectors confers pathogenicity on ALB28-1

Virulence assays to evaluate the role of T3Es include different approaches. Compared to the above experiment to evaluate the virulence of HZAU091 carrying effectors from HA4-1, gene mutation and complementation was a more classical way to evaluate the virulence. Therefore, we constructed the mutants by substituting the entire CDS region of the predicted effectors into the CDS region of antibiotic genes in HA4-1 strain genome. It should be clarified that in order to rigorously verify the virulence function of RipBS, the ΔRipBS mutant used in the following experiments is the triple mutant of three copy numbers of RipBS (Figure S2). The mutants exhibit the same morphology and growth curves as the wild type strains, which illustrated that the pathogenicity difference was mainly due to the absence of the candidate effectors (Figure S3). Then the virulence of successfully mutated strains (ΔRipA5, ΔRipBS, ΔHyp6, ΔRipS6, and ΔRipO1) and their complementary strains was tested (Figures 6A–J). After 12 days of mutated strains' inoculation, all plants showed wilting symptoms except for that inoculated by ΔRipA5 and HA4-1 which grew healthy (Figure 6A). All plants inoculated with complementation strains showed resistance at the same time (Figures 6A, C, E, G, I). When RipS6 was mutated, the wilt symptom of ALB28-1 was the most severe (Figure 6I), and the pathogenic process was the most rapid during the invasion (Figure 6J). The DI of the mutant strains was ΔRipS6 > ΔRipBS > ΔRipO1 > ΔHyp6 > ΔRipA5 = HA4-1 (Figures 6B, D, F, H, J). All these mutated strains were infiltrated into ALB28-1 leaves to verify the core avirulence effector as the complementation strains, but none of them resulted in the disappearance of the HR (Figure S4), which might be as a result of the effector functional redundancy.

Taken together, with the combination of the pathogenicity results of the virulent strain HZAU091 carrying effectors from HA4-1 and the mutant strains and its complementary strains,

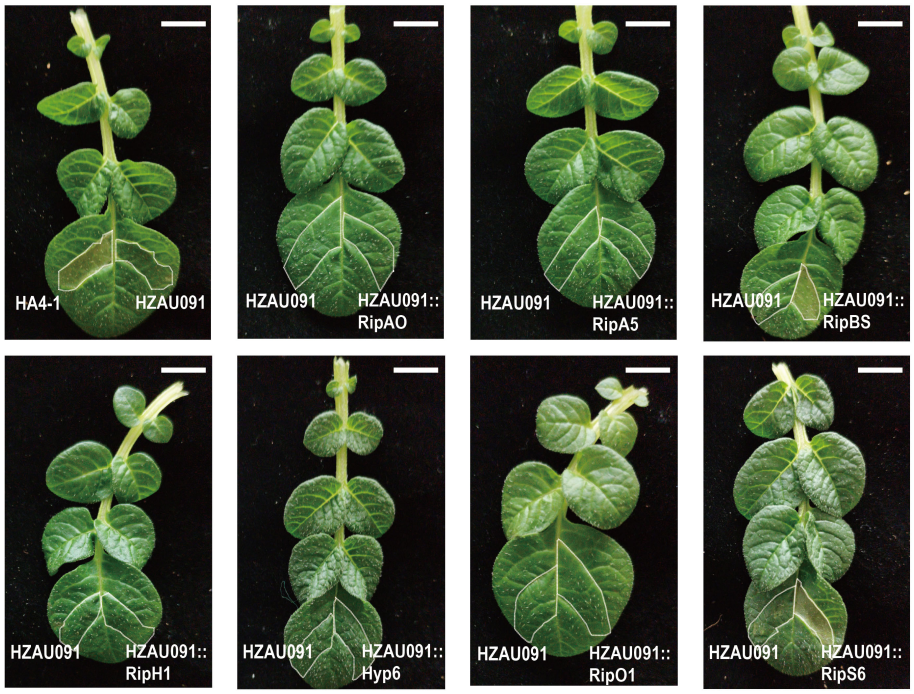

FIGURE 5
HZAU091 carrying RipBS and RipS6 elicited the HR of ALB28-1 leaves. All candidate effectors of HA4-1 were introduced into HZAU091. HA4-1 (avirulent) could cause HR in ALB28-1 leaves while HZAU091 (virulent) failed. HA4-1 and HZAU091 were wild type controls. HZAU091::RipBS and HZAU091::RipS6 could elicit the HR as HA4-1. All bacterial strains were resuspended at OD_{600} = 0.1 (≈1 × 10^8CFU/mL) and infiltrated into 12 ALB28-1 leave replicates. The experiments were repeated at least three times with similar results. The white scale bar indicates 1 cm. The photo was taken at 3 dpi.

RipBS and RipS6 were regarded as key avirulence effectors that could be recognized by ALB28-1. Apart from the above experiments conducted using the resistance host ALB28-1, the host-specific recognition was then confirmed by using an HA4-1 susceptible host *Solanum tuberosum L.* cultivar E3 (Figure S5). E3, inoculated with HA4-1, HA4-1 ΔRipBS, and HA4-1 ΔRipS6, showed wilting symptoms with no significant difference (Figure S5A). *R. s* strains HZAU091 carrying RipS6 and RipBS also conferred virulence to E3 with no significant difference (Figure S5B). Future work is needed to gain further understanding of the molecular function of RipBS and RipS6.

RipBS is a novel T3E unique in *R. solanacearum* strains

Since RipBS was predicted as T3Es only by the bioinformatic method (Tan et al., 2019), this study experimentally supplemented the demonstration utilizing the Cya reporter system. In this system, the CyaA protein could be delivered into the plant cell when T3SS perceived the signal peptide of the predicted effectors (Mukaihara et al., 2010). If the core element of T3SS was abolished, the T3Es would lose the ability to be delivered into the host plant cells to trigger or suppress the plant immunity. Therefore, *hrpB*, encoding the structure component of theT3SS, was mutated and used as a negative control. Since RipO1 was previously discovered in other strains as a definite T3E (Peeters et al., 2013), we used it as a positive control. Then all recombinant plasmids, carrying both effector gene and the *cyaA* gene, were introduced into the HA4-1 and HA4-1 ΔhrpB, and all these *R. solanacearum* strains were infiltrated into the potato tubers for 28 days in dark. With the successful delivery of the fusion protein $RipBS^{SP}$-Cya and $RipO1^{SP}$-Cya to the host plant cell, Cya protein was perceived by plants and robustly elevated the concentration of cAMP due to the cascade reactions. When the *hrpB* of HA4-1 was mutated, no significant rise in concentration was observed in any experimental groups (Figure 7A). This result proved that RipBS was secreted through the type III secretion system and was a novel T3E in the *R. solanacearum*.

In this experiment, when the T3Es prediction of HA4-1 was initially made, RipBS was not within the range of the prediction results. However, RipBS was originally predicted using bioinformatics methods as a new T3E (Tan et al., 2019). Therefore, it was speculated that RipBS can be classified in this experiment as some other effector proteins. The sequence of RipBS was then compared with the effector protein with multiple copies in HA4-1. It was found that RipBS was classified into the RipAC multi-copy sequences of HA4-1. As shown in a phylogenetic tree of RipAC sequences among all sequenced *R. solanacearum* strains, HA4-1 presented at least three RipAC copy numbers (Figure 7B). The nucleotide sequence of *RipBS* was identical to the unique copy from HA4-1 RipAC. Then the amino acid sequence of this unique RipAC copy was also blasted in UniproKB and the result showed the alignment with *Xanthomonas campestris* pv. *campestris* XopAC as RipBS alignment (Figure S6). In summary, the T3Es prediction result was rectified. That is, RipBS was identified as a novel T3E rather than a copy of RipAC.

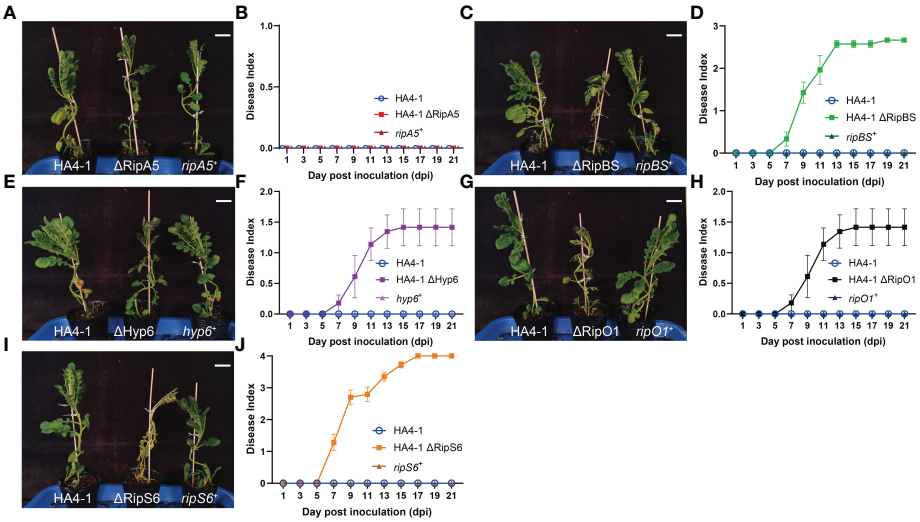

FIGURE 6
Mutation in predicted T3Es increased virulence of HA4-1. **(A, C, E, G, I)** The phenotypes of ALB28-1 inoculated with HA4-1, HA4-1 mutants and their complementation strains at 15 dpi. White scale bar indicates 5 cm. ALB28-1 was resistant to HA4-1, HA4-1 ΔRipA5 and all complementation strains, while susceptible to other HA4-1 mutants. **(B, D, F, H, J)** The disease index of ALB28-1 inoculated with HA4-1, HA4-1 effector mutants and their complementation strains within 21 days. The concentration of the bacterial suspension was $1x10^8$ CFU/mL. Error bars represent mean ± SD for three representative experimental replicates. The DI values of healthy plants were presented with zero value. The experiments were repeated at least three times with similar results.

Discussion

This work determined the pathogenicity of HA4-1 and HZAU091 to a wild potato accession ALB28-1. ALB28-1 was resistant to HA4-1 while susceptible to HZAU091 (Figures 1A, B). The genome sequence of HZAU091 was sequenced and the comparative genomics analysis confirmed that HZAU091 was more closely related to HA4-1 on the genome level (Figure 2). Using the comparative genomics method, seven distinct effectors were predicted in HA4-1, among which Hyp6 was found to present only in HA4-1 compared with HZAU091 (Figure 3A). The virulence assays conducted with HZAU091 harboring HA4-1 effectors and with T3E mutated HA4-1 clones, demonstrated that certain predicted effectors have a strong role in conferring avirulence to *R. solanacearum* in the wild potato. In particular, our study revealed that RipS6 and RipBS, a novel predicted effector, substantially contribute to the resistance of ALB28-1 against *R. solanacearum* (Figures 4A, 6I).

RipBS was first predicted as a novel effector in the *R. solanacearum* (Tan et al., 2019), but was not identified by the gene expression experiment. In this work, RipBS was predicted to possess an *hrpII* box (Table S4) and was confirmed as a T3E based on the cAMP experiment using the Cya reporter system (Figure 7A). The amino acid alignment of RipBS with RipAC homologs and XopAC revealed that RipBS had a closer relationship with the *Xanthomonas campestris* pv. *Campestris* (Xcc) effector XopAC than with the *Ralstonia solanacearum* effector RipAC (Figure 7B). XopAC is also named AvrAC due to its avirulence ability. XopAC can trigger the immunity of Arabidopsis ecotype Col-0 relying on the LRR (Leucine-rich repeat)and fic domains (Xu et al., 2008; Guy et al., 2013). However, AvrAC has also been reported as a virulence factor that can suppress plant immunity by specifically targeting the plant immune kinases BIK1 and RIPK1 with its uridine 5'-monophosphate transferase activity and inhibiting flg22-induced MAPK activation by targeting the RLCKVII (Feng et al., 2012; Yamaguchi et al., 2013). By contrast, the host developed decoy substrate PBL2 and pseudokinase RKS1 as well as ZAR1 to recognize and consume AvrAC to make a successful intercept for BIK1 and trigger the plant immunity (Wang et al., 2015). When RipBS was mutated, the pathogenicity of the RipBS-mutant strain showed an obvious increase (Figures 6C, D), illustrating that plants may lose the target effector to recognize and trigger immunity. Thus, RipBS was demonstrated to be an avirulence effector in HA4-1. The mechanism of how RipBS confer avirulence remained to be discovered. Since RipBS also possessed the LRR and fic domains as XopAC, we hypothesized that these domains also contribute to its biological function.

RipS6 may act as an avirulence effector as its mutation led to strong virulence to HA4-1 in ALB28-1. It is worth noting that in our findings, RipS6 was also present in the GMI1000 genome (Figure 3A), while the inoculation result indicated that GMI1000 were virulent to ALB28-1 (Figure 1A). For effector protein prediction, we amplified all predicted protein gene fragments using polymerase chain reactions and sequenced them, and compared with the GMI1000 reference effectors. $RipS6^{GMI1000}$ has multiple missense mutations at the nucleotide level compared with $RipS6^{HA4-1}$ (Table S4). Therefore, it is speculated that the missense mutations in GMI1000 may alter the biological function of RipS6, and that ALB28-1 may not recognize $RipS6^{GMI1000}$ and trigger the plant immunity. RipS6 belongs to the RipS (SKWP) family, which contains 12–18 tandem repeats of a novel 42aa motif (Mukaihara and Tamura, 2009). In this effector family, RipS1 has been reported

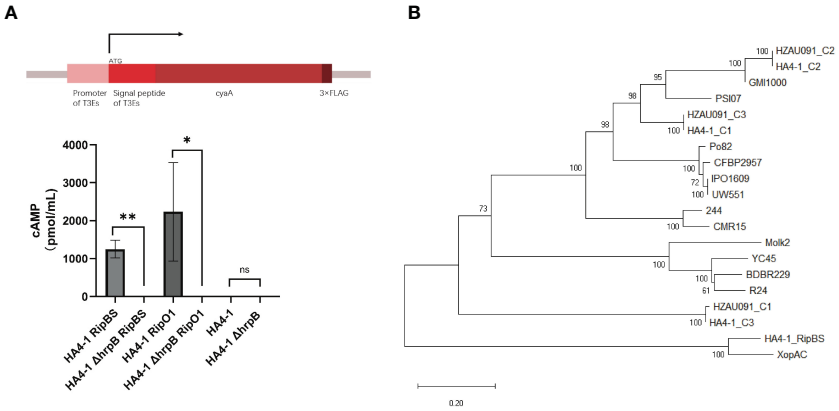

FIGURE 7
RipBS was identified as a novel effector. **(A)** The Cya reporter system to identify the T3Es based on the gene expression study method. HA4-1 ΔhrpB was a core T3SS system mutated strain that lost the ability to deliver the T3Es into the plant cells. HA4-1 ΔhrpB strains acted as controls. Error bars represent mean ± SD for three biological replicates. Asterisks indicate significant differences (Student's *t* test, $*p < 0.05$, $**p < 0.01$). ns means no significant difference. The DI values of healthy plants were presented with zero value. **(B)** The phylogenetic tree of RipBS in all *R. solanacearum* strains containing RipAC (C1, C2, C3 indicated different copies of RipAC in either HA4-1 or HZAU091).

to suppress the flg22-induced ROS (Landry et al., 2020). RipS4 (previously named RSc1839) can contribute to bacterial fitness (Macho et al., 2010). The RipS multiprotein of OE1-1, a Japanese *R. solanacearum* strain, has been proven to collectively contribute to bacterial virulence to eggplant. In the meantime, RipS1, RipS4, and RipS5 are the major RipS effectors for disease development (Chen et al., 2021). However, few mechanisms of how the SKWP family modulates plant immunity have been reported. Our study first proved that the effector RipS6 reduce bacterial virulence to potato.

The inoculation results of HA4-1 mutant strains showed that RipBS, RipS6, RipO1, and Hyp6 all contribute to the avirulence to ALB28-1, while only RipBS and RipS6 could reduce the virulence of HZAU091 according to the inoculation of the virulent strain HZAU091 carrying these two effectors in HA4-1. The leaf inoculation results also showed that HZAU091::RipS6 and HZAU091::RipBS are the only effectors that could still cause HR as HA4-1 (Figure 5). The introduction of RipS6, RipO1, and Hyp6 failed to significantly reduce the plant susceptibility caused by HZAU091 infection. In many cases, some effectors could inhibit the ETI (Effector-Triggered Immunity) triggered by another effector or ETI-associated components, for example, RipAY could inhibit the ETI triggered by RipE1 (Sang et al., 2020), XopQ inhibits cell death triggered by ETI-associated MAP kinase cascade MAPKKKα MEK2/SIPK and by several *R/avr* gene pairs (Teper et al., 2014). It was speculated that some effectors inside HZAU091 may also inhibit the ETI elicited by RipO1 and Hyp6 of HA4-1. To confirm this hypothesis and uncover the effector inhibitor, RipS6, RipO1, and Hyp6 of HA4-1 can be complemented into the HZAU091 mutant strain of a certain effector and then perform inoculation experiments in future studies.

The leaf inoculation results showed that single effector mutated strains could still cause HR as HA4-1 (Figure S4). Effector functional redundancy may explain this result, for example, RipB, RipAA, and RipP1 contribute in part to the avirulence of RS1000 (Nakano and Mukaihara, 2019). Several effector proteins in HA4-1 may be recognized by ALB28-1 leaves to trigger the immune response. To investigate whether the HR was related to these candidate effectors, introducing the candidate effector into HAZU091. All chosen effectors introduced into HZAU091 were infiltrated into ALB28-1 leaves. HZAU091::RipS6 and HZAU091::RipBS elicited the HR which HZAU091 and other HZAU091 complementation strains failed (Figure 5). To uncover the effector function in the future, RipBS/RipS6 double mutant strains and even multiple mutant strains should be constructed.

Our research results identified the effectors from HA4-1 that could boost plant immunity, conforming that comparative genomics and T3Es repertoires analysis of different virulence strains was a useful way to identify core avirulence effectors for the plants that lack well-known resistance resources. Based on comparative genomics and pathogenicity assays of two strains under the same genetic background, researchers can shed more light on these areas. The results of this research could be beneficial to promoting the study of the interaction mechanism between potato and *R. solanacearum*, and further uncovering the resistance gene to bacterial wilt. However, only one wild potato accession was used in this study. Researchers still face significant challenges in advancing the development of commercial potato bacterial wilt resistance breeding.

Data availability statement

The datasets presented in this study can be found in online repositories. The names of the repository/repositories and accession number(s) can be found in the article/Supplementary Material.

Author contributions

MH and XT conducted the experiments. HC and BS conceived the research and designed the experiments and supervised the molecular biology experiments. YW helped to screen the potato bacterial resistance material. MH wrote the manuscript. BS, XT, HC, BW, and DC guided the paper writing. All authors contributed to the article and approved the submitted version.

Funding

This work was funded by the National Natural Science Foundation of China grant 31871686, 32201789, the Earmarked Fund for Modern Agro-Industry Technology Research System of China (No. CARS-09-P07), and the grant (2022A1515110018) from Basic and Applied Basic Research Foundation of Guangdong Province.

Conflict of interest

The authors declare that the research was conducted in the absence of any commercial or financial relationships that could be construed as a potential conflict of interest.

Publisher's note

Supplementary material

The Supplementary Material for this article can be found online at: https://www.frontiersin.org/articles/10.3389/fpls.2023.1075042/full#supplementary-material

References

Alikhan, N.-F., Petty, N. K., Ben Zakour, N. L., and Beatson, S. A. (2011). BLAST ring image generator (BRIG): Simple prokaryote genome comparisons. *BMC Genomics* 12, 402. doi: 10.1186/1471-2164-12-402

Chen, L., Lei, N., Kiba, A., Hikichi, Y., and Ohnishi, K. (2021). Contribution of RipS type III effector family of *Ralstonia solanacearum* Japanese strain OE1-1 to disease development in eggplant. *J. Gen. Plant Pathol.* 87, 77–82. doi: 10.1007/s10327-020-00977-5

Cheng, D., Zhou, D., Wang, Y., Wang, B., He, Q., Song, B., et al. (2021). *Ralstonia solanacearum* type III effector RipV2 encoding a novel E3 ubiquitin ligase (NEL) is required for full virulence by suppressing plant PAMP-triggered immunity. *Biochem. Biophys. Res. Commun.* 550, 120–126. doi: 10.1016/j.bbrc.2021.02.082

Cunnac, S., Boucher, C., and Genin, S. (2004). Characterization of the *cis* -acting regulatory element controlling HrpB-mediated activation of the type III secretion system and effector genes in *Ralstonia solanacearum*. *J. Bacteriol.* 186, 2309–2318. doi: 10.1128/JB.186.8.2309-2318.2004

Deng, W., Marshall, N. C., Rowland, J. L., McCoy, J. M., Worrall, L. J., Santos, A. S., et al. (2017). Assembly, structure, function and regulation of type III secretion systems. *Nat. Rev. Microbiol.* 15, 323–337. doi: 10.1038/nrmicro.2017.20

Feng, F., Yang, F., Rong, W., Wu, X., Zhang, J., Chen, S., et al. (2012). A *Xanthomonas* uridine 5′-monophosphate transferase inhibits plant immune kinases. *Nature* 485, 114–118. doi: 10.1038/nature10962

Flor, H. H. (1971). Current status of the gene-For-Gene concept. *Annu. Rev. Phytopathol.* 9, 275–296. doi: 10.1146/annurev.py.09.090171.001423

Genin, S., and Denny, T. P. (2012). Pathogenomics of the *Ralstonia solanacearum* species complex. *Annu. Rev. Phytopathol.* 50, 67–89. doi: 10.1146/annurev-phyto-081211-173000

Guy, E., Lautier, M., Chabannes, M., Roux, B., Lauber, E., Arlat, M., et al. (2013). *xopAC*-triggered immunity against xanthomonas depends on *Arabidopsis* receptor-like cytoplasmic kinase genes *PBL2* and *RIPK*. *PloS One* 8, e73469. doi: 10.1371/journal.pone.0073469

Jain, C., Rodriguez-R, L. M., Phillippy, A. M., Konstantinidis, K. T., and Aluru, S. (2018). High throughput ANI analysis of 90K prokaryotic genomes reveals clear species boundaries. *Nat. Commun.* 9, 5114. doi: 10.1038/s41467-018-07641-9

Konstantinidis, K. T., and Tiedje, J. M. (2005). Genomic insights that advance the species definition for prokaryotes. *Proc. Natl. Acad. Sci.* 102, 2567–2572. doi: 10.1073/pnas.0409727102

Landry, D., González-Fuente, M., Deslandes, L., and Peeters, N. (2020). The large, diverse, and robust arsenal of *Ralstonia solanacearum* type III effectors and their in planta functions. *Mol. Plant Pathol.* 21, 1377–1388. doi: 10.1111/mpp.12977

Machida-Hirano, R. (2015). Diversity of potato genetic resources. *Breed. Sci.* 65, 26–40. doi: 10.1270/jsbbs.65.26

Macho, A. P., Guidot, A., Barberis, P., Beuzón, C. R., and Genin, S. (2010). A competitive index assay identifies several *Ralstonia solanacearum* type III effector mutant strains with reduced fitness in host plants. *Mol. Plant-Microbe Interactions®* 23, 1197–1205. doi: 10.1094/MPMI-23-9-1197

Monteiro, F., Solé, M., van Dijk, I., and Valls, M. (2012). A chromosomal insertion toolbox for promoter probing, mutant complementation, and pathogenicity studies in *Ralstonia solanacearum*. *Mol. Plant-Microbe Interactions®* 25, 557–568. doi: 10.1094/MPMI-07-11-0201

Moon, H., Pandey, A., Yoon, H., Choi, S., Jeon, H., Prokchorchik, M., et al. (2021). Identification of RipAZ1 as an avirulence determinant of *Ralstonia solanacearum* in *Solanum americanum*. *Mol. Plant Pathol.* 22, 317–333. doi: 10.1111/mpp.13030

Morel, A., Guinard, J., Lonjon, F., Sujeeun, L., Barberis, P., Genin, S., et al. (2018). The eggplant AG91-25 recognizes the type III-secreted effector RipAX2 to trigger resistance to bacterial wilt (*Ralstonia solanacearum* species complex): RipAX2 triggers ETI in eggplant AG91-25. *Mol. Plant Pathol.* 19, 2459–2472. doi: 10.1111/mpp.12724

Mukaihara, T., and Tamura, N. (2009). Identification of novel *Ralstonia solanacearum* type III effector proteins through translocation analysis of *hrpB*-regulated gene products. *Microbiology* 155, 2235–2244. doi: 10.1099/mic.0.027763-0

Mukaihara, T., Tamura, N., and Iwabuchi, M. (2010). Genome-wide identification of a Large repertoire of *Ralstonia solanacearum* type III effector proteins by a new functional screen. *Mol. Plant-Microbe Interactions®* 23, 251–262. doi: 10.1094/MPMI-23-3-0251

Nakano, M., and Mukaihara, T. (2019). The type III effector RipB from *Ralstonia solanacearum* RS1000 acts as a major avirulence factor in *Nicotiana benthamiana* and other *Nicotiana* species. *Mol. Plant Pathol.* 20, 1237–1251. doi: 10.1111/mpp.12824

Noroy, C., and Meyer, D. F. (2017). Comparative genomics of the zoonotic pathogen *Ehrlichia chaffeensis* reveals candidate type IV effectors and putative host cell targets. *Front. Cell. Infect. Microbiol.* 6. doi: 10.3389/fcimb.2016.00204

Oh, E.-J., Hwang, I. S., Park, I. W., and Oh, C.-S. (2022). Comparative genome analyses of *Clavibacter michiganensis* type strain LMG7333T reveal distinct gene contents in plasmids from other *Clavibacter* species. *Front. Microbiol.* 12. doi: 10.3389/fmicb.2021.793345

Pandey, A., Moon, H., Choi, S., Yoon, H., Prokchorchik, M., Jayaraman, J., et al. (2021). *Ralstonia solanacearum* type III effector RipJ triggers bacterial wilt resistance in *Solanum pimpinellifolium*. *Mol. Plant-Microbe Interactions®* 34, 962–972. doi: 10.1094/MPMI-09-20-0256-R

Patil, V. U., Gopal, J., and Singh, B. P. (2012). Improvement for bacterial wilt resistance in potato by conventional and biotechnological approaches. *Agric. Res.* 1, 299–316. doi: 10.1007/s40003-012-0034-6

Peeters, N., Guidot, A., Vailleau, F., and Valls, M. (2013). *Ralstonia solanacearum* , a widespread bacterial plant pathogen in the post-genomic era: Ralstonia solanacearum and bacterial wilt disease. *Mol. Plant Pathol.* 14, 651–662. doi: 10.1111/mpp.12038

Prior, P., Ailloud, F., Dalsing, B. L., Remenant, B., Sanchez, B., and Allen, C. (2016). Genomic and proteomic evidence supporting the division of the plant pathogen *Ralstonia solanacearum* into three species. *BMC Genomics* 17, 90. doi: 10.1186/s12864-016-2413-z

Prior, P., Allen, C., and Elphinstone, J. (1998). *Bacterial wilt disease* (Berlin, Heidelberg: Springer Berlin Heidelberg). doi: 10.1007/978-3-662-03592-4

Rich, A. E. (1983). *Potato diseases* (New York: Academic Press).

Sabbagh, C. R. R., Carrere, S., Lonjon, F., Vailleau, F., Macho, A. P., Genin, S., et al. (2019). Pangenomic type III effector database of the plant pathogenic ralstonia spp. *PeerJ* 7, e7346. doi: 10.7717/peerj.7346

Safni, I., Cleenwerck, I., De Vos, P., Fegan, M., Sly, L., and Kappler, U. (2014). Polyphasic taxonomic revision of the *Ralstonia solanacearum* species complex: proposal to emend the descriptions of *Ralstonia solanacearum* and *Ralstonia syzygii* and reclassify current *R. syzygii* strains as *Ralstonia syzygii* subsp. *syzygii* subsp. nov., *R. solanacearum* phylotype IV strains as *Ralstonia syzygii* subsp. *indonesiensis* subsp. nov., banana blood disease bacterium strains as *Ralstonia syzygii* subsp. *celebesensis* subsp. nov. and *R. solanacearum* phylotype I and III strains as *Ralstonia pseudosolanacearum* sp. nov. *Int. J. Syst. Evol. Microbiol.* 64, 3087–3103. doi: 10.1099/ijs.0.066712-0

Salanoubat, M., Genin, S., Artiguenave, F., Gouzy, J., Mangenot, S., Arlat, M., et al. (2002). Genome sequence of the plant pathogen ralstonia solanacearum. *Nature* 415, 497–502. doi: 10.1038/415497a

Sang, Y., Yu, W., Zhuang, H., Wei, Y., Derevnina, L., Yu, G., et al. (2020). Intra-strain elicitation and suppression of plant immunity by *Ralstonia solanacearum* type-III effectors in *Nicotiana benthamiana*. *Plant Commun.* 1, 100025. doi: 10.1016/j.xplc.2020.100025

Setubal, J. C., Almeida, N. F., and Wattam, A. R. (2018). "Comparative genomics for prokaryotes," in *Comparative genomics methods in molecular biology*. Eds. J. C. Setubal, J. Stoye and P. F. Stadler (New York, NY: Springer New York), 55–78. doi: 10.1007/978-1-4939-7463-4_3

Shah, S. M. A., Khojasteh, M., Wang, Q., Taghavi, S. M., Xu, Z., Khodaygan, P., et al. (2021). Genomics-enabled novel insight into the pathovar-specific population structure of the bacterial leaf streak pathogen *Xanthomonas translucens* in small grain cereals. *Front. Microbiol.* 12. doi: 10.3389/fmicb.2021.674952

Sharma, P., Johnson, M. A., Mazloom, R., Allen, C., Heath, L. S., Lowe, T. M., et al. (2022). Meta-a nalysis of the *Ralstonia solanacearum* species complex (RSSC) based on comparative evolutionary genomics and reverse ecology. *Microb. Genomics* 8, 14. doi: 10.1099/mgen.0.000791

Tan, X., Qiu, H., Li, F., Cheng, D., Zheng, X., Wang, B., et al. (2019). Complete genome sequence of sequevar 14M ralstonia solanacearum strain HA4-1 reveals novel type III effectors acquired through horizontal gene transfer. *Front. Microbiol.* 10. doi: 10.3389/fmicb.2019.01893

Teper, D., Salomon, D., Sunitha, S., Kim, J.-G., Mudgett, M. B., and Sessa, G. (2014). *Xanthomonas euvesicatoria* type III effector XopQ interacts with tomato and pepper 14-3-3 isoforms to suppress effector-triggered immunity. *Plant J.* 77, 297–309. doi: 10.1111/tpj.12391

Wale, S., Platt, B. H. W., and Cattlin, N. D. (2008). *Diseases, pests and disorders of potatoes: A colour handbook* (London: Manson publ).

Wan, X., and Yang, Y. (2022). Complete genome sequence analysis of *Ralstonia solanacearum* strain PeaFJ1 provides insights into its strong virulence in peanut plants. *Front. Microbiol.* 13, 14. doi: 10.3389/fmicb.2022.830900

Wang, G., Roux, B., Feng, F., Guy, E., Li, L., Li, N., et al. (2015). The decoy substrate of a pathogen effector and a pseudokinase specify pathogen-induced modified-self recognition and immunity in plants. *Cell Host Microbe* 18, 285–295. doi: 10.1016/j.chom.2015.08.004

Wang, L., Wang, B., Zhao, G., Cai, X., Jabaji, S., Seguin, P., et al. (2017). Genetic and pathogenic diversity of *Ralstonia solanacearum* causing potato brown rot in China. *Am. J. Potato Res.* 94, 403–416. doi: 10.1007/s12230-017-9576-2

Xu, R.-Q., Blanvillain, S., Feng, J.-X., Jiang, B.-L., Li, X.-Z., Wei, H.-Y., et al. (2008). AvrAC $_{Xcc8004}$, a type III effector with a leucine-rich repeat domain from *Xanthomonas campestris* pathovar campestris confers avirulence in vascular tissues of *Arabidopsis thaliana* ecotype col-0. *J. Bacteriol.* 190, 343–355. doi: 10.1128/JB.00978-07

Yamaguchi, K., Yamada, K., and Kawasaki, T. (2013). Receptor-like cytoplasmic kinases are pivotal components in pattern recognition receptor-mediated signaling in plant immunity. *Plant Signal. Behav.* 8, e25662. doi: 10.4161/psb.25662

Zheng, X., Li, X., Wang, B., Cheng, D., Li, Y., Li, W., et al. (2019). A systematic screen of conserved *Ralstonia solanacearum* effectors reveals the role of RipAB, a nuclear-localized effector that suppresses immune responses in potato. *Mol. Plant Pathol.* 20, 547–561. doi: 10.1111/mpp.12774

Frontiers in
Plant Science

Cultivates the science of plant biology and its applications

The most cited plant science journal, which advances our understanding of plant biology for sustainable food security, functional ecosystems and human health.

Discover the latest Research Topics

See more →

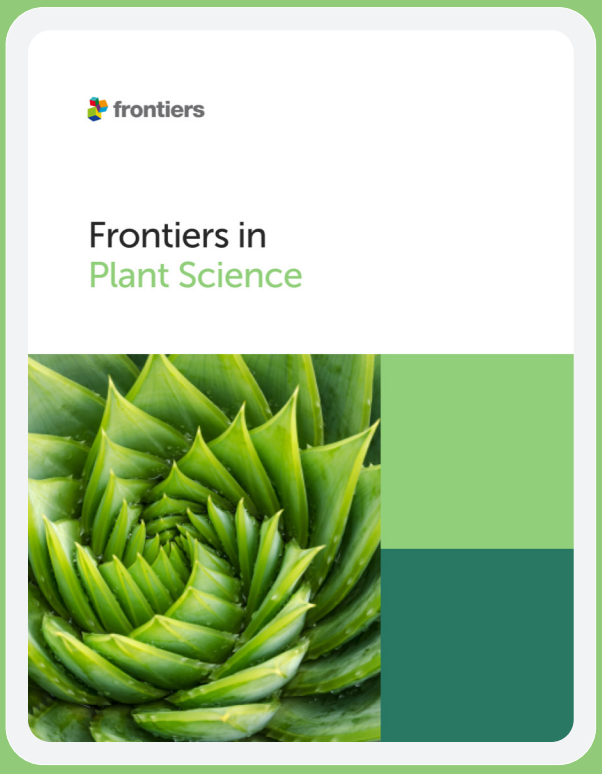

Frontiers

Avenue du Tribunal-Fédéral 34
1005 Lausanne, Switzerland
frontiersin.org

Contact us

+41 (0)21 510 17 00
frontiersin.org/about/contact